

VOLUME 80

DECEMBER 2, 1976

NUMBER 25

JPCHAx

THE JOURNAL OF

PHYSICAL
CHEMISTRY



PUBLISHED BIWEEKLY BY THE AMERICAN CHEMICAL SOCIETY

THE JOURNAL OF PHYSICAL CHEMISTRY

BRYCE CRAWFORD, Jr., *Editor*
STEPHEN PRAGER, *Associate Editor*
ROBERT W. CARR, Jr., C. ALDEN MEAD, *Assistant Editors*

EDITORIAL BOARD: C. A. ANGELL (1973-1977), F. C. ANSON (1974-1978), V. A. BLOOMFIELD (1974-1978), J. R. BOLTON (1976-1980), L. M. DORFMAN (1974-1978), H. L. FRIEDMAN (1975-1979), H. L. FRISCH (1976-1980), W. A. GODDARD (1976-1980), E. J. HART (1975-1979), W. J. KAUFMANN (1974-1978), R. L. KAY (1972-1976), D. W. McCLURE (1974-1978), R. M. NOYES (1973-1977), W. B. PERSON (1976-1980), J. C. POLANYI (1976-1980), S. A. RICE (1976-1980), F. S. ROWLAND (1973-1977), R. L. SCOTT (1973-1977), W. A. STEELE (1976-1980), J. B. STOTHERS (1974-1978), W. A. ZISMAN (1972-1976)

Published by the
AMERICAN CHEMICAL SOCIETY
BOOKS AND JOURNALS DIVISION
D. H. Michael Bowen, Director

Editorial Department: Charles R. Bertsch,
Head; Marianne C. Brogan, Associate
Head; Celia B. McFarland, Joseph E.
Yurvati, Assistant Editors

Graphics and Production Department:
Bacil Guiley, Head

Research and Development Department:
Seldon W. Terrant, Head

Advertising Office: Centcom, Ltd., 50 W.
State St., Westport, Conn. 06880.

© Copyright, 1976, by the American
Chemical Society. No part of this publication
may be reproduced in any form without
permission in writing from the American
Chemical Society.

Published biweekly by the American
Chemical Society at 20th and Northampton
Sts., Easton, Pennsylvania 18042. Second
class postage paid at Washington, D.C. and
at additional mailing offices.

Editorial Information

Instructions for authors are printed in
the first issue of each volume. Please conform
to these instructions when submitting man-
uscripts.

Manuscripts for publication should be
submitted to *The Journal of Physical
Chemistry*, Department of Chemistry, Uni-
versity of Minnesota, Minneapolis, Minn.
55455. Correspondence regarding **accepted
papers and proofs** should be directed to the
Editorial Department at the ACS Easton
address.

Page charges of \$60.00 per page are as-
sessed for papers published in this journal.
Ability to pay does not affect acceptance or
scheduling of papers.

Bulk reprints or photocopies of indi-
vidual articles are available. For information
write to Business Operations, Books and
Journals Division at the ACS Washington
address.

Requests for **permission to reprint**
should be directed to Permissions, Books and
Journals Division at the ACS Washington
address. The American Chemical Society and
its Editors assume no responsibility for the
statements and opinions advanced by con-
tributors.

Subscription and Business Information

1976 Subscription rates—including surface
postage

	U.S.	PUAS	Canada, Foreign
Member	\$24.00	\$29.75	\$30.25
Nonmember	96.00	101.75	102.25
Supplementary material	15.00	19.00	20.00

Air mail and air freight rates are avail-
able from Membership & Subscription Ser-
vices, at the ACS Columbus address.

New and renewal subscriptions should
be sent with payment to the Office of the
Controller at the ACS Washington address.

Changes of address must include both old
and new addresses with ZIP code and a recent
mailing label. Send all address changes to the
ACS Columbus address. Please allow six
weeks for change to become effective. **Claims**
for missing numbers will not be allowed if loss
was due to failure of notice of change of ad-
dress to be received in the time specified; if

claim is dated (a) North America—more than
90 days beyond issue date, (b) all other for-
eign—more than 1 year beyond issue date; or
if the reason given is "missing from files".
Hard copy claims are handled at the ACS
Columbus address.

Microfiche subscriptions are available
at the same rates but are mailed first class to
U.S. subscribers, air mail to the rest of the
world. Direct all inquiries to Business Oper-
ations, Books and Journals Division, at the
ACS Washington address or call (202) 872-
4444. **Single issues** in hard copy and/or mi-
crofiche are available from Special Issues
Sales at the ACS Washington address. Cur-
rent year \$4.75. Back issue rates available
from Special Issues Sales. **Back volumes** are
available in hard copy and/or microform.
Write to Special Issues Sales at the ACS
Washington address for further information.
Microfilm editions of ACS periodical pub-
lications are available from volume 1 to the
present. For further information, contact
Special Issues Sales at the ACS Washington
address. **Supplementary material** must be
ordered directly from Business Operations,
Books and Journals Division, at the ACS
Washington address.

	U.S.	PUAS, Canada	Other Foreign
Microfiche Photocopy	\$2.50	\$3.00	\$3.50
1-7 pages	4.00	5.50	7.00
8-20 pages	5.00	6.50	8.00

Orders over 20 pages are available only on
microfiche, 4 × 6 in., 24X, negative, silver
halide. Orders must state photocopy or mi-
crofiche if both are available. Full biblio-
graphic citation including names of all au-
thors and prepayment are required. Prices
are subject to change.

American Chemical Society
1155 16th Street, N.W.
Washington, D.C. 20036
(202) 872-4600

Member & Subscription Services
American Chemical Society
P.O. Box 3337
Columbus, Ohio 43210
(614) 421-7230

Editorial Department
American Chemical Society
20th and Northampton Sts.
Easton, Pennsylvania 18042
(215) 258-9111

Volume 80, Number 25 December 2, 1976

JPCHAx 80(25) 2717-2810 (1976)

ISSN 0022-3654

- Kinetics of the Reaction $\text{OH} + \text{HNO}_2 \rightarrow \text{H}_2\text{O} + \text{NO}_2$ at High Temperatures Behind Shock Waves
 . . . **Robert A. Fifer** 2717
- Anion Radicals of Aromatic Ketones in Amine Solutions as Studied by Radiolysis
 . . . **Mikio Hoshino,* Shigeyoshi Arai, and Masashi Imamura** 2724
- Photoreduction of Silver Ion in Aqueous and Alcoholic Solutions
 . . . **Hiroshi Hada,* Yoshiro Yonezawa, Akio Yoshida, and Atsuhiko Kurakake** 2728
- Thermodynamic Properties of Liquids, Including Solutions. 13. Molecular and Intermolecular
 Properties from Excess Enthalpies . . . **Maurice L. Huggins** 2732
- High Field Conductance of Some Acids, Bases, and Salts
 . . . **Thomas J. Gilligan, III, and Andrew Patterson, Jr.*** 2735
- The Electrochemistry of Nitrobenzene and *p*-Nitrobenzaldehyde Studied by Transmission
 Spectroelectrochemical Methods in Sulfolane
 . . . **N. R. Armstrong, N. E. Vanderborgh, and Rod K. Quinn*** 2740
- An Investigation of the Self-Association of 2-Pyrrolidinone in Cyclohexane and Carbon
 Tetrachloride by Means of Spectroscopic and Dielectric Polarization Measurements
 . . . **Judith A. Walmsley,* E. Jean Jacob, and H. Bradford Thompson** 2745 ■
- Mean Activity Coefficients for the Simple Electrolyte in Aqueous Mixtures of Polyelectrolyte
 and Simple Electrolyte. The Mixed Counterion System Na^+ , Ca^{2+} , Cl^- ,
 Polystyrenesulfonate
 . . . **Jan C. T. Kwak,* Nancy J. Morrison, Ester J. Spiro, and Kunihiko Iwasa** 2753 ■
- Infrared Studies of Reactions on Oxide Surfaces. 7. Mechanism of the Adsorption of Water and
 Ammonia on Dehydroxylated Silica . . . **B. A. Morrow,* I. A. Cody, and Lydia S. M. Lee** 2761
- Dipole Moment Derivatives, Polar Tensors, and Effective Charges of Ammonia and Phosphine
 . . . **A. B. M. S. Bassi and Roy E. Bruns*** 2768
- Light Scattering Study of Local Structures in Solutions: Chloroform-Ethanol System
 . . . **Tadashi Kato and Tsunetake Fujiyama*** 2771
- Dielectric Studies of Amino Acid Conformation . . . **Joseph A. Walder** 2777
- Study of Relaxational Mechanisms in Dimethyl Sulfoxide in Water by Optical
 Digital-Correlation Spectroscopy . . . **P. W. Drake and R. Meister*** 2780
- The Significant Determination of the Permanent Dipole Moment of a Solute in Solution
 . . . **R. Finsy* and R. Van Loon*** 2783
- A Study of the Solvent Effect on the Lowest Triplet State of Hydroxybenzaldehydes
 . . . **K. A. Martin, G. Moller, and A. M. Nishimura*** 2788
- Effects of Intermolecular Interaction on Protein Diffusion in Solution
 . . . **Wilfrid B. Veldkamp* and Joseph R. Votano** 2794
- Kinetics of Dissociation of Ferric Chloride Complexes. Stability Constants of Inner- and
 Outer-Sphere Complexes . . . **H. A. Schwarz* and R. W. Dodson** 2801

- A Simple Theory of Surface Tension at Low Vapor Pressure . **H. Ted Davis*** and **L. E. Scriven** 2805
 Pulse Radiolysis Study of Geminate Recombination in Charge Transfer Systems
 . . . **Koichiro Hayashi, Dagmar Lindenau, Wolfram Schnabel, and Masahiro Irie*** 2807

■ Supplementary material for this paper is available separately (consult the masthead page for ordering information); it will also appear following the paper in the microfilm edition of this journal.

* In papers with more than one author, the asterisk indicates the name of the author to whom inquiries about the paper should be addressed.

AUTHOR INDEX

- | | | | |
|----------------------------|----------------------|--------------------------|--------------------------|
| Arai, S., 2724 | Hada, H., 2728 | Lindenau, D., 2807 | Schwarz, H. A., 2801 |
| Armstrong, N. R., 2740 | Hayashi, K., 2807 | Martin, K. A., 2788 | Scriven, L. E., 2805 |
| Bassi, A. B. M. S., 2768 | Hoshino, M., 2724 | Meister, R., 2780 | Spiro, E. J., 2753 |
| Bruns, R. E., 2768 | Huggins, M. L., 2732 | Moller, G., 2788 | Thompson, H. B., 2745 |
| Cody, I. A., 2761 | Imamura, M., 2724 | Morrison, N. J., 2753 | Vanderborgh, N. E., 2740 |
| Davis, H. T., 2805 | Irie, M., 2807 | Morrow, B. A., 2761 | Van Loon, R., 2783 |
| Dodson, R. W., 2801 | Iwasa, K., 2753 | Nishimura, A. M., 2788 | Veldkamp, W. B., 2794 |
| Drake, P. W., 2780 | Jacob, E. J., 2745 | Patterson, A., Jr., 2735 | Votano, J. R., 2794 |
| Fifer, R. A., 2717 | Kato, T., 2771 | Quinn, R. K., 2740 | Walder, J. A., 2777 |
| Finsy, R., 2783 | Kurakake, A., 2728 | Schnabel, W., 2807 | Walmsley, J. A., 2745 |
| Fujiyama, T., 2771 | Kwak, J. C. T., 2753 | Yonezawa, Y., 2728 | Yoshida, A., 2728 |
| Gilligan, T. J., III, 2735 | Lee, L. S. M., 2761 | | |

THE JOURNAL OF PHYSICAL CHEMISTRY

Registered in U. S. Patent Office © Copyright, 1976, by the American Chemical Society

VOLUME 80, NUMBER 25 DECEMBER 2, 1976

Kinetics of the Reaction $\text{OH} + \text{HNO}_2 \rightarrow \text{H}_2\text{O} + \text{NO}_2$ at High Temperatures Behind Shock Waves

Robert A. Fifer

Pitman-Dunn Laboratory, U.S. Army Frankford Arsenal, Philadelphia, Pennsylvania 19137 (Received June 14, 1976)

Publication costs assisted by the U.S. Army Frankford Arsenal

The kinetics of nitrous acid decomposition has been studied over the temperature range 1000–1400 K, and at pressures of 3.5–11 atm, using a shock tube relaxation technique. Mixtures of NO, NO₂, and H₂O in Ar containing nitrous acid due to the equilibrium $\text{NO} + \text{NO}_2 + \text{H}_2\text{O} \leftrightarrow 2\text{HNO}_2$ (3) were heated by incident shock waves, and the rate of HNO₂ decomposition was followed by spectroscopically monitoring the increase in NO₂ concentration as the above equilibrium shifts to the left. The results are interpreted in terms of a two-step decomposition mechanism: $\text{HNO}_2 \leftrightarrow \text{OH} + \text{NO}$ (1, -1); $\text{OH} + \text{HNO}_2 \rightarrow \text{H}_2\text{O} + \text{NO}_2$ (2). Due to the high ratio of (NO) to (HNO₂) employed, it was found that reaction 1 was in equilibrium, reaction 2 being the rate-determining step under these conditions. The observed rate of reaction, together with the equilibrium constant for reaction 1, provides a measurement of k_2 . This rate constant is found to have a near zero activation energy and a value of $k_2 = 1.55 \times 10^{12} \text{ cm}^3 \text{ mol}^{-1} \text{ s}^{-1}$ at the temperatures of these experiments. This can be combined with the temperature-dependent equilibrium constant for this reaction to give $k_{-2} = 8.3 \times 10^{12} \exp(-42\,000/RT) \text{ cm}^3 \text{ mol}^{-1} \text{ s}^{-1}$ for the reverse reaction of nitrogen dioxide with water. The data also provide a lower limit for the rate constant for the unimolecular decomposition of HNO₂ of $k_1 = 5.5 \times 10^{12} \exp(-48\,000/RT) \text{ s}^{-1}$.

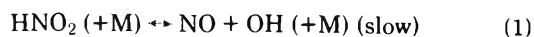
Introduction

Under ordinary conditions, nitrous acid is unstable with respect to decomposition and consequently does not exist in a pure gaseous state. As a result, very little is known about the gas-phase reactions of this molecule. This is unfortunate, since nitrous acid may play an important role in atmospheric chemistry, as well as in the production of nitrogen oxides in high-temperature combustion systems.

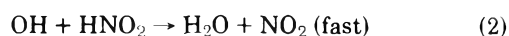
The rate of formation of HNO₂ in mixtures of NO, NO₂, and H₂O has been studied near room temperature.¹⁻³ This reaction, although apparently heterogeneous, is quite rapid at room temperature; from this it has been assumed¹ that the reverse reaction (i.e., HNO₂ decomposition) is similarly rapid. Based on an extrapolation of its assumed low-temperature instability, it has generally been proposed in the literature that nitrous acid will be even less stable at higher temperatures and will therefore not be important in systems at elevated temperatures. On the other hand, Asquith and Tyler⁴ observed HNO₂ formation, with a very slow subsequent rate of decomposition (half-life ~10 min), in a study of the H₂O₂ + NO reaction at 550 K. They concluded that nitrous acid may be

much more stable than had previously been thought. This was confirmed by Atkins and Cox,⁵ who showed that under certain experimental conditions dilute mixtures of nitrous acid can be prepared and stored for many hours with very little decomposition.

Nitrous acid would be expected to decompose by at least two different mechanisms. At low temperatures it apparently decomposes by some bimolecular, and sometimes heterogeneous, mechanism involving reaction of one HNO₂ molecule with either a second HNO₂ molecule or one of its equilibrium decomposition products (NO, NO₂, H₂O, HNO₃, N₂O₃, etc.). On the other hand, at higher temperatures, dilute mixtures would be expected to decompose via a unimolecular bond dissociation mechanism. By analogy with the nitric acid decomposition reaction^{6,7} this is



$$\Delta H = 50 \text{ kcal/mol}$$

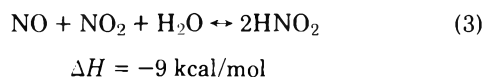


$$\Delta H = -41 \text{ kcal/mol}$$

Since the bond dissociation energies of HNO_2 and HNO_3 are similar, nitrous acid might be expected to be at least as stable as nitric acid at high temperatures.

There have been several recent studies at low temperatures and subatmospheric pressures of the reverse of reaction 1 in the third-order region.⁸⁻¹⁴ These investigations were prompted by the proposed importance of OH radicals in photochemical smog formation and by the proposed role of reaction -1, and the corresponding $\text{OH} + \text{NO}_2$ reaction, in converting reactive oxides of hydrogen and nitrogen, which catalytically destroy atmospheric ozone, to more stable products. Although good agreement has been found among the studies for the low-temperature third-order rate constant k_{-1} , attempts to obtain the high-pressure limiting second-order rate constants $k_{-1\infty}$ by either theoretical calculation^{10,15} or extrapolation to higher pressures^{11,14} have led to widely varying results. Clearly, a study of HNO_2 decomposition at high pressure could provide the information about the reverse reaction needed for atmospheric modeling, while high-temperature studies of HNO_2 decomposition would provide in addition values for k_1 and/or k_2 applicable to combustion systems.

In the present study the thermal decomposition of nitrous acid by reactions 1 and 2 has been investigated for the first time, using what might be called a shock tube chemical relaxation technique. Mixtures of NO, NO_2 , and H_2O in argon diluent were prepared. These contained HNO_2 due to the equilibrium



The equilibrium mixtures were then suddenly compressed and heated by incident shock waves and the subsequent rate of nitrous acid decomposition followed by spectroscopically monitoring the increase in NO_2 concentration as the above equilibrium shifted to the left due to reactions 1 and 2.

Experimental Section

The shock tube used in this study, as well as all of the associated gas mixing and handling equipment, is constructed of stainless steel. The shock tube has a 122-cm driver section and a 335-cm test section, both having a polished 53-mm bore. The quartz observation windows are located 274-cm downstream from the diaphragm. Their inside surfaces are cylindrically ground to a 53-mm radius to conform to the inner surface of the shock tube. The velocity of the shock wave is measured using platinum thin film resistance gauges, four of which are located at 500-mm intervals along the downstream end of the test section. The amplified signals from the last three gauges sequentially start and stop two digital electronic timers (HP-5304A), which measure to the nearest tenth of a microsecond (accuracy $\pm 0.5 \mu\text{s}$) the transit time of the shock wave over the two 500-mm distances. The observation windows are located midway between the last two gauges; the shock transit time between these gauges is therefore used for the temperature calculation.

For most experiments, 0.032 in. (0.81 mm) thick soft aluminum diaphragms were used; these were scored with an "X" to burst reproducibly at driver gas pressures of 500–550 psia (3450–3790 kN/m^2). Most shocks were driven by helium. The temperature was varied by changing the initial sample pressure. A few shocks were driven by hydrogen; for these the sample pressures were approximately twice as high for the same temperature range. In order to extend the range of

pressures covered to lower values, a few experiments were carried out using 0.025 in. (0.64 mm) and 0.020 in. (0.51 mm) thick diaphragms, which were scored to burst at about 420 psia (2900 kN/m^2) and 300 psia (2070 kN/m^2), respectively. However, with decreasing sample pressure it became increasingly difficult to measure the rate of reaction due to the decreasing ratio of HNO_2 to NO_2 in the mixture.

Light from a dc tungsten lamp was focused to the center of the shock tube through a 1.5-mm vertical slit placed near the first window. The light emerging from the opposite window passed through a second slit and was focused onto the entrance slit of a 0.25-m grating monochromator (JA-82-410) set to 4500 Å. Entrance and exit slits were 2.5 mm and the grating dispersion was 33 Å/mm, giving a band width of about 85 Å. The light was detected by an RCA 1P28 photomultiplier and the resulting signal was recorded photographically from a Tektronix 7603 oscilloscope operated in the dc mode, generally at a 50 $\mu\text{s/cm}$ writing speed.

Nitrous acid absorbs from 3000 to 4000 Å, with the strongest bands in the 3400–3700-Å region at room temperature.^{16,17} Since NO_2 also absorbs strongly in this region, it was not considered practical to attempt to measure the reaction rate using the time-dependent decrease in HNO_2 absorption. Rather, the increase in NO_2 absorption was followed. This can be measured at higher wavelengths where HNO_2 does not absorb. The 4500-Å wavelength for NO_2 was thought to be the best compromise between staying sufficiently far from HNO_2 absorption bands to prevent any interference while still having a fairly strong NO_2 absorption. Tests at higher wavelengths (4500–5500 Å) showed that the measured rates were independent of wavelength at all wavelengths tested.

The reaction mixtures were prepared from Ar, NO, NO_2 , and H_2O to a total pressure of 800 Torr in a 35-l. stainless-steel tank. This provided sufficient gas for several experiments. In order to produce a reasonable amount of HNO_2 via equilibrium reaction 3, a relatively high percentage of NO was used in most mixtures. The amount of H_2O was, of course, limited by its room-temperature vapor pressure. Although high NO_2 concentrations favor high HNO_2 concentrations, nevertheless a high HNO_2 to NO_2 ratio was desirable for greatest sensitivity since the increase in NO_2 concentration was used to follow the reaction rate; this necessitated the use of small NO_2 concentrations. The nine mixtures used had the percentages (the remainder being argon) listed in Chart I. These percentages are those that would result if no HNO_2 formed in the mixtures, i.e., if all HNO_2 were converted by reaction -3 into NO, NO_2 , and H_2O .

The mixtures were prepared as follows. Water vapor (usually 16 Torr) was first added to the storage tank. The desired amount of NO_2 was then added using a 4% mixture of NO_2 in Ar. (In preparing mixtures containing NO_2 , due account was taken of the pressure- and temperature-dependent NO_2 - N_2O_4 equilibrium in determining the equivalent amount of monomeric NO_2 present.) The NO was added next. Although nitrous acid formed as the NO was added, the amount formed was very small relative to NO, and the associated small pressure decrease was easily corrected for. Finally, argon was added to bring the final pressure to 800 Torr.

The argon used was Matheson Ultra High Purity (min. 99.999%). The NO_2 was obtained from Matheson (min. 99.5%) and was vacuum distilled prior to use. The water was degassed by pumping on it for several minutes. The NO was prepared from NaNO_2 and H_2SO_4 solutions as described elsewhere.¹⁸ After two or three fractional distillations, the gas was passed through a 2.4-m column of silica gel at -98°C .¹⁹ This reduced

Chart I

	NO	H ₂ O	NO ₂
B	33.88	2.25	0.25
C	33.86	2.00	0.23
D	33.88	2.00	0.13
E	12.50	2.00	0.25
F	33.88	0.75	0.25
G	33.88	2.00	0.42
H	33.88	2.00	0.19
I	33.88	1.97	0.12
J	12.50	1.94	0.12

the N₂O impurity to less than 0.01%, as determined by infrared spectroscopy.

For each mixture, initial incident shock temperatures, T_2 , were computed as a function of shock velocity using standard shock equations,²⁰ assuming ideal gas behavior and no reaction. Temperature-dependent enthalpy polynomials for Ar, NO, H₂O, and NO₂ were fit to data in the JANNAF tables²¹ for use in these computations. The density ratio across the shock wave, ρ_2/ρ_1 , was also calculated for each shock and used both to determine the density behind the shock wave from the initial pressure, P_1 , and to convert all measured times or rates from laboratory to gas-particle coordinates.²⁰

An initial calculation showed that it was not necessary to include HNO₂ in the computation of T_2 and ρ_2/ρ_1 . Due to the small concentrations of HNO₂ in the mixtures the error introduced by not taking the HNO₂ equilibrium reaction into account was well within the experimental error in the temperature due to uncertainty in the shock velocity.

Corrections to the temperature, densities, and measured rates for the effects of boundary layer formation, shock deceleration, and heat of reaction²² were considered but found to be unimportant. The deceleration and boundary layer corrections were negligible because of the short measurement times and high pressures employed. Errors due to the overall endothermicity of the reaction are negligible because of the low heat of reaction (+4.5 kcal/mol HNO₂) and high dilutions used.

Results

Figure 1 shows the appearance of the NO₂ absorption traces at 4500 Å for two experiments. There is a sudden decrease in transmittance when the shock wave passes the window position resulting from compression of the gases at the shock front. This is followed by a slower decrease due to NO₂ formation as the HNO₂ decomposes. Except at the lowest temperatures, the NO₂ absorption eventually approached a steady state level during the measurement time due to completion of reaction. This steady state NO₂ absorption, as well as the change in absorption resulting from reaction, always correlated reasonably well with that calculated from the initial composition of the mixture. This indicated that no appreciable quantities of N₂, NO₃, etc., are formed and is consistent with reactions 1 and 2 being the only important reactions in the system.

For each experiment, the rate of NO₂ formation was determined using the equation

$$\frac{d[\text{NO}_2]}{dt} = - \frac{0.4343S}{1000C(\rho_2/\rho_1)I_i L \epsilon(T)} \text{ mol/cm}^3 \text{ s} \quad (\text{I})$$

where S is the initial slope, C is the seconds per unit horizontal distance on the photograph, I_i is the distance between the zero percent baseline and the trace at $t = t_i$ (i.e., after shock compression but before reaction begins), L is the diameter of the

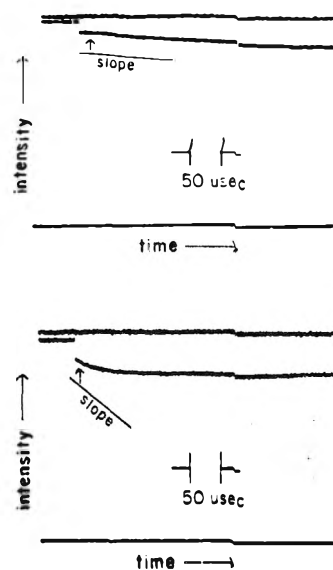


Figure 1. Time-dependent absorption traces for NO₂ at 4500 Å for two experiments. The upper and lower straight lines in each case are the "100%" and "0%" transmiss on baselines, recorded before the experiment. Top: expt C1, 1123 K, 6.18 atm. Bottom: expt C3, 1254 K, 9.94 atm.

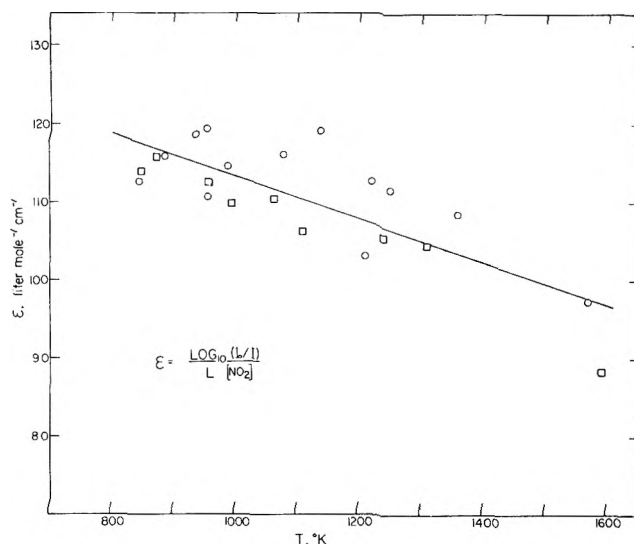


Figure 2. Measured extinction coefficients for NO₂ at 4500 Å as a function of temperature, determined from shocks in two different mixtures, both containing 0.5% NO₂ in argon.

shock tube, and $\epsilon(T)$ is the decadic extinction coefficient ($\text{l. mol}^{-1} \text{ cm}^{-1}$) of NO₂ at 4500 Å at the temperature of the experiment.

The extinction coefficient of NO₂ as a function of temperature was determined in a separate set of 22 experiments involving shocks in mixtures containing 0.5% NO₂ in argon. The results are shown in Figure 2. The extinction coefficient was found to have a negative temperature coefficient at 4500 Å and could be represented by

$$\epsilon(T) = 140.1 - 0.0274(T) \text{ l. mol}^{-1} \text{ cm}^{-1} \quad (\text{II})$$

over the temperature range 850–1600 K. The measured $\epsilon(T)$ are very close to those reported in previous determinations^{23,24} at 4360 Å.

According to reactions 1 and 2, one molecule of NO₂ is

TABLE I: Experimental Parameters

Expt	T_1 , K	P_1 , Torr	u_1 , mm/ μ s	T_2 , K	ρ_2/ρ_1	[M] $\times 10^5$ mol/cm ³	[NO] $\times 10^6$ mol/cm ³	[H ₂ O] $\times 10^7$ mol/cm ³	[NO ₂] $\times 10^8$ mol/cm ³	[HNO ₂] $\times 10^8$ mol/cm ³	log k s ⁻¹	log k_2 mol ⁻¹ cm ³ s ⁻¹
B1	295	325	1.046	1028	3.642	6.43	21.72	13.71	8.39	15.39	2.08	12.06
B2	295	275	1.092	1094	3.736	5.58	18.86	11.93	7.65	12.61	2.74	12.13
B3	296	225	1.150	1184	3.846	4.69	15.83	10.06	6.87	9.70	3.42	12.13
B4	297	450	1.116	1131	3.777	9.18	30.97	19.46	11.11	23.66	3.09	12.11
B5	299	375	1.173	1221	3.876	7.79	26.32	16.62	10.29	18.40	3.78	12.16
B6	300	300	1.076	1076	3.689	5.92	19.98	12.67	8.43	12.72	2.73	12.30
B7	300	265	1.105	1118	3.747	5.31	17.93	11.40	7.81	10.92	2.94	12.17
C1	293	325	1.110	1123	3.774	6.71	22.65	12.67	7.91	15.05	2.76	11.91
C2	293	275	1.149	1180	3.844	5.78	19.53	10.96	7.18	12.26	3.12	11.85
C3	293	449	1.195	1254	3.926	9.65	32.60	18.51	4.24	15.64	3.59	11.91
D1	293	500	1.141	1169	3.825	10.47	35.37	20.06	4.37	17.43	3.00	11.92
D2	293	450	1.174	1220	3.884	9.56	32.32	18.35	4.20	15.51	3.43	11.99
D3	293	395	1.228	1307	3.977	8.60	29.05	16.52	4.01	13.47	4.04	12.04
D4	293	270	1.144	1173	3.830	5.66	19.13	10.92	3.10	7.96	3.09	12.05
D5	293	225	1.174	1221	3.885	4.78	16.17	9.25	2.80	6.36	3.26	11.89
E1	294	251	1.143	1307	3.521	4.82	5.99	9.29	8.56	6.98	4.55	12.15
E2	293	550	1.117	1260	3.484	10.49	13.00	19.92	15.73	20.98	4.42	12.17
E3	293	477	1.145	1311	3.524	9.20	11.41	17.53	14.27	17.45	4.77	12.23
E4	293	327	1.090	1214	3.443	6.16	7.65	11.82	10.35	10.11	3.99	12.15
E5	293	270	1.082	1200	3.430	5.07	6.30	9.75	8.82	7.71	3.73	12.02
E6	293	225	1.048	1142	3.375	4.16	5.17	8.02	7.46	5.87	3.36	12.12
F1	293	250	1.158	1208	3.838	5.25	17.75	3.56	9.33	7.60	3.43	12.11
F2	293	600	1.089	1102	3.712	12.19	41.17	7.92	18.21	24.52	2.88	12.25
F3	293	500	1.155	1204	3.834	10.49	35.44	6.88	16.34	19.77	3.47	12.07
F4	293	415	1.185	1251	3.886	8.83	29.82	5.84	14.30	15.53	3.59	11.90
F5	293	350	1.256	1370	4.001	7.66	25.90	5.12	12.84	12.64	4.80	12.41
F6	293	250	1.117	1145	3.764	5.15	17.41	3.49	9.15	7.45	2.88	12.05
F7	293	200	1.152	1199	3.829	4.19	14.17	2.87	7.71	5.54	3.39	12.18
F8	293	150	1.238	1339	3.971	3.26	11.02	2.25	6.24	3.83	4.40	12.33
F9	293	153	1.222	1312	3.946	3.30	11.17	2.28	6.31	3.91	4.37	12.46
G1	293	300	1.098	1103	3.749	6.15	20.75	11.33	16.10	19.50	2.96	12.13
G2	293	497	1.147	1178	3.842	10.45	35.20	18.92	24.08	39.63	3.81	12.30
G4	293	340	1.070	1063	3.694	6.87	23.17	12.61	17.47	22.80	2.67	12.17
G5	293	240	1.164	1204	3.872	5.09	17.15	9.43	13.95	14.81	3.82	12.23
G6	293	200	1.212	1282	3.902	4.27	14.41	7.96	12.14	11.59	4.35	12.27
G7	293	165	1.222	1298	3.918	3.54	11.94	6.63	10.41	8.90	4.34	12.18
H1	293	300	1.117	1133	3.785	6.21	20.99	11.83	5.74	11.89	2.96	12.09
H3	293	450	1.151	1183	3.848	9.48	32.00	17.93	7.55	20.54	3.87	12.56
H5	293	300	1.114	1129	3.781	6.21	20.97	11.82	5.73	11.87	3.17	12.34
H6	293	250	1.153	1188	3.853	5.27	17.81	10.07	5.16	9.50	3.79	12.52
H7	293	225	1.186	1239	3.911	4.82	16.27	9.21	4.87	8.38	3.99	12.38
H8	293	190	1.166	1207	3.875	4.03	13.62	7.73	4.27	6.61	3.59	12.23
I1	293	270	1.147	1178	3.836	5.67	19.16	10.78	3.05	7.85	3.19	12.11
I2	293	550	1.129	1151	3.803	11.45	38.68	21.60	4.48	19.21	3.14	12.19
I4	293	425	1.218	1291	3.961	9.21	31.14	17.43	4.09	14.49	4.15	12.24
I5	293	300	1.130	1152	3.805	6.25	21.12	11.87	3.22	8.92	3.14	12.26
I7	293	250	1.166	1208	3.871	5.30	17.90	10.08	2.93	7.16	3.21	11.93
I8	293	215	1.194	1251	3.920	4.61	15.59	8.79	2.70	5.95	3.80	12.24
I9	293	180	1.242	1332	4.003	3.94	13.33	7.53	2.45	4.81	4.38	12.34
J1	293	400	1.048	1141	3.373	7.38	9.19	13.93	4.80	8.27	3.29	12.16
J2	293	599	1.084	1202	3.432	11.25	13.99	21.13	6.41	14.40	3.99	12.34
J3	293	495	1.136	1293	3.510	9.51	11.83	17.89	5.78	11.45	4.77	12.53
J4	293	400	1.057	1156	3.388	7.42	9.23	13.99	4.82	8.31	3.72	12.47
J5	293	342	1.091	1214	3.443	6.44	8.02	12.17	4.38	6.84	4.16	12.51
J6	293	285	1.131	1284	3.504	5.47	6.80	10.34	3.90	5.43	4.61	12.51

formed in reaction 2 for every molecule of HNO₂ that dissociates in step 1. Therefore, for each experiment, the apparent first-order rate constant, k , for reaction 1 was calculated from $k = (d[\text{NO}_2]/dt)/[\text{HNO}_2]_i$ where $[\text{HNO}_2]_i$ is the initial concentration of nitrous acid behind the shock wave. The $[\text{HNO}_2]_i$ were calculated as follows: From the pressure of the gas mixture admitted to the shock tube, P_1 , and the known composition of the mixture (assuming no HNO₂), effective partial

pressures P^0 of NO, H₂O, and NO₂ were readily calculated. By an iterative procedure, the value of α , the partial pressure of each reactant consumed, was then determined for which the equilibrium constant for reaction 3 calculated from the equation

$$K_3 = \frac{(2\alpha)^2}{(P^0_{\text{NO}} - \alpha)(P^0_{\text{H}_2\text{O}} - \alpha)(P^0_{\text{NO}_2} - \alpha)} \text{ atm}^{-1} \quad (\text{III})$$

agrees with the reported equilibrium constant²⁵⁻²⁷ for this reaction at the starting temperature, T_1 , of the experiment (i.e., the room temperature, usually 293 K). The equilibrium partial pressure of HNO_2 is therefore 2α , and this can be used, with the ideal gas law and ρ_2/ρ_1 , to determine $[\text{HNO}_2]_1$, and thereby k .

The results for the 55 experiments carried out are given in Table I, which gives for each the initial temperature (T_1) and pressure (P_1), the measured shock velocity (u_1), the calculated shock temperature (T_2), the density ratio (ρ_2/ρ_1), the total post-shock density $[M]$, the initial post-shock concentrations of NO , H_2O , NO_2 , and HNO_2 , the apparent first-order rate constant (k), and k_2 , to be defined below.

Figure 3 shows an Arrhenius plot for k . Least-squares analysis gives

$$k = 4.2 \times 10^{12} \exp(-49\,500/RT) \text{ s}^{-1} \quad (\text{IV})$$

The apparent activation energy is very close to what would be expected for reaction 1 in the limiting high-pressure region ($E_a \sim \Delta E^\circ = 48 \text{ kcal/mol}$). However, there are systematic differences between the results for the different mixtures which cast doubt on the interpretation that k is the limiting high-pressure first-order rate constant ($k_{1\infty}$) for this reaction. In particular, a close examination of Figure 3 shows that the points are generally high for those mixtures with high $[\text{HNO}_2]/[\text{NO}]$ ratios (e.g., mixtures E, J) and generally low for those mixtures with low $[\text{HNO}_2]/[\text{NO}]$ ratios (e.g., mixtures D, I). This suggests that the reverse of reaction 1 is playing a role under the conditions of these experiments; that is, reactions -1 and 2 are competing with each other for the hydroxyl radicals produced by reaction 1.

Accordingly, we shall include in our analysis this reverse reaction. Making the steady state approximation for OH and considering only reactions 1, -1, and 2, we can write:

$$\frac{d[\text{OH}]}{dt} = 0 = k_1[\text{HNO}_2][M]^x - k_{-1}[\text{OH}][\text{NO}][M]^x - k_2[\text{OH}][\text{HNO}_2] \quad (\text{V})$$

where x may vary from 0 to 1 depending on whether the reaction is in the high-pressure, transition, or low-pressure region. Solving for $[\text{OH}]$ and substituting into

$$k = \frac{d[\text{NO}_2]/dt}{[\text{HNO}_2]} = k_2[\text{OH}] \quad (\text{VI})$$

gives:

$$k = \frac{k_2 k_1 [\text{HNO}_2][M]^x}{k_{-1}[\text{NO}][M]^x + k_2[\text{HNO}_2]} \quad (\text{VII})$$

Two limiting cases may be considered: (A) If $k_{-1}[\text{NO}][M]^x \gg k_2[\text{HNO}_2]$

$$k = \frac{k_2 K_1 [\text{HNO}_2]}{[\text{NO}]} \quad \text{where } K_1 = k_1/k_{-1} \quad (\text{VIIa})$$

(B) If $k_2[\text{HNO}_2] \gg k_{-1}[\text{NO}][M]^x$

$$k = k_1[M]^x \quad (\text{VIIb})$$

Case A corresponds to the situation where reactions 1 and -1 are in equilibrium, reaction 2 being the slow, rate-determining, step. In case B reaction 1 is the rate-determining step, reaction 2 being sufficiently fast that it does not affect the rate of reaction.

Calculations were carried out which involved fitting eq VII to the measured k in an attempt to determine k_1 and k_2 from the experimental data. These calculations showed that the

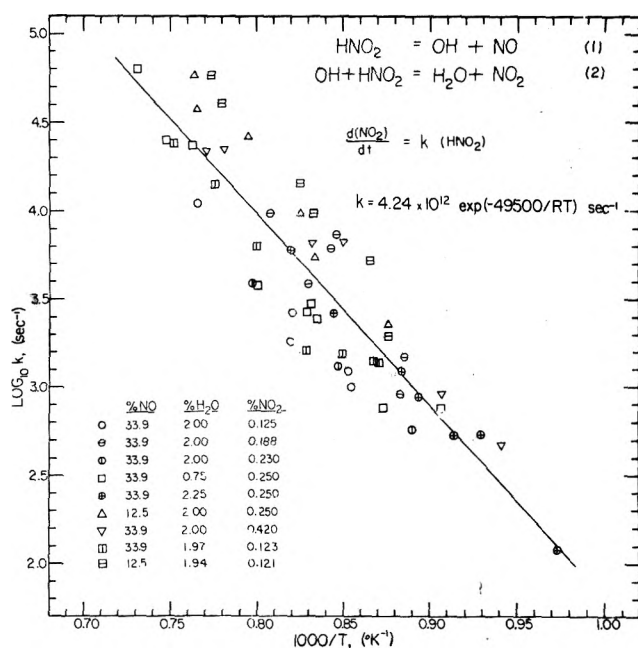


Figure 3. Arrhenius plot for the measured apparent first-order rate constants.

value of the preexponential factor A in the kinetic expression for k_1 (i.e., $k_1 = A \exp(-E_a/RT) \text{ s}^{-1}$, where $E_a \sim 48\,000 \text{ cal/mol}$) must be at least $5.5 \times 10^{12} \text{ s}^{-1}$, with k_2 between 1×10^{12} and $2 \times 10^{12} \text{ cm}^3 \text{ mol}^{-1} \text{ s}^{-1}$, in order for the calculated k to show a variation with $[\text{HNO}_2]/[\text{NO}]$ similar to that observed. For such values of k_1 and k_2 , $k_{-1}[\text{NO}] > k_2[\text{HNO}_2]$ for all experiments. (The value of k_{-1} is calculated from k_1 and the equilibrium constant K_1 .) Consequently, the experimental data correspond more closely to case A than case B, and thus provide a measure of k_2 rather than k_1 .

Equation VIIa can therefore be used to determine k_2 for each experiment from the measured k , K_1 at the temperature of the experiment,²⁸ and the starting concentrations of HNO_2 and NO . An Arrhenius plot for the k_2 calculated in this way is shown in Figure 4. Least-squares analysis gives $k_2 = 6.92 \times 10^{12} \exp(-3500/RT) \text{ cm}^3 \text{ mol}^{-1} \text{ s}^{-1}$. An activation energy of 2-4 kcal/mol is not unreasonable for this reaction. However, considering the small activation energy and the degree of scatter in the data, the calculated 3.5 kcal/mol activation energy is probably not statistically significant. We prefer, therefore, to report only an average value of

$$k_2 = (1.55 \pm 0.5) \times 10^{12} \text{ cm}^3 \text{ mol}^{-1} \text{ s}^{-1} \quad (\text{VIII})$$

over the temperature range of these experiments. This is the first determination of this rate constant. The error limits shown are estimates based on the probable maximum uncertainties in the measured rates and calculated HNO_2 concentrations. (The square of the HNO_2 concentration enters into the calculation of k_2 from the measured rates.) The calculated k_2 also makes use of the equilibrium constant K_1 . Consequently, if the published high-temperature free-energy functions²¹ for OH, NO, or the two isomers of HNO_2 are revised significantly at some future date, the value of k_2 reported above should be adjusted accordingly.

Finally, an expression for k_{-2} can be calculated from k_2 and the equilibrium constant K_2 . Assuming no activation energy for k_2 , and again assuming *cis*- and *trans*- HNO_2 to be in equilibrium, this gives:

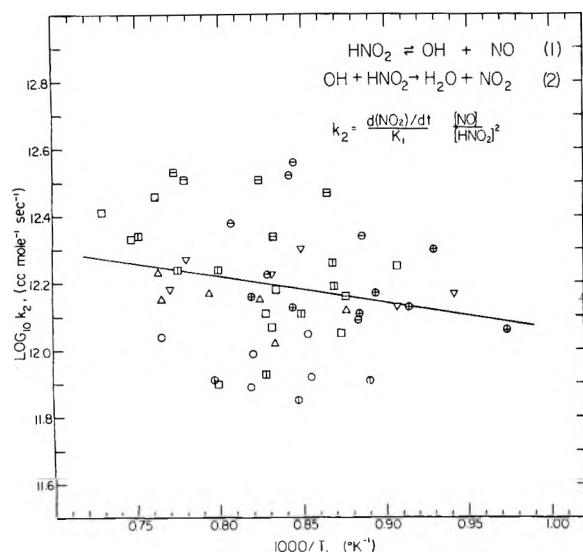


Figure 4. Arrhenius plot for the rate constants for reaction 2 calculated from eq VIIa.

$$k_{-2} = 8.3 \times 10^{12} \exp(-42000/RT) \text{ cm}^3 \text{ mol}^{-1} \text{ s}^{-1} \quad (\text{IX})$$

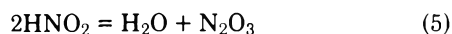
for the nitrogen dioxide-water reaction in the temperature range of this study. This is the first reported value for this rate constant.

Discussion

Consideration of Other Reactions. Three additional reactions were considered as possible complicating processes for this reaction system. The first was N_2O_3 formation and decomposition. Dinitrogen trioxide is formed via the equilibrium reaction



In order to determine the amount of N_2O_3 present in these mixtures, it is convenient to subtract reaction 4 from reaction 3 to yield



Since the equilibrium constant for reaction 5 is roughly 0.86 at room temperature,²¹ it follows that in the mixture the ratio $[\text{HNO}_2]/[\text{N}_2\text{O}_3] \sim 1.2[\text{H}_2\text{O}]/[\text{HNO}_2]$. Since $[\text{H}_2\text{O}]/[\text{HNO}_2]$ was typically about 20 in these experiments, the $[\text{N}_2\text{O}_3]$ should have been only a few percent or less of $[\text{HNO}_2]$, and it was therefore reasonable to assume that the decomposition of this small amount of N_2O_3 following shock heating did not significantly affect the measured rate of reaction. Due to the low bond dissociation energy of N_2O_3 (~ 10 kcal/mol), the dissociation of any N_2O_3 present should occur immediately behind the shock front before any significant amount of HNO_2 has decomposed.

The second reaction considered was



which could compete with reactions -1 and 2 for hydroxyl radicals. The rate constant for this reaction is probably somewhat less than that of reaction 2 at high temperature and perhaps about equal to that of reaction -1. However, the equilibrium constant for this reaction ($K_6 = 5 \times 10^5 \text{ cm}^3/\text{mol}$ at 1200 K) is such that for any reasonable OH concentration only very low concentrations of HNO_3 can form. Nitric acid formation is therefore probably not important in this system,

unless, as seems unlikely, it is removed by a subsequent reaction that forms some stable product in addition to those already being considered.

The third reaction considered was nitrous acid isomerization:



In this study it has been assumed that the rate of isomerization is fast compared to the rates of the reactions being measured and that this rate consequently does not affect the kinetics of nitrous acid decomposition. Although the rate of isomerization has never been measured, Hisatsune²⁹ has calculated $k_7 = 1.33 \times 10^{13} \exp(-10900/RT) \text{ s}^{-1}$ by using a transition state model. This gives $k_7 = 1.4 \times 10^{11} \text{ s}^{-1}$, or a half-life of $5.0 \times 10^{-12} \text{ s}$ at 1200 K. Since this is fast compared to the rates of reactions 1 and 2, the assumption of equilibrium between the two isomers during decomposition of nitrous acid is undoubtedly justified. It is not, of course, possible to determine which isomer is reacting in this system. (If one isomer is principally responsible for reaction, the equilibrium constant for the isomerization ($K_7 \sim 1.25$ at 1200 K) is, in effect, buried in the experimentally determined rate constant.) However, since it has been shown³⁰ that the O-H bond is unusually long and has a low vibrational frequency in *cis*- HNO_2 compared to the *trans* isomer, it is reasonable to speculate that it is the *cis* isomer that is chiefly responsible for the abstraction reaction 2, the rate constant for which was determined in this study.

Values of the Measured Rate Constants. It is of interest to compare k_2 with the various estimates that have been either recommended or used for atmospheric considerations and high-temperature combustion modeling. One approach has been to assume that k_2 can be approximated by the rate constant for the corresponding nitric acid reaction ($\text{OH} + \text{HNO}_3 \rightarrow \text{H}_2\text{O} + \text{NO}_3$). On this basis, for example, Tsang³¹ suggests $k_2 = 3.6 \times 10^{11} \exp(-800/RT) \text{ cm}^3 \text{ mol}^{-1} \text{ s}^{-1}$. This gives $k_2 = 2.6 \times 10^{11}$ at 1200 K, which is a factor of 3 lower than found here. Demerjian, Kerr, and Calvert³² recommended using one-half the rate constant for the reaction $\text{OH} + \text{H}_2\text{CO} \rightarrow \text{H}_2\text{O} + \text{HCO}$, based on the argument that since the enthalpies of the two reactions are similar the rate constants per abstractable hydrogen atom must also be similar. However, since the rate constant for the formaldehyde reaction is greater than $10^{13} \text{ cm}^3 \text{ mol}^{-1} \text{ s}^{-1}$ at the temperatures of these experiments,^{33,34} this method overestimates k_2 by more than an order of magnitude. Clearly chemical analogies have not been reliable in estimating k_2 . Finally, it may be noted that in a recent study of the photochemical decomposition of nitrous acid, Cox has estimated $k_2 = 1.1 \times 10^{12} \text{ cm}^3 \text{ mol}^{-1} \text{ s}^{-1}$ at room temperature.³⁵ Since this is almost identical with the value found here at temperatures 700–1100 K higher, this estimate, if correct, would indicate that this reaction has an activation energy very close to zero.

Only a lower limit ($5.5 \times 10^{12} \exp(-48000/RT) \text{ s}^{-1}$) can be established here for k_1 , the first-order rate constant for nitrous acid unimolecular decomposition. This may be compared with theoretical RRKM calculations reported by Tsang¹⁵ for the reverse reaction as a function of density for temperatures up to 1000 K. At 1000 K and a density of $5.3 \times 10^{-5} \text{ mol}/\text{cm}^3$, Tsang's calculations indicate $k_{-1} \sim 7 \times 10^{11} \text{ cm}^3 \text{ mol}^{-1} \text{ s}^{-1}$, which combined with the equilibrium constant²⁸ gives $k_1 \sim 5.3 \times 10^3 \text{ s}^{-1}$. The lower limit determined here yields $1.8 \times 10^2 \text{ s}^{-1}$ at 1000 K. Thus, at 1000 K, Tsang's RRKM calculations are not inconsistent with these results and indicate a value for k_1 more than an order of magnitude greater than the lower limit determined here. The RRKM calculations indicate that

the reaction is probably still in the fall off region at these temperatures and pressures.

Requirements for Measuring $k_{1\infty}$. In retrospect, it can be seen that under somewhat different conditions it should be possible to measure $k_{1\infty}$ using the shock tube relaxation technique described here. Two requirements must be met. The first is for much lower $[\text{NO}]/[\text{HNO}_2]$ ratios than employed in this study, in order to prevent the recombination reaction -1 from competing with reaction 2 for the OH radicals produced in the initial dissociation. The second requirement is for much higher pressures, in order to bring the unimolecular decomposition closer to the high-pressure limit. The first requirement can be partially met by using mixtures with somewhat lower $[\text{NO}]/[\text{NO}_2]$ ratios. However, as this ratio is decreased, the $[\text{HNO}_2]/[\text{NO}_2]$ ratio also decreases, making the rate of NO_2 formation more difficult to follow. The best solution might be to follow the reaction rate by a different technique, for example, by directly monitoring HNO_2 via its infrared absorption. In this case the $[\text{HNO}_2]/[\text{NO}_2]$ ratio would no longer be a limiting factor (at least as long as reaction 6 does not cause complications), and much lower $[\text{NO}]/[\text{HNO}_2]$ ratios could be obtained. Another approach would be to add to the mixture a radical scavenger that can remove OH faster than NO does in reaction -1. The requirement for higher pressures requires a shock tube equipped to operate at proportionately higher diaphragm bursting pressures, or alternatively, a combustion driven (heated driver gas) shock tube. For example, with a shock tube designed to operate at bursting pressures of about 4000 psi, initial and post-shock pressures roughly an order of magnitude higher than in this study would be possible.

References and Notes

- (1) L. G. Wayne and D. M. Yost, *J. Chem. Phys.*, **19**, 41 (1951); **18**, 767 (1950).
- (2) R. F. Graham and B. J. Tyler, *J. Chem. Soc., Faraday Trans. 1*, **68**, 683 (1972).
- (3) For discussion of ref 1 and 2, see R. F. Hampson and D. H. Stedman, *J. Phys. Chem. Ref. Data*, **2**, 267 (1973).
- (4) P. L. Asquith and B. J. Tyler, *J. Chem. Soc. D*, 744 (1970).
- (5) D. H. F. Atkins and R. A. Cox, *U.K. At. Energy Res. Establish., Rep.*, **R7615** (1973).
- (6) H. Harrison, H. S. Johnston, and E. R. Hardwick, *J. Am. Chem. Soc.*, **84**, 2478 (1962), and references therein.
- (7) K. Glänzer and J. Troe, *Ber. Bunsenges. Phys. Chem.*, **78**, 71 (1974).
- (8) A. A. Westenberg and N. DeHaas, *J. Chem. Phys.*, **57**, 5375 (1972).
- (9) J. G. Anderson and F. Kaufman, *Chem. Phys. Lett.*, **16**, 375 (1972).
- (10) C. Morley and I. W. M. Smith, *J. Chem. Soc., Faraday Trans. 2*, **68**, 1016 (1972).
- (11) F. Stuhl and H. Niki, *J. Chem. Phys.*, **57**, 3677 (1972).
- (12) J. G. Anderson, J. J. Margitan, and F. Kaufman, *J. Chem. Phys.*, **60**, 3310 (1974).
- (13) C. J. Howard and K. M. Evenson, *J. Chem. Phys.*, **61**, 1943 (1974).
- (14) R. Atkinson, D. A. Hansen, and J. N. Pitts, Jr., *J. Chem. Phys.*, **62**, 3284 (1975).
- (15) W. Tsang, "Chemical Kinetics Data Survey, VI", R. F. Hampson, Ed., NBSIR-207 (Institute for Materials Research, National Bureau of Standards, Washington, D.C., 1973).
- (16) G. W. King and D. Moule, *Can. J. Chem.*, **40**, 2057 (1962).
- (17) H. S. Johnston and R. Graham, *Can. J. Chem.*, **52**, 1415 (1974).
- (18) G. Brauer, Ed., "Handbook of Preparative Inorganic Chemistry", Academic Press, New York, N.Y., 1963, p 486.
- (19) E. E. Hughes, *J. Chem. Phys.*, **35**, 1531 (1961).
- (20) See, for example: E. F. Greenz and J. P. Toennies, "Chemical Reactions in Shock Waves", Academic Press, New York, N.Y., 1964.
- (21) JANNAF Thermochemical Tables, 2nd ed, D. R. Stull and H. Prophet, Ed., *Natl. Stand. Ref. Data Ser., Natl. Bur. Stand.*, **No. 37** (1971).
- (22) R. L. Belford and R. A. Strehlow, *Annu. Rev. Phys. Chem.*, **20**, 247 (1969).
- (23) R. E. Huffman and N. Davidson, *J. Am. Chem. Soc.*, **81**, 2311 (1959).
- (24) E. Zimet, *J. Chem. Phys.*, **53**, 515 (1970).
- (25) P. G. Ashmore and B. J. Tyler, *J. Chem. Soc.*, 1017 (1961).
- (26) D. M. Waldorf and A. L. Babb, *J. Chem. Phys.*, **39**, 432 (1963).
- (27) The equilibrium constant data of Ashmore and Tyler ($K_3 = 1.56 \text{ atm}^{-1}$ at 293 K) were used in preference to that of Waldorf and Babb, whose equilibrium constants are roughly a factor of 2 higher, and are not as consistent with the increases in NO_2 absorption during reaction observed in the experiments reported here. Equilibrium constants for reaction 3 can also be calculated from data in the JANNAF Tables, assuming *cis*- and *trans*-nitrous acid to be in equilibrium with each other. This gives $K_3 = 0.8$ at 293 K, which is a factor of 2 lower than that of Ashmore and Tyler. The effect of using the data of Waldorf and Babb would have been to increase $[\text{HNO}_2]$ and decrease k by about 20%.
- (28) Over the temperature range of these experiments (1100-1500 K), JANNAF data indicated that the equilibrium constant K_1 can be represented with sufficient accuracy by $K_1 = 209.0 \exp(-47750/RT) \text{ mol/cm}^3$, assuming *cis*- and *trans*- HNO_2 to be in equilibrium.
- (29) I. C. Hisatsune, *J. Phys. Chem.*, **72**, 269 (1968).
- (30) A. P. Cox, A. H. Brittain, and D. J. Finnigan, *Trans. Faraday Soc.*, **67**, 2179 (1971).
- (31) W. Tsang, *J. Phys. Chem. Ref. Data*, **2**, 276 (1973).
- (32) K. L. Demerjian, J. A. Kerr, and J. G. Calvert, *Adv. Environ. Sci. Technol.*, **4**, 172 (1974).
- (33) V. N. Kondratiev, "Rate Constants of Gas Phase Reactions, Reference Book", English translation: R. M. Fristrom, Ed., COM-72-10014, Office of Standard Reference Data, NBS (NTIS, Springfield, Va., 1972).
- (34) Wm. E. Wilson, Jr., *J. Phys. Chem. Ref. Data*, **1**, 535 (1972).
- (35) R. A. Cox, *J. Photochem.*, **3**, 175 (1974).

Anion Radicals of Aromatic Ketones in Amine Solutions as Studied by Radiolysis

Mikio Hoshino,*

The National Institute for Environmental Studies, Yatabe-machi, Ibaraki 300-21, Japan

Shigeyoshi Arai, and Masashi Imamura

The Institute of Physical and Chemical Research, Wako-shi, Saitama 351, Japan (Received April 26, 1976)

Publication costs assisted by The Institute of Physical and Chemical Research

Amine solutions of benzophenone and acetophenone have been studied by using matrix isolation and pulse radiolysis techniques at various temperatures. In the case of benzophenone, the anion radical produced in *sec*-butylamine solution at 77 K has an absorption peak at 780 nm, whereas the peak locates at 680 nm at 153 K. The former peak is ascribed to a presolvated benzophenone anion radical and the latter to a solvated one. This solvated benzophenone anion radical was found to be in equilibrium with the ketyl radical in primary and secondary amine solutions. The enthalpy change (ΔH) was obtained for these systems to be ca. 6 kcal/mol. In a triethylamine solution at 183 K, the benzophenone anion radical has an absorption peak at 760 nm. The equilibrium between the anion and ketyl radicals was not observed in this solution. The acetophenone anion radical in the *sec*-butylamine solution showed the spectral shift due to solvation. An equilibrium between the anion and ketyl radicals was also studied.

Introduction

The benzophenone anion radical has been studied extensively in photochemistry and radiation chemistry since Porter and Wilkinson's observation in alkaline alcohol solution by flash photolysis.¹

In previous papers, we have reported the time-dependent spectral shift of the benzophenone anion radical in alcohol solution observed by pulse radiolysis,² and the spectral shift of the anion radical in alcohol solution by raising the temperature from 4 to ca. 80 K.³ These facts have been interpreted based on the solvent reorientation around the anion radical. The other aromatic ketones showed similar behavior in alcohol solutions.

Recently, flash and laser photolysis studies of benzophenone in amine solutions have been carried out at room temperature.^{4,5} Transients were the benzophenone anion radical and/or ketyl radical. However, the dynamic behavior of these transients is still unknown in amine solutions.

In the present work, we have performed pulse radiolysis and γ radiolysis studies on the solvation and successive reactions of benzophenone and acetophenone anion radicals in primary, secondary, and tertiary amine solutions. The solvated benzophenone anion radical was found to be in equilibrium with the ketyl radical in primary and secondary amine solutions. The ketyl radical produced probably forms hydrogen bonding with an imino anion in primary and secondary amine solutions.

Detailed reaction mechanisms are discussed on the basis of solvation and its related equilibrium of the anion radical with the ketyl radical.

Experimental Section

Benzophenone from Wako Pure Chemical Industries was recrystallized from an ethanol solution. Acetophenone was used without further purification. *sec*-Butylamine, *n*-propylamine, isopropylamine, diisopropylamine, and triethylamine, guaranteed reagents from Wako Pure Chemical Industries, were refluxed on sodium metal and fractionally distilled. These amines were stored on a metallic alloy of so-

dium and potassium in vacuo. All the samples were prepared in vacuo to avoid moisture and oxygen.

The irradiation cell for matrix study had an optical path length of 2 mm. γ -Ray irradiation and measurements of absorption spectra were carried out at 77 K on a Cary 14 R spectrometer. Samples were warmed after irradiation in a simple way where they were drawn out for a definite time from liquid nitrogen in a dewar vessel.

The cells and apparatus for pulse radiolysis were essentially the same as described in earlier papers.^{6,7} The energy and duration of pulses were 2.7 MeV and 1.0 μ s, respectively. Samples were cooled by blowing cold nitrogen gas which was supplied from a liquid nitrogen container equipped with an electric heater at the bottom.

Results

Benzophenone Anion Radical. Figure 1 shows the absorption spectra obtained by γ irradiation of a *sec*-butylamine solution containing 10 mol % benzophenone at 77 K. The spectrum for the solution without warming has a peak at 780 nm and a small peak at 560 nm. The main peak gradually shifted to shorter wavelengths upon warming of the solution, and its final location was at 680 nm. When the solution was further warmed, the 680-nm band decreased without shift and then disappeared completely. There was no band appearing concurrently with the decay of the 680-nm band. During the shift from 780 to 680 nm the intensity of the band was found to increase by a factor of almost 2. Such a phenomenon was not observed when ethanol was used as a matrix.³

Figure 2 shows the spectra obtained by pulse radiolysis of a liquid *sec*-butylamine solution of 3 mol % benzophenone at various temperatures. The spectrum at room temperature had an intense band at 560 nm, which agrees with the well-known band of a benzophenone ketyl radical. As the temperature was decreased, the intensity of the 560-nm band decreased and the other band which is due to the benzophenone anion radical appeared at 680 nm. When the solution was irradiated at 193 K, only the 680-nm band was observable.

A clear isosbestic point is seen at about 580 nm in Figure 2, indicating an equilibrium between the ketyl and anion radi-

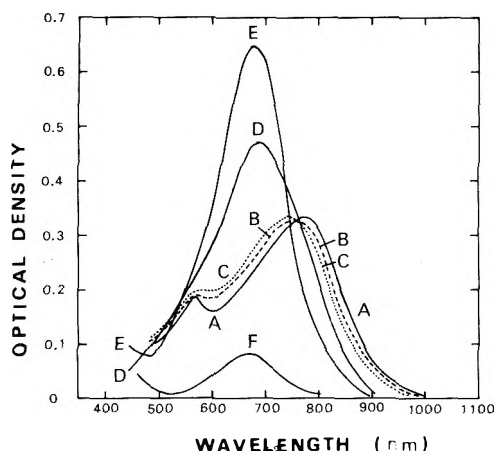


Figure 1. Absorption spectra for a γ -irradiated *sec*-butylamine solution containing 10 mol % benzophenone at 77 K: (A) before warming; (B) warmed for 65 s; (C) for 95 s; (D) for 135 s; (E) for 185 s; (F) for 285 s. Irradiation and optical measurement carried out at 77 K.

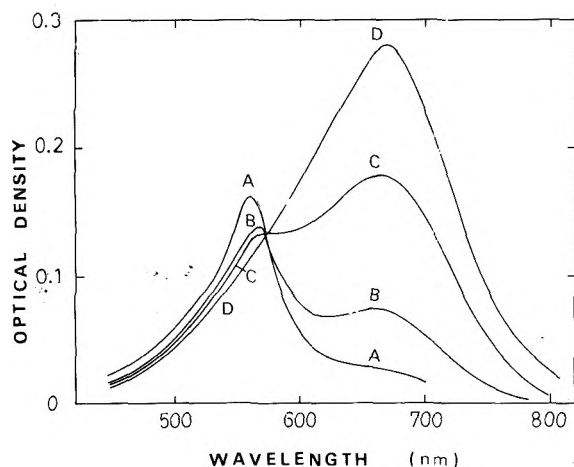


Figure 2. Absorption spectra for a pulse-irradiated *sec*-butylamine solution of 3 mol % benzophenone. Every spectrum obtained at 25 μ s after the pulse: (A) 291 K; (B) 258 K; (C) 222 K; (D) 193 K.

calcs. From a comparison of the peak intensities for the solution at 291 and 193 K, the value of $\xi_{680}G_{291 K}/\xi_{560}G_{193 K}$ is obtained to be 1.7, where ξ and G express the molar extinction coefficient and G value of the transients, respectively.

Figure 3 represents the spectra determined at various times after the pulse for the solution at 230 K. Each spectrum shows the same shape, irrespective of the time. This fact means that the ratio of the absorbing species at 560 and 680 nm is constant throughout their decays. In all primary and secondary amine solutions and at all temperatures studied, the decay behavior of the 560- and 680-nm bands was very similar to each other and fits the second-order rate law. On the basis that the molar extinction coefficient of a benzophenone ketyl radical is $3.7 \times 10^3 \text{ M}^{-1} \text{ cm}^{-1}$, the rate constant for the decay of the radical is evaluated as $1.5 \times 10^7 \text{ M}^{-1} \text{ s}^{-1}$ in the *sec*-butylamine solution at room temperature.⁸

n-Propylamine, isopropylamine, and diisopropylamine solutions gave essentially the same results as that observed for the *sec*-butylamine solution. In a triethylamine solution, however, the spectrum obtained immediately after the pulse had an intense band at 560 nm and a weak band at 760 nm even at 183 K, as shown in Figure 4. Furthermore, the 760-nm band disappeared almost completely within 100 μ s after the

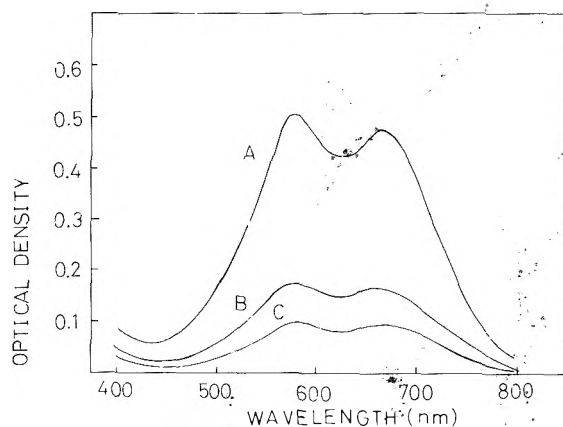


Figure 3. Absorption spectra for a pulse-irradiated *sec*-butylamine solution of 3 mol % benzophenone at 230 K. A, B, and C determined at 0.5, 10.5, and 20.5 ms after the pulse, respectively.

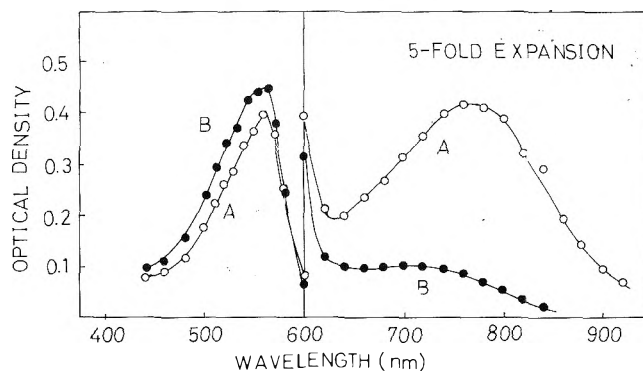


Figure 4. Absorption spectra for a pulse-irradiated triethylamine solution of 4 mol % benzophenone at 183 K. A and B determined at 2 and 47 μ s after the pulse, respectively. The ordinate is fivefold expanded in the region above 600 nm.

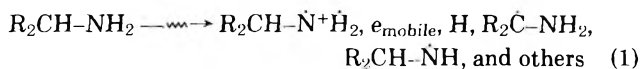
pulse, although the lifetime of the 560-nm band was as long as 0.3 s. The decay of the 760-nm band was accompanied by the formation of an appreciable portion of the 560-nm band. Hence, no equilibrium exists between both absorbing species in this solution.

Acetophenone Anion Radical. Figure 5 shows the transient absorption spectra obtained by the pulse radiolysis of the *sec*-butylamine solution containing 3 mol % acetophenone at 173 K. The spectrum observed immediately after the pulse decayed over the wavelengths studied. The spectral shape did not change during the decay of the band. This species is ascribed to the acetophenone anion radical.

γ radiolysis of the *sec*-butylamine solution containing 3 mol % acetophenone was carried out at 77 K. As shown in Figure 6, the absorption band obtained before warming was at longer wavelengths than that obtained after warming the solution. The shape of the latter band was quite similar to that observed for the pulse radiolysis at 173 K.

Discussion

Absorption Spectra of the Benzophenone Anion Radical in Amine Solutions. A possible reaction mechanism may be represented for amine solutions from the analogy of alcohols as:



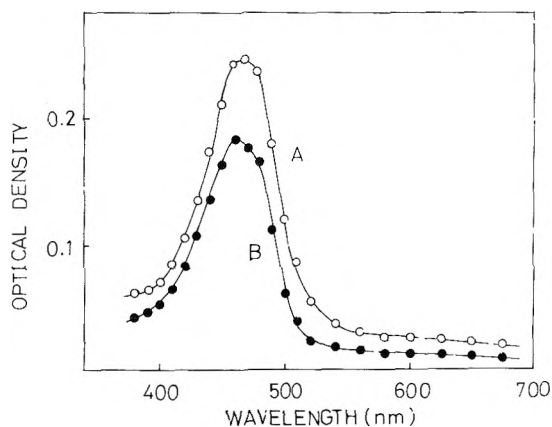


Figure 5. Absorption spectra for a pulse-irradiated *sec*-butylamine solution of 3 mol % acetophenone at 173 K: A and B determined at 5 and 130 μ s after the pulse, respectively.

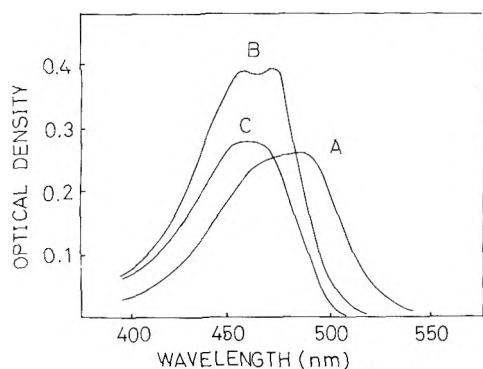
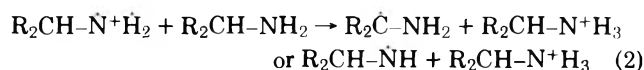
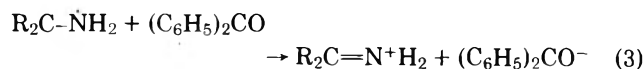


Figure 6. Absorption spectra for a γ -irradiated *sec*-butylamine solution containing 3 mol % acetophenone at 77 K: (A) before warming; (B) warmed for 60 s; (C) for 140 s.



The amine cation radical may produce a relatively stable protonated cation and a neutral amine radical in which an odd electron localizes on a carbon or nitrogen atom as shown in reaction 2.

When benzophenone molecules are present, they capture mobile electrons to form benzophenone anion radicals. The anion radical may additionally be produced by the following reaction of benzophenone and the neutral amine radical:



In Table I are listed the peak wavelengths of the benzophenone anion radical produced in several kinds of amine solutions. Our previous studies have shown that the absorption peak of a presolvated benzophenone anion radical locates at 780 nm and that of a solvated one at 640 nm in an ethanol solution.^{2,3} In the present study, it is reasonable to assign the 780- and 680-nm bands observed in *sec*-butylamine to the presolvated and solvated anion radicals, respectively.

The pulse radiolysis results of a triethylamine solution are evidently different from those of primary and secondary amine solutions. The spectrum had the peaks at 760 and 560 nm. The latter band is obviously due to the ketyl radical, while the former can be assigned to the anion radical.

TABLE I: Absorption Peak Wavelengths of the Benzophenone Anion Radical in Amine Solutions (in nm)

	<i>s</i> -BA ^a	<i>n</i> -PA ^b	<i>i</i> PA ^c	(<i>i</i> -P) ₂ A ^d	TEA ^e
77 K	780				
193 K	680	680	660	680	760

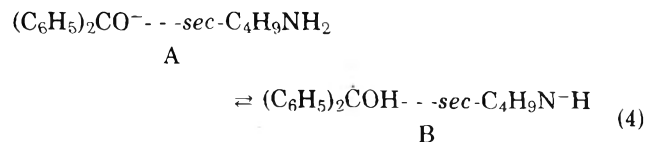
^a *sec*-Butylamine. ^b *n*-Propylamine. ^c Isopropylamine. ^d Diisopropylamine. ^e Triethylamine.

A large shift of the absorption band due to solvation was observed for alcohol and primary and secondary amine solutions. This fact suggests that the H in OH, NH₂, and NH groups approaches an oxygen atom of the benzophenone anion radical in the solvated state. It is likely that the anion radical is a hydrogen bonded complex with a solvent molecule in these solvents.

A significant increase in band intensity on going from 780 to 680 nm does not result from the difference in extinction coefficients between solvated and presolvated anion radicals, because such an increase was not seen in an ethanol solution. Reactive species trapped in the *sec*-butylamine solution probably produces additional benzophenone anion radicals at temperatures higher than 77 K according to reaction 3.

Absorption Spectra of the Acetophenone Anion Radical in sec-Butylamine Solution. The absorption band of the anion radical produced in the *sec*-butylamine solution shows a spectral shift to shorter wavelengths by warming the solution. An increase in the band intensity of the anion radical was also observed similarly to the case of the benzophenone anion radical. Because the absorption band of the acetophenone ketyl radical locates at shorter wavelengths, we were unable to observe it in the wavelength region studied. The transient absorption spectrum observed for the pulse radiolysis of acetophenone in *sec*-butylamine solution at 173 K is in good agreement with the spectrum obtained after warming the solution at 77 K. Therefore, the 460-nm band of the acetophenone anion radical is due to the solvated species.

Equilibrium between the Anion Radical and the Ketyl Radical. The existence of the isobestic point and the similar decay behavior observed for the *sec*-butylamine solution of benzophenone leads to a conclusion that the anion radical is in equilibrium with the ketyl radical. Since the equilibrium is not established in a triethylamine solution, the reaction is considered to be proton transfer from a solvent molecule to an anion radical



where A and B are the solvated benzophenone anion radical and the ketyl radical hydrogen bonded with the *sec*-butylimino anion. If the ketyl radical and *sec*-butylimino anion formed by reaction 4 are free in the solution, the ratio of [A] to [(C₆H₅)₂COH] depends on the concentration of *sec*-C₄H₉N⁻H, as expressed in the equation, [A]/[(C₆H₅)₂COH] = [*sec*-C₄H₉N⁻H]/K, where K is the equilibrium constant of reaction 4. This relation is contrary to the experimental finding that the ratio is constant throughout their decays.

From K = [B]/[A] and [A] + [B] = [C₀], one obtains

$$\begin{aligned} K &= ([C_0] - [A])/[A] = (\xi_a I [C_0] \\ &\quad - \xi_a I [A])/ \xi_a I [A] = (D_0 - D_a)/D_a \quad (5) \end{aligned}$$

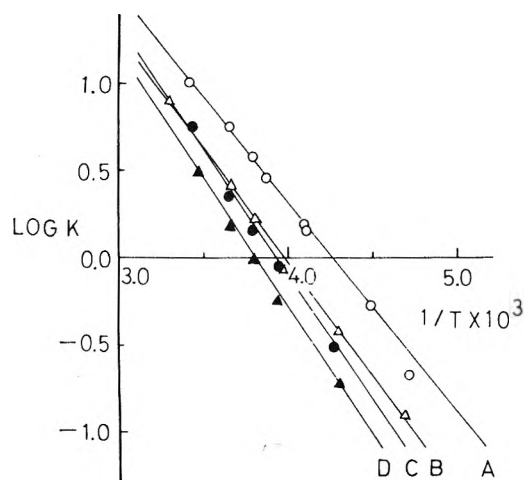


Figure 7. Logarithmic plots of K values against $1/T$ obtained with the systems of benzophenone-amines: (A) *sec*-butylamine; (B) diisopropylamine; (C) isopropylamine; (D) *n*-propylamine.

where ξ_a , l , and D_a are a molar extinction coefficient of the anion radical, an optical path length, and an optical density at 680 nm, respectively. D_0 is equal to $\xi_a l [C_0]$ and corresponds to the optical density at 680 nm for the solution at 193 K, where the equilibrium shifts far to the left. Equation 5 is valid only when $[C_0]$ is constant, irrespective of temperature studied. This condition may be satisfied in the present experiment, since all the spectra have an isobestic point over the entire temperature range studied. In Figure 7 are shown the logarithmic plots of K values against $1/T$ in four amine solutions. The good straight lines gave the values of enthalpy change (ΔH) of 5.5 kcal/mol for *sec*-butylamine, 6.6 kcal/mol for *n*-propylamine, 6.3 kcal/mol for isopropylamine, and 5.9 kcal/mol for diisopropylamine solutions (Table II).

In the pulse radiolysis of the *sec*-butylamine solution of acetophenone, it is difficult to examine the equilibrium between the anion radical and the ketyl radical, since the ketyl radical has the absorption band below 400 nm. A C-T absorption due to acetophenone and amine prevented observation at short wavelengths. However, by assuming this equilibrium, the apparent K values were obtained at various temperatures by using eq 5 as in the case of benzophenone. Logarithmic plots of the K values against $1/T$ give a convex curvature as shown in Figure 8, indicating complex features of this equilibrium. The apparent ΔH values were estimated to be 4.1 kcal/mol from the slope of the plots in the lower temperature region and 2.0 kcal/mol from that in the higher temperature region.

A number of studies have been published on the photochemical reduction of benzophenone in amine solutions and/or solutions containing amines.^{4,5,9,10} The well accepted mechanism involves the formation of a charge transfer triplet state followed by its direct dissociation into a ketyl radical and a neutral amine radical

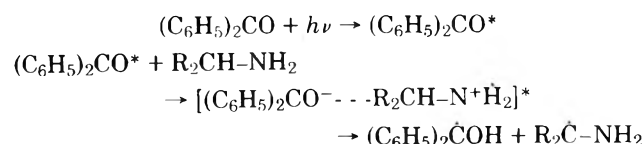


TABLE II: ΔH for the Equilibrium between the Benzophenone Anion and the Ketyl Radical^a

	<i>s</i> -BA	<i>n</i> -PA	<i>i</i> -PA	(<i>i</i> -P) ₂ A
ΔH , kcal/mol	5.5	6.6	6.3	5.9

^a Abbreviations are the same as in Table I.

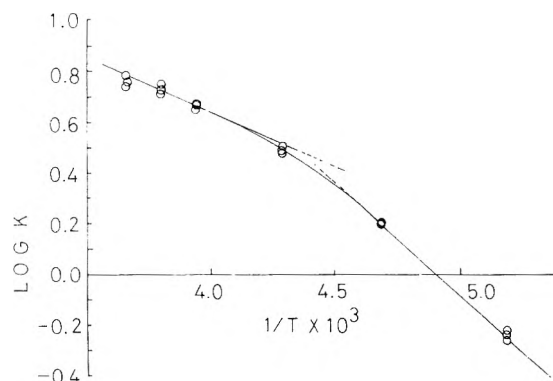
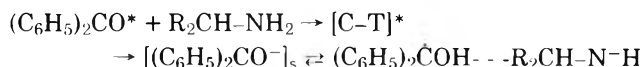


Figure 8. Logarithmic plots of apparent K values against $1/T$ obtained with a system of acetophenone-*sec*-butylamine.

However, the other pathway for the formation of the ketyl radical is more conceivable from the results obtained here. A benzophenone anion radical produced from a charge transfer triplet state may abstract a proton from a neighboring amine molecule according to reaction 4 and form the ketyl radical.

When the *sec*-butylamine solution of 3 mol % benzophenone was irradiated by uv light at 173 K, the benzophenone anion radical was observed together with an unspecified yellow species that is more stable than the anion radical.¹¹ The benzophenone ketyl radical was not detected at this temperature. These results should support the reaction mechanism that the benzophenone anion radical is initially produced in the *sec*-butylamine solution upon uv irradiation. The reaction mechanism is



Acknowledgment. The authors express their thanks to Dr. Akira Kira for his kind assistance in the matrix isolation experiment and for stimulating discussions throughout this study.

References and Notes

- (1) G. Porter and F. Wilkinson, *Trans. Faraday Soc.*, **57**, 1686 (1961).
- (2) M. Hoshino, S. Arai, and M. Imamura, *J. Phys. Chem.*, **78**, 1473 (1974).
- (3) M. Hoshino, S. Arai, M. Imamura, and A. Namiki, *Chem. Phys. Lett.*, **26**, 582 (1974).
- (4) R. S. Davidson, P. F. Lanteth, and M. Santanam, *J. Chem. Soc., Perkin Trans. 2*, 2351 (1972).
- (5) S. Arimitsu and H. Masuhara, *Chem. Phys. Lett.*, **22**, 543 (1973).
- (6) A. Kira, S. Arai, and M. Imamura, *Rep. Inst. Phys. Chem. Res. (Jpn.)*, **47**, 139 (1971).
- (7) S. Arai, M. Hoshino, and M. Imamura, *J. Phys. Chem.*, **79**, 702 (1975).
- (8) B. W. Hodgson, J. P. Keene, E. J. Land, and A. J. Swallow, *J. Chem. Phys.*, **63**, 3761 (1975).
- (9) S. G. Cohen and R. J. Baumgarten, *J. Am. Chem. Soc.*, **87**, 2996 (1965).
- (10) A. H. Parola, A. W. Rose, and S. G. Cohen, *J. Am. Chem. Soc.*, **97**, 6202 (1975).
- (11) M. Hoshino and S. Arai, unpublished results.

Photoreduction of Silver Ion in Aqueous and Alcoholic Solutions

Hiroshi Hada,* Yoshiro Yonezawa, Akio Yoshida, and Atsuhiko Kurakake

Department of Industrial Chemistry, Faculty of Engineering, Kyoto University, Yoshida, Kyoto, Japan (Received November 19, 1975; Revised Manuscript Received August 30, 1976)

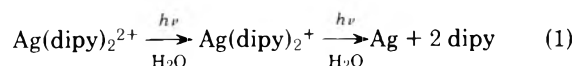
Publication costs assisted by Kyoto University

Aqueous and alcoholic solutions of silver perchlorate have been photolyzed by 253.7-nm light. The primary reaction of the photolysis is assumed to be electron transfer from solvent molecule to silver ion: $(\text{Ag}^+, \text{ROH})_{\text{cage}} + h\nu \rightarrow (\text{Ag}, \text{ROH}^+)_{\text{cage}}$. Variations of the mean quantum yield of silver atom formation with the concentrations of silver ion, hydrogen ion, and alcohols added are systematically interpreted by the concept that reactive species are surrounded by the solvent cage. It is proposed that the number of solvent molecules composing a cage would be about 10. The quantum yield increases with reaction temperature. Apparent activation energies of the quantum yields are about 2–6 kcal/mol.

Introduction

The reactions of metal ions in aqueous solution have received attention for many years in photochemistry and radiation chemistry.^{1–4} In particular, the photolysis and radiolysis of aqueous solutions of Fe(II, III)^{5–10} and Ce(III, IV)^{11–13} have been the subject of much research. In these systems, existence of reverse reactions by the actinic light used for forward photochemical reaction brings about some complications.

On the other hand, there are very few reports on the photochemistry of silver compounds in solution. The only silver complex which has been quantitatively investigated seems to be $\text{Ag}(\text{dipy})_2^{2+}$. Balzani and Carassiti found that in aqueous solutions this complex undergoes a photoredox decomposition through a two-step process:¹⁴



Quantum yields ranging from 10^{-1} (253.7 nm) to 10^{-3} (436 nm) were obtained for the disappearance of $\text{Ag}(\text{dipy})_2^{2+}$. A photoreaction mechanism involving the oxidation of a pseudo-coordinated water molecule was proposed.

It has also been shown that γ radiolysis of silver salt solutions at 77 K yields silver atoms which were attributed to the electron-capture reaction^{15–17}



The dose–yield curve for Ag was obtained by using the ESR technique and a reaction mechanism in the frozen system was discussed.¹⁷ Pukies, Roebke, and Henglein investigated several fast processes of the reduction of silver ion in aqueous solution by the pulse-radiolysis technique and confirmed that the formation of nuclei of colloid silver requires some milliseconds at room temperature.¹⁸

We have found that irradiation of aqueous and alcoholic solutions of silver perchlorate with 253.7-nm light produces colloid silver. The colloid silver can be quantitatively collected and the amount of silver is easily measured by the differential potentiometric titration method.^{19,20} Complications due to the reverse photochemical reaction would be negligible in this case. Silver perchlorate is suitable for the study of the photochemistry of the silver ion in solution because it is easily soluble in both water and alcohols and does not show any

absorption at wavelengths longer than 210 nm due to the perchlorate anion.

Photooxidation of alcohols by several metal ions at 77 K has been studied by the ESR technique.²¹ However, little has been known about the photochemistry of the silver ion in alcohols. Also, it seems that the photochemistry of metal ions in concentrated solutions up to 10 M has not been developed at present. We have thus undertaken the study of the photoreduction of silver ion in aqueous and alcoholic solutions with particular regard to the effects of silver and hydrogen ion concentrations as well as reaction temperature. It is proposed that the primary reaction of the photoreduction will be electron transfer from the solvent molecule to the silver ion. Photochemical reaction in the liquid phase proceeds under the influence of the solvent cage.²² It is suggested that variations of the mean quantum yield of silver atom formation with the concentrations of silver ion, hydrogen ion, and alcohol added are systematically interpreted by the introduction of the concept of solvent cage.

Experimental Section

Apparatus and Procedure. A 15-W sterilization lamp, Type GT-1511N (Toshiba Co. Ltd.), was used as the light source. A filter solution of cobalt sulfate was adequate to cut off wavelengths shorter than 253.7 nm. The incident intensities on the reaction vessel were measured by the use of the ferrioxalate actinometer with the quantum yields determined by Hatchard and Parker.²³ The reaction cell was a rectangular quartz vessel of $1 \times 1 \times 4$ cm. The temperature of reaction vessel could be kept constant by a thermostat.

After irradiation, the reaction mixture was left in the dark at 20 °C for 24 h to obtain stable colloid silver. It was then collected by means of a sintered glass filter and washed completely with a large excess of distilled water. The remainder was dissolved by nitric acid and then neutralized by aqueous ammonia. After addition of acetic acid, it was diluted to 100 ml and submitted to differential potentiometric titration. The silver ion concentration was determined by measuring the maximum electromotive force of the concentration cell constructed during a stepwise titration with 10^{-4} or 10^{-5} M potassium iodide solution.

Absorption spectra of silver perchlorate solutions were recorded on a MPS-5000 spectrophotometer (Shimadzu Seisakusho Co. Ltd.). Hydrogen ion concentration was measured

on a Type M-4 pH meter (Horiba Seisakusho Co. Ltd.).

Calculation of Quantum Yield. When x_t and x_0 are the amounts of 10^{-4} M potassium iodide solution equivalent to the sample solution being subjected to the photochemical and thermal reactions, respectively, the number of silver atoms in question, ΔP , is

$$\Delta P = 6.02 \times 10^{16}(x_t - x_0) \quad (3)$$

ΔP ranged from 10^{17} to 10^{18} atoms under the present experimental conditions. The mean quantum yield of silver atom formation, Φ , is expressed as

$$\Phi = \frac{\Delta P}{q_0(1 - T)t} \quad (4)$$

where q_0 and T denote the number of incident photons and transmittance of the solution at 253.7 nm, respectively, and t is irradiation time in hours. q_0 was chosen to be 5.54×10^{18} or 1.18×10^{19} photons/h in this work. We have determined the quantum yield under a wide range of silver and hydrogen ion concentrations in silver perchlorate solution at several reaction temperatures.

Materials. Silver perchlorate purchased from Nakarai Chemical Co. Ltd. was recrystallized. Water and alcohols were carefully distilled in pyrex vessel before use.

Results

Absorption Spectra. Absorption spectra of silver perchlorate in water and several alcohols are given in Figure 1. Broad absorption extending from less than 210 to 260 nm has been found to be characteristic of the presence of silver ion in these solvents.²⁴⁻²⁶ Molar extinction coefficients in alcohols are about twice as large as that in water. The absorption at 253.7 nm will not be contaminated by that of the solvent molecules, because it lies in the absorption tail of these solutions. It is noticed that 94% of the incident light (253.7 nm) is absorbed by the 1 M aqueous solution in the reaction vessel having a pathlength of 1 cm. Absorption spectra did not show any characteristic change over the silver perchlorate concentrations from 10^{-5} to 1 M for both aqueous and alcoholic solutions.

Dependence of the Silver Atom Formed on the Irradiation Time. The amount of the elemental silver formed in the 1 M aqueous solution was followed with the time of irradiation at 25 °C. During irradiation times of less than 1 h, the amount of elemental silver formed increases linearly. After prolonged irradiation, the apparent quantum yield gradually decreases, probably due to side reactions or the filter effect of reaction products. We have therefore determined the mean quantum yield after 1-h irradiation throughout this work.

Quantum Yield of Aqueous Solution. Quantum yields of silver formation were determined over a wide range of silver perchlorate concentrations at 25 °C and are given in Figure 2. A nearly constant value of 0.008 was observed at concentrations lower than 1 M, but at higher concentrations the quantum yield rapidly increases to 0.032 at 11.5 M.

Irradiation of both 1 and 9 M solutions were carried out at 25-80 °C. It is found that the mean quantum yield obeys the Arrhenius-type relation. Apparent activation energies derived from the Arrhenius plot are given in Table I.

Variation of the quantum yield with addition of perchloric acid is shown in Figure 3. The quantum yield decreases with an increase of perchloric acid and is reduced to nearly one-half at 4 M and to one-tenth at 7 M.

We photolyzed the 1 M solution with 253.7-nm light of $q_0 = 1.44 \times 10^{21}$ photons/h for 10 h. The increase of hydrogen ion

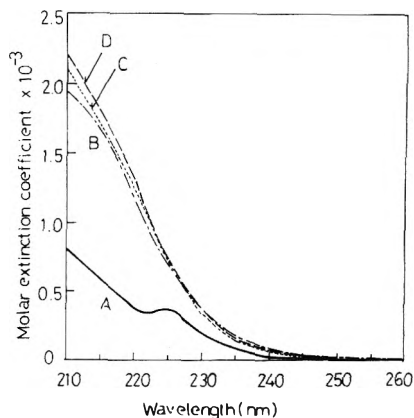


Figure 1. Absorption spectra of silver perchlorate in (A) water, (B) ethanol, (C) 2-propanol, (D) 2-methyl-2-propanol. The molar extinction coefficient is calculated from the optical density and silver perchlorate concentration.

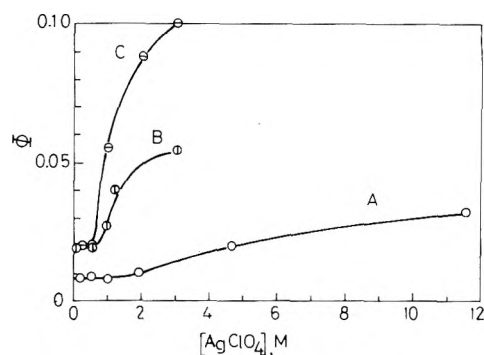


Figure 2. Dependence of the mean quantum yield Φ on the silver perchlorate concentration at 25 °C: (A) water, (B) ethanol, (C) 2-propanol.

TABLE I: Apparent Activation Energies of the Mean Quantum Yield

Solvent	[AgClO ₄], M	E _{act} , kcal/mol
Water	1	2.28 ± 0.09
	9	2.50 ± 0.04
Ethanol	1	5.64 ± 0.28
	3	3.37 ± 0.17
2-Propanol	1	4.70 ± 0.07
	3	3.38 ± 0.26

concentration during the irradiation was 1.57×10^{-4} mol and the amount of elemental silver formed was 1.48×10^{-4} mol at 25 °C. This means that nearly equimolar amounts of silver atom and hydrogen ion are produced in the photochemical reaction.

It is found that addition of 1 M sodium perchlorate to 1 M silver perchlorate solution has no effect on the quantum yield. The present reaction is relatively insensitive to the concentration of perchlorate anion.

Quantum Yield of Alcoholic Solutions. Ethanol and 2-propanol solutions of silver perchlorate are also photosensitive to 253.7-nm light but 2-methyl-2-propanol solution is not. Quantum yields were determined over a wide range of silver perchlorate concentrations at 25 °C and are given in Figure 2. As is the case for aqueous solutions, the quantum yields are nearly constant at low concentration and then rapidly in-

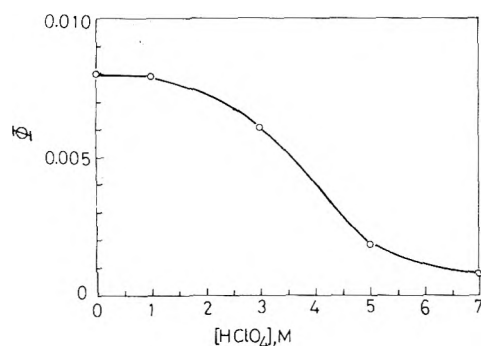


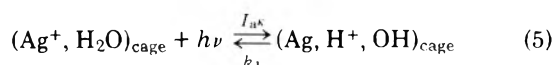
Figure 3. Dependence of Φ on the perchloric acid concentration at 25 °C. $[\text{AgClO}_4]$ is 1 M.

crease. The effect of reaction temperature over 20–60 °C on both 1 and 3 M solutions was also examined. The results are given in Table I.

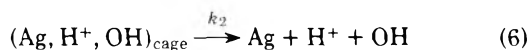
Photolyses of 1 M silver perchlorate in mixtures of water and some alcohols were also carried out. Variation of the quantum yield with the concentration of alcohol is described in Figure 4. It increases with the addition of 2-propanol, whereas it decreases with 2-methyl-2-propanol. In the former, quantum yield is almost constant at first and then rapidly increases at about 1 M of 2-propanol.

Discussion

The photolysis of silver perchlorate in aqueous solution will proceed by electron transfer from the water molecule to silver ion, followed by the immediate decomposition of H_2O^+ into H^+ and OH



where the subscript cage means that reactants are surrounded by the cage composed of solvent molecules. I_a is the number of photons absorbed in the reaction system per unit volume and unit time and κ is the fraction of the electron transfer reaction from the photoexcited state of the species $(\text{Ag}^+, \text{H}_2\text{O})_{\text{cage}}$. k_1 denotes the rate constant of the backward reaction. The solvent cage gradually decomposes and the silver atoms will finally convert to colloid silver out of the cage



where k_2 denotes the rate constant of cage decomposition reaction.

The OH radical will experience several complex processes and be converted to O_2 at last. We carried out the pyrogallol test to confirm the formation of O_2 gas.^{27–30} The reaction cell and analysis cell made of rectangular quartz of $1 \times 1 \times 4$ cm were connected with a high vacuum line. Two cells were filled with 1 M silver perchlorate solution and the pyrogallol reagent prepared by the method of Hoffmann,²⁹ respectively. The volume of the vacuum system was reduced to about 50 cm³ in order to obtain high sensitivity for the detection of O_2 gas. Irradiation by 253.7-nm light of $q_0 = 1.60 \times 10^{20}$ photons/h for 2 h caused a distinct coloring of the pyrogallol reagent. Uv absorption spectra of this reagent showed an increase of longer wavelength absorption at more than 550 nm which was not evident before irradiation. This reaction scheme also agrees with the observation that elemental silver and hydrogen ions are produced in nearly equal amount during the photolysis of 1 M silver perchlorate solution.

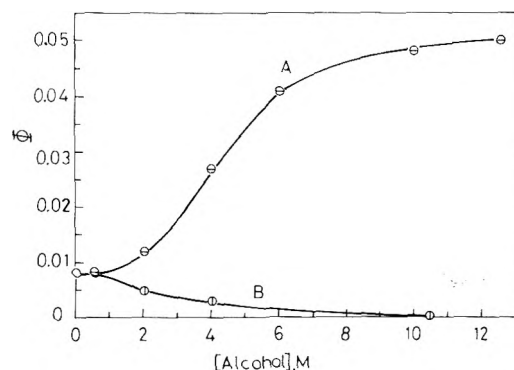


Figure 4. Dependence of Φ on the concentrations of added (A) 2-propanol and (B) 2-methyl-2-propanol at 25 °C. $[\text{AgClO}_4]$ is 1 M.

We attempt to interpret the dependence of the quantum yield on the various reaction conditions with the concept of solvent cage. Assuming the stationary concentration of $(\text{Ag}, \text{H}^+, \text{OH})_{\text{cage}}$, quantum yield is expressed as

$$\Phi = \frac{1}{I_a} \frac{d[\text{Ag}]}{dt} \quad (7a)$$

$$= \frac{1}{I_a} k_2 [(\text{Ag}, \text{H}^+, \text{OH})_{\text{cage}}] \quad (7b)$$

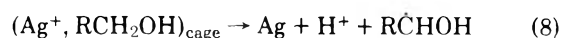
$$= \frac{\kappa k_2}{k_1 + k_2} \quad (7c)$$

In this approximation, quantum yield is determined by the product of κ and the ratio of the rate of cage decomposition reaction to net reactions.

Figure 2 shows that the quantum yield is nearly constant below 5 mol % and then rapidly increases with increasing silver ion concentrations. The point of inflection of the curve corresponds to about 10 mol % of silver perchlorate. At the lower concentrations, the solvent cage will be formed and decompose individually without being affected by each other. So, it is assumed that the values of 5 and 10 mol % may be used as a measure of the size of a solvent cage. From a simple calculation, the number of water molecules composing a cage would be about 10. This solvent cage will contain both one silver ion and one water molecule or their decomposition products.

According to Figure 3, quantum yield is nearly constant at first and then decreases with increasing perchloric acid concentration more than 1 M. It has been confirmed that dissolution of colloid silver by the added acid does not occur in this case. We suppose that addition of perchloric acid accelerates the back reaction in eq 5, reducing the quantum yield. The dependence of the quantum yield on perchloric acid concentration seems to be related at least in part to the formation of a solvent cage around the reactive species.

The similarity of the dependence of the quantum yield on the silver perchlorate concentration between aqueous and alcoholic solutions (Figure 2) prompts us to assume that silver atom is formed by the same mechanism in both cases. An analogous reaction scheme as eq 5 and 6 brings about the formation of silver atom, hydrogen ion, and radical species



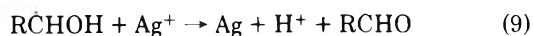
This radical will finally transform to aldehyde.

We carried out the phenylhydrazine test^{31,32} to confirm the formation of acetaldehyde from ethanol and acetone from 2-propanol, respectively. An alcoholic solution of 2,4-dinitrophenylhydrazine containing phosphoric acid was added

to the 1 M silver perchlorate solution previously irradiated by 253.7-nm light of $q_0 = 4.0 \times 10^{19}$ photons/h for 1 h. Uv absorption spectra of them gave a characteristic peak at 354 nm (acetaldehyde 2,4-dinitrophenylhydrazone) from ethanol and 364 nm (acetone 2,4-dinitrophenylhydrazone) from 2-propanol which were not distinct in unirradiated solutions, respectively. Addition of ethanolic sodium hydroxide induced the large bathochromic shift of the above peak to 430 nm for both dinitrophenylhydrazones.³²

As is the case of aqueous solutions, Figure 2 also suggests that the number of alcohol molecules composing a cage would be about 10.

It is found that the quantum yield increases in the order: 2-methyl-2-propanol \ll water $<$ ethanol $<$ 2-propanol. This order seems to be related at least in part to the ease of abstraction of α hydrogen from these molecules. The forward reaction of eq 5 and 6 is accelerated if the radical species resulting from electron transfer reacts with the solvent. Since the presence of α hydrogen appears to be a requirement for radical trapping by the alcohol, photolysis does not proceed in 2-methyl-2-propanol solution. We should also attend that the RCHOH radical in eq 8 is capable of reducing an additional silver ion



This reaction may play a significant role in increasing the quantum yield in the alcoholic solution especially at low silver perchlorate concentration.

The quantum yield begins to increase when the ratio of 2-propanol to water reaches to about 5 mol % in Figure 4. Recently, Carey and Langford investigated the scavenging effect of several alcohols in the photoreduction of ferric perchlorate in water.³³ The differences of our result against theirs are that the quantum yield increases not linearly with increasing 2-propanol concentration of more than 0.5 M and then attains a constant value which corresponds to the quantum yield of pure 2-propanol solution and that 2-methyl-2-propanol of more than 0.5 M one-sidedly suppresses the reaction. Though we did not examine the scavenging effect of alcohols of less than 0.5 M, we suppose that the effect shown in Figure 4 will be due mainly to the inclusion of alcohol molecules into the solvent cage initially composed of water molecules only.

It is observed that the quantum yield increases with reaction temperature. Apparent activation energies summarized in Table I are about 2–6 kcal/mol. It seems plausible at sight that the apparent activation energy is ascribed to the cage decomposition reaction of eq 6 in the dilute solution. However, it is shown that the magnitude of apparent activation energies for both dilute and concentrated solutions is almost the same so that, these activation energies may not be responsible for the cage decomposition process only. It is noticed that they are as large as that of the diffusor process in solution.³⁴ The observed activation energy would be due to several complex processes not clarified at present.

Figure 2 shows that the quantum yield in the concentrated solution is two to five times larger than that in the dilute one. Heidt et al. and Hayon and Weiss observed that the quantum yields of photooxidation of cerous perchlorate¹¹ and ferrous sulfate⁶ increase with increasing reactant concentration. The maximum concentration used in our work is quite larger than

theirs. In such a case, physical properties of the solution will considerably change, so that, application of the simple picture of solvent cage may be impossible. Though uv spectra of aqueous and alcoholic solutions over 10^{-5} to 1 M do not show any characteristic change due to the formation of new species, it may be possible that some photosensitive cluster³⁵ plays significant role in promoting the photochemical reaction in the concentrated solution. As the study of high-concentration photochemistry has not yet been developed, the lack of information renders such a discussion rather speculative. We think at present that the photoreduction of the silver ion in the concentrated solution would proceed through a reaction scheme considerably different from eq 5 and 6.

References and Notes

- (1) A. W. Adamson, W. L. Waltz, E. Zinato, D. W. Watts, P. D. Fleischauer, and R. D. Lindholm, *Chem. Rev.*, **68**, 541 (1968).
- (2) V. Balzani and V. Carassiti, "Photochemistry of Coordination Compounds", Academic Press, New York, N.Y., 1970.
- (3) G. Stein, Ed., "Radiation Chemistry of Aqueous Systems", Wiley, New York, N.Y., 1968.
- (4) A. Henglein, W. Schnabel, and J. Wendenburg, "Einführung in die Strahlenchemie mit praktischen Anleitungen", Verlag Chemie, Weinheim/Bergstr., West Germany, 1969.
- (5) T. Rigg and J. Weiss, *J. Chem. Phys.*, **20**, 1194 (1952).
- (6) E. Hayon and J. Weiss, *J. Chem. Soc.*, 3866 (1960).
- (7) L. J. Heidt, M. G. Mullin, W. B. Martin, Jr., and A. M. J. Beatty, *J. Phys. Chem.*, **66**, 336 (1962).
- (8) M. G. Adamson, D. L. Baulch, and F. S. Dainton, *Trans. Faraday Soc.*, **58**, 1388 (1962).
- (9) G. V. Buxton, S. P. Wilford, and R. J. Williams, *J. Chem. Soc.*, 4957 (1962).
- (10) P. L. Airey and F. S. Dainton, *Proc. R. Soc. London, Ser. A*, **291**, 340, 478 (1966).
- (11) (a) L. J. Heidt and M. E. Smith, *J. Am. Chem. Soc.*, **70**, 2476 (1948); (b) L. J. Heidt and A. F. McMillan, *ibid.*, **76**, 2135 (1954); (c) L. J. Heidt and J. Berestecki, *ibid.*, **77**, 2049 (1955).
- (12) F. Hussain and R. G. W. Norrish, *Proc. R. Soc. London, Ser. A*, **275**, 161 (1963).
- (13) (a) R. W. Matthews, H. A. Mahlman, and T. J. Sworski, *J. Phys. Chem.*, **74**, 2475 (1970); (b) R. W. Matthews and T. J. Sworski, *ibid.*, **79**, 681 (1975).
- (14) (a) V. Balzani, A. Bertoluzza, and V. Carassiti, *Bull. Soc. Chim. Belg.*, **71**, 821 (1962); (b) V. Carassiti, G. Condorelli, and L. L. Costanzo, *Ann. Chim. (Rome)*, **54**, 303 (1964).
- (15) (a) L. Schields, *J. Chem. Phys.*, **44**, 1685 (1966); *Trans. Faraday Soc.*, **62**, 1042 (1966); (b) L. Schields and M. C. R. Symons, *Mol. Phys.*, **11**, 57 (1966).
- (16) R. A. Zhitnikov and A. L. Orzeli, *Sov. Phys. Solid State*, **7**, 1559 (1966).
- (17) B. L. Bales and L. Kevan, *Chem. Phys. Lett.*, **3**, 484 (1969); *J. Phys. Chem.*, **74**, 1098 (1970).
- (18) V. J. Pukies, W. Roebke, and A. Henglein, *Ber. Bunsenges. Phys. Chem.*, **72**, 842 (1968).
- (19) F. Lühr, *Z. Wiss. Photogr.*, **27**, 283 (1929).
- (20) Y. Konishi, H. Hada, and M. Tamura, *J. Chem. Soc. Jpn.*, **92**, 829 (1971).
- (21) (a) D. Greatorex and T. J. Kemp, *Trans. Faraday Soc.*, **67**, 56, 1576 (1971); *J. Chem. Soc., Faraday Trans. 1*, **68**, 121 (1972); (b) D. Greatorex, R. J. Hill, T. J. Kemp, and T. J. Stone, *ibid.*, **68**, 2059 (1972); (c) A. Cox and T. J. Kemp, *ibid.*, **71**, 2490 (1975).
- (22) T. Franck and E. Rabinowitch, *Trans. Faraday Soc.*, **30**, 120 (1934).
- (23) (a) C. A. Parker, *Proc. R. Soc. London, Ser. A*, **220**, 104 (1953); (b) C. G. Hatchard and C. A. Parker, *ibid.*, **235**, 518 (1956).
- (24) H. Fromherz and W. Menscricck, *Z. Phys. Chem.*, **B3**, 1 (1929).
- (25) E. Rabinowitch, *Rev. Mod. Phys.*, **14**, 112 (1942).
- (26) H. Hosoya and S. Nagakura, *Bull. Chem. Soc. Jpn.*, **37**, 249 (1964).
- (27) R. P. Anderson, *J. Ind. Eng. Chem.*, **7**, 587 (1915).
- (28) J. W. Shipley, *J. Am. Chem. Soc.*, **38**, 1687 (1916).
- (29) F. Hoffmann, *Z. Angew. Chem.*, **35**, 325 (1922).
- (30) P. M. E. Hauser, *Bull. Soc. Chim. Fr.*, **33**, 1141 (1923).
- (31) E. A. Braude and E. R. H. Jones, *J. Chem. Soc.*, 498 (1945).
- (32) L. A. Jones, J. C. Holmes, and R. B. Seligman, *Anal. Chem.*, **28**, 191 (1956).
- (33) J. H. Carey and C. H. Langford, *Inorg. Nucl. Chem. Lett.*, **10**, 591 (1974).
- (34) S. Glasstone, K. J. Laidler, and H. Eyring, "The Theory of Rate Processes", McGraw-Hill, New York, N.Y., 1941, p 525.
- (35) T. H. Lilley, *Water, Compr. Treat.*, **3**, 266 (1973).

Thermodynamic Properties of Liquids, Including Solutions. 13. Molecular and Intermolecular Properties from Excess Enthalpies¹

Maurice L. Huggins

135 Northridge Lane, Woodside, California 94062 (Received August 9, 1976)

The author's theoretical equation for the excess enthalpy of binary mixtures of simple molecules contains three intermolecular parameters: (1) an energy parameter, measuring the energy change when contacts between like molecules are replaced by contacts between unlike molecules; (2) an equilibrium constant, measuring the relative probabilities of contacts of the three types; and (3) the ratio of the contacting molecular surface areas of the two species. These parameters have been calculated for 44 systems at 25 °C from published experimental data. Approximate contacting molecular surface areas have been calculated for 22 substances.

1. Introduction

Several years ago² I presented a new solution theory, in which the concentration dependence of the molal excess enthalpy (H^E) is related to three parameters: (1) an energy parameter (ϵ_{Δ}) measuring the change of energy when contacts ($\alpha\alpha$, $\beta\beta$) between like units are replaced by contacts ($\alpha\beta$) between unlike units; (2) an equilibrium constant (K) measuring the relative probabilities of contacts of the three types, as functions of concentration; (3) the ratio ($r_{\sigma} = \sigma_{\beta}^0/\sigma_{\alpha}^0$) of the contacting molecular surface areas of the two types of unit.

For binary solutions of simple rigid molecules, I tentatively assumed, with experimental justification, that each of the three parameters is (at a given temperature) constant, independent of the concentration. I deduced equations, based on this assumption, relating the magnitudes of the parameters to the shape and scale of the curve for the dependence of H^E on the mole fractions of the components. With these equations the parameters are easily calculated from three points on an accurate H^E curve.

Using the very precise H^E data now available for a number of binary mixtures of simple rigid molecules, I have recently shown³ that the three parameters are accurately constant over the whole composition range, within the probable error of the data.

In this paper I report values of the parameters, deduced on the assumption of parameter constancy, for 44 binary mixtures.

2. Calculation and Tabulation of the Parameters

The three theoretical parameters are related to the concentration dependence of H^E by the equations⁴

$$H^E = \epsilon_{\Delta} x_1 z_2 g_K \quad (1)$$

$$z_2 = 1 - z_1 = \frac{r_{\sigma} x_2}{x_1 + r_{\sigma} x_2} \quad (2)$$

$$g_K = 2[(1 + K' z_1 z_2)^{1/2} - 1]/K' z_1 z_2 \quad (3)$$

$$K' = 4 \left(\frac{1}{K} - 1 \right) \quad (4)$$

In reporting experimental measurements of H^E , it is customary for the experimenters to give the parameters of a smoothing equation, usually with the standard deviation of the experimental points from that equation. The smoothing equation is usually in the Redlich-Kister form:

$$H^E = x_1 x_2 [a_0 + a_1(x_1 - x_2) + a_2(x_1 - x_2)^2 + \dots] \quad (5)$$

My customary procedure is to calculate H^E from the smoothing equation for mole fractions (x_2) of 0.3, 0.5, and 0.7; and then, using eq 1-4, to compute ϵ_{Δ} , K , and r_{σ} . The values obtained are listed in Table I, with (in most cases) the standard deviations of the experimental data points from the theoretical curves and from the empirical smoothing curves of the experimenters. The number of parameters (p) in the experimenters' smoothing equation is also listed. As already noted, $p = 3$ for my theoretical equation. The ratio $\sigma_{\beta}^0/\sigma_{\alpha}^0$ in column 5 will be explained in the next section. The energy parameters and standard deviations are in J mol^{-1} .

3. Discussion

Ideally, the theoretical equations apply only to mixtures of molecules that are chemically uniform as regards their interactions with other molecules. Nevertheless, I have included in the table many solutions containing components for which this is not strictly the case, with the idea that the departures of the actual H^E curves from those for similar ideal systems are probably less than the departures of the experimenters' smoothing curves from the true curves. Empirically, at least, the calculated parameters for these systems should be useful.

ϵ_{Δ} determines the scale of the H^E vs. x_2 curve. K determines its fatness (the increase in spread as H^E decreases from its maximum value). r_{σ} determines its skewness. See Figure 1 of ref 3.

The standard deviations from the empirical smoothing curves are rough measures of the probable inaccuracy of the theoretical parameters deduced from these curves. Direct comparisons of the standard deviations from the theoretical curves with those from the empirical curves are significant only if the number of parameters in the equation for the empirical curve is the same or less than 3, the number in the theoretical equation. Comparisons in such cases show that the theoretical equation represents the data as well as the empirical smoothing equation, in most cases, even though the former was calculated to give agreement at only three concentrations, whereas the parameters of the empirical equation were calculated to give the best overall agreement.

If the molecules of a component of a solution are not rigid, but flexible as in the normal alkanes, my theoretical equation for the excess enthalpy should be applicable, provided in-

TABLE I: Intermolecular Parameters

Components $\alpha + \beta$	Parameters				Standard dev			Ref
	ϵ_{Δ}	K	r_{σ}	$\sigma_{\beta}^0/\sigma_{\alpha}^0$	Theor	Emp	p	
Benzene + CCl ₄	479	0.743	1.09	1.07	0.08	0.06	4	5
	473	0.744	1.10	1.07	0.34	0.33	3	6
	476	0.744	1.07	1.07		0.18	3	7
	484	0.724	1.05	1.07		0.11	4	8
	432	1.155	1.09	1.07		0.5	3	9
Benzene + cycloheptane	2724	1.038	1.23	1.23	4.7	4.5	3	10
Benzene + cyclohexane	3144	0.865	1.117	1.13	0.43	0.19	4	5
	3136	0.867	1.119	1.13		0.3	4	11
	3130	0.866	1.126	1.13	0.26	0.16	4	12
	3142	0.876	1.115	1.13	1.18	1.11	4	6
	3130	0.866	1.120	1.13			3	7
	3153	0.782	1.119	1.13	2.9	3.0	3	8
	3037	1.13	1.06	1.13	7.0	6.9	4	10
Benzene + cyclooctane	2723	1.12	1.33	1.3	6.3	4.7	4	10
Benzene + cyclopentane	2367	1.05	1.11	1.19	4.5	4.8	4	10
Benzene + 1,3-dioxane	-543	1.156	0.99	0.99	0.9	0.9	3	13
Benzene + furan	353	0.981	0.828	0.83	0.9	0.5	5	13
Benzene + <i>n</i> -heptane	3117	0.878	1.61		5.3	5.3	3	8
Benzene + <i>n</i> -hexane	3552	0.46	1.56				3	14
	3090	0.75	1.63				3	15
	3283	0.84	1.70	1.5	3.7	3.8	3	8
Benzene + isoctane	2178	1.032	2.624	2.7	4.7	0.7	3	16
Benzene + OMCTS ^a	249	1.082	1.160	1.16	0.26	0.28	3	17
	252	1.049	1.148	1.16	0.01	0.02	3	18
	811	0.867	1.326	1.29	1.14	1.12	4	19
Benzene + <i>m</i> -xylene	793	0.925	1.250	1.21	0.85	0.76	4	19
Benzene + <i>o</i> -xylene	587	0.845	1.396	1.45	0.62	0.59	4	19
Benzene + <i>p</i> -xylene	387	1.304	0.435		0.97	0.31	5	11
1-Butanol + methanol	708	0.933	1.095	1.06	0.13	0.14	3	20
CCl ₄ + cyclohexane	707	1.000	1.120	1.06			3	18
	660	1.64	1.22	1.06	1.0	1.4	3	21
	673	1	1	1.06	2.1	2.2	2	22
	343	0.942	1.121	1.11	0.13	0.14	3	21
	325	1.013	1.116	1.11	0.52	0.51	3	23
CCl ₄ + diethyl ether	-1675	1.94	1.02	1.02	13.8	6.1	3	24
CCl ₄ + <i>n</i> -hexane	1108	1.06	1.27		8.6	7.4	3	25
	1089	0.84	1.53		3.9	3.8	2	26
	1062	0.89	1.53		4.9	5.3	3	27
CCl ₄ + <i>n</i> -octane	953	2.21	1.89		9.7	9.0	2	25
CCl ₄ + OMCTS ^a	458	0.901	2.685	2.5	0.2	0.2	4	16
CCl ₄ + <i>n</i> -pentane	1061	1.04	1.20		8.5	7.4	2	25
Chloroform + diethyl ether	-8528	3.01	0.96	0.96	29	15	5	28
Cycloheptane + toluene	2478	0.934	0.935	0.94	4.1	4.5	4	10
Cyclohexane + cyclopentane	84	1.148	1.788	1.05	0.08	0.07	3	20
Cyclohexane + 2,3-dimethylbutane	574	1.110	1.126	1.12		0.05	4	29
Cyclohexane + 1,4-dioxane	6527	0.73	1.14	1.14	10	8	5	13
Cyclohexane + <i>n</i> -heptane	743	0.865	2.006				3	18
	786	0.730	1.936		1.6	1.5	3	8
	684	0.868	1.881		0.47	0.09	4	30
	687	0.839	1.894		0.58	0.21	4	6
	669	0.983	1.867			2.1	3	18
Cyclohexane + <i>n</i> -hexane	685	0.877	1.873		1.15	1.20	4	31
	633	1.43	1.67		2.7	2.7	2	32
	685	0.868	1.895		1.26	1.05	3	33
	612	1.224	1.285	1.3	0.79	0.82	3	8
	1201	0.900	2.459	2.39	1.5	1.3	4	22
	2265	1.083	1.179	1.03	3.2	3.1	4	10
	2013	0.842	1.469	1.14	2.0	2.2	3	8
Cyclooctane + toluene	2337	1.244	0.995	0.9	8.4	6.6	3	10
Cyclopentane + <i>cis</i> -decalin	-546	1.022	0.887	0.89	0.49	0.49	3	34
Cyclopentane + <i>trans</i> -decalin	-1121	1.034	0.919	0.92	1.01	1.01	3	34
Cyclopentane + OMCTS ^a	593	1.338	2.194	2.3	0.6	0.2	3	35
Cyclopentane + tetrachloroethylene	931	0.947	1.053	1.05	0.14	0.33	3	36
<i>n</i> -Heptane + toluene	1950	0.898	0.720		0.73	0.72	3	8
Isooctane + OMCTS ^a	2207	0.809	1.855	2.1	0.4	1.4	3	32
Toluene + <i>m</i> -xylene	161	1.036	1.110	1.11	0.09	0.09	3	17
Toluene + <i>o</i> -xylene	185	0.995	1.030	1.04	0.16	0.15	3	17
Toluene + <i>p</i> -xylene	67	1.015	1.283	1.25	0.11	0.10	3	17

^a OMCTS = octamethylcyclotetrasiloxane.

TABLE II: Relative Contacting Surface Areas

Component	σ^0	Component	σ^0
Benzene	(1.00)	1,3-Dioxane	0.99
CCl ₄	1.07	1,4-Dioxane	1.29
Chloroform	1.14	Ethylbenzene	1.81
Cycloheptane	1.23	Furan	0.83
Cyclohexane	1.13	Isooctane	1.5
Cyclooctane	1.3	OMCTS	2.7
Cyclopentane	1.19	Tetrachloroethylene	1.25
cis-Decalin	1.06	Toluene	1.16
trans-Decalin	1.09	m-Xylene	1.29
Diethyl ether	1.09	o-Xylene	1.21
2,3-Dimethylbutene	1.27	p-Xylene	1.45

tramolecular contacts between the segments are impossible or unlikely. I have therefore included in the table some systems with short chain normal alkane components (pentane, hexane, heptane). With much longer chains intramolecular contacts, varying in number as the concentration changes, would be expected. This should lead to calculated r_σ values that are not ratios of the true intermolecularly contacting molecular surface areas. This effect will be dealt with in future papers.

It should not be expected that the contacting surface area of a given component is precisely the same in its solutions with other components. If, however, the differences are small, one can calculate from the r_σ values approximate areas for each component, relative to that for a given component, e.g., benzene. From the r_σ values in Table I, I have computed the approximate σ^0 values (relative to that for benzene) listed in Table II.

Appropriate ratios of the areas in Table II are given in column 5 of Table I, for comparison with the r_σ values calculated from the curve shapes. From these comparisons it is evident that Table II can be used to predict approximate values of r_σ for many systems other than those included in Table I.

I cannot emphasize too strongly that the accuracy of the parameters in the tables depends on the accuracy of the experimental data from which they were calculated. I have included in Table I several comparisons of parameters for the same system, calculated from data published by different investigators. These comparisons show the approximate magnitudes of the differences in parameter values to be expected.

Included in the table are some solutions for which the standard deviations are quite large, hence the calculated parameters must be considered only rough approximations. Even rough approximations are sometimes useful, however.

I shall make no attempt now to interpret the meanings of the theoretical parameters in terms of intermolecular contact energies, molecular structures, etc.

4. Conclusion

I gratefully express my indebtedness to the experimenters whose data I have used. I hope that this paper contributes to a better understanding of the fundamental significance and importance of their work.

References and Notes

- (1) Presented at the 4th International Conference on Chemical Thermodynamics, Montpellier, France, Aug 27, 1975.
- (2) M. L. Huggins, *J. Phys. Chem.*, **74**, 371 (1970).
- (3) M. L. Huggins, *J. Phys. Chem.*, **80**, 1317 (1976).
- (4) M. L. Huggins, *Polymer*, **12**, 389 (1971).
- (5) R. H. Stokes, K. N. Marsh, and R. P. Tomlins, *J. Chem. Thermodyn.*, **1**, 211 (1969).
- (6) S. Murakami and G. C. Benson, *J. Chem. Thermodyn.*, **1**, 559 (1969).
- (7) C. G. Savini, D. R. Winterhalter, L. H. Kovach, and H. C. Van Ness, *J. Chem. Eng. Data*, **11**, 40 (1966).
- (8) G. W. Lundberg, *J. Chem. Eng. Data*, **9**, 193 (1964).
- (9) T. J. Findlay and P. J. Kavanagh, *J. Chem. Thermodyn.*, **6**, 361 (1974).
- (10) A. E. P. Watson, I. A. McLure, J. E. Bennett, and G. C. Benson, *J. Phys. Chem.*, **69**, 2751 (1965).
- (11) A. E. Pope, H. D. Pflug, B. Dacre, and G. C. Benson, *Can. J. Chem.*, **45**, 2665 (1967).
- (12) M. B. Ewing, K. N. Marsh, R. H. Stokes, and C. W. Tuxford, *J. Chem. Thermodyn.*, **2**, 751 (1970).
- (13) A. W. Andrews and K. W. Morcom, *J. Chem. Thermodyn.*, **3**, 519 (1971).
- (14) H. K. De Q. Jones and B. C.-Y. Lu, *J. Chem. Eng. Data*, **11**, 488 (1966).
- (15) V. S. Schnaible, H. C. Van Ness, and J. M. Smith, *AIChE J.*, **3**, 147 (1957).
- (16) K. N. Marsh and R. P. Tomlins, *Trans. Faraday Soc.*, **66**, 783 (1970).
- (17) S. Murakami, V. T. Lam, and G. C. Benson, *J. Chem. Thermodyn.*, **1**, 397 (1969).
- (18) J. M. Sturtevant and P. A. Lyons, *J. Chem. Thermodyn.*, **1**, 201 (1969).
- (19) J. Singh, H. D. Pflug, and G. C. Benson, *J. Phys. Chem.*, **72**, 1939 (1968).
- (20) M. B. Ewing and K. N. Marsh, *J. Chem. Thermodyn.*, **2**, 351 (1970).
- (21) J. R. Goates, R. J. Sullivan, and J. B. Ott, *J. Phys. Chem.*, **63**, 589 (1959).
- (22) B. S. Harsted and E. S. Thomsen, *J. Chem. Thermodyn.*, **6**, 549 (1974).
- (23) T. Boublik, V. T. Lam, S. Murakami, and G. C. Benson, *J. Phys. Chem.*, **73**, 2356 (1969).
- (24) D. F. Gray, I. D. Watson, and A. G. Williamson, *Austr. J. Chem.*, **21**, 379 (1968).
- (25) J. M. Berryman and E. L. Heric, *Can. J. Chem.*, **50**, 3799 (1968).
- (26) T. G. Bissell, G. E. Okator, and A. G. Williamson, *J. Chem. Thermodyn.*, **3**, 393 (1971).
- (27) W. M. Recko and K. Sadowska, *Bull. Acad. Pol. Sci.*, **20**, 73 (1972).
- (28) L. A. Beath and A. G. Williamson, *J. Chem. Thermodyn.*, **1**, 51 (1969).
- (29) M. B. Ewing and K. N. Marsh, *J. Chem. Thermodyn.*, **6**, 35 (1974).
- (30) K. N. Marsh and R. H. Stokes, *J. Chem. Thermodyn.*, **1**, 223 (1969).
- (31) M. L. McGlashan and H. F. Stoeckli, *J. Chem. Thermodyn.*, **1**, 589 (1969).
- (32) B. S. Harsted and E. S. Thomsen, *J. Chem. Thermodyn.*, **6**, 557 (1974).
- (33) H. Watts, E. C. W. Clarke, and D. N. Glew, *Can. J. Chem.*, **46**, 815 (1968).
- (34) D. E. G. Jones, I. A. Weeks, and G. C. Benson, *Can. J. Chem.*, **49**, 2481 (1971).
- (35) K. N. Marsh, *J. Chem. Thermodyn.*, **2**, 359 (1970).
- (36) J. Polák, S. Murakami, V. T. Lam, and G. C. Benson, *J. Chem. Eng. Data*, **15**, 323 (1970).

High Field Conductance of Some Acids, Bases, and Salts

Thomas J. Gilligan, III,^{1a,b} and Andrew Patterson, Jr.*

Sterling Chemistry Laboratory, Yale University, New Haven, Connecticut 06520 (Received June 28, 1976)

Publication costs assisted by Yale University

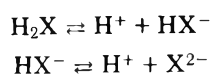
High field conductance quotients are reported for a wide variety of acids, bases, and salts of differing valence type. An extension of the Onsager theory for weak electrolytes is shown to account adequately for the conductance quotients of stepwise-dissociating compounds. A careful study of the cell constants of conductance cells used allows a claim of increased precision of the results. The applicability is considered of some recent corrections to the theory for the Wien effect.

Introduction

In what follows we describe some of the results of a high field conductance investigation of a number of acids, bases, and salts having different valence types. Bass and Moore² have advanced a model of nervous excitation based on the Wien dissociation effect. The ions H^+ , K^+ , and Na^+ are of principal importance in this model; it seemed desirable therefore to determine if stepwise dissociation of compounds such as sodium hydrogenoxalate or tartaric acid was amenable to theoretical interpretation using available theories of high field conductance behavior. The study was purposely made wide-ranging and exploratory, in part to include a spread of electrochemical characteristics (K_a 's, α 's, λ^0 's, etc.), and in part to see if examples could be found to test recent theoretical proposals involving lower-field ion-atmosphere shielding³ or higher-field dissociation kinetic⁴ effects. Among others, we shall be concerned with three different kinds of experimental results: (1) the dependence of the quotient $\Delta\Lambda/\Lambda(0)$, the high field conductance quotient (HFCQ), vs. field strength; (2) the concentration dependence of the HFCQ at two different field strengths, 110.0 and 237.5 kV/cm; and (3) at high fields, 150 kV/cm and above, the deviation from the expected linearity of the HFCQ plots of a number of compounds. Details of the measurements are to be found in Gilligan's dissertation;^{1a} selected results which exemplify typical behavior and the theoretical implications of these results are presented here. The only previous study of this type, by Schiele,⁵ did not report the temperatures and concentrations of the sample solutions, nor was a theoretical interpretation available.

Theoretical

For electrolytes which undergo stepwise dissociation, the only theory of high field conductance available is that of Onsager⁶ for the "Second Wien Effect" (Wien effect II), the practical use of which is described by Bailey and Patterson⁷ and Freitag and Patterson.⁸ The theory can be applied without ambiguity to single-step dissociations such as found with acetic acid, but must be modified for a dissociation that yields more than two ions. Taking as an example the dissociation of a dibasic acid



we begin with Onsager's theory⁶ for the Wien effect II where

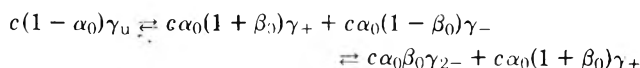
$$\begin{aligned} K(X) &= K(0)F(b) = K(0)(1 + b + b^2/3 + b^3/18 + \dots) \\ b &= z_i^2 z_j^2 (\lambda_i + \lambda_j) 9.6857 V / (z_j \lambda_i \\ &\quad + z_i \lambda_j) D T^2 \quad \text{in } H_2O \text{ at } 25^\circ C \end{aligned}$$

At zero field

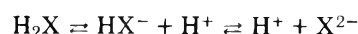
$$K(0) = c \alpha_0^2 \gamma_{\pm}^2 / (1 - \alpha_0) \gamma_u$$

where α is the degree of dissociation, γ_{\pm} , the mean activity coefficient for the ions, and γ_u , the activity of the undissociated electrolyte, assumed to be unity. At any nonzero field, γ_{\pm} is also assumed to be unity because the increasing field decreases the ion atmosphere, thus allowing γ_{\pm} to approach unity. If $K(0)$ and the field strength are known, the degree of dissociation at any field strength can be calculated.

The first step is to set up the equilibrium situation:



for



If each equilibrium is considered separately then

$$\begin{aligned} K_1(0)F(b) &= K_1(X) = (c \gamma_{\pm}^2 \alpha^2 / (1 - \alpha))(1 - \beta^2) \\ K_2(0)F(b) &= K_2(X) = (c \alpha \beta \gamma_{2-} (1 + \beta)) / (1 - \beta) \end{aligned}$$

where α is the degree of dissociation for step one and β is the degree of dissociation for step two. The single-ion activity coefficients for the anion, cation, and dianion are substituted for the mean activity coefficients using the method of Spiro⁹

$$\log \gamma_i = -0.5090 z_i^2 I^{1/2} / (1 + I^{1/2}) \quad \text{with } I = 1/2 \sum c_i z_i^2$$

(Spiro included the concentration of the associated electrolyte in the total ionic strength. We have made calculations both with and without its inclusion for chosen cases.) The concentration of the individual ions, c_i , can be determined from the equilibrium. For step two, since the electrolyte is unsymmetrical, $z_i \neq z_j$, it is necessary to use the single ion conductivities to give the values of b used to calculate $F(b)$.

The theoretical HFCQ curve is then calculated in the following manner: Initially β is set equal to zero and the activity coefficients are set equal to one. Using the equations outlined above, α is calculated at zero field. This value is used to find β . Then α is recalculated using the β determined in the preceding step and a new β is calculated using the new α . The new values for α and β determine the concentration of the indi-

vidual ions, and these concentrations are summed to give the total ionic strength. From this the single ion activity coefficients for the anion, cation, and dianion are calculated. Having these quantities, one returns to the calculation of α and β and calculates another new set of values for α and β . These in turn are used to determine new activity coefficients. If the two sets differ by less than a certain amount, the next step in the calculation of $\Delta\Lambda/\Lambda(0)$ is performed. If not, the process is repeated using the newest set of values.

Having obtained values for α and β , we can obtain the zero field Λ by summing the contributions of each ion. The contribution of each ion is obtained by multiplying the single ion conductivity (SIC) of each ion by the fraction of that electrolyte present as ions. Thus $\lambda_1 = \lambda_1^0(\alpha + \alpha\beta)$, $\lambda_2 = \lambda_2^0(\alpha - \alpha\beta)$, and $\lambda_3 = \lambda_3^0\alpha\beta$, and

$$\Lambda = \lambda_1 + \lambda_2 + \lambda_3$$

This then is used as $\Lambda(0)$. The use of λ^0 , the infinite dilution⁵ value, in the computation of the HFCQ is an approximation, but it is not a bad one since the HFCQ involves dividing and thus cancelling most of the error. One could rectify these approximations by using concentration-dependent conductance equations and first Wien effect theory.¹⁰ However, we judged this unnecessary since an unambiguous choice of experimental single-ion conductivities is not possible for most of the electrolytes we have studied.

The α and β at nonzero fields are calculated by setting the activity coefficients equal to one for the entire calculation. (See ref 3 and 8 and the discussion below.) The value of b is calculated at a specified field and from this $F(b)$ and then $K_1(X)$ are found. $K_1(X)$, with $\beta = 0$, determines α . Then using the necessary valence factor, a different b is calculated (at the same field as previously) for step two. This yields a different $F(b)$ and then $K_2(X)$. $K_2(X)$ is used to calculate β . This β replaces $\beta = 0$ in a new calculation of α . The new α then yields a new β . The two sets are compared as before and the calculation continues until successive sets are equal within specified limits. From the last set, the total Λ can be calculated as was done at zero field, and the theoretical HFCQ obtained.

Experimental Section

The apparatus and methods have been described elsewhere.^{7,8} In some measurements cells were used with 0.50-mm spacing, instead of 1.0 mm. Particular care was taken to determine and follow the cell constants of all cells by the method of Jones and Bradshaw.¹¹ It has been found that the cell constants of cells made with identical 16-mm diameter electrodes using construction techniques as reasonably identical as possible within hand-made glass working procedures^{7,8} may vary as much as $\pm 2.2\%$ from the average value; this probably results from variations in electrode spacing. In comparing the results of measurements obtained in different cells, we have normalized all conductance quotients to an average cell constant of 0.441 (for 1.0-mm cells), or equivalently normalized cell spacing or value of the electrical field. A detailed study of tartaric acid^{1a} justified this procedure. The precision is thus limited only by the reproducibility of the data, but the accuracy is limited to $\pm 2.2\%$ until a method is devised for measuring the electrode spacing in situ.

The other important element in the field strength, $X = V/d$, is the voltage. The voltage has been determined simultaneously with the conductance bridge null^{7,8} using a storage oscilloscope (Tektronix 549), a calibrated capacitive voltage divider (Jennings P-6014), and a calibrated Tektronix

preamplifier Type Z. The accuracy of the measurement is probably better than 0.1%, but since the square pulses being measured have a greater pulse-height variation than this, the maximum error in voltage is probably 1%.

The electrolytes studied were: the monobasic acids acetic, monochloroacetic, crotonic, and 2-furoic; the salts potassium citrate, sodium succinate, dipotassium tartrate, potassium hydrogen tartrate, sodium hydrogen oxalate, potassium dihydrogen phosphate; the dibasic acids fumaric, maleic, malic, malonic, oxalic, orthophthalic, tartaric, itaconic, methylsuccinic, succinic; the tribasic acids citric, phosphoric, and arsenic; the diamines ethylenediamine, 1,4-diaminobutane, 1,5-diaminopentane, 1,6-diaminohexane, and piperazine; and the amines *n*-amylamine, benzylamine, α -phenylethylamine, piperidine, and the slightly soluble base, silver oxide.

The measurements were all made relative to a reference electrolyte, either potassium chloride or hydrochloric acid solution, as was best suited to the polarization behavior of the solution under study.

Results and Discussion

The details of the study are given by ref 1a. The usual expected form of a HFCQ plot vs. field for a weak electrolyte is a curve from the origin followed by a linear increase the slope of which depends upon the value of K_a . Numerous deviations were found.

1-1 Acids. Acetic acid has been studied extensively before,^{5,7} since its particular degree of dissociation maximizes the observable Wien effect II. At 25.00 °C and a field of 150.0 kV/cm our measured HFCQ of 6.65×10^{-4} M acetic acid was 7.32%; the theoretical result is 8.45%. Bailey⁷ at a different concentration, 7.41×10^{-4} M, obtained a result of 7.52%; a decrease in the HFCQ of 0.05, to 7.47%, would be expected if Bailey's work were to have been done at the concentration we employed. Figure 1 of Bailey's paper⁷ is entirely characteristic of the present results. The remaining difference between the two sets of results must be the consequence of the much more precise measurement of applied exciting voltage in the present work. On the basis of measured conductances, Bailey's cell turns out to have had the same cell constant as the median cell constant of our 1.0-mm cells, to which all our data have been reduced. The results for the other monobasic acids at 150.0 kV/cm at 25 °C are: monochloroacetic, 0.83% at 1.05×10^{-4} M; 2-furoic, 1.58% at 1.18×10^{-4} M; monochlorobenzoic, 3.88% at 1.63×10^{-4} M; and crotonic acid, 6.85% at 5.78×10^{-4} M. In each case the theoretical result is about 15% higher than the experimental at 150 kV/cm. The present results confirm the finding of Bailey that the experimental effect, especially at higher fields, is lower than that predicted by theory, but extends it to all the weak acids studied. Bailey and Patterson⁷ attributed the disparity to concentration polarization, but the present study rules out this possibility, as it includes acids whose K_a 's range over 10^2 -fold. Since the HFCQ's exhibit the proper order of increase as the K_a 's of the acids decrease, and since the differences from theory are all of the same magnitude, there is no basis on which to suspect any error in the K_a 's employed. Also, the same differences have been observed in the dibasic acids studied (see below). Discussion of the possible source of this difference is postponed to the section of Corrections to Theory.

Acid Salts. To test the applicability to stepwise dissociation of the extended Onsager theory described above, sodium hydrogen tartrate, sodium hydrogen oxalate, and potassium dihydrogen phosphate and other salts were studied. Those just

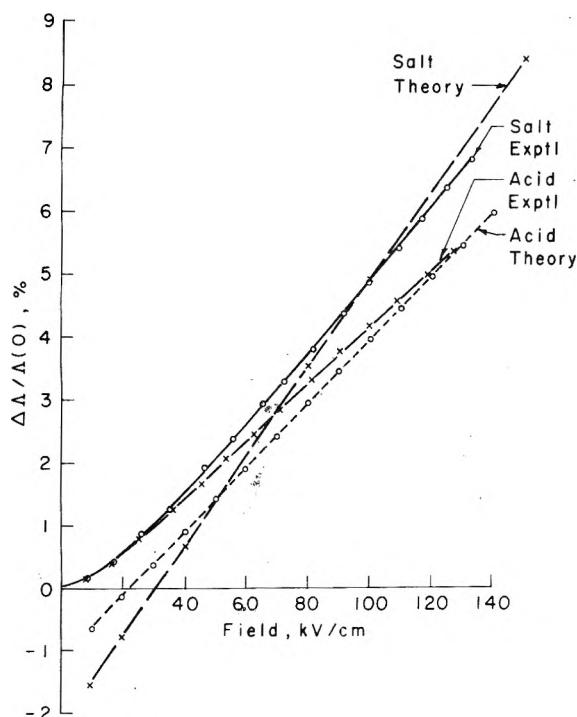


Figure 1. High field conductance quotient, percent, as function of field, kilovolts per centimeter, for a 1.372×10^{-4} M solution of sodium hydrogen tartrate, above, and for a 8.211×10^{-5} M solution of tartaric acid, below, at 25 °C. In each case the experimental results are connected by a solid curve, the theoretical calculations by a dotted curve. Theoretical constants were: SIC's $\lambda_1^0(\text{H}^+) = 349.8$, $\lambda_2^0(\text{HX}^-) = 27.0$, and $\lambda_3^0(\text{X}^{2-}) = 63.2$; dissociation constants, $K_1 = 9.17 \times 10^{-4}$, $K_2 = 4.30 \times 10^{-5}$.

named may be regarded (to an approximation in the case of KDP, since its K_3 is very small) as acid salts of dibasic acids; their use avoids a common ion (H^-) which would otherwise be present if a dibasic acid were studied, the first ionization step of which were substantially complete. Figure 1, for the tartrate, typifies the results. (The data for the parent acid are plotted to the same scale for comparison; see below.) The agreement between the experiment and theory is adequate, as it is also for the oxalate, Figure 2. In the case of the phosphate, Figure 3, the plot is quite similar; considering the small size of the effect and the tenfold difference in scale, the agreement is very good indeed. The curves all exhibit the characteristic loop of theory below the experimental at lower fields, a situation which becomes extreme when 3–3 electrolytes¹² are studied. It is due to the shielding by the ion atmosphere, not accounted for in the Onsager theory.⁶

The results indicate that the method chosen for calculating the theoretical Wien effect II is valid for those salts of weak, nonsymmetrical associating electrolytes which dissociate into several different ions. The use of single-ion activity coefficients to obtain the degree of dissociation at zero field, of SIC's to calculate b , $F(b)$, and $K(X)$, and of products of SIC's and the resulting degrees of dissociation to calculate the change of conductivity, all are shown to yield good agreement between theory and experiment in the case of these stepwise dissociations.

Dibasic Acids. Ten dibasic acids, listed above, and having K_1 's ranging from 5.3×10^{-2} to 6.2×10^{-5} , K_2 's ranging from 2.5×10^{-5} to 8.3×10^{-7} , and a diversity of SIC's were studied. Data for tartaric, oxalic, and phosphoric acids are given in Figures 1–3.

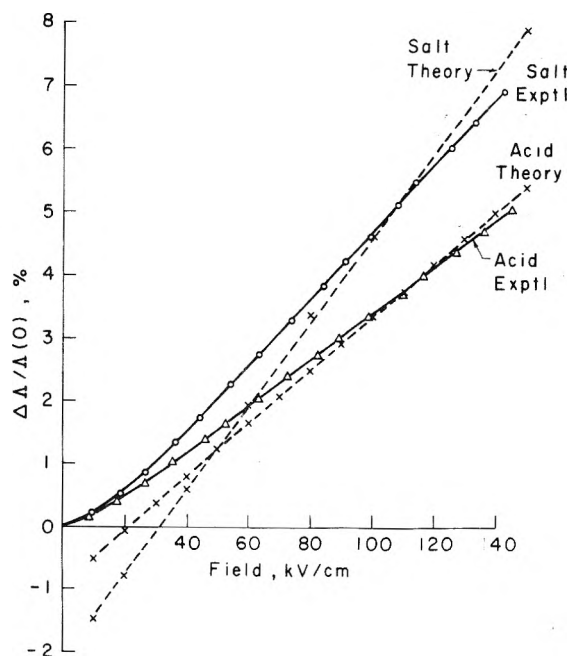


Figure 2. High field conductance quotient, percent, as function of field, kilovolts per centimeter, for a 1.444×10^{-4} M solution of sodium hydrogen oxalate, above, and for a 7.290×10^{-5} M solution of oxalic acid, below, at 25 °C. In each case the experimental results are joined by a solid curve and the theoretical calculations by a dotted curve. Theoretical constants were: SIC's, $\lambda_1^0 = 349.8$, $\lambda_2^0 = 40.2$, $\lambda_3^0 = 74.2$; dissociation constants, $K_1 = 5.36 \times 10^{-2}$, $K_2 = 5.41 \times 10^{-5}$.

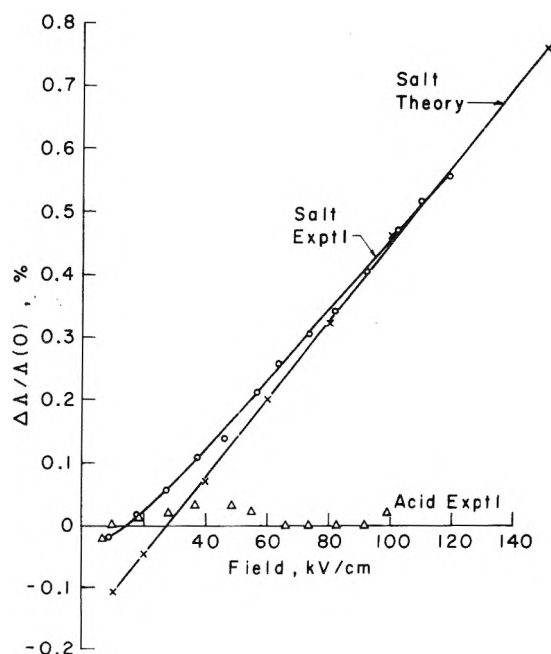


Figure 3. High field conductance quotient, percent, as function of field, kilovolts per centimeter, for a 3.469×10^{-4} M solution of potassium dihydrogen phosphate, above, and for a 7.49×10^{-5} M solution of phosphoric acid, below, at 25 °C. Note the HFCQ scale is expanded by a factor of 10 from those of Figure 1 and 2. The experimental results for the salt are shown as circles and the theoretical calculations as X's. The experimental results for the acid, which cluster around the zero HFCQ axis, are essentially zero within the precision of the measurement. The theoretical HFCQ for phosphoric acid, relative to hydrochloric acid, is zero when it is regarded as a strong acid. The theoretical constants were: SIC's (λ^0 's), $[\text{K}^+] = 73.52$, $[\text{H}^+] = 349.8$, $[\text{H}_2\text{PO}_4^-] = 51.2$, $[\text{HPO}_4^{2-}] = 81.0$; dissociation constant $K_2 = 6.31 \times 10^{-8}$.

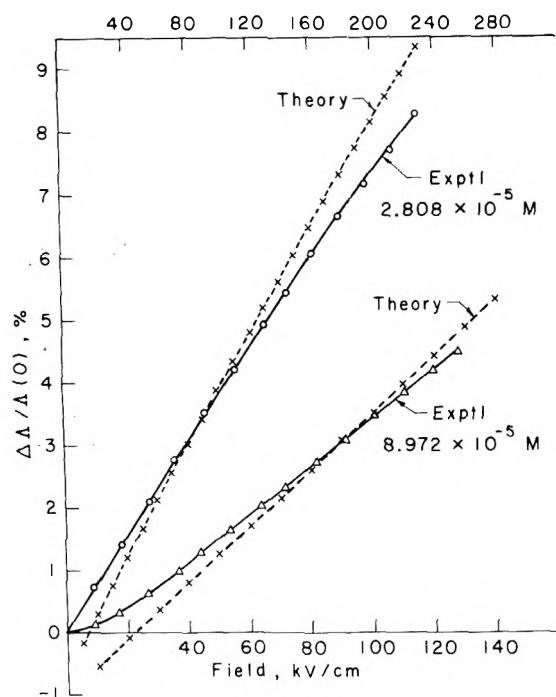


Figure 4. High field conductance quotient, percent, as a function of field, kilovolts per centimeter, for a 2.808×10^{-5} M solution of fumaric acid, above, and for a 8.972×10^{-5} M solution, below, at 25°C . The field scale at the top of the graph should be used for the upper curves. The experimental results are joined by a solid curve, the theoretical calculations by a dotted curve. The theoretical constants were: SIC's, $\lambda_1^0 = 349.8$, $\lambda_2^0 = 42.3$, $\lambda_3^0 = 61.8$; dissociation constants, $K_1 = 8.04 \times 10^{-4}$, $K_2 = 2.50 \times 10^{-5}$.

Fumaric and Malonic Acids. Figure 4 illustrates data for fumaric acid. Determinations were made in two different types of cells, having 1.0- and 0.50-mm spacings; the data accordingly extend to higher fields. Although it is not easy to discern on plots to this scale, the results at the higher fields (above 150 kV/cm) bend toward the abscissa. The theoretical calculations do likewise. These results may be compared with those for malonic acid under similar conditions, Figure 5. In this case the data and theoretical calculations tend upward, away from the abscissa, at higher fields. The size of the overall effect is smaller. The K_a 's are as follows: fumaric $K_1 = 8.04 \times 10^{-4}$, $K_2 = 2.50 \times 10^{-5}$; malonic $K_1 = 1.42 \times 10^{-4}$, $K_2 = 2.01 \times 10^{-6}$. Since with weak electrolytes heretofore studied a smaller K_a is expected to yield a larger HFCQ, these results might appear surprising. Further, at 110.0 kV/cm, the effect of varying the concentration of fumaric acid is to cause the HFCQ to decrease as concentration increases; at 237.5 kV/cm, the HFCQ increases with increasing concentration. In the case of malonic acid, at both fields the HFCQ increases as concentration increases. At a concentration of 6×10^{-5} M and at zero field, α_0 for fumaric acid is 0.9603, β_0 is 0.3377; for malonic acid $\alpha_0 = 0.9620$ while β_0 is a tenth as large, $\beta_0 = 0.0342$.

Tartaric acid, Figure 1, behaves in much the same way as fumaric acid because the two have similar degrees of dissociation, but the downward curvature of the HFCQ at higher fields is even more pronounced as a result of the higher value of β . For tartaric acid, $\alpha_0 = 0.9681$, $\beta_0 = 0.4414$ at 4×10^{-4} M.

Oxalic acid, Figure 2, at 7.28×10^{-5} M, has the first ionization step essentially complete, 99.89%; the situation is thus that of a one-step dissociation with excess hydrogen ion. This results in a lower HFCQ (for the acid) than for the acid salt.

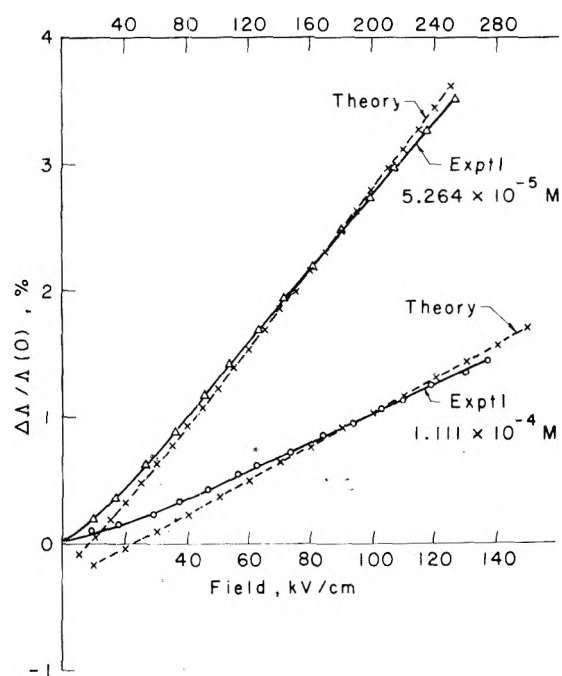


Figure 5. High field conductance quotient, percent, as a function of field, kilovolts per centimeter, for a 5.264×10^{-5} M solution of malonic acid, above, and for a 1.111×10^{-4} M solution, below, at 25°C . The field scale at the top of the graph should be used for the upper curves. The experimental results are joined by a solid curve, the theoretical calculations by a dotted curve. The theoretical constants were: SIC's, $\lambda_1^0 = 349.8$, $\lambda_2^0 = 39.1$, and $\lambda_3^0 = 64.0$; dissociation constants, $K_1 = 1.42 \times 10^{-4}$, $K_2 = 2.01 \times 10^{-6}$.

The HFCQ at 110 kV/cm increases as concentration increases, as it does with fumaric acid.

Phosphoric acid, Figure 3, exhibits a very small and essentially unchanging HFCQ when measured vs. hydrochloric acid as reference, which is to say it behaves as a strong 1-1 electrolyte. The results cluster around the $\Delta\Lambda/\Lambda(0)$ axis within the error limits of the experiment. The average value of the quotient is +0.010%, +0.034 and -0.023 deviation, maximum. This is to be expected, since the first step is essentially complete while the second is negligible. Arseric acid behaves in the same way.

The variations from strict linearity of the plots of HFCQ vs. field are the consequence of an interplay of factors, some of which are disturbed by the applied field. If the solute is a dibasic acid the first ionization step of which is nearly complete, and for which there is an appreciable degree of ionization by step two (e.g., fumaric acid is 97.3% ionized, first step, 40.9% ionized, second step, at 2.8×10^{-5} M) then at equilibrium and zero field, appreciable $[\text{H}^+]$ is provided by step two, and the ionization according to step one is less than it would have been in the absence of a second ionization step. At non-zero fields, more hydrogen ions are added by both steps 1 and 2. The increase from step 2 causes the increase from step 1 to be less than the expected linear increase with field, because of common ion effects. This negative deviation of α from the expected linearity is characteristic of all multiple dissociating acids; the deviation will be larger, the larger the degree of dissociation of the second ionization step.

Because the anion concentration always increases with increasing field, β will always show a positive deviation from the expected linearity. However, when α is far below unity, that is, when the first ionization step is not substantially complete, this increase in the anion concentration with field is larger and

β will show an even larger positive deviation from linearity. The influence of increasing β will depend on its magnitude relative to decreasing α , and a competition for dominance results. If the opposite deviations of α and β cancel each other, the theoretical HFCQ vs. field curve will be linear. If the negative deviation from linearity of α predominates then the theoretical curve will turn downward. If the positive deviation of β predominates, the curvature will be upward.

The concentration dependence of the theoretical results which match the experimental results can now be explained in terms of three competing factors: shifts in the activity coefficients, changes in the curvature with changing concentration, and the effect of increasing concentration on the slope of the $\Delta\Lambda/\Lambda(0)$ vs. field strength plot. As the concentration increases, the activity coefficients will cause a downshift of the entire plot by the same amount. If the curvature changes, this too will affect the concentration behavior. This effect should be most prominent at the high fields. This curvature changes with concentration as follows: the deviation becomes less negative with increasing concentration because of the lessening influence of the hydrogen ions and this results in a net increase in $\Delta\Lambda/\Lambda(0)$ with increasing concentration. The magnitude of this increase will depend on the field strength and the relative degrees of dissociation for both steps with the second step having the largest potential for increase. As mentioned previously, an increase in concentration causes both α and β to drop. For a simple electrolyte an increase in the concentration will cause an increase in $\Delta\Lambda/\Lambda(0)$ at a given field strength. This concentration effect alters the slope of the plot and therefore should have its greatest influence at high field strengths. It is not a linear increase, but increases more slowly at higher concentrations. For the dibasic acids, this effect will influence both α and β , but the influence of β will diminish more rapidly than α . Therefore the concentration dependence of $\Delta\Lambda/\Lambda(0)$ depends on the competition between the negative influence of the activity coefficient and the positive influences of the changing curvature and the increasing concentration.

Because all these factors interact with each other, it is unproductive to undertake further verbal description; the test of adequacy of the model and extended theory described above must be against experimental results. It has been found that the theoretical behavior calculated matches the experimental results obtained, including the details of high field curvature and the concentration dependence as illustrated by the results just given.

Diamines. Five diamines were examined; all showed unexceptional behavior and rather poorer agreement between theory and experiment than with the salts and diacids studied. The diamines are the base counterparts of the dicarboxylic acids and a similar theory may be applied. The K_b 's and SIC's were in some cases of doubtful validity or else unavailable. Figure 6 illustrates the behavior of 1,6-diaminohexane for which K_b 's are available¹³ but for which SIC's must be estimated. On the basis of reasonable assumptions about ion size, etc., we have chosen SIC's, given in the figure legend, which give good agreement with the experiment.

Weak Bases. Six amines were studied which act as weak bases in solution. The agreement between theory and experiment was poorer, with the exception of benzylamine, than with any of the other electrolytes studied. In addition to the unavailability of reliable electrochemical data, in the case of the stronger of these bases, carbon dioxide contamination is a possible adverse influence in spite of strenuous efforts to avoid it. The presence of carbon dioxide in effect changes the

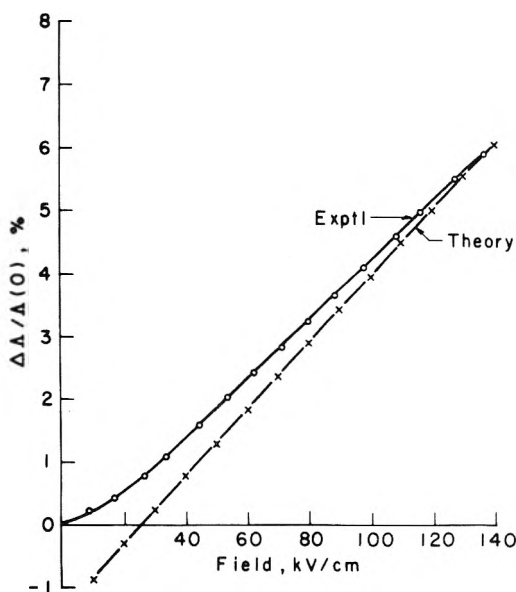


Figure 6. High field conductance quotient, percent, as a function of field, kilovolts per centimeter, for a 1.208×10^{-4} M solution of 1,6-diaminohexane at 25 °C. The experimental results are plotted as circles, the theoretical calculations as 'x's. The theoretical constants were: SIC's, $\lambda_1^0(\text{OH}^-) = 199.2$, $\lambda_2^0 = 45$, $\lambda_3^0 = 60$; dissociation constants, $K_1 = 8.53 \times 10^{-4}$, $K_2 = 6.92 \times 10^{-5}$.

$K(0)$ of the compound being studied; its influence should be about the same for all the bases since the techniques of solution preparation were carefully standardized, but it would cause the greatest divergence where the HFCQ is the smallest. This is essentially what was observed. Schiele⁵ commented on his poorer results with bases. Onsager⁶ has suggested that the larger and slower ions found in weak bases might cause greater deviations between experiment and theory. Whichever of these items may be the cause of our poorer agreement, it is not unlike that which has been observed before.

Corrections to Theory

Onsager's associates Liu³ and Provencher⁴ have advanced two kinds of corrections to the theory of high field conductance. Liu accounts for the shielding of the Coulomb forces by the Debye-Hückel ion atmosphere which was neglected by Onsager in the theory of Wien effect II, through the inclusion of an additional term in the $F(b)$ expression when κ and β obey certain inequalities:

$$K(X) = K(0) \left[F(b) + \frac{2\kappa^2 q^2}{b} \ln(1 + b/\kappa q) \right] \quad \beta \gg \kappa$$

or

$$K(X) = K(0)[1 + 2\kappa q + b^2/3\kappa q] \quad \beta \ll \kappa$$

in terms of the Debye-Hückel potential. For the Onsager-Kim potential,¹⁰ the result is

$$K(X) = K(0) \left[F(b) + \frac{2\kappa^2 q^2}{b} \ln \frac{b}{\kappa q} \right] \quad \beta \gg \kappa$$

Unfortunately, with the electrolytes used in this study, the corrections are valid only at very low fields, or for concentrations or higher fields outside our experimental range. With acetic acid at 6.85×10^{-4} M, $\kappa = \beta$ at 23.5 kV/cm; it is surprising that the Liu correction gives excellent agreement with theory up to about 10 kV/cm. For the high field approximation

$\beta \gg \kappa$, at 150 kV/cm β is only 6.4 times larger than κ , far from the requirement $\beta \gg \kappa$.

The theory of Onsager and Provencher⁴ is applicable to associated electrolytes where the rate of recombination of ions is at least comparable to the rate permitted by diffusion, and where the lifetime of the associated species is comparable to the relaxation time of the ionic atmosphere. Under these circumstances there is an additional mechanism for the relaxation of the asymmetric charge distribution of the ion atmosphere around a moving ion and the dissociation kinetics may be affected. The magnitude of these effects cannot be estimated at present, but the Provencher mechanisms offer potential ways of explaining some of the experimental deviations, as of weak monobasic acids, from theory. The Liu corrections would be of much greater importance with examples like 3-3 electrolytes, which will be the subject of a separate discussion.

References and Notes

- (1) (a) Submitted in partial fulfilment of the requirements for the degree of Doctor of Philosophy, Yale University, June, 1972; *Diss. Abstr. Int. B*, **33**, 2011B (1972); Order No. 72-29, 542. (b) Present address: Department of Chemical Engineering, Carnegie-Mellon University, Schenley Park, Pittsburgh, Pa. 15213.
- (2) L. Bass and W. J. Moore in "Structural Chemistry and Molecular Biology", A. Rich and N. R. Davidson, Ed., W. H. Freeman, San Francisco, Calif., 1968, pp 356-369.
- (3) L. Onsager and C. T. Liu, *Z. Phys. Chem. (Leipzig)*, **228**, 428 (1965).
- (4) L. Onsager and S. W. Provencher, *J. Am. Chem. Soc.*, **90**, 3134 (1968).
- (5) J. Schiele, *Ann. Phys.*, **13**, 811 (1932).
- (6) L. Onsager, *J. Chem. Phys.*, **2**, 599 (1934).
- (7) F. E. Bailey and A. Patterson, *J. Am. Chem. Soc.*, **74**, 4756 (1952).
- (8) H. Freitag and A. Patterson, *J. Electrochem. Soc.*, **108**, 529 (1961).
- (9) K. N. Marsh, M. Spiro, and M. Selvaratnam, *J. Phys. Chem.*, **67**, 699 (1963).
- (10) L. Onsager and S. K. Kim, *J. Phys. Chem.*, **61**, 198 (1957).
- (11) G. Jones and B. C. Bradshaw, *J. Am. Chem. Soc.*, **55**, 1780 (1933).
- (12) D. Berg and A. Patterson, *J. Am. Chem. Soc.*, **75**, 1484 (1953).
- (13) D. D. Perrin, "Dissociation Constants of Organic Bases in Aqueous Solutions", Butterworths, London, 1965.

The Electrochemistry of Nitrobenzene and *p*-Nitrobenzaldehyde Studied by Transmission Spectroelectrochemical Methods in Sulfolane

N. R. Armstrong,[†] N. E. Vanderborgh,[‡]

Department of Chemistry, University of New Mexico, Albuquerque, New Mexico 87131

and Rod K. Quinn*

Sandia Laboratories, Albuquerque, New Mexico 87115 (Received November 4, 1975; Revised Manuscript Received September 2, 1976)

Publication costs assisted by Sandia Laboratories

Transmission spectroelectrochemistry experiments have been used to study the electrochemical reductions of nitrobenzene and *p*-nitrobenzaldehyde in sulfolane. The reduction intermediates of both these aromatic compounds are sufficiently long-lived in sulfolane to be amenable to study by these techniques. Nitrobenzene undergoes a single one-electron, chemically reversible reduction at $E_{p,c} = -1.875$ V vs. AgRE. This was verified by analysis of the visible absorption spectrum for the reduction species; two maxima were observed at 348 nm ($\epsilon 5.7 \times 10^3$ M⁻¹ cm⁻¹) and 465 nm ($\epsilon 4.1 \times 10^3$ M⁻¹ cm⁻¹). *p*-Nitrobenzaldehyde undergoes two one-electron reductions ($E_{p,1} = -1.528$ V, $E_{p,2} = -2.114$ V vs. AgRE), which are accompanied by following chemical reactions. A mechanism is shown involving formation of a parent-radical anion complex and an unusually low reproporationation reaction rate ($k_f = 5.4 \pm 0.7 \times 10^2$ M⁻¹ s⁻¹ at 50 °C). Verification of the proposed mechanism is assisted by digital simulation techniques and a newly developed differential treatment of the spectroelectrochemical data.

Introduction

Recently a cyclic voltammetric study of the reductions of benzaldehyde and substituted benzaldehydes in sulfolane was reported.¹ These data showed that upon cathodic electrolysis these compounds produce long-lived intermediates. This area was additionally explored using ring-disk electrochemical techniques and kinetic parameters have been obtained for the chemical reactions following charge transfer.²

[†] Current address: Department of Chemistry, Michigan State University, East Lansing, Mich. 48823.

[‡] Current address: Los Alamos Scientific Laboratory, Los Alamos, N. Mex. 87544.

We report here the transmission spectroelectrochemical study of two particular compounds, nitrobenzene and *p*-nitrobenzaldehyde, which extends the information presented previously.¹⁻³ The study of benzaldehyde, *p*-cyano- and *p*-phenylbenzaldehyde reductions by the same techniques will be reported in a subsequent publication.⁴

Throughout these investigations, the rather unique solvent properties of sulfolane have been evident. Rates of both heterogeneous charge transfer and homogeneous chemical reactions have been noticeably retarded when compared with other solvent media.¹⁻³ These solvent effects on reaction rates are confirmed by the spectroelectrochemical characterization of the *p*-nitrobenzaldehyde reduction mechanism.

The reduction intermediates of nitrobenzene and *p*-nitrobenzaldehyde have been studied previously by spectroscopic techniques including uv-visible spectrophotometry,⁵⁻⁹ and electron spin resonance spectroscopy.¹⁰⁻¹⁵ Electrochemical reductions produce one-electron adducts, the radical anions. The absorption maximum for the nitrobenzene radical anion species has been shown to occur at 464 nm in DMF.⁹ Alkali metal reductions of nitrobenzene in a variety of solvents produce differing chemical species which show unique optical absorption quite different from that found using electrochemical reduction.^{5,6}

Transmission spectroelectrochemical techniques have been well documented. These methods provide both qualitative and quantitative information and serve to elucidate both heterogeneous and homogeneous reactions.¹⁶⁻²¹ Techniques of digital simulation seem to present a powerful method of interpreting spectroelectrochemical information.^{16,19-21} These methods have been utilized here to obtain features of the reduction processes of nitrobenzene and *p*-nitrobenzaldehyde which cannot be determined by alternate electrochemical techniques.

Experimental Section

Purification procedures have been previously described¹ for all chemicals except nitrobenzene. This compound was distilled under reduced pressure from molecular sieves (Linde 4A). Prepared solutions were further purified by argon displacement of dissolved oxygen. This procedure in sulfolane solution takes over 1 h. All solutions were 0.1 M with respect to tetrabutylammonium perchlorate (TBAP).

The spectroelectrochemical cell used for these studies was similar in design to one described previously.²² Optically transparent electrodes (OTE) were platinum films, 15-30 nm thick, vapor deposited on quartz substrates. The geometric area of the OTE (that part used as the electrolysis site) was 0.308 cm².

The original cyclic voltammograms for nitrobenzene and *p*-nitrobenzaldehyde were recorded with respect to a previously described Ag⁺|AgClO₄ reference electrode.¹ Peak potentials are cited vs. this reference couple. All other experiments were conducted using a silver plate anodized in perchlorate medium as the reference electrode. This was positioned in a 1.0 cm diameter tube terminated by a fine glass frit. The potential stability of this electrode was acceptable, better than ±10 mV over a period of several hours.

Electrochemical experiments were performed at 50 °C. Temperature was monitored with a thermistor probe built directly into the cell cavity. Temperature was determined using an operational amplifier configuration described previously.²³ Temperature was maintained by pumping thermostating oil through four hollow bolts which held the cell together. An identical cell served for the reference cell in the spectral measurements.

Typical experimental procedure involved recording a cyclic voltammogram for the compound of interest at a sweep rate of 16.7 mV/s. This was then compared with previous current-voltage data taken at bulk electrodes. Oxygen levels were also confirmed to be less than electrochemically detectable (10⁻⁴ M) during these voltammograms. The OTE was then poised at the potential of interest (usually several hundred millivolts past the cyclic voltammetric peak potential) and then rapid and short (<50 nm) wavelength scans were made to identify regions of special spectral interest. This process was repeated several times; spectra were constructed graphically from specific absorbances found 15 s after the

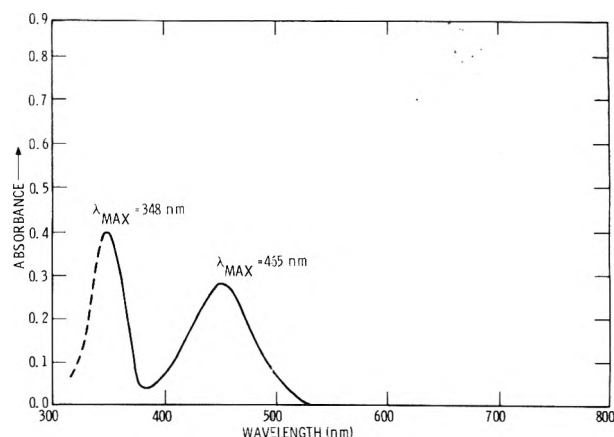


Figure 1. Absorption spectrum of the nitrobenzene reduction intermediate. The potential was stepped past the reduction peak potential (-1.875 V).

initiation of electrolysis. These spectra differ only in amplitude from those found at shorter time intervals. A reference spectroelectrochemical cell was placed in the reference beam of the spectrophotometer so that parent compound absorbance is absent from the product spectra.

The absorbance at a single wavelength was also monitored as a function of time. This was done either, during the "potential step experiments" by rapidly switching the OTE from a point before the electrolysis wave to a potential past the peak potential, or, during the "cyclic voltammetric experiments" by observing spectral behavior while a triangular waveform, slope of 2 V/min, was applied to the OTE.

Results and Discussions

The results of this study show a variety of homogeneous chemical reactions following the primary reduction step of *p*-nitrobenzaldehyde. The nitrobenzene reduction behavior expected of a chemically stable radical anion species.⁹

Information taken from cyclic voltammograms of nitrobenzene confirm that the compound undergoes a chemically reversible, single, one-electron transfer in sulfolane ($E_{p,c}$ for the reduction is -1.875 V vs. (Ag⁺|AgClO₄) while the peak current ratio is 1.00 at sweep rates down to 10 mV/s). The absorption spectrum for the reduced species is shown in Figure 1. The dashed line indicates the spectral region where the OTE shows significant absorbance and the spectrophotometer sensitivity is therefore decreased. These sulfolane data show good agreement with similar work in DMF.⁹

Potential step experiments were performed with the spectrophotometer set at both wavelengths of maximum absorbance (348 and 465 nm). The absorbance-time behavior was consistent with a reduction occurring under strict diffusion control. The absorbance (*A*) showed a linear dependence with the square root of electrolysis time for both wavelength maxima, for electrolysis times up to 16 s. Extinction coefficients of the absorbing species were estimated from the slope of the *A* vs. *t*^{1/2} plots¹⁶ (Table I).

The 348- and 465-nm peaks either represent the same species or one peak is attributable to a species which is in rapid chemical equilibrium with the radical anion. As discussed later these two possibilities are not distinguishable.

The cyclic voltammogram for *p*-nitrobenzaldehyde is shown in Figure 2. This voltammogram was taken on the Pt OTE and showed two apparent one-electron steps with widely separated peak potentials ($E_{p,c}$ at -1.528 and -2.114 V vs. Ag⁺|AgClO₄).

TABLE I: Absorption Bands and Extinction Coefficients for Reduction Intermediates of *p*-Nitrobenzaldehyde and Nitrobenzene

Compound	λ_{max} , nm	Extinction coeff, $\text{M}^{-1} \text{cm}^{-1}$	
		Apparent ^a	Corrected ^b
<i>p</i> -Nitrobenzaldehyde (PNB)	390 ^c	2.5×10^4	3.1×10^4
	663 ^c	1.5×10^4	1.6×10^4
	450 ^d	2.0×10^4	
Nitrobenzene (PhNO_2)	348	5.7×10^3	
	465	4.1×10^3	

^a Derived from the zero-time extrapolation of the slope of the absorbance/ $t^{1/2}$ plot. ^b Derived from the digital simulation mechanism. ^c Present after the first one-electron addition. ^d Present after the second one-electron addition.

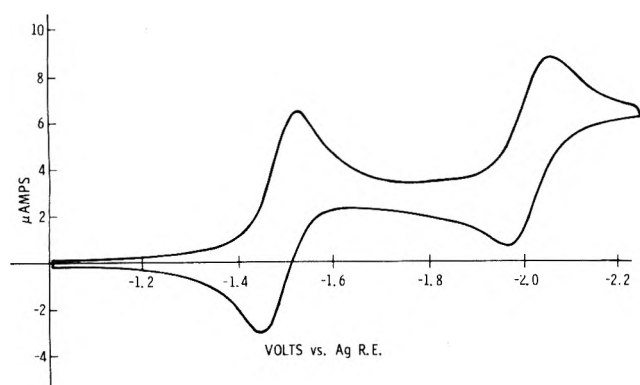


Figure 2. Cyclic voltammogram of the two-step reduction of 2.58 mM *p*-nitrobenzaldehyde in sulfolane at the Pt OTE. Potential scan starts at -1.0 V vs. AgRE at a scan rate of 16.7 mV/s.

This agrees with previous work obtained in DMF.²⁴ The first reduction wave was chemically reversible² and analogous to the one-electron nitrobenzene reduction. The peak potential is anodically shifted 350 mV from that found for nitrobenzene which is the expected result for the inductive effect caused by the carbonyl group.¹ The second electron addition indicated a slow chemical reaction following charge transfer; the cyclic voltammetric peak current ratios are less than unity at sweep rates less than 200 mV/s.¹

Spectral information obtained for this two step reduction is shown in Figure 3. The solid line represents a spectrum taken when the potential of the OTE was stepped beyond the second peak potential for PNB. Three important bands were seen at 390, 663, and ~ 450 nm. If the potential of the OTE was stepped beyond the first peak potential of PNB, only the 390- and 663-nm bands were seen (i.e., no evidence of the 450-nm band shown in Figure 5 was seen). The 663-nm band is broad, with some unresolved structure. The shape of this band did not change during any of the various electrochemical experiments. In all potential step experiments described below, the absorbance contribution of the 390-nm band to the absorbance vs. time behavior of the 450-nm band was resolved. Under diffusion controlled, one-electron reduction conditions, the absorbance vs. $t^{1/2}$ behavior of the 390- and 663-nm bands was linear up to 16 s. Absorbance vs. $\text{time}^{1/2}$ behavior for the 450-nm band under diffusion controlled, two-electron reduction conditions, was nonlinear, however, further suggesting a chemical reaction occurs to remove the species causing that absorbance. This reaction is probably not one involving the

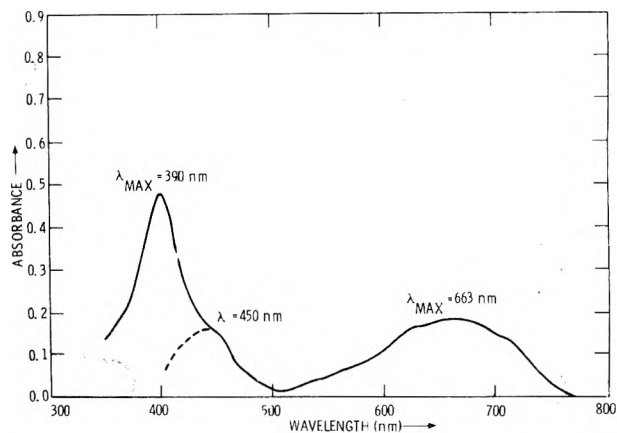


Figure 3. Absorption spectrum of the *p*-nitrobenzaldehyde reduction intermediates. The potential was stepped past the reduction peak potential and the absorbances were measured 15 s after initiation of electrolysis: solid line (—), spectrum taken at the first reduction process; broken line (---), shoulder added to the original spectrum at the second reduction process.

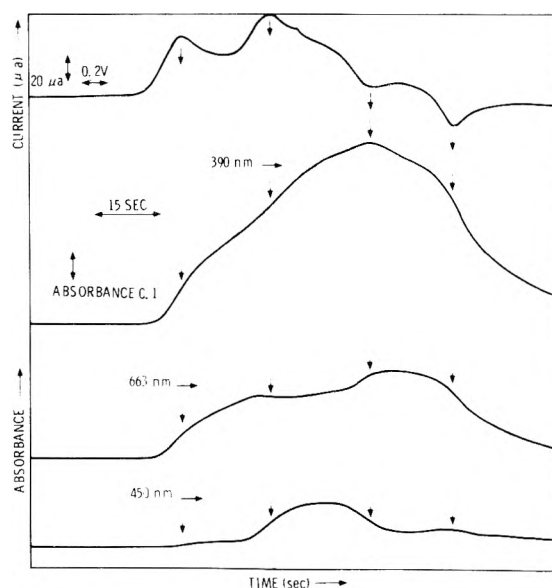


Figure 4. Spectroelectrochemical results for the two-electron reduction of 2.58 mM *p*-nitrobenzaldehyde in sulfolane. The upper curve is the current-time behavior of the controlled potential scan. Note the two reduction steps prior to potential scan reversal. The lower three curves are the absorbance vs. time plots at 390, 663, and 450 nm taken under the cyclic voltammetric conditions.

PNB dianion with solution impurities such as dissolved oxygen. The stability of the *p*-nitrobenzaldehyde and nitrobenzene one-electron reduction intermediates, both of which should be affected by dissolved oxygen, support this hypothesis. Extinction coefficient information was obtained by estimating the slope of the $A/t^{1/2}$ relationship for each wavelength maximum extrapolated to zero time.¹⁶

The absorbance/time behavior was monitored for each of the band maxima during a cyclic voltammetric experiment (Figure 4). The 390- and 663-nm peaks both increase at the onset of the first reduction wave. The 663-nm peak remains at a constant absorbance during the second reduction process while the 390-nm peak continues to increase. The 450-nm peak does not increase until the onset of the second reduction process. (Some small spectral overlap is noticed during the first reduction step and was not removed from this figure.)

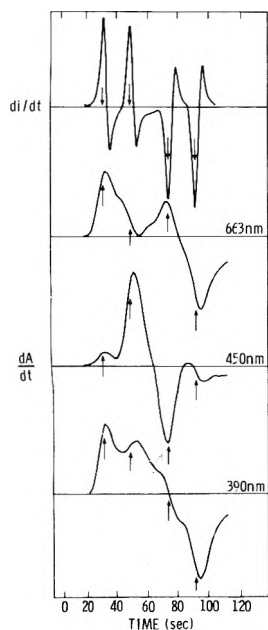
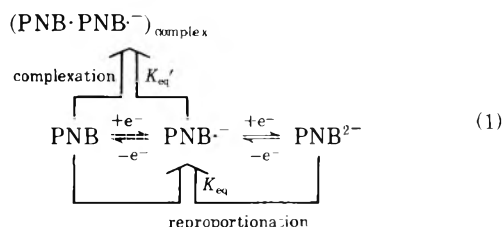


Figure 5. Differential data treatment for current-time and absorbance-time results from *p*-nitrobenzaldehyde reduction in sulfolane. The upper trace is the graphical presentation of dI/dt vs. time, whereas the bottom three curves are the dA/dt behavior of the three absorption maxima on the same time scale; 663, 450, and 390 nm, respectively (spectral overlap of the 390-nm band with the 450-nm band is uncorrected).

Both the current-time and absorbance-time data from Figure 4 were digitized and then differentiated using a least-squares smoothing routine. The results of this treatment are shown in Figure 5. The uppermost trace is a representation of dI/dt vs. time for the cyclic voltammogram. The dA/dt vs. time behavior for each of the band maxima are shown on the same time scale. The 390-nm band shows two maxima of dA/dt values, at the onset of the first reduction process (the first peak in dI/dt), and at the onset of the second reduction process (the second peak in dI/dt), and two minima of dA/dt at the reoxidation peaks of the dianion and one-electron intermediates.

Disregarding the spectral overlap of the 390-nm band in the 450-nm band data, the concentration of this species maximizes only with the onset of the second reduction process (dA/dt reaches a maximum). As the second reduction proceeds dA/dt reaches zero for the 663-nm band. Upon the onset of the oxidation of the dianion species, the 663-nm band once again shows a sharp increase (dA/dt reaches a maximum).

These data can be explained on the basis of a simple re-proportionation reaction between the PNB dianion and unreduced parent, and the formation of a complex between the unreduced parent and radical anion.



The 390-nm band (PNB^-) increases during the production of the dianion, PNB^{2-} (450-nm band) because of its continued production from the re-proportionation reaction.

The concentration of the parent-ion complex increases in

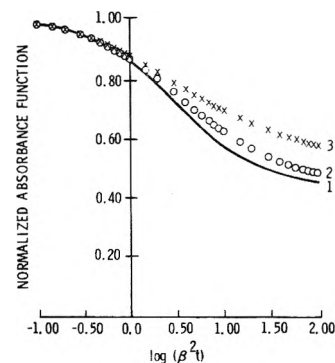


Figure 6. Digitally simulated working curve for the re-proportionation reaction of the dianion species and the parent *p*-nitrobenzaldehyde. Normalized absorbance function is plotted vs. the logarithm of the kinetic parameter, $\beta^2 t$. (1) $K_{\text{eq}}' C_{\text{bulk}} = 0$; (2) $K_{\text{eq}}' C_{\text{bulk}} = 1$; (3) $K_{\text{eq}}' C_{\text{bulk}} = 10$.

the reaction layer along with the radical anion during the first reduction step. During the second reduction, there is competition for the parent species for the complexation reaction and the re-proportionation of the dianion, thus the complex reaches an effective steady state concentration ($dA_{663}/dt = 0$ in Figure 5). During the post-oxidation wave, radical anion and parent molecule are present in high concentration and a maximum rate in complex formation is observed (dA_{663}/dt reaches a maximum).

The 663-nm band is broad, intense and a low energy electronic transition which is consistent with the radical anion-parent complex suggested here. We have assumed the simplest 1:1 stoichiometry of the complex. There is no evidence to suggest more complicated species than this. Such species have been proposed for other aromatic systems.²⁵ Weakly dimerized or complexed intermediates have also been suggested for the two electron, *o*-toluidine oxidation and methyl viologen reduction.^{16-18,20}

The equilibrium constant for the PNB re-proportionation reaction was estimated from the Nernst relationship:^{16-18,20,21}

$$K_{\text{eq}} = k_f/k_b = \exp[nF(E_{p,2} - E_{p,1})/RT] = (1.5 \times 10^9 \text{ M}^{-1}) \quad (2)$$

Digital simulation techniques were applied to determine the rate coefficient (k_f) for this re-proportionation reaction.^{16,20,21} Diffusion profiles of the various solution species were computed assuming a diffusion-controlled production of the dianion species (PNB^{2-}) (potential step past the second peak potential). The other species were the product of the re-proportionation reaction, i.e., the radical anion (PNB^-); and the parent complex with the radical anion ($\text{PNB} \cdot \text{PNB}^-$)_{complex}. Several diffusion profiles were computed using various values of the dimensionless kinetic parameter, $\beta^2 t$, which has been described before for digital simulation purposes:^{15,19}

$$\beta^2 t = k_f C_{\text{bulk}} t_k \quad (3)$$

where k_f is the forward rate coefficient, C_{bulk} is the bulk concentration, and t_k is the time after initiation of electrolysis. Values of normalized absorbance,¹⁶ α , were plotted for various values of $\beta^2 t$ ($0.1 \leq t \leq 100$) (Figure 6). Case 1 shows a working curve for the simple re-proportionation and is the same as for previously reported studies.²⁰ Cases 2 and 3 are for inclusion of parent-ion complexation expressed by the dimensionless equilibrium parameter $K_{\text{eq}}' C_{\text{bulk}}$. Increasing values of $K_{\text{eq}}' C_{\text{bulk}}$ cause less deviation of α from 1.0 (i.e., the repro-

TABLE II: Typical Calculations of the Forward Rate Coefficient, k_f , for the PNB Disproportionation

t, s	Absorbance	α^a	$\log \beta^2 t$	$k_f, M^{-1} s^{-1}$
(1) $T = 31^\circ C$				
2.5	0.048	0.782 ^b		
5.0	0.062	0.712 ^b		
7.5	0.086	0.807	0.31	127
10.0	0.098	0.798	0.33	99
12.5	0.106	0.770	0.46	107
15.0	0.113	0.751	0.53	105
17.5	0.119	0.732	0.59	103
20.0	0.126	0.725	0.62	97
Av of all runs = 122 ± 17				
(2) $T = 40^\circ C$				
2.5	0.055	0.779 ^b		
5.0	0.075	0.749 ^b		
7.5	0.092	0.751	0.53	210
10.0	0.101	0.715	0.65	208
12.5	0.107	0.676	0.79	229
15.0	0.114	0.659	0.86	225
17.5	0.120	0.642	0.93	226
20.0	0.126	0.631	0.99	227
Av of all runs = 229 ± 8				
(3) $T = 50^\circ C$				
2.5	0.058	0.713	0.54	645
5.0	0.076	0.659	0.68	445
7.5	0.085	0.602	0.89	481
10.0	0.094	0.578	1.00	465
12.5	0.099	0.543	1.18	563
15.0	0.105	0.527	1.30	619
17.5	0.109	0.506 ^b		
20.0	0.112	0.486 ^b		
Av of all runs = 536 ± 73				

^a α = normalized absorbance = $A_{\lambda,t} \pi^{1/2} / 2(C^b)(Dt)^{1/2} \epsilon_{450nm}$.
^b Rejected values. The value of $K_{eq} C_{bulk}$ used for these calculations was $5 \times 10^2 M^{-1}$; $C_{bulk} = 2.15 mM$, $\lambda_{max} 450 nm$ (PNB²⁻), $\epsilon_{450} 2.0 \times 10^4 M^{-1} cm^{-1}$.

portionation reaction rate is slower). Values of k_f were computed from the working curve for various values of α determined experimentally.^{16,19}

$$\alpha = A / [(2/\pi)Dt]^{1/2} C_{bulk} \epsilon R \quad (4)$$

The working curve was chosen which provided the k_f with the smallest average deviation for all values of $\beta^2 t$, and used the smallest value of $K_{eq} C_{bulk}$. Other simulated mechanisms do not fit the data as well as that demonstrated in Table II. The assumption of parent-ion complexation was necessary to obtain the minimum average deviation in k_f . The simulation of this reaction is given in greater detail in ref 4.

The estimated rate coefficient, k_f , at 50 °C is small for bimolecular charge transfer. The apparent activation energy determined from the temperature dependence of k_f (Table II) is correspondingly large, $E_{act} = 14.7$ kcal/mol and $\Delta S^\ddagger = -2.4$ eu. Reproportionation reactions have been compared to the values predicted by the Marcus model for electron transfer.²⁷ Radii of the parent molecule and the dianion can be assumed less than 5 Å, charge transfer can be assumed to occur across an 8–10-Å barrier, and the standard free energy of the reaction can be determined from the separation in peak potentials from the cyclic voltammograms ($\Delta G^\circ = -13.4$ kcal/mol). Under these assumptions, a k_f value of over $10^7 M^{-1} s^{-1}$ was calculated. Differences in this predicted value and experimental values may result from errors in the determi-

nation of k_f or appreciable rearrangement energies which are neglected in the usual Marcus treatment.

Small errors in the extinction coefficient of the dianion can lead to negative deviations in the digital simulation value found for k_f by more than two orders of magnitude. This rate coefficient was also determined by measuring the rate of decay of the 450-nm absorbance after a potential-step-followed-by-relaxation experiment,¹⁷ which yields a value of k_f independent of the value for the extinction coefficient. The average rate coefficient found by this method was $2.0 \times 10^2 M^{-1} s^{-1}$ at 50 °C, which is in good agreement with the value determined by digital simulation.

Other abnormally small rates of charge transfer and homogeneous chemical reaction have been observed in sulfolane.^{1,2,4,29,30} The small rates for reproportionation may be explained by assuming large, unpredicted rearrangement energies in the charge transfer process including large solvent reorganization energies. The solvation of these radical anion and dianion species by sulfolane may not be well described by a simple dielectric continuum assumption.²⁷ This solvent shows liquid crystal properties at room temperature with ordering in two dimensions.²⁸ The temperature dependence of k_f was observed over a wide enough temperature range to assume differing levels of solvent ordering. Long-range ordering has been postulated for other solvents such as Me₂SO.^{29,30} The low apparent rate of reproportionation could be partially a result of the rearrangement of solvation of the dianion and parent species in this semicrystalline solvent medium. This observation is supported by the relatively large temperature dependence of the reproportionation rate which parallels qualitatively the temperature dependence of the solvent viscosity.²⁸

The spectroelectrochemical technique has been a useful addition to the investigation of the reduction of *p*-nitrobenzaldehyde, nitrobenzene, and similar compounds.¹⁻⁴ The visibly colored complex of the *p*-nitrobenzaldehyde radical anion with the parent molecule observed in this study has not been seen previously in ESR or visible spectrophotometric experiments of the chemically produced species.⁵⁻¹⁵ It should also be pointed out that this species does not show unique electrochemical behavior either in ring-disk voltammetric experiments or cyclic voltammetric experiments.^{1,2} In addition, a slow reproportionation reaction has been observed to occur between the *p*-nitrobenzaldehyde dianion and the parent molecule, which may be due to unpredicted solvent rearrangement energies.

Acknowledgments. We gratefully acknowledge D. M. Mattox and G. J. Kominiak of Sandia Laboratories for preparing the transparent metal film electrodes used in this study. One of us (N.R.A.) acknowledges the Associated Western Universities for financial support through an AWU/AEC Graduate Fellowship at Sandia Laboratories.

This work was supported by the U.S. Energy Research and Development Administration.

References and Notes

- (1) N. R. Armstrong, R. K. Quinn, and N. E. Vanderborgh, *Anal. Chem.*, **46**, 1759 (1974).
- (2) N. R. Armstrong, R. K. Quinn, and N. E. Vanderborgh, *J. Electrochem. Soc.*, **122**, 615 (1975).
- (3) N. R. Armstrong, R. K. Quinn, and N. E. Vanderborgh, *J. Electrochem. Soc.*, **123**, 646 (1976).
- (4) N. R. Armstrong, Ph.D. Dissertation, University of New Mexico, 1974.
- (5) V. Kalyanaraman, C. N. R. Rao, and M. V. George, *Tetrahedron Lett.*, **55**, 4889 (1969).
- (6) C. N. R. Rao, V. Kalyanaraman, and M. V. George, *Appl. Spectrosc. Rev.*,

- 3, 154 (1970).
- (7) A. Ishitani, K. Kuwata, H. Tsobomura, and S. Hagakura, *Bull. Chem. Soc. Jpn.*, **36**, 1357 (1963).
- (8) B. Kastening, *Electrochim. Acta*, **9**, 241 (1964).
- (9) E. Wells, *Anal. Chem.*, **45**, 2022 (1973).
- (10) D. Geske and A. Maki, *J. Am. Chem. Soc.*, **82**, 2671 (1960).
- (11) A. Maki and D. Geske, *J. Am. Chem. Soc.*, **83**, 1852 (1961).
- (12) P. Rieger and G. Fraenkel, *J. Chem. Phys.*, **37**, 2811 (1962).
- (13) P. Rieger and G. Fraenkel, *J. Chem. Phys.*, **39**, 609 (1963).
- (14) N. Steinberger and G. Fraenkel, *J. Chem. Phys.*, **40**, 723 (1964).
- (15) T. Fujinaga, V. Deguchi, and K. Umamoto, *Bull. Chem. Soc. Jpn.*, **37**, 822 (1964).
- (16) T. Kuwana and N. Winograd in "Electroanalytical Chemistry", Vol. 7, A. J. Bard, Ed., Marcel Dekker, New York, N.Y., 1974, pp 1-78.
- (17) J. Strojek and T. Kuwana, *J. Electroanal. Chem.*, **16**, 471 (1968).
- (18) T. Kuwana and J. Strojek, *Discuss. Faraday Soc.*, **45**, 134 (1968).
- (19) N. Winograd, H. Blount, and T. Kuwana, *J. Phys. Chem.*, **73**, 3456 (1969).
- (20) J. Strojek, T. Kuwana, and S. Feldberg, *J. Am. Chem. Soc.*, **90**, 1355 (1968).
- (21) N. Winograd and T. Kuwana, *J. Am. Chem. Soc.*, **93**, 4343 (1971).
- (22) F. Hawkridge and T. Kuwana, *Anal. Chem.*, **45**, 1021 (1973).
- (23) N. E. Vanderborgh and W. D. Spall, *Anal. Chem.*, **40**, 256 (1968).
- (24) Y. Kargin, V. Kondrانيا, and H. Semakhina, *Izv. Akad. Nauk. Ser. Khim.*, **2**, 278 (1970).
- (25) L. J. Andrews and R. M. Keefer, "Molecular Complexes in Organic Chemistry", Holden-Day, San Francisco, Calif., 1964, pp 55-62.
- (26) N. Katkova and S. Shein, *Kinet. Katal.*, **13**, 492 (1972).
- (27) R. A. Marcus, *J. Chem. Phys.*, **43**, 679 (1965).
- (28) M. Della Monica, L. Jannelli, and U. Lamanna, *J. Phys. Chem.*, **72**, 1068 (1968).
- (29) B. Case in "Reactions of Molecules at Electrodes", N. S. Hush, Ed., Wiley-Interscience, New York, N.Y., 1971, pp 45-134.
- (30) H. L. Schafer and W. Schaffernicht, *Angew. Chem.*, **72**, 618 (1970).
- (31) L. Meites, "Polarographic Techniques", 2d ed, Interscience, New York, N.Y., 1965, pp 267-278.

An Investigation of the Self-Association of 2-Pyrrolidinone in Cyclohexane and Carbon Tetrachloride by Means of Spectroscopic and Dielectric Polarization Measurements

Judith A. Walmsley,* E. Jean Jacob, and H. Bradford Thompson

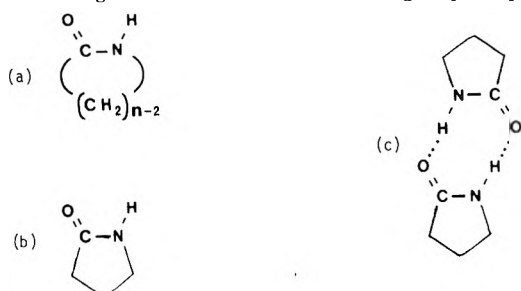
Department of Chemistry, University of Toledo, Toledo, Ohio 43606 (Received May 20, 1976)

Publication costs assisted by the University of Toledo

The self-association of 2-pyrrolidinone in cyclohexane and in carbon tetrachloride has been investigated using infrared and Raman spectroscopy and dielectric polarization measurements. In CCl_4 solutions up to 0.3 M the results have been interpreted as being indicative of the presence of monomers, dimers, and trimers. A computer fit of the data gives a dimerization constant, K_1 , of $118 \pm 30 \text{ M}^{-1}$ and a trimerization constant, K_2 , of $15 \pm 10 \text{ M}^{-1}$. The dipole moments of the species in CCl_4 are 3.74, 1.64, and 3.8 D for the monomer, dimer, and trimer, respectively. The Raman and infrared spectra show that the dimer probably has a cyclic, essentially planar structure and, along with the magnitude of the dipole moment, suggest that the trimer is also a cyclic species. The presence of some acyclic dimer and trimer as well as small amounts of higher oligomers cannot be excluded. In cyclohexane the predominant species appear to be the monomer and dimer although no model system was found which would best fit the experimental electric moment data. The dipole moment of the monomeric species in cyclohexane has been found to be 3.3 D by a graphical procedure. Self-association of 2-pyrrolidinone does not occur in 1,4-dioxane and the dipole moment in this solvent is 3.80 D.

Introduction

The structure of lactams is of scientific interest because they provide small molecule models for the amide group in peptides. Aside from this they present a challenging hydrogen bonding question, in particular in nonpolar solvents. A generalized formula for lactams (a), the formula of 2-pyrrolidinone (b), and the structure of its cyclic dimer (c) are shown, where n = ring size. When $n > 9$ the amide group adopts the



trans conformation, when $n < 9$ it adopts the cis conformation and when $n = 9$ both cis and trans isomers coexist.¹⁻³ Dielectric polarization measurements indicate that the trans lactams undergo self-association in non-polar solvents forming chain oligomers while cis lactams form predominantly cyclic dimers.³

Numerous infrared spectroscopic investigations of dilute solutions of 2-pyrrolidinone and other cis lactams in carbon tetrachloride have been reported. In all cases the data and the thermodynamic parameters derived from it were interpreted on the basis of a two species system: monomer and cyclic dimer.⁴⁻⁹ However, in their study of ϵ -caprolactam in CCl_4 , Lord and Porro noted that they did not obtain a constant value for the dimerization constant for solutions with a concentration greater than about 0.2 M.⁹ Vapor phase osmometry was used to investigate the function of ring size on the self-association of a series of lactams in benzene¹⁰ and equilibrium constants and thermodynamic parameters were determined assuming a monomer-dimer system. Ebullioscopic mea-

measurements⁸ and NMR spectroscopy^{11,12} have also been employed to study the hydrogen bonding of lactams.

Huisgen and Walz³ studied the dielectric polarization of a series of lactams in benzene and observed for the cis lactams that the molar polarization decreased as the concentration increased. They interpreted this effect to be caused by the formation of cyclic dimers of low dipole moment. The dipole moment of a planar cyclic dimer is expected to be very small due to cancellation of the dipole moments of the two monomeric units. More recently dielectric relaxation techniques have been used to examine two cis lactams in several nonpolar solvents.^{13,14} Besides the monomer and dimer species, a trimer was included in this interpretation of the experimental data. However, the evidence for the presence of a trimeric species came mainly from the computer fit of the data and was not conclusive. Dimerization and trimerization constants were calculated for 2-pyrrolidinone and ϵ -caprolactam in cyclohexane.¹³ The infrared and Raman spectra indicate the existence of cyclic dimers and chain oligomers in the liquid state and cyclic dimers in the solid state.¹⁵

An X-ray crystal structure of 4-iodomethyl-2-pyrrolidinone has shown this compound to be a dimer consisting of two symmetry related structures held together by hydrogen bonds.¹⁶ We have calculated the dihedral angle between the two amide planes to be 15°, showing that the dimer ring is nearly planar in the crystal.

We have used infrared and Raman spectroscopy and dielectric polarization measurements to examine 2-pyrrolidinone in carbon tetrachloride over a range of concentrations and have found that it is necessary to consider the system to be composed of three species: monomer, dimer, and trimer. Equilibrium constants for the dimerization and trimerization have been determined from the dielectric polarization data. Although we do not have conclusive evidence it is believed that the dimer and trimer exist predominantly in the cyclic form as opposed to an acyclic form. 2-Pyrrolidinone has also been examined in cyclohexane and no concrete evidence for the existence of trimers has been found. However it was not possible to determine an association constant from the dielectric polarization measurements because a satisfactory model system could not be found.

Experimental Section

Materials. 2-Pyrrolidinone was purified by a double fractional distillation. The second distillation was carried out using a 30-cm heated fractionating column containing a tantalum spiral and the fraction boiling at 94 °C at 1.7–1.8 Torr was used for measurements (freezing point = 25.2 °C). The sample was chromatographically pure as determined by glpc. 2-Pyrrolidinone was stored in a desiccator and all transfers were carried out in a glove bag under a nitrogen atmosphere.

The solvents for infrared and Raman spectral studies were spectral quality and were dried over molecular sieves. The solvents for static permittivity and refractive index measurements were distilled through a jacketed, heated, glass column which was 4 ft in length and which was packed with stainless steel curlings. Cyclohexane was refluxed over sodium metal overnight, fractionally distilled, and stored over sodium ribbon. Carbon tetrachloride was refluxed over P₄O₁₀ and fractionally distilled from it. 1,4-Dioxane was stirred with activated alumina for 6 h to destroy peroxides. It was decanted from the Al₂O₃, refluxed over sodium metal for 24 h and fractionally distilled. Dioxane and carbon tetrachloride sol-

vent bottles were stored in plastic bags containing desiccant.

The solutions for spectral measurements were prepared by adding 2-pyrrolidinone from a calibrated dropper to an oven-dried, weighed volumetric flask, weighing, and diluting to the mark with solvent. For static permittivity and refractive index measurements, the solutions were prepared in the same manner except the oven-dried volumetric flasks were cooled and stoppered in a glove bag under N₂ and the dilution with the solvent was done in the glove bag.

Apparatus. The heterodyne beat method^{17a,18} was used to measure the dielectric constants of the solutions. The apparatus as described previously^{19,20} has been improved by the replacement of the original variable capacitor with a General Radio Type 874-VCL precision capacitor and by replacement of the fixed and variable oscillator circuits with transistorized circuits, essentially as described by Brown and Hill.²¹ The measurements were made at 333 kHz and the variable oscillator was balanced at 180 Hz above null, using a 3:1 Lissajous figure.¹⁸ A glass cell was used which had a holding chamber for thermal equilibration of solutions. Pure solvents were used for standardization of the cell. Dielectric constant measurements were reproducible to within 0.0002.

The refractive index measurements (sodium D line) were made with a Bausch and Lomb dipping refractometer and these measurements have a precision of 7×10^{-6} . The dielectric constant and refractive index measurements were done at 25 °C with a temperature control of ± 0.005 °C.

Infrared spectra were obtained on a Perkin-Elmer 621 at room temperature using 0.1- or 1.0-mm matched NaCl cells for the solution spectra. Raman spectra were obtained on a custom-built Raman spectrometer designed by Dr. D. F. Burow²² of this department. The exciting source was the 514.5-nm line of an argon ion laser.

Computer fitting of the dielectric polarization data was done on a PDP-8/I computer.

Theory and Data Treatment

The calculations of the electric moments were done employing the method of Guggenheim.^{23a,24} In this method the dipole moment, dielectric constant, and refractive index are related by the expression

$$\frac{\epsilon - n^2}{(\epsilon + 2)(n^2 + 2)} = \frac{\epsilon_0 - n_0^2}{(\epsilon_0 + 2)(n_0^2 + 2)} + \left[\frac{4\pi N\mu^2}{27kT} + P_a \right] c \quad (1)$$

where ϵ is the dielectric constant of the solution, n is the refractive index of the solution, ϵ_0 and n_0 refer to the values for the pure solvent, N is Avogadro's number, k is the Boltzmann constant, T is the absolute temperature, μ is the dipole moment, P_a is the atomic polarization of the solute, and c is the concentration of the solute.

The atomic polarization term in eq 1 is usually small with respect to the electronic polarization. The latter is accounted for by the molar refraction and enters into the Guggenheim expression via the refractive index terms. Since a positive error is introduced in the molar refraction when the refractive indices used are those measured with visible radiation rather than the values extrapolated to infinite wavelength, the molar refraction is frequently used for the sum of the electronic and atomic polarizations.¹⁸ In the absence of a reasonable estimate of the atomic polarization for 2-pyrrolidinone, that approximation has been used in the treatment of this data.

For a system containing a single type of solute species, a plot of the term $(\epsilon - n^2)/(\epsilon + 2)(n^2 + 2)$ vs. c expressed in mol/ml results in a straight line whose slope equals $4\pi N\mu^2/27kT$. This

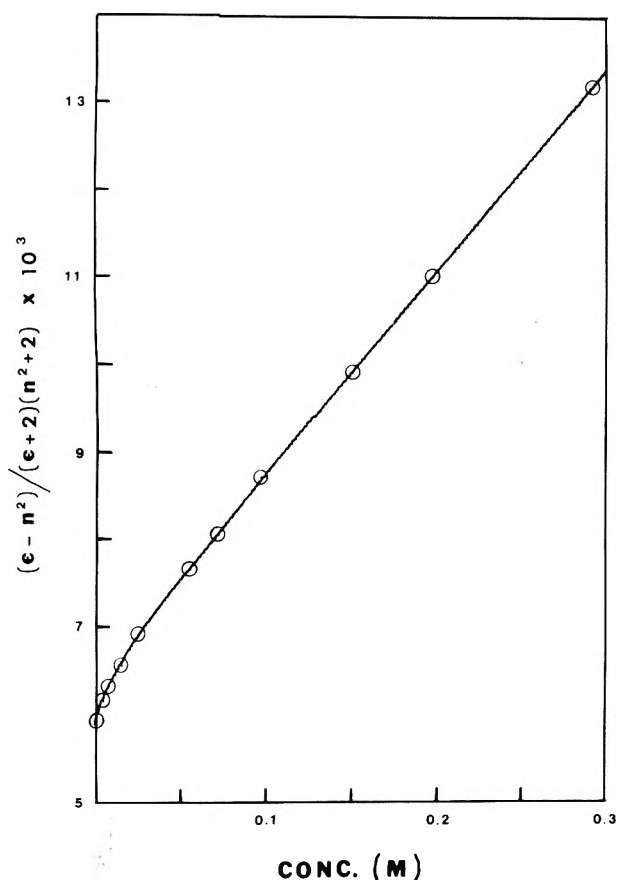


Figure 1. Plot of the dielectric polarization data for 2-pyrrolidinone in CCl_4 at 25 °C: (○) experimental; (—) calculated

type of plot results in a curve if several different solute species, each possessing a different dipole moment, exist in solution simultaneously. (See Figures 1 and 4.)

The apparent μ^2 calculated for a specified concentration of solute in a multicomponent system is the weighted sum of the contributions of the μ_i^2 of the individual components:

$$\mu_{\text{app}}^2 = \sum_i \mu_i^2 \alpha_i \quad (2)$$

where α is the fraction of a particular species; i.e., $\text{mol}_i / \text{mol}_{\text{total solute as monomer}}$. Substituting eq 2 into eq 1 and neglecting the atomic polarization as discussed above gives

$$\frac{\epsilon - n^2}{(\epsilon + 2)(n^2 + 2)} = \frac{\epsilon_0 - n_0^2}{(\epsilon_0 + 2)(n_0^2 + 2)} + \frac{4\pi Nc}{27kT} \sum_i \mu_i^2 \alpha_i \quad (3)$$

If c , the total solute concentration, has been calculated on the basis of all the material existing as monomer or as the simplest units, then eq 3 becomes

$$\frac{\epsilon - n^2}{(\epsilon + 2)(n^2 + 2)} = \frac{\epsilon_0 - n_0^2}{(\epsilon_0 + 2)(n_0^2 + 2)} + \frac{4\pi N}{27kT} (\mu_1^2 c_1 + \mu_2^2 c_2 + \dots + \mu_i^2 c_i) \quad (4)$$

For a system of two species, monomer and dimer, the reaction and equilibrium expression can be written:

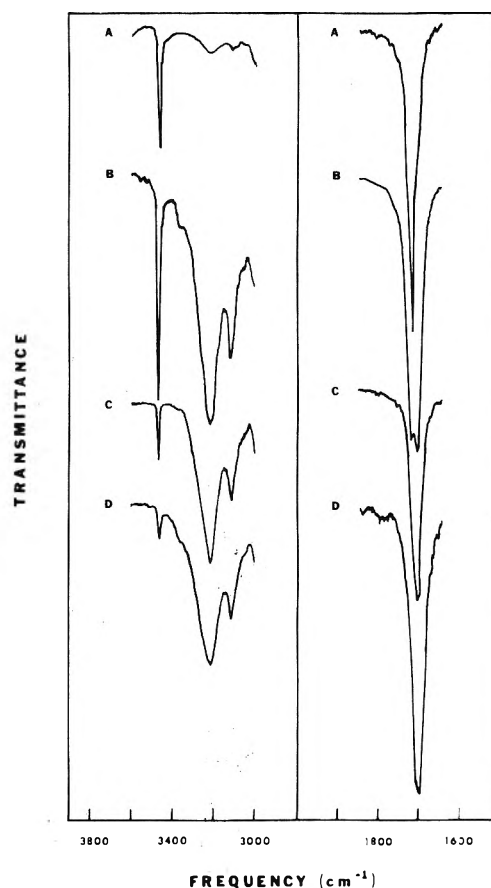
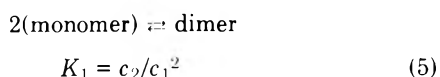


Figure 2. Infrared spectra of 2-pyrrolidinone in CCl_4 : (A) 0.001 M (1.0-mm cell), (B) 0.01 M (1.0-mm cell), (C) 0.05 M (0.1-mm cell), (D) 0.27 M (0.1-mm cell).

where the subscripts 1 and 2 now refer to the monomer and dimer, respectively, and K_1 is the dimerization constant. The law of conservation of mass requires that

$$c = c_1 + 2c_2 \quad (6)$$

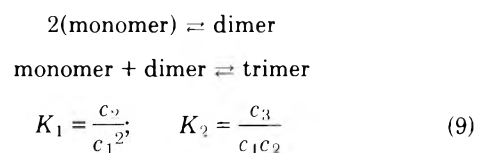
or

$$c = c_1 + 2K_1 c_1^2 \quad (7)$$

Then eq 4 becomes

$$\frac{\epsilon - n^2}{(\epsilon + 2)(n^2 + 2)} = \frac{\epsilon_0 - n_0^2}{(\epsilon_0 + 2)(n_0^2 + 2)} + \frac{4\pi N}{27kT} (\mu_1^2 c_1 + \mu_2^2 K_1 c_1^2) \quad (8)$$

Similarly if a three species model system composed of monomer, dimer, and trimer is considered the equilibrium expression, mass balance equation, and Guggenheim equation are



where the subscript 3 denotes the trimeric species.

$$c = c_1 + 2c_2 + 3c_3 \quad (10)$$

or

$$c = c_1 + 2K_1c_1^2 + 3K_1K_2c_1^3 \quad (11)$$

$$\frac{\epsilon - n^2}{(\epsilon + 2)(n^2 + 2)} = \frac{\epsilon_0 - n_0^2}{(\epsilon_0 + 2)(n_0^2 + 2)} + \frac{4\pi N}{27kT} (\mu_1^2c_1 + \mu_2^2K_1c_1^2 + \mu_3^2K_1K_2c_1^3) \quad (12)$$

The analysis of the dielectric polarization data of the carbon tetrachloride and cyclohexane solutions was done using a linear least-squares computer fit of the experimental data to a specific model system. After a model had been chosen, an equilibrium constant or set of equilibrium constants was arbitrarily chosen. The mass balance equation, such as eq 11, was solved for c_1 in terms of c and $K(s)$ and the value of c_1 for each data point substituted into the Guggenheim expression. The dipole moments and the value of the intercept²⁵ at infinite dilution were then determined by a linear least-squares fit of the data. These values were used to calculate a "theoretical" $\epsilon - n^2/(\epsilon + 2)(n^2 + 2)$ term and the standard deviation of the theoretical from the experimental was determined. The equilibrium constant(s) was changed systematically until the best fit of the experimental data to the model was obtained.

Within a given model system a minimum in the standard deviation of the Guggenheim terms was taken as the criterion for the best fit. Inappropriate models did not give minima in the standard deviation upon variation of the equilibrium constants.

Graphical determination of the monomer moments of 2-pyrrolidinone in carbon tetrachloride and cyclohexane was done by plotting ϵ and n^2 vs. w , the concentration of solute in g/ml. The dipole moments were calculated from the equation^{2,3b}

$$\mu_1^2 = \frac{27kT}{4\pi N} \left[\frac{M_1\beta}{(\epsilon_0 + 2)^2} - \frac{M_1\eta}{(n_0^2 + 2)^2} \right] \quad (13)$$

where M_1 is the molecular weight of the monomer and

$$\beta = \lim_{w \rightarrow 0} \left(\frac{\partial \epsilon}{\partial w} \right); \quad \eta = \lim_{w \rightarrow 0} \left(\frac{\partial n^2}{\partial w} \right) \quad (14)$$

Results

2-Pyrrolidinone in CCl₄. Permittivity and refractive index measurements were made on a series of 10 solutions varying in concentration from 0.003 to 0.3 M, and on pure carbon tetrachloride. A plot of the data is shown in Figure 1 where the points represent the experimental data.

Choice of a monomer-dimer model for this system and a computer treatment of the dielectric polarization data according to eq 5-8 does not give a minimum in the standard deviation of the fit; i.e., no best fit is obtained. As the value of K_1 is increased, the standard deviation of the fit decreases and appears to do so without limit. Meanwhile the calculated values of the monomer moment, μ_1 , become unrealistically large.

A three-species model composed of monomers, dimers, and trimers, as expressed by eq 9-12, gave a good fit to the experimental data. The standard deviation of the computer fit falls within the deviations expected due to experimental errors. In the calculations of the association constants and dipole moments, no assumptions have been made regarding the structure of the associated species; i.e., whether they are cyclic, acyclic, or a mixture of both. The association constants and

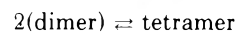
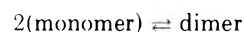
TABLE I: Association Constants and Dipole Moments of 2-Pyrrolidinone in CCl₄ at 25 °C

K_1, M^{-1}		K_2, M^{-1}	
118 ± 30		15 ± 10	
μ_1, D	μ_2, D	μ_3, D	
3.74 ± 0.21	1.64 ± 0.19	3.8 ± 0.8, -0.2	
3.5 ^a			

^a Graphically determined.

dipole moments are given in Table I. By virtue of the method by which the computations were performed the values of the association constants are not simply related to the standard deviation of the fit. Therefore, error limits on K_1 and K_2 are approximate values which were determined by applying random deviations (within $\pm\sigma$) to the experimental $\epsilon - n^2/(\epsilon + 2)(n^2 + 2)$ terms to produce a new set of "experimental" points. The new set of data was then treated in the same manner as the real data, resulting in values of K_1 , K_2 , and dipole moments. This was repeated for several sets of pseudo-experimental data. The error limits on the dipole moments were determined from the estimated deviations in the association constants. This was done by assuming that K_1 and K_2 had values corresponding to their maximum deviations and calculating the dipole moments from the fit of the experimental data with these sets of association constants.

A second three-species model composed of monomers, dimers, and tetramers was considered. In this case the equilibria were assumed to be



This model also yielded a minimum in the standard deviation of the fit, but it was not as good a fit as for the monomer-dimer-trimer model.

The carbonyl and N-H stretching regions of the infrared spectra of solutions of 2-pyrrolidinone in CCl₄ are shown in Figure 2. In the 3500-3000-cm⁻¹ region the sharp band at 3460 cm⁻¹ is the $\nu(\text{N-H})$ ²⁶ absorption of nonhydrogen bonded (free) N-H groups^{1,2,5,7,15} while the two broad bands at 3210 and 3110 cm⁻¹ are associated with hydrogen bonded N-H groups.^{2,5,15} Of the latter two bands, the higher frequency band has been assigned to the stretching vibration of the hydrogen N-H and the lower frequency band to a combination of the C=O stretching and N-H in-plane bending vibrations in Fermi resonance with the $\nu_{\text{assoc}}(\text{N-H})$ vibration.²⁷ There is a disagreement regarding the origin of the lower frequency band, but both of the bands due to associated N-H groups are believed to arise from a dimeric structure.^{1,6,15} As the concentration increases the absorbance of the free N-H stretching vibration decreases while that of the associated species increases, with no apparent change or shift in frequencies. Even at a concentration of 0.27 M there is still an easily detectable amount of free N-H.

While the N-H stretching region is more informative regarding the amount of nonhydrogen bonded N-H, the carbonyl group stretching region is more informative with respect to the presence of associated species. The infrared frequencies at various concentrations are listed in Table II. The band at 1716 cm⁻¹ is due to the absorption of free C=O of the monomer.^{2,15} At a concentration somewhere between 0.01 and 0.05 M this band becomes undetectable because of its decreasing

TABLE II: Infrared Frequencies of 2-Pyrrolidinone in the N-H and C=O Stretching Regions

Solvent	Concn, M	$\nu(\text{N-H})_{\text{free}}$, cm^{-1}	$\nu(\text{N-H})_{\text{assoc}}$, cm^{-1}	Comb ^a band, cm^{-1}	$\nu(\text{C=O})_{\text{free}}$, cm^{-1}	$\nu(\text{C=O})_{\text{dimer}}$, cm^{-1}	$\nu(\text{C=O})_{\text{b}}$, cm^{-1}
CCl_4	0.27	3461	3213	3110			1698
	0.10	3460	3208	3105			1698
	0.05	3460	3211	3110		1701	
	0.01	3460	3210	3110	1716	1701	
	0.001	3461	~3210	~3110	1715	1701	
Cyclohexane	0.10	3464	3205	3117		1711	
	0.01	3462	3205	3115	1732	1712	
	0.005				1732	1712	
	0.001				1733	1711	
1,4-Dioxane	0.27		3335		1710		
	0.10		3335		1710		
	0.07		3335		1709		
Liquid			3252	3117			1690 ^c

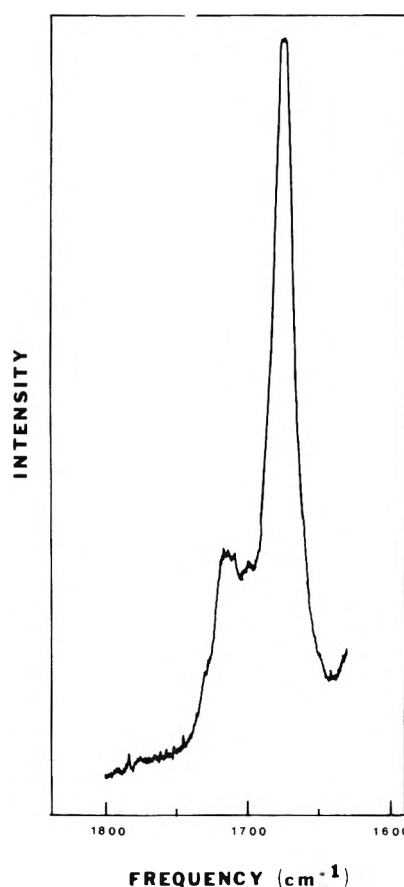
^a Combination of C=O stretching and N-H in-plane deformation vibrations. ^b Contains contributions from dimer and oligomer. ^c Broad.

intensity, but a broadening of the $\nu_{\text{assoc}}(\text{C=O})$ band is observed. The band at 1701 cm^{-1} we assign to the absorption of a hydrogen bonded carbonyl in a dimeric species. Above 0.05 M this band shifts to 1698 cm^{-1} , indicating the presence of a third species or possibly more than one additional species. Rey-Lafon and co-workers¹⁵ report the carbonyl stretching vibration at 1699 cm^{-1} in a 1 M solution in CCl_4 , so it appears that no further shift in this band occurs upon increasing the concentration to this value.

The Raman spectrum in the $1850\text{--}1600\text{-cm}^{-1}$ region for a 0.21 M solution of 2-pyrrolidinone is shown in Figure 3 and the frequencies for two concentrations and the liquid are listed in Table III. Three bands are found in this region and are given the following assignments. The band at 1712 cm^{-1} is assigned to the free C=O groups, most probably from monomeric species. The intense band at 1672 cm^{-1} is assigned to the symmetric stretch of hydrogen bonded carbonyl groups in a planar cyclic dimer in accord with the similar assignment of the band at 1659 cm^{-1} in the liquid by Rey-Lafon.¹⁵ A planar cyclic dimer structure possesses C_{2h} symmetry and the $\nu_s(\text{C=O})$ vibration has A_g symmetry, being Raman active, but not infrared active. A depolarization spectrum of the pure liquid reveals that the band at 1658 cm^{-1} is nearly completely polarized as is expected for a vibration having A_g symmetry. The asymmetric carbonyl stretching vibration for a planar cyclic dimer structure possesses C_{2h} symmetry and the $\nu_s(\text{C=O})$ vibration has A_g symmetry, being Raman active, but not infrared active. A depolarization spectrum of the pure A molecule having C_{2h} symmetry has no coincidences in the infrared and Raman spectra and should be easily identified. Unfortunately, due to solvent interference in some regions and the presence of other species of lower symmetry, it has not been possible to analyze the complete spectrum.

A poorly resolved band in the Raman at approximately 1696 cm^{-1} is attributed to the presence of one or more additional species, more highly polymerized than the dimer. The Raman spectra correlate with the infrared in indicating the presence of at least three species in CCl_4 solutions at concentrations above 0.05 M.

2-Pyrrolidinone in Cyclohexane. Permittivity and refractive index measurements were made on a series of nine solutions varying in concentration from 0.005 to 0.052 M, and on the pure solvent. The upper end of the concentration range was limited by the relatively slight solubility of pure 2-pyr-

Figure 3. Raman spectrum of 0.21 M 2-pyrrolidinone in CCl_4 .

rolidinone in cyclohexane, as compared to solvents such as CCl_4 , benzene, and dioxane. A saturated solution of 2-pyrrolidinone in cyclohexane at 22°C is approximately 0.1 M. A plot of the dielectric polarization data is shown in Figure 4 where the points represent the experimental data.

Numerous models were chosen for this system in an attempt to fit the dielectric polarization data, but none of them resulted in a satisfactory fit. Of these, the monomer-dimer model did result in a minimum in the standard deviation, but this fit was no better than that from any other model. Con-

TABLE III: Raman Frequencies of 2-Pyrrolidinone in the N-H and C=O Stretching Regions

Solvent	Concn, M	$\nu(\text{N-H})_{\text{free}}$, cm^{-1}	$\nu(\text{N-H})_{\text{assoc}}$, cm^{-1}	Comb ^a band, cm^{-1}	$\nu(\text{C=O})_{\text{free}}$, cm^{-1}	$\nu(\text{C=O})_{\text{dimer}}$, cm^{-1}	$\nu(\text{C=O})_{\text{oligomer}}$, cm^{-1}
CCl ₄	0.21	3459	3182	3101	1712	1673	1696
	0.11	3458	~3189	~3100	1712	1670	~1696
Liquid						1658	1698

^a Combination of C=O stretching and N-H in-plane deformation vibrations.

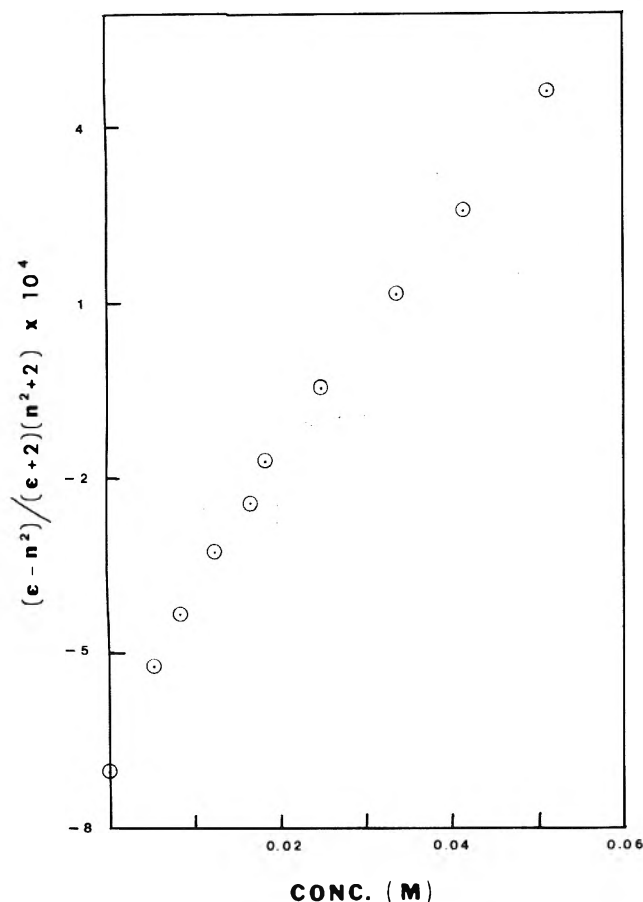


Figure 4. Plot of the dielectric polarization data for 2-pyrrolidinone in cyclohexane at 25 °C.

sequently, we do not report an association constant for 2-pyrrolidinone in cyclohexane. Other models which were tried were: (a) monomer-dimer-trimer, (b) monomer-dimer-tetramer, (c) monomer-trimer, (d) dimer-trimer. The magnitude of the association constant(s) and the dipole moments obtained in attempting to fit a model to the experimental data and the direction in which they change in going from one model choice to another lead us to believe that this system probably contains two major species with only very small amounts, if any, of additional species.

A value of 3.3 D for the dipole moment of the monomer in cyclohexane has been determined graphically. This is lower than the value of 3.55 D in benzene³ and considerably lower than the predicted moment of 4.10 D in nonpolar solvents given by Hopmann.¹³

The infrared spectra in the N-H and C=O stretching regions are shown in Figure 5. The $\nu(\text{N-H})$ region is shown for just the two more concentrated solutions because interference due to solvent absorptions in this region becomes appreciable

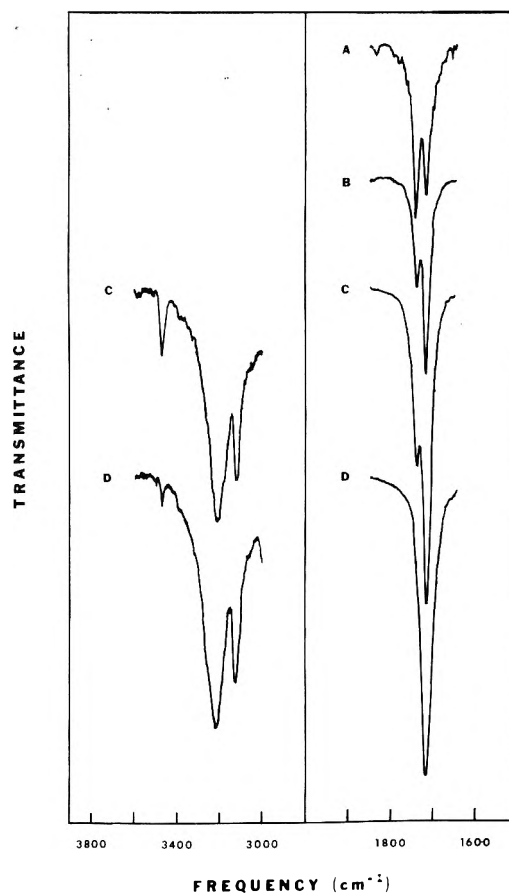


Figure 5. Infrared spectra of 2-pyrrolidinone in cyclohexane: (A) 0.001 M (1.0 mm cell), (B) 0.005 M (1.0-mm cell), (C) 0.01 M (1.0-mm cell), (D) 0.10 M (0.1-mm cell).

in more dilute solutions. The observed frequencies are summarized in Table II. The band at 3462 cm^{-1} due to the stretching vibration of free N-H groups is less intense relative to the 3205-cm^{-1} band in a 0.01 M solution in cyclohexane than is the case of the corresponding bands in a 0.01 M solution in CCl₄, indicative of a greater concentration of associated species in the cyclohexane.

In the carbonyl stretching region, two bands are observed. The higher frequency band at 1732 cm^{-1} , which increases in intensity as the 2-pyrrolidinone concentration decreases, is due to free C=O groups and is assigned to the carbonyl stretching vibration of the monomeric species. The lower frequency band at 1712 cm^{-1} increases in intensity with increasing solute concentration and has been assigned to the $\nu(\text{C=O})$ of hydrogen bonded carbonyl groups, probably in a dimeric species. The fact that the 1712-cm^{-1} band does not shift or exhibit any noticeable broadening from $5 \times 10^{-4}\text{ M}$ up to approximately the limit of solubility suggests that no other more highly associated species are being formed in ap-

preciable quantity. As was the case in the $\nu(\text{N-H})$ region, by comparing the relative intensities of the two carbonyl bands at the same concentrations in cyclohexane and in CCl_4 it can be seen that the equilibrium lies further toward the associated species in cyclohexane than in CCl_4 .

Unfortunately it was impossible to obtain Raman spectra of 2-pyrrolidinone in cyclohexane because of interference of solvent bands. However, in light of the strong evidence for the existence of planar, or approximately planar, cyclic dimers in the liquid and in CCl_4 solutions, it is very likely that the same type of dimer species would exist in cyclohexane. The low solubility and the high value of the free C=O stretching frequency of 2-pyrrolidinone in cyclohexane indicate that the lactam interacts very little with this solvent. Under such circumstances the formation of a cyclic dimer appears even more favorable. Accordingly, the band in the infrared at 1712 cm^{-1} is tentatively assigned to the $\nu_{\text{as}}(\text{C=O})$ of a planar cyclic dimer.

2-Pyrrolidinone in Dioxane. The dipole moment of 2-pyrrolidinone in 1,4-dioxane was determined and found to be $3.80 \pm 0.01\text{ D}$. This agrees well with the value of 3.79 D at 30°C reported by Lee and Kumler.²⁸ The dipole moment was determined from measurements on a series of five solutions varying in concentration from 0.016 to 0.05 M plus the pure solvent. The plot of $\epsilon - n^2/(\epsilon + 2)(n^2 + 2)$ vs. concentration (mol/ml) resulted in a straight line, indicative of the presence of a single species. The infrared spectra also indicate the presence of one solute species in dioxane. In the N-H stretching region a single, broad absorption occurs at 3335 cm^{-1} ; there is no absorption in the region of nonhydrogen bonded N-H . In the C=O stretching region, a single absorption is again observed, occurring at 1710 cm^{-1} . This band does not split or shift upon changing the concentration. It is concluded that 2-pyrrolidinone does not undergo self-association in dioxane, but that oxygen atoms of the dioxane form hydrogen bonds with the N-H of the 2-pyrrolidinone.^{18,23c}

Discussion

2-Pyrrolidinone and other cis lactams do not exhibit the simple behavior in nonpolar solvents that early investigators had anticipated. Because most studies were conducted on very dilute solutions using spectroscopic techniques the presence of trimers or higher n -mers was undetected until recent dielectric loss measurements.^{13,14} In view of the abundance of species which have been found to exist in systems undergoing self-association through hydrogen bonding,^{29,30} it is perhaps surprising that species besides the monomer and dimer have not been sought.

The behavior of cis lactams and carboxylic acids in nonpolar solvents is analogous in several respects. First they both have a propensity for the formation of cyclic dimers containing eight-membered rings and second the apparent dielectric properties of the dimers are similar.^{3,23d} It has not been possible to explain all the experimental data on carboxylic acid solutions on the basis of a monomer-dimer model³⁰ and in several instances a monomer-dimer-chain oligomer model has been used to explain the data on acetic acid in CCl_4 .^{31,32} The analysis of these systems is hampered by the lack of experimental methods sensitive enough to distinguish between very similar species sometimes present in very low concentrations and by the coexistence of multiple species.

A combined consideration of the spectroscopic and dielectric polarization data for 2-pyrrolidinone in CCl_4 shows the necessity of including species more highly polymerized than the dimer and suggests that the important species is a

trimer. However, the existence of still higher oligomers cannot be excluded at this time. That a planar, cyclic dimer is present is quite certain and all our data point to a cyclic trimer, but acyclic dimers and trimers may also be present. The value of the dimerization constant, K_1 , is approximately the same or slightly lower than the literature values determined spectroscopically for a monomer-dimer model. The latter are summarized in Table IV. The magnitude and the direction of the difference between dimerization constants based on a monomer-dimer-trimer model and those based on a monomer-dimer model are dependent upon the structure of the species (cyclic or acyclic) and upon assumptions made about the system and, therefore, are difficult to predict. Dimerization constants from infrared measurements usually have been calculated^{5,7,8} assuming that the stretching vibration of free N-H groups arises only from monomeric structures and that the remainder of the 2-pyrrolidinone exists as the cyclic dimer. If nonhydrogen bonded N-H groups from an acyclic structure are contributing to the $\nu_{\text{free}}(\text{N-H})$, and it may not be possible to distinguish between the $\nu(\text{N-H})$ of monomer and that of chain end groups,^{29a} then an error is introduced causing the dimerization constant to appear too small. On the other hand, the neglect of species other than the monomer and dimer will cause the dimerization constant to appear too large. Using dielectric polarization data no assumption concerning the structure of a particular species is necessary.

The dipole moment of 3.74 D for the monomer in carbon tetrachloride is slightly lower than the value of 3.80 D in dioxane. It is higher than the value of 3.5 D determined graphically and the value of 3.55 D in benzene³ also determined graphically. Graphical determinations in multicomponent systems are prone to large errors because it is necessary to determine the slope of the tangent to the curve at infinite dilution. For comparison, the vapor phase moment of formamide is 3.71 D ³³ and its moments in benzene and dioxane are 3.37 and 3.86 D , respectively.³⁴

The dipole moment of the dimer in CCl_4 as calculated by the computer fit of the data is 1.64 D . Huisgen and Walz³ reported a dimer moment of 2.2 D in benzene, using a monomer-dimer model. As stated earlier the dipole moment of a planar, cyclic dimer structure is expected to be zero or very small due to cancellation of the moments. Relatively high dipole moments have also been observed for carboxylic acid dimers in solution.³⁵ These high apparent moments have been explained most often as resulting from a large atomic polarization of the dimer^{17b,23d} which is inadequately compensated for in the usual assumptions that the atomic polarization is about 5–10% of the electronic polarization or that errors in the refractive index measurements essentially correct for neglect of the atomic polarization term. The assumptions about the normal magnitude of the atomic polarization have been arrived at from measurements on molecules containing ordinary bonds. However, the carboxylic acid and lactam cyclic dimers are held together by very weak bonds and it seems reasonable that these molecules will have a number of low frequency stretching, bending, and twisting vibrations due to the dimer ring which could significantly increase the atomic polarization.

Another possible source of the high dipole moment of the dimer species would be the coexistence of cyclic and acyclic dimer structures. An acyclic dimer is expected to have a dipole moment greater than that of the monomer. In such a situation the μ^2 observed would be equal to a weighted average of the μ_{cyclic}^2 and μ_{acyclic}^2 . This would be experimentally indistinguishable from the case where there is a cyclic dimer having

TABLE IV: Summary of Dimerization Constants Determined Spectroscopically for 2-Pyrrolidinone in CCl₄

$K_D,^a \text{ M}^{-1}$	$t, ^\circ\text{C}$	Ref
160 ± 20	22	13
116 ± 2	25	8
150^b	25	7
290^c	25	5

^a Based on a monomer-dimer model. ^b Calculated from the thermodynamic parameters given in the reference. ^c Recalculated from molal⁻¹ units assuming the density to be that of pure CCl₄.

a large atomic polarization. It may be possible to decide between the two choices by studying a given cis lactam in a variety of nonpolar solvents. The atomic polarization of a cyclic dimer should be approximately the same in all the solvents, but the equilibrium between cyclic and acyclic dimer structures may be highly solvent dependent.

The trimer moment of 3.8 D in CCl₄ has been interpreted as indicating that the trimer has predominantly a cyclic structure. In trans lactams where chain oligomers are formed the molar polarization increased over that of the monomer as the concentration increased.³ Therefore, it is believed that an acyclic trimer structure would possess a dipole moment considerably greater than that of the monomer. There is no apparent reason to expect a cyclic trimer structure to have a zero dipole moment since the cyclic dimer does not. Similarly to the dimeric species, the presence of some acyclic trimer along with the cyclic trimer cannot be eliminated as a possibility at this time. It should be noted here that using molecular models a planar, cyclic trimer structure has unfavorable angles for hydrogen bonding. By allowing the nitrogen atoms to have a pyramidal geometry, numerous configurations of a cyclic trimer are possible. Although we do not have any evidence for nonplanarity of the amide group in 2-pyrrolidinone in solution, we felt it valid to consider the possibility of a nonplanar nitrogen atom in the preparation of models because the dimer ring in 4-iodomethyl-2-pyrrolidinone is not completely planar (vide supra) and because a few nonplanar cis amides have been reported.^{1,36,37}

Further support for a cyclic, as opposed to an acyclic, trimer comes from the infrared data. The ratio of the absorptivities per N-H group of the free N-H stretching vibration at 3460 cm⁻¹ in CCl₄ to that of the associated N-H stretching vibration at 3210 cm⁻¹ is related to the concentration, c , and absorbance, A , as expressed in

$$\frac{a_{\text{free}}}{a_{\text{assoc}}} = \frac{A_{3460} c_{\text{assoc N-H}}}{A_{3210} c_{\text{free N-H}}} \quad (15)$$

The absorptivity ratio should be a constant and its constancy or lack of it can be used to test a chosen model system. The equilibrium constants in Table I were used to calculate the concentrations of monomers, dimers, and trimers. Assumptions were then made about the structure of each species and the concentrations of free and associated N-H groups were computed. For example, a molecule of acyclic trimer contains two associated N-H groups plus one free N-H group. When it was assumed that all the dimer and all the trimer exist as cyclic structures, the ratio $a_{\text{free}}/a_{\text{assoc}}$ calculated for a series of spectra ranging in total concentration from 0.01 to 0.27 M was constant to within $\pm 8\%$ and the deviations were random. However assuming all the dimer to be cyclic and all the trimer acyclic led to ratios which decreased as the total concentration

of 2-pyrrolidinone increased, indicating that this latter assumption about the nature of the species was incorrect.

That 2-pyrrolidinone exists in an associated state in cyclohexane is apparent from the infrared spectra and from a cryoscopic study which gave a molecular weight of 169.6 at a concentration of 0.013 m (0.010 M). The theoretical molecular weight of the dimer is 170.21. This large amount of association and the limited solubility of 2-pyrrolidinone in this solvent are believed to be the reasons for our inability to find a model which would satisfactorily fit the dielectric polarization data. In order to determine a dimerization constant, considerable data on solutions less concentrated than 0.01 M are required. Both of the dimerization constants reported in the literature^{8,13} were determined from measurements on solutions whose concentrations were 0.01 M or greater. Hopmann has used a monomer-dimer-trimer model to fit data obtained by a dielectric relaxation technique and has reported a dimerization constant of 1600 M⁻¹ and a trimerization constant of 40 M⁻¹.¹³ From a study of ϵ -caprolactam and 2-pyrrolidinone in nonpolar solvents he concluded that trimerization occurred in cyclohexane and, to a lesser extent, in CCl₄, but did not occur in benzene.

Contrary to Hopmann's findings, the infrared spectra in the carbonyl stretching region indicate trimer or higher oligomer formation in CCl₄, but not in cyclohexane. However, this does not constitute proof that trimerization does not occur at all in cyclohexane. In general the type and degree of self-association which occurs seems to be dependent upon the nature of the solvent and upon its interaction with the solute.

Acknowledgments. This research was supported by the National Science Foundation. We wish to thank Mr. Max Diem for running the Raman spectra and Dr. Duane F. Burow for his helpful discussions.

Supplementary Material Available: Tables of the concentration, dielectric constant, and refractive index data for Figures 1 and 2 are available (1 page). Ordering information is available on any current masthead page.

References and Notes

- H. E. Hallam and C. M. Jones, *J. Mol. Struct.*, **1**, 413 (1968).
- C. Y. S. Chen and C. A. Swenson, *J. Phys. Chem.*, **73**, 2999 (1969).
- R. Huisgen and H. Walz, *Chem. Ber.*, **89**, 2616 (1956).
- M. Tsuboi, *Bull. Chem. Soc. Jpn.*, **24**, 75 (1951).
- H. E. Auffsprung, S. D. Christian, and J. D. Worley, *Spectrochim. Acta*, **20**, 1415 (1964).
- W. Klemperer, M. W. Cronyn, A. H. Maki, and G. C. Pimentel, *J. Am. Chem. Soc.*, **76**, 5846 (1954).
- C. Y. S. Chen and C. A. Swenson, *J. Phys. Chem.*, **73**, 1363 (1969).
- K. Wagner, G. Rudakoff, and P. Frolich, *Z. Chem.*, **15**, 272 (1975).
- R. C. Lord and T. J. Porro, *Z. Electrochem.*, **64**, 672 (1960).
- G. Montaudo, S. Caccamese, and A. Recca, *J. Phys. Chem.*, **79**, 1554 (1975).
- L. F. Blackwell, P. D. Buckley, K. W. Jolley, and I. D. Watson, *Aust. J. Chem.*, **25**, 67 (1972).
- J. M. Purcell, H. Susi, and J. R. Cavanaugh, *Can. J. Chem.*, **47**, 3655 (1969).
- R. F. W. Hopmann, *J. Phys. Chem.*, **78**, 2341 (1974).
- L. Hellemans and L. De Maeyer, *J. Chem. Phys.*, **63**, 3490 (1975).
- M. Rey-Lafon, M.-T. Forel, and J. Lascombe, *J. Chim. Phys.*, **64**, 1435 (1967).
- A. L. Ball, R. Desiderato, and G. R. Freeman, *Cryst. Struct. Commun.*, **2**, 565 (1973).
- N. E. Hill, W. E. Vaughn, A. H. Price, and M. Davies, "Dielectric Properties and Molecular Behavior", Van Nostrand-Reinhold, London, 1969: (a) p 124; (b) pp 261-264.
- H. B. Thompson, *J. Chem. Educ.*, **43**, 66 (1966).
- H. B. Thompson and M. T. Rogers, *J. Chem. Educ.*, **32**, 20 (1955).
- H. B. Thompson and C. C. Sweeney, *J. Phys. Chem.*, **64**, 221 (1960).
- M. G. Brown and D. J. T. Hill, *J. Chem. Educ.*, **47**, 484 (1970).
- M. Diem, J. L. Fry, and D. F. Burow, *J. Am. Chem. Soc.*, **95**, 253 (1973).
- J. W. Smith, "Electric Dipole Moments", Butterworths, London, 1955: (a) p 58; (b) p 60; (c) pp 311-313; (d) pp 306-312.

- (24) E. A. Guggenheim, *Trans. Faraday Soc.*, **45**, 714 (1949).
 (25) The value of the intercept was determined by the data fit in order that the experimental intercept (pure solvent) would be weighted no more heavily than any other experimental point.
 (26) The symbol ν is used to denote the stretching vibration of the indicated group.
 (27) T. Miyazawa, *J. Mol. Spectrosc.*, **4**, 168 (1960).
 (28) C. M. Lee and W. D. Kumler, *J. Am. Chem. Soc.*, **83**, 4593 (1961).
 (29) G. C. Pimentel and A. L. McClellan, "The Hydrogen Bond", W. H. Freeman, San Francisco, Calif., 1960, (a) p 96.
 (30) M. D. Joesten and L. J. Schaad, "Hydrogen Bonding", Marcel Dekker, New York, N.Y., 1974, pp 279-290.
 (31) M. A. Goldman and M. T. Emerson, *J. Phys. Chem.*, **77**, 2295 (1973), and references therein.
 (32) J. T. Bulmer and H. F. Shurvell, *J. Phys. Chem.*, **77**, 256 (1973).
 (33) R. J. Kurland and E. B. Wilson, *J. Chem. Phys.*, **27**, 585 (1957).
 (34) W. W. Bates and M. E. Hobbs, *J. Am. Chem. Soc.*, **73**, 2151 (1951).
 (35) H. A. Pohl, M. E. Hobbs, and P. M. Gross, *J. Chem. Phys.*, **9**, 408 (1941).
 (36) F. K. Winkler and J. D. Dunitz, *J. Mol. Biol.*, **59**, 169 (1971).
 (37) J. Smolikova, M. Tichy, and K. Blaha, *Collect. Czech. Chem. Commun.*, **41**, 413 (1976).

Mean Activity Coefficients for the Simple Electrolyte in Aqueous Mixtures of Polyelectrolyte and Simple Electrolyte. The Mixed Counterion System Na^+ , Ca^{2+} , Cl^- , Polystyrenesulfonate

Jan C. T. Kwak,* Nancy J. Morrison, Ester J. Spiro, and Kunihiko Iwasa

Department of Chemistry, Dalhousie University, Halifax, Nova Scotia, Canada (Received July 30, 1976)

Publication costs assisted by the National Research Council of Canada

Activity coefficients of NaCl and CaCl_2 , measured with a galvanic cell method, in aqueous polyelectrolyte solutions containing Na^+ , Ca^{2+} , Cl^- , and poly(styrenesulfonate) $^-$ ions are reported. The measurements were performed with series of solutions at constant polyion and constant chloride ion concentrations, and varying Na^+ to Ca^{2+} ratios. Polystyrenesulfonate concentrations of 0.0505, 0.02, 0.01, and 0.005 equiv/kg of water were used, chloride concentrations varied from excess polyelectrolyte to excess chloride. The results are compared to theoretical predications based on Manning's limiting laws for the activity of the small ions. They show, on one hand, the expected increase in the activity coefficient of NaCl as the Na^+ equivalent fraction x_{Na} decreases, as well as the decrease in the CaCl_2 activity coefficient as the Ca^{2+} equivalent fraction x_{Ca} decreases, but in the CaCl_2 case the activity coefficient does not drop to zero, as predicted by counterion condensation theory. It is shown that a semiempirical modification of the limiting laws, based on the assumption that a certain fraction of Ca^{2+} ions remains uncondensed, leads to reasonable agreement with the experimental results for $\gamma_{\pm}(\text{CaCl}_2)$ at low x_{Ca} values, without appreciably influencing the theoretical predictions for $\gamma_{\pm}(\text{CaCl}_2)$ at high x_{Ca} values, and for $\gamma_{\pm}(\text{NaCl})$, both of which are in good agreement with the experimental results.

The measurement of the activities of the simple electrolytes in polyelectrolyte solutions to which both uni-univalent and di-univalent electrolytes have been added is of considerable practical and theoretical importance. Such mixtures approximate the composition of many biological fluids, in which typically Na^+ , K^+ , Ca^{2+} , Mg^{2+} , Cl^- , and a colloid or polymeric anion are the major ionic constituents. The colloid or polymeric anion may be an ionic polysaccharide, a protein, DNA or RNA, etc. From a theoretical point of view, so far two approaches have been used to describe the thermodynamic properties of mixed counterion-polyelectrolyte solutions. Manning¹ applied his limiting laws, which incorporate both condensation and Debye-Hückel type effects, to mixed counterion systems in the absence of added electrolyte. In this paper we will make extensive use of Manning's description of these systems. Dolar, Skerjanc, and co-workers²⁻⁶ have applied the so-called cell model, which solves the Poisson-Boltzmann equation for specified boundary conditions, to mixed counterion systems in order to calculate osmotic coefficients, heats of mixing and heats of dilution, and volume changes on dilution in salt-free systems. In two previous papers^{7,8} we reported

measurements of the mean activity coefficient of the added electrolyte in mixtures of salts of poly(styrenesulfonic acid) with simple chloride salts containing a common cation. Na^+ , K^+ , Mg^{2+} , and Ca^{2+} salts were studied using an electrochemical technique. The choice of polystyrenesulfonate as the polymer ion was made on the basis of its well-known structural parameters, the degree of purification obtainable, and stability of the polymer, and because of the large amounts of thermodynamic and transport data available for salts of this polyion. In this paper we report measurements of the mean activity coefficients of NaCl and of CaCl_2 in aqueous mixtures containing Na^+ , Ca^{2+} , Cl^- , and PSA^- , where PSA^- stands for a polymer segment carrying one unit of negative charge (i.e., one sulfonate group). As in any multicomponent system, there are a number of possibilities for varying the composition of the mixtures. We chose to vary the Na^+ to Ca^{2+} ratio while keeping the polyion and the Cl^- molality constant, and did this for a number of polyion molalities and polyion to the Cl^- molality ratios. Thus, we report values for $\gamma_{\pm}(\text{NaCl})$ and $\gamma_{\pm}(\text{CaCl}_2)$ as a function of the equivalent Na^+ fraction at constant polyion molality m_p and constant polyion to chloride

molality ratio X . We will compare our results to values predicted from Manning's treatment of this case. We will show the detailed results of the limiting laws for activity coefficients in mixed valency counterion systems later, but it is useful to briefly outline the major results now. Basically, condensation theory,⁹ as applied by Manning to mixed counterion systems without added salt,¹ predicts that for a given polyion concentration, mixtures with high equivalent fractions of the divalent counterion (region I) will exhibit the normal partial condensation of the divalent counterion, but the univalent counterion is not condensed at all. In mixtures with high equivalent fractions of the univalent counterion (region III), all divalent counterions are condensed on the polyion, making their activity zero. In addition, part of the univalent counterions are condensed as well. In between these two regions, there is a region (region II) where the divalent counterion is completely condensed, but where the univalent counterion is not yet condensed. In systems with added simple electrolyte, the situation is qualitatively the same, but the transition points between the three regions now depend on the composition of the added electrolyte (Figure 1). Thus, counterion condensation theory predicts a very striking dependence of the divalent counterion activity coefficient on the ionic composition of the mixture, and of course the situation in region III invites comparison with the behavior of Ca^{2+} or Mg^{2+} in the cellular fluid. As before, we stress that only purely electrostatic interactions are considered in Manning's description,¹ as well as in cell model calculations.²⁻⁶

It is the aim of this paper to study a system in which contributions from "special" interactions are expected to be minimal. Our results in similar systems with only one counterion⁸ seem to bear out that this is indeed the case. It may well be that special interactions do play a role in systems with other charged groups on the polymer (e.g., carboxylic groups) or with counterions which do not have a closed shell electronic structure, and extensions of our measurements to such systems will be of considerable interest.

Very few experimental results for thermodynamic or transport properties in mixed counterion polyelectrolyte solutions have been reported. Osmotic coefficients, heats of mixing, heats of dilution, and volume changes on dilution for univalent-divalent counterion mixtures of polystyrenesulfonate were determined by Dolar and Skerjanc²⁻⁶ at a number of polyion concentrations. The cell model as well as Manning's theory predict a maximum in the osmotic coefficient ϕ when plotted as a function of the equivalent fraction of univalent counterions. This maximum was indeed observed, but at higher univalent ion equivalent fractions than predicted.

The only activity coefficient measurements in mixed counterion polyelectrolyte systems of which we are aware were performed by Rinaudo and Milas¹⁰ on salt-free mixtures of sodium and calcium carboxymethylcellulose (CMC), using two CMC samples, one of moderate and one of high charge density. Although the Na^+ and Ca^{2+} single ionic activity coefficients reported by these authors are subject to the usual uncertainties of such measurements, the results show the two major effects given above, i.e., the increase in the activity coefficient of Na^+ as its equivalent fraction decreases, and a strong decrease in the Ca^{2+} activity coefficient as the Ca^{2+} equivalent fraction decreases. Moreover, their results clearly show the influence of the charge density of the polyion, at least in qualitative agreement with the theoretical expressions given below.

Interesting though necessarily qualitative information regarding polyion-small ion interactions in mixed valency

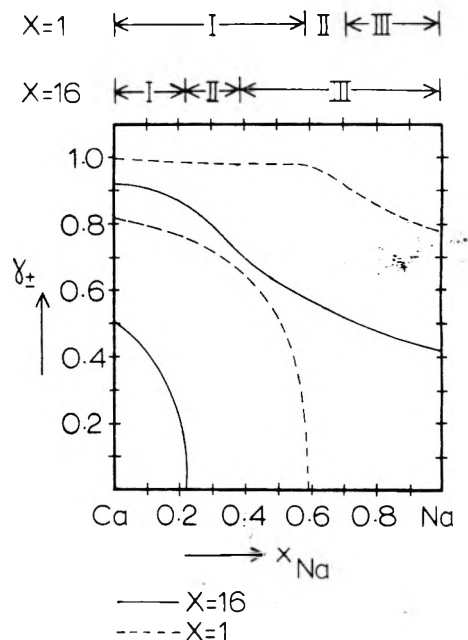


Figure 1. Limiting law predictions for $\gamma_{\pm}(\text{CaCl}_2)$ (lower two curves) and $\gamma_{\pm}(\text{NaCl})$ (upper two curves): full lines, $X = 16$; broken lines, $X = 1$.

counterion systems has come from dielectric increment and from nuclear magnetic relaxation measurements performed in recent years. Minakata et al.¹¹ and Mandel and co-workers^{12,13} found that the reduced dielectric increment exhibits a maximum as the equivalent fraction of the univalent ion is increased. It seems that the interpretation of dielectric increment data is still rather difficult. More direct information has come from the ^{23}Na nuclear magnetic relaxation measurements of Leyte et al.¹⁴ Using mixtures of sodium and barium polystyrenesulfonate, these authors demonstrated the removal of the Na^+ ion from the polyion as the Ba^{2+} content of the mixture increased. They also concluded that at least the larger part of the Ba^{2+} resides near the polyion, but is not bound to a single fixed charge.

We will now consider in detail the activity coefficients of NaCl and of the CaCl_2 in the three regions mentioned earlier. In doing so, we will closely follow Manning's treatment of the mixed valency counterion system (ref 1, pp 17-22), which gave all relevant equations for the salt-free systems. Moreover, Manning¹⁵ and DeMarky and Manning¹⁶ considered such systems under excess uni-univalent salt conditions to derive expressions for the free energy per charged group of the polyion. In their case, the condition of excess salt, although stated, was not used explicitly in the derivations involved. For these reasons we will only give a brief summary of the premises underlying our treatment and then proceed to give the final results. We refer to Manning's papers for a more detailed description. It should be pointed out that although we will compare our results to these limiting laws, which are based on counterion condensation theory, the expressions derived are strictly valid only for line and point charges without any interactions between the line charges. Both the introduction of finite radii, and therefore of repulsive forces, and of polyion-polyion interactions may seriously affect the condensation phenomenon. Such an effect would be noticed especially in the mixed counterion systems studied here, because a breakdown of the prediction of complete condensation of the divalent counterion in regions II and III would completely alter the predicted activity coefficients. Aside from this

modeling problem, one might also ask whether complete condensation of any ion is possible even in the limiting case, because in certain respects complete condensation seems to contradict conventional thermodynamic arguments. We defer a detailed discussion of the counterion condensation problem to a later publication, and will use this paper to compare our experimental results to the limiting laws, which will enable us to detect where the most serious deviations occur.

Consider a system $\text{Na}^+, \text{Ca}^{2+}, \text{Cl}^-, \text{P}^- + \text{H}_2\text{O}$. All concentrations are given as molalities. The polymer concentration m_P is defined as the number of charged groups P^- per kilogram of H_2O (notice this definition is different from the one used in ref 8). We further define $X = m_P/m_{\text{Cl}}$, the charge density parameter $\xi = e|\beta|/DkT^{1.8}$ with e the proton charge, $|\beta|$ the charge in a unit length of polyion, D the dielectric constant, k Boltzmann's constant, and T the temperature; $x_{\text{Na}} = 1 - x_{\text{Ca}} = m_{\text{Na}}/(m_{\text{Na}} + 2m_{\text{Ca}})$ is the equivalent fraction of Na^+ ions. In our work, we find it more convenient to work with x_{Na} or x_{Ca} , X , and m_P as the three composition variables, rather than m_P , m_{A^+} , and $r = 2m_{\text{B}^{2+}}/m_P$ used by DeMarky and Manning,¹⁶ but the resulting equations can easily be converted. In our notation, $r = x_{\text{Ca}}(1 + X^{-1})$. As before, it is assumed that condensation of counterions takes place when ξ exceeds a critical value which depends on the valency of the counterion, $\xi_{\text{crit}} = 1$ for univalent counterions and 0.5 for divalent counterions.

Condensed counterions are assumed to have zero activity. Uncondensed counter- and coions are influenced by the net remaining charge of the polyion. This causes a lowering of their activity given by^{17,18}

$$\ln \gamma_i = -\frac{1}{2}\xi\lambda m_P z_i^2 \kappa^{-2} \quad (1)$$

where $\lambda = 4\pi e^2/DkT$, z_i is the valency of ion i , and κ^2 is the Debye-Hückel screening parameter,¹⁷ given by $\kappa^2 = \lambda \sum_i m_i z_i^2$ the summation i being over all small ions. γ_i is the molal activity coefficient of ion i .

Manning distinguishes three cases for the charge density parameter and his reasoning can easily be applied to the salt added systems. In all cases, our equations can be compared to Manning's results (ref 1) by setting $X = \infty$.

Case 1. $\xi < 1/2$. Neither of the two counterions (Na^+ and Ca^{2+}) condenses, and all activity coefficients are given by eq 1, which in our notation reads:

$$\ln \gamma_i = -\frac{1}{2}\xi z_i^2 \{1 + 2X^{-1} + (1 - x_{\text{Na}})(1 + X^{-1})\}^{-1} \quad (2)$$

Case 2. $1/2 < \xi < 1$. Two regions can now be distinguished:

Region I: Mixtures rich in Ca^{2+} , with enough Ca^{2+} to make $\xi_{\text{net}} = 1/2$. m_{Ca} must exceed $1/2 m_P(1 - 1/2\xi^{-1})$, or $(1 - 1/2\xi^{-1})(1 + X^{-1})^{-1} < x_{\text{Ca}}$.

Only Ca^{2+} condenses, the fraction Ca^{2+} condensed equals $1/2(m_P/m_{\text{Ca}})(1 - 1/2\xi^{-1})$. The remaining uncondensed Ca^{2+} ions as well as the Na^+ and Cl^- ions are described by eq 1 for a polyion with $\xi = 1/2$. We obtain

$$\ln \gamma_{\text{Na}^+} = \ln \gamma_{\text{Cl}^-} = -8^{-1} \{1 + 3\xi X^{-1} - x_{\text{Na}}\xi(1 + X^{-1})\}^{-1} \quad (3)$$

$$\ln \gamma_{\text{Ca}^{2+}} = -\frac{1}{2} \{1 + 3\xi X^{-1} - x_{\text{Na}}\xi(1 + X^{-1})\}^{-1} + \ln \{1 - X(1 - 1/2\xi^{-1})(1 - x_{\text{Na}})^{-1}(1 + X)^{-1}\} \quad (4)$$

In (4), we recognize the first term on the right-hand side as a "Debye-Hückel" term, and the second term as a "condensation" term.

Region II: $x_{\text{Ca}} < (1 - 1/2\xi^{-1})(1 + X^{-1})^{-1}$. There is not enough Ca^{2+} to make $\xi_{\text{net}} = 1/2$. All Ca^{2+} condenses, but because $\xi < 1$, no Na^+ condenses. ξ_{net} will equal $\xi \{1 - (1 - x_{\text{Na}})(1 + X^{-1})\}$.

$$\ln \gamma_{\text{Na}^+} = \ln \gamma_{\text{Cl}^-} = -\frac{1}{2}\xi \{x_{\text{Na}}(1 + X^{-1}) - X^{-1}\}^2 \times \{x_{\text{Na}}(1 + X^{-1}) + X^{-1}\}^{-1} \quad (5)$$

$$\gamma_{\text{Ca}^{2+}} = 0 \quad (6)$$

Case 3. $1 < \xi$. Now, three regions can be distinguished. In the first region, there is enough Ca^{2+} present to make $\xi_{\text{net}} = 1/2$, in the second region there is not enough Ca^{2+} to make $\xi_{\text{net}} = 1/2$, but enough to make $\xi_{\text{net}} = 1$. In the third region there is not enough Ca^{2+} to make $\xi_{\text{net}} = 1$, and additional Na^+ has to condense.

Region I: Enough Ca^{2+} to make $\xi_{\text{net}} = 1/2$. m_{Ca} must exceed $1/2 m_P(1 - 1/2\xi^{-1})$, or $(1 - 1/2\xi^{-1})(1 + X^{-1})^{-1} < x_{\text{Ca}}$. The expressions for $\ln \gamma_{\text{Na}^+}$, $\ln \gamma_{\text{Cl}^-}$, and $\ln \gamma_{\text{Ca}^{2+}}$ are identical with those in region I of case 2 (eq 3 and 4).

Region II: Enough Ca^{2+} to make $\xi_{\text{net}} = 1$, but not enough to make $\xi_{\text{net}} = 1/2$. $1/2 m_P(1 - \xi^{-1}) < m_{\text{Ca}} < 1/2 m_P(1 - 1/2\xi^{-1})$, or $(1 - \xi^{-1})(1 + X^{-1})^{-1} < x_{\text{Ca}} < (1 - 1/2\xi^{-1})(1 + X^{-1})^{-1}$. All Ca^{2+} will be condensed, but no Na^+ is condensed yet. ξ_{net} will have an intermediate value between $1/2$ and 1: $\xi_{\text{net}} = \xi \{1 - (1 - x_{\text{Na}})(1 + X^{-1})\}$. The expressions for $\ln \gamma_{\text{Na}^+}$, $\ln \gamma_{\text{Cl}^-}$, and $\gamma_{\text{Ca}^{2+}}$ are identical with those in region II of case 2 (eq 5 and 6).

Region III. Not enough Ca^{2+} to make $\xi_{\text{net}} = 1$, $m_{\text{Ca}} < 1/2 m_P(1 - 1/\xi)$ or $x_{\text{Ca}} < (1 - \xi^{-1})(1 + X^{-1})^{-1}$. All Ca^{2+} condenses, but still additional Na^+ has to condense. The fraction Na^+ condensed equals $1 - (m_P/m_{\text{Na}})(\xi^{-1} + X^{-1})$. As before, the remaining uncondensed Na^+ is described by eq 1, for a polyion with $\xi_{\text{net}} = 1$. We obtain

$$\ln \gamma_{\text{Na}^+} = -\frac{1}{2}(1 + 2\xi X^{-1})^{-1} + \ln \{(\xi^{-1} + X^{-1})x_{\text{Na}}^{-1}(1 + X^{-1})^{-1}\} \quad (7)$$

where again we recognize the first term on the right-hand side as a Debye-Hückel term and the second term as a condensation term. Also

$$\ln \gamma_{\text{Cl}^-} = -\frac{1}{2}(1 + 2\xi X^{-1})^{-1} \quad (8)$$

Again, the activity coefficient of Ca^{2+} equals zero.

In all cases, mean activity coefficients for NaCl and CaCl_2 are defined by $\gamma_{\pm}^2(\text{NaCl}) = \gamma_{\text{Na}^+}\gamma_{\text{Cl}^-}$ and $\gamma_{\pm}^3(\text{CaCl}_2) = \gamma_{\text{Ca}^{2+}}\gamma_{\text{Cl}^-}^2$. Thus, $\gamma_{\pm}(\text{CaCl}_2)$ is zero in the regions where all Ca^{2+} is condensed.

The vinylic backbone type polyelectrolyte used in this study has a charge density parameter $\xi = 2.8$, thus we will consider the equations derived for case 3, $\xi > 1$, in some detail. In regions I and II, the Na^+ ion is not condensed, and the Na^+ and Cl^- are influenced by the polyion atmosphere only. However because of the presence of Ca^{2+} , even this Debye-Hückel term is much smaller than in the case when no Ca^{2+} is present (compare eq 3 with eq 8). Thus, as x_{Na} approaches 0, the Na^+ and Cl^- ions are effectively screened from the influence of the polyion, and their activity coefficients and $\gamma_{\pm}(\text{NaCl})$ reach high values. In region III, increasingly more Na^+ condenses as x_{Na} approaches 1 and γ_{Na^+} and $\gamma_{\pm}(\text{NaCl})$ are decreased correspondingly. On the other hand, condensation theory predicts that the Ca^{2+} ion has a finite activity only in region I, and is completely condensed in regions II and III. The values of x_{Ca} , where the transitions between regions I and II and between regions II and III takes place, depend on the composition of the added salt. It is for this reason that DeMarky and Manning used r , the ratio of the equivalent concentration of divalent ions over m_P , as the main composition variable. In our notation, the transition points will shift to lower x_{Ca} values as $X (= m_P/m_{\text{Cl}})$ decreases for systems at constant m_P . (Notice that all expressions for the activity coefficients derived before are of course independent of m_P , but m_P does enter as a composition variable because $m_P + m_{\text{Cl}} = 2m_{\text{Ca}} + m_{\text{Na}}$)

Figure 1 shows the transition points for the cases $X = 16$ and $X = 1$, as well as the limiting law curves for $\gamma_{\pm}(\text{NaCl})$ and $\gamma_{\pm}(\text{CaCl}_2)$. We notice that as X decreases, both γ_{\pm} curves shift to higher values, and that region II becomes smaller. Figure 2 of Manning's paper (ref 1) shows the curves for γ_{Na^+} and $\gamma_{\text{Ca}^{2+}}$ in the salt free case. Our curves for $X = 16$ closely approximate the salt-free case.

The limiting laws do not account for Debye-Hückel type interactions between the remaining small ions. As before,⁸ we will empirically correct for these interactions by dividing the measured value of γ_{\pm} by γ_{\pm}^0 , where γ_{\pm}^0 is activity coefficient of the pure electrolyte under consideration at the same ionic strength as the total added electrolyte mixture in the polyelectrolyte solution:

$$\gamma_{\pm}(\text{corr}) = \gamma_{\pm}(\text{measd})/\gamma_{\pm}^0 \quad (9)$$

This is an obvious generalization of the correction procedure which proved successful in mixtures with only one counterion,^{7,8,18-20} and was shown to be theoretically justified.²¹ In applying this method in mixed valency counterion systems, a slight ambiguity arises in calculating the ionic strength of the added electrolyte mixture, because at low Ca^{2+} equivalent fractions a large part or all of the Ca^{2+} is condensed. However, for the concentration range covered in this work, the difference between using the actual ionic strength (i.e., taking into account the expected condensation of the Ca^{2+} ion) and the stoichiometric ionic strength was found not to appreciably alter the correction term, and we have used the latter method throughout.

Experimental Section

Sodium poly(styrenesulfonate) (NaPSA) was kindly supplied by the Dow Chemical Co., Midland, Mich. (designation SC 1585, average mol wt 5×10^5). Purification procedures, conversion to the Na^+ and Ca^{2+} form, and concentration determinations of the final stock solutions were described earlier.^{7,8} "Ultrapure" NaCl (Ventron Co., Beverly, Mass.) and analytical grade CaCl_2 were used without further purification. Carefully prepared and analyzed NaCl and NaPSA stock solutions and CaCl_2 and CaPSA stock solutions were mixed and diluted by weight to obtain four series of NaCl-NaPSA and four series of CaCl_2 -CaPSA mixtures, with matching polyion molalities m_p . For each of the four polyion concentrations used ($m_p = 0.0505, 0.0200, 0.0100$, and 0.00500) mixtures with matching values of X were prepared ($X = 16, 9, 4, 1$, and 0.25). A total of 16 NaCl-NaPSA and 16 CaCl_2 -CaPSA starting mixtures were prepared which had pairs of identical PSA and Cl^- concentrations. These pairs could be mixed by weight to obtain a series of Na/Ca mixtures with constant m_p and X .

Na^+ glass electrodes (Fisher Scientific) and Ca^{2+} liquid membrane electrodes (Orion Research Inc., Cambridge, Mass.) were used in conjunction with an Ag|AgCl electrode. Electrodes were the same as described before;^{7,8} potentials were measured using a 616 digital electrometer (Keithley Instruments, Cleveland, Ohio). The electrometer was calibrated vs. a Leeds and Northrup K-4 potentiometer, and found to be accurate within 0.1%.

Activity coefficients for NaCl and CaCl_2 standard solutions used for the calibration curve were interpolated from literature values.²²

In order to check some of our results with an independent, nonelectrochemical technique, a number of Donnan exclusion experiments were performed, both in the single counterion systems (NaCl + NaPSA and CaCl_2 + CaPSA) and in a number of Na^+ - Ca^{2+} mixtures. In the experiments with a

NaCl-CaCl₂ mixture as the outside solution, no difference in the final outcome was observed when either NaPSA or CaPSA or a mixture of both was used as the starting solution inside the dialysis bag. Generally, equilibration periods of 5 to 7 days were used. Ca^{2+} , Cl^- , and total cation concentrations were determined for the inside and outside solutions. Unexpectedly, the Cl^- determination using Mohr's titration was not interfered with by the polyelectrolyte,²³ in fact the presence of PSA seems to result in a sharper end point. In some of the experiments with NaCl-CaCl₂ mixtures very low concentrations of Ca^{2+} had to be used to obtain final values for x_{Ca} of the inside solutions which were in the range required. In these cases, the Ca^{2+} concentration of the outside solution could not be determined accurately, but was kept constant by using a large outside volume and repeated solution changes. Still, it is impossible with Donnan exclusion measurements to cover the whole x_{Ca} range or to use mixtures with low m_p , and it is not feasible to perform series of measurements at constant m_p and X .

Results and Discussion

The measurement of electrolyte activities in mixed electrolyte solutions using ion selective electrodes, especially with electrodes other than the H^+ or Na^+ glass electrodes, has not yet reached the degree of accuracy and repeatability of other thermodynamic measurement techniques, e.g., vapor pressure measurements. Yet, in many cases it is the only method available: for instance, in the case of low solution concentration or with multiionic mixtures. Both the Na^+ glass electrode and the Ca^{2+} liquid membrane electrode were shown to behave satisfactorily in single counterion polyelectrolyte mixtures.^{7,8} In fact, since our last report we have improved the repeatability of the Ca^{2+} electrodes by more stringent calibration-measurement sequences, and in CaCl_2 -CaPSA mixtures the Ca^{2+} electrode now has a precision only slightly less than the Na^+ glass electrode in NaCl-NaPSA mixtures. The Nernst slope of the cell Ca^{2+} electrode | CaCl_2 |AgCl|Ag was never lower than 87 mV (theoretical value 88.8 mV/decade CaCl_2 activity), and independent measurements of the same mixture gave a repeatability of ± 0.005 in $\gamma_{\pm}(\text{CaCl}_2)$. No interference problem of Ca^{2+} on the Na^+ glass electrode is expected, however, the Ca^{2+} electrode clearly responds to Na^+ at high Na^+ concentrations and high total ionic strengths.²⁴⁻²⁶ We therefore tested both the Na^+ and the Ca^{2+} electrodes in aqueous NaCl-CaCl₂ mixtures of constant ionic strength using the Na^+ or Ca^{2+} electrode together with a Ag|AgCl electrode. The NaCl-CaCl₂ system has been studied by a number of authors using electrochemical²⁵⁻²⁸ or isopiestic²⁹ techniques and the general conclusion is that the linear form of Harned's rule holds for both NaCl and CaCl_2 , at least in the relatively high ionic strength mixtures studied. Although there are discrepancies in the values reported for the linear Harned coefficients, they are generally small enough to warrant the assumption that for ionic strengths below 0.1 M, $\gamma_{\pm}(\text{NaCl})$, and $\gamma_{\pm}(\text{CaCl}_2)$ at constant I should be virtually independent of x_{Na} or x_{Ca} , at least within the precision of our galvanic cell results. Our results for $\gamma_{\pm}(\text{NaCl})$ and $\gamma_{\pm}(\text{CaCl}_2)$ in NaCl-CaCl₂ mixtures of constant ionic strength ($I = 0.1, 0.05$, and 0.01) are shown in Figure 2. In this figure the symbols X at $x_{\text{Na}} = 0$ and $x_{\text{Na}} = 1$ indicate the values respectively for $\gamma_{\pm}^0(\text{CaCl}_2)$ and $\gamma_{\pm}^0(\text{NaCl})$ (i.e., their pure solution values). As Figure 2 indicates, the results for both $\gamma_{\pm}(\text{NaCl})$ and $\gamma_{\pm}(\text{CaCl}_2)$ are reasonably independent of x_{Na} or x_{Ca} , and we may conclude that at least at ionic strengths below 0.1 M the Ca^{2+} electrode responds satisfactorily to Ca^{2+} activity changes without in-

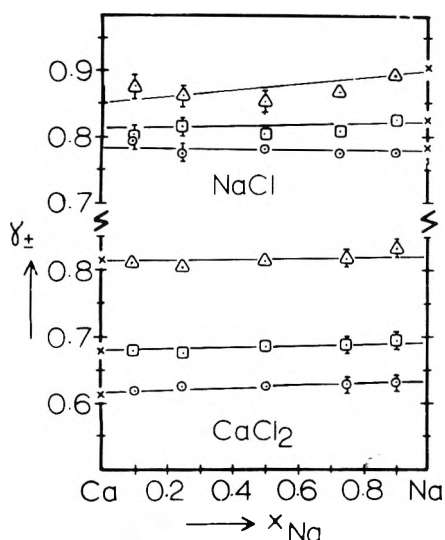


Figure 2. Activity coefficients of NaCl (upper three curves) and CaCl₂ (lower three curves) in NaCl-CaCl₂ mixtures of constant ionic strength: Δ , $I = 0.1$; \square , $I = 0.05$; \circ , $I = 0.01$.

terference from Na⁺. The results in the NaCl-CaCl₂ mixtures could be duplicated within experimental error with different, independently prepared mixtures. In the polyelectrolyte solutions, the Na⁺ electrode results were reproducible within measurement error (± 0.005 in γ_{\pm} , or ± 0.005 mV) over the whole x_{Na} range (down to $x_{Na} = 0.1$), but the Ca²⁺ electrode results generally were not reliable for mixtures with $x_{Ca} < 0.2$, and no results are reported in this region. In general, no results for $\gamma_{\pm}(\text{CaCl}_2)$ are reported for mixtures where $a_{\pm}(\text{CaCl}_2)$ falls below approximately 2×10^{-4} M.

Results for $\gamma_{\pm}(\text{NaCl})$ and $\gamma_{\pm}(\text{CaCl}_2)$ as a function of x_{Na} at constant m_p and X , for a total of 16 measurement series (m_p values 0.0505, 0.0200, 0.0100, and 0.00500, with X values of 16, 9, 4, 1, and 0.25 for the 0.0505 and 0.0200 series, and 4, 1, and 0.25 for the 0.01 and 0.005 series) are presented in Table I, together with the values of γ_{\pm}^0 for each solution.³⁰ Figures 3-7 show the results for $\gamma_{\pm}(\text{corr})$ (eq 1) at each of the X values studied. In these figures, we have tried to show all data points, however, because of the overlap of $\gamma_{\pm}(\text{corr})$ values, some points had to be deleted for reasons of clarity.

Table II compares the values for $\gamma_{\pm}(\text{NaCl})$ and $\gamma_{\pm}(\text{CaCl}_2)$ in a number of Donnan exclusion experiments to interpolated values from our galvanic cell measurement series. Taking into account the limited accuracy of the Donnan exclusion experiments, especially in the case of Na⁺-Ca²⁺ mixtures, and, in the case of the mixtures, the fairly large uncertainty in obtaining interpolated values for $\gamma_{\pm}(\text{CaCl}_2)$, the agreement between these two types of experiments is very satisfactory. Our galvanic cell results in the single counterion systems are very well corroborated by the Donnan exclusion results, at least in the concentration ranges where the Donnan method can be applied. In the Na⁺-Ca²⁺ mixtures the experimental uncertainty is larger with both types of measurements, but one of the major conclusions we will draw later, i.e., the fact that $\gamma_{\pm}(\text{CaCl}_2)$ does not drop as fast as predicted by the limiting law when x_{Na} is increased, is substantiated by the Donnan exclusion results.

In the case of galvanic cell measurements, a measurement series at constant m_p and X is made by starting with the CaCl₂-CaPSA mixture and adding the matching NaCl-NaPSA mixture in successive steps (weight method), measuring the cell potentials at each x_{Na} value. In a number of

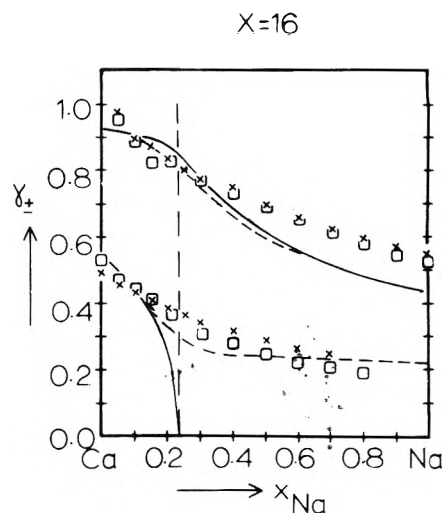


Figure 3. $\gamma_{\pm}(\text{corr})$ values for NaCl (upper points) and CaCl₂ (lower points) at $X = 16$: \times , $m_p = 0.05$; \square , $m_p = 0.02$: full lines, limiting laws; broken lines, eq 11, 13 (NaCl) and 12, 15 (CaCl₂) with $\epsilon = 0.1$.

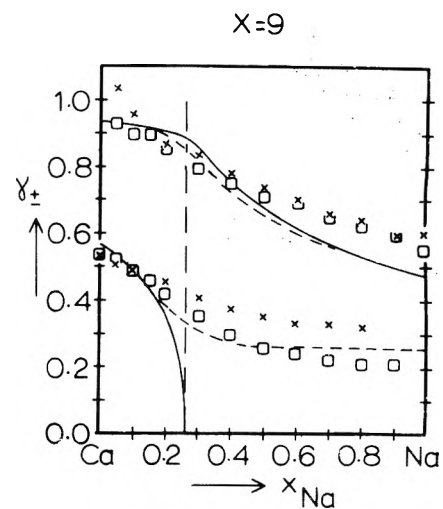


Figure 4. $\gamma_{\pm}(\text{corr})$ values for NaCl (upper points) and CaCl₂ (lower points) at $X = 9$: \times , $m_p = 0.05$; \square , $m_p = 0.02$: full lines, limiting laws; broken lines, eq 11, 13 (NaCl) and 12, 15 (CaCl₂) with $\epsilon = 0.1$.

cases, duplicate mixtures were prepared independently and the measured cell potentials always agreed within the standard limit of error (ca. ± 0.5 mV). The agreement with our earlier results for the CaCl₂-CaPSA system⁸ and for the NaCl-NaPSA system⁷ is excellent, in all cases within the error limits caused by the uncertainty in the concentration determinations of the PSA stock solutions. The internal consistency of the results in the mixtures is good in the case of the NaCl activity coefficients, as can be seen from the independence of the corrected values of $\gamma_{\pm}(\text{NaCl})$ from m_p . The only exceptions to this independence are a number of high values (i.e., $\gamma_{\pm}(\text{NaCl}) > 1$) in mixtures with low x_{Na} and low X , i.e., mixtures with low Na⁺ equivalent fractions and high chloride concentrations. However, this occurs only in mixtures with $x_{Na} = 0.05$, and in the $m_p = 0.05$, $X = 0.25$ series up to $x_{Na} = 0.6$. It can probably be attributed to large uncertainties in the mixture composition (for the $x_{Na} = 0.05$ points) and to a breakdown of the assumption that $\gamma_{\pm}^0(\text{NaCl})$ is independent of x_{Na} for the high ionic strength mixtures, which may also be derived from the $I = 0.1$ data in Figure 2. In any case, only in

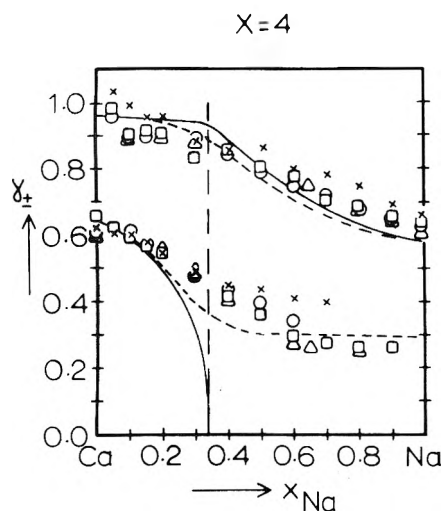


Figure 5. $\gamma_{\pm}(\text{corr})$ values for NaCl (upper points) and CaCl_2 (lower points) at $X = 4$: X, $m_p = 0.05$; \square , $m_p = 0.02$; \circ , $m_p = 0.01$; Δ , $m_p = 0.005$; full lines, limiting laws; broken lines, eq 11, 13 (NaCl) and 12, 15 (CaCl_2) with $\epsilon = 0.1$.

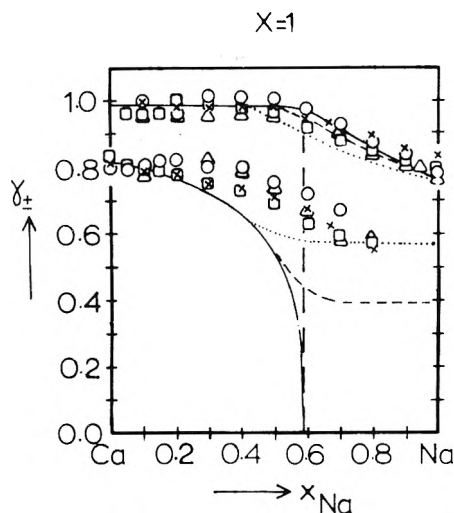


Figure 6. $\gamma_{\pm}(\text{corr})$ values for NaCl (upper points) and CaCl_2 (lower points) at $X = 1$: X, $m_p = 0.05$; \square , $m_p = 0.02$; \circ , $m_p = 0.01$; Δ , $m_p = 0.005$; full lines, limiting laws; broken lines, eq 11, 13 (NaCl) and 12, 15 (CaCl_2); - - - -, $\epsilon = 0.1$; , $\epsilon = 0.3$.

a few mixtures are the positive deviations observed larger than the maximum error limits, and the general trends in the $\gamma_{\pm}(\text{corr})$ values are not influenced. The values obtained for $\gamma_{\pm}(\text{CaCl}_2)$ show an excellent internal consistency for mixtures rich in Ca^{2+} , but the spread in $\gamma_{\pm}(\text{corr})$ values for mixtures with $x_{\text{Ca}} < 0.7$ between the different m_p series is outside the expected limit of error. The largest deviation seems to be between the $m_p = 0.05$ and the $m_p = 0.02$ series at high X values, where the difference can reach about 0.07 units in $\gamma_{\pm}(\text{corr})$. This difference may well indicate the increased experimental error in these mixtures, but on the other hand the trend to higher $\gamma_{\pm}(\text{CaCl}_2)$ values at a given x_{Ca} as m_p increases was in both qualitative and quantitative agreement with the results from preliminary measurement series which are not reported here. Taking into account the results from the Donnan exclusion measurements, we can certainly conclude that the curves for $\gamma_{\pm}(\text{corr})$ of CaCl_2 given in Figures 3–7 reliably indicate the range of γ_{\pm} values encountered for the polyion concentration range studied.

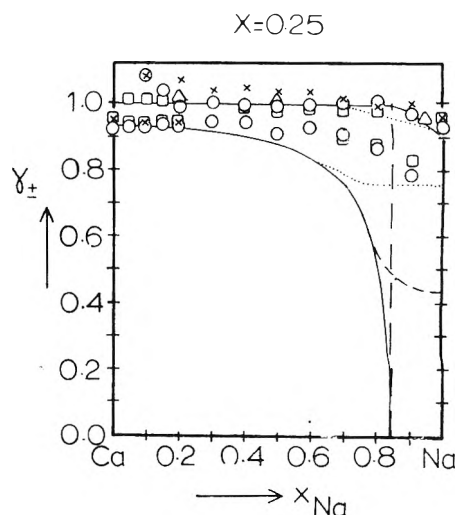


Figure 7. $\gamma_{\pm}(\text{corr})$ values for NaCl (upper points) and CaCl_2 (lower points) at $X = 0.25$: X, $m_p = 0.05$; \square , $m_p = 0.02$; \circ , $m_p = 0.01$; Δ , $m_p = 0.005$; full lines, limiting laws; broken lines, eq 11, 13 (NaCl) and 12, 15 (CaCl_2), - - - -, $\epsilon = 0.1$; , $\epsilon = 0.5$.

We will now consider in detail the trends observed in the experimental curves for $\gamma_{\pm}(\text{NaCl})$ and $\gamma_{\pm}(\text{CaCl}_2)$ (both of which are already corrected for the small ion interactions) as shown in Figures 3–7, and compare them to the limiting law predictions (eq 3–8 suitably combined to give γ_{\pm}). The full lines in these figures show the limiting law predictions for $\gamma_{\pm}(\text{CaCl}_2)$ (lower curves) and $\gamma_{\pm}(\text{NaCl})$ (upper curves), which can be compared directly to the $\gamma_{\pm}(\text{corr})$ data points given. First of all, as was discussed above, in most cases we do not find a significant m_p dependence of the $\gamma_{\pm}(\text{corr})$ values, in the range of polyelectrolyte concentrations studied. In the one case where the m_p dependence is outside the experimental error ($\gamma_{\pm}(\text{CaCl}_2)$ in the $m_p = 0.05$ series at higher x_{Na} values), there is no clear trend, and the qualitative conclusions remain the same. This m_p independence is one of the basic justifications for applying the limiting laws at finite concentrations. The three major effects predicted by condensation theory and the limiting laws are (see Figure 1) the following:

(1) As X decreases, the transition points between regions I and II, and between regions II and III shift to higher x_{Na} values (because these transition points are at certain fixed values of $2m_{\text{Ca}}/m_p$).

(2) As x_{Na} decreases, the fraction of Na^+ ions condensed decreases and the Debye–Hückel term for the Cl^- ions and the uncondensed Na^+ ions decreases, leading to a substantial increase of $\gamma_{\pm}(\text{NaCl})$.

(3) As Na^+ is added to a pure Ca^{2+} mixture, the fraction of Ca^{2+} ions condensed increases rapidly toward the last part of region I, and in regions II and III $\gamma_{\pm}(\text{CaCl}_2)$ is zero.

The $\gamma_{\pm}(\text{NaCl})$ data points are in remarkable agreement with the limiting law predictions. Both: the increase in $\gamma_{\pm}(\text{NaCl})$ as x_{Na} decreases, and the X -dependent point where $\gamma_{\pm}(\text{NaCl})$ levels off at a value close to one, are in virtual quantitative agreement with the theoretical predictions. At the Na^+ side, the experimental values for $\gamma_{\pm}(\text{NaCl})$ in mixtures with high X values are higher than the limiting law predictions in quantitative agreement with earlier findings.^{7,8,31} However we may conclude that it is possible to quantitatively predict $\gamma_{\pm}(\text{NaCl})$ values in these multiionic mixtures, and thus we can also have confidence in predictions of the single ionic activity coefficients of the Na^+ ion. As was shown in our previous paper,⁸ no difference could be detected

TABLE II: Comparison of Results for $\gamma_{\pm}(\text{NaCl})$ and $\gamma_{\pm}(\text{CaCl}_2)$ from Donnan Exclusion Measurements (I) with Interpolated Results from Electrochemical Cells (II)

m_p	x_{Na}	X	$\gamma_{\pm}(\text{NaCl})$		$\gamma_{\pm}(\text{CaCl}_2)$	
			I	II	I	II
0.0352	1	9.67	0.54	0.537		
0.0411	1	26	0.48	0.50		
0.0502	0	0.67			0.542	0.541
0.0492	0	2.61			0.525	0.512
0.0480	0	3.80			0.513	0.495
0.0451	0	5.05			0.498	0.490
0.0506	0.25	1.86	0.78	0.82	0.46	0.47
0.0366	0.65	1.80	0.74	0.75	0.42	0.39
0.0487	0.63	2.56	0.69	0.71	0.39	0.38

between $\gamma_{\pm}(\text{NaCl})$ in NaCl-NaPSA mixtures and $\gamma_{\pm}(\text{KCl})$ in KCl-KPSA mixtures. Additional measurements of alkali chloride activity coefficients in a natural polyelectrolyte with sulfonate fixed charges (dextransulfonate) also failed to detect significant differences between the mean activity coefficients of the four alkali chlorides.³² It therefore seems that the electrostatic model employed by the limiting laws, suitably corrected for the small ion interactions and taking into account positive deviations at high X and high x_{Na} values, can be used to predict activity coefficients of the alkali metal ions in multiionic polyelectrolyte solutions, with a reliability normally in the order of $\pm(0.01-0.02)$ units in γ_{\pm} or in γ_{+} .

Turning now to the $\gamma_{\pm}(\text{CaCl}_2)$ values, we notice that the situation is quite different. Although the data do show the expected decrease in $\gamma_{\pm}(\text{corr})$ as x_{Na} increases, the decrease is gradual, and at no point do the activity coefficients become zero or even close to zero. Although the decrease in $\gamma_{\pm}(\text{CaCl}_2)$ may seem relatively small, it should be pointed out that this still corresponds to a substantial decrease in $\gamma_{\text{Ca}^{2+}}$. For instance, if we use the activity coefficients of the Cl^{-} ion as given by the limiting law (eq 3, 5, and 8) to calculate $\gamma_{\text{Ca}^{2+}}$ from our $\gamma_{\pm}(\text{corr})$ data for CaCl_2 , the decrease in $\gamma_{\text{Ca}^{2+}}$ as x_{Na} increases is seen to be gradual but still substantial, even though there is no sharp transition point (Figure 8). In Figure 8, it is of interest to note the excellent quantitative agreement for mixtures of different X at the Ca side. This again points out how well the corrected limiting laws describe the single divalent counterion mixtures. Clearly, using eq 5 and 8 in regions II and III to calculate $\gamma_{\text{Cl}^{-}}$ is not fully justified in view of our experimental results for γ_{\pm} , but the results obtained for $\gamma_{\text{Ca}^{2+}}$ are certainly indicative of the fact that the Ca^{2+} activity coefficient, although low, does not drop to zero. It should also be pointed out that the $\gamma_{\pm}(\text{CaCl}_2)$ values reported here are in agreement with Donnan exclusion measurements (Table II), making it very unlikely that the nonzero activity of CaCl_2 is a measurement artifact. Rinaudo and Milas¹⁰ did report that the single ion activity coefficient of Ca^{2+} in salt free $\text{Na}^{+}-\text{Ca}^{2+}$ counterion mixtures of a high charge density carboxymethylcellulose dropped to zero at an x_{Na} value between 0.3 and 0.4 (the limiting law predicts the transition point between regions I and II at $x_{\text{Na}} = 0.15$ for their CMC sample). However it is not possible to detect activity coefficients below 0.01 at these low concentrations, and therefore it is certainly possible that $\gamma_{\text{Ca}^{2+}}$ had a low but finite value, which would still lead to appreciable, nonzero values for $\gamma_{\pm}(\text{CaCl}_2)$, because of the averaging effect of the Cl^{-} ion. Manning¹ quotes work by Dolar and Juznic,³³ not available to us, on single ion activity coefficients of Pb^{2+} in $\text{H}^{+}-\text{Pb}^{2+}$ polystyrenesulfonate mixtures, where the Pb^{2+} activity coefficient is certainly smaller

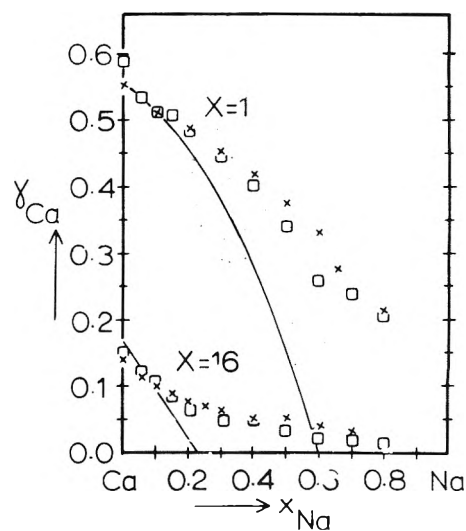


Figure 8. $\gamma_{\text{Ca}^{2+}}$ calculated from $\gamma_{\pm}(\text{corr})$ values for CaCl_2 assuming $\gamma_{\text{Cl}^{-}}$ is given by eq 3, 5, and 8: upper points, $X = 1$; lower points, $X = 16$: full lines, eq 4.

than our values for Ca^{2+} in comparable $\text{Na}^{+}-\text{Ca}^{2+}$ mixtures, but still finite activities are reported. Krakauer,³⁴ using a dye-colorimetric method, measured the "bound to unbound" ratios for Mg^{2+} in $\text{Na}^{+}, \text{Mg}^{2+}, \text{Cl}^{-}$, polynucleotide mixtures, where the polynucleotide was poly(A + 2U). His mixtures contained a considerable excess of NaCl. He did not observe a sharp transition point in the bound to unbound Mg^{2+} ratio as the Mg^{2+} to polynucleotide ratio was decreased. Such a transition point would correspond to the point where all Mg^{2+} is condensed. Manning observed that the deviations from the limiting laws in Krakauer's work became smaller as the NaCl excess decreased. Indirect information about the state of binding of the divalent counterion has come from NMR data on polyelectrolyte solutions with univalent-divalent counterion mixtures. Leyte et al.¹⁴ detected a strong increase in the ^{23}Na spin-lattice relaxation rate as the Ba^{2+} content of the mixtures increased. This closely corresponds to the increase in $\gamma_{\pm}(\text{corr})$ for NaCl reported here. However by comparing this increase to model calculations based on either a site-bound (fixed) Ba^{2+} ion or a more loosely bound Ba^{2+} ion, they also concluded that the larger part of the Ba^{2+} resides near the polyion, but is not bound to one particular charge. Unfortunately, these measurements cannot yet give quantitative information on the position of the divalent ion, especially not in mixtures with high Na^{+} mole fractions, i.e., regions II and III which are of most interest to our discussion here. The os-

otic coefficient measurements of Dolar et al.²⁻⁴ show the expected maximum in the osmotic coefficient as the equivalent fraction of the univalent ions increases, but at higher univalent ion equivalent fractions than predicted. Thus, there seems to be considerable evidence that condensation theory and the limiting laws, derived by combining the condensation concept with a Debye-Hückel type treatment of polyion-small ion interactions, give a correct qualitative description of the mixtures studied here, but the actual transitions between the various regions may not be as sharp, and the lowering of the divalent ion activity coefficient not as strong as predicted.

There are a number of possible causes for the disagreement between our results for $\gamma_{\pm}(\text{CaCl}_2)$ in regions II and III and the theoretical predictions based on counterion condensation theory. Phenomenological modifications of the theory, based on the assumption that the fraction of condensed ions is actually smaller than what is predicted by condensation theory, could for instance either use the assumption that the net charge density of the polyion is higher because of incomplete condensation of all counterions, or the assumption that in regions of low x_{Ca} not all the Ca^{2+} ions are condensed, as seems evident from the experimental results. Both assumptions lead to finite values of $\gamma_{\text{Ca}^{2+}}$ in regions II and III. We have examined both methods, and will present the results of the second method, because the first mentioned assumption leads to certain inconsistencies, especially in region II.

We will assume that a certain fraction ϵ of all Ca^{2+} ions will remain uncondensed throughout regions II and III. We will also assume ϵ to be constant over the whole x_{Na} range. The introduction of this parameter clearly is a departure from condensation theory, forced by our experimental results. Thus, ϵ essentially is an extra parameter used to fit the calculated values for both $\gamma_{\pm}(\text{NaCl})$ and $\gamma_{\pm}(\text{CaCl}_2)$ to the experimental results at a given X , retaining the framework of condensation theory. When $\epsilon = 0$ eq 10-15 revert back to the corresponding equations from the unmodified theory. The assumption that ϵ does not depend on x_{Na} (realizing that in region I a larger fraction may remain uncondensed, depending on ξ) limits the number of adjustable parameters to one. The net charge density parameter ξ_{net} (i.e., the effective ξ of the partially neutralized charges of the polyion) is still $\frac{1}{2}$ in region I and 1 in region III, and must be modified in region II:

$$\xi_{\text{net}} = \xi \{x_{\text{Na}}(1 + X^{-1})(1 - \epsilon) - X^{-1} + \epsilon(1 + X^{-1})\} \quad (10)$$

Now, the transition points between the regions are determined by the right-hand side of eq 10 for $\xi_{\text{net}} = \frac{1}{2}$ and $\xi_{\text{net}} = 1$, and these transition points are shifted toward smaller x_{Na} values. The functional forms of γ_{\pm} are unchanged in region I.

In region II, the activity coefficients are given by

$$\ln \gamma_{\pm}(\text{NaCl}) = -\frac{1}{2}\xi^{-1}\xi_{\text{net}}^2[(1 - 2\epsilon)x_{\text{Na}}(1 + X^{-1}) + 2(1 + X^{-1})\epsilon + X^{-1}]^{-1} \quad (11)$$

$$\ln \gamma_{\pm}(\text{CaCl}_2) = 2 \ln \gamma_{\pm}(\text{NaCl}) + \frac{1}{3} \ln \epsilon \quad (12)$$

with ξ_{net} given by eq 10.

In Region III

$$\ln \gamma_{\text{Cl}^-} = -\frac{1}{2}[1 + 2\xi X^{-1} + \epsilon\xi(1 - x_{\text{Na}})(1 + X^{-1})]^{-1} \quad (13)$$

$$\ln \gamma_{\pm}(\text{NaCl}) = \ln \gamma_{\text{Cl}^-} + \frac{1}{2} \ln \{[\xi^{-1} + X^{-1} - \epsilon(1 - x_{\text{Na}})(1 + X^{-1})]x_{\text{Na}}^{-1}(1 + X^{-1})^{-1}\} \quad (14)$$

$$\ln \gamma_{\pm}(\text{CaCl}_2) = 2 \ln \gamma_{\text{Cl}^-} + \frac{1}{3} \ln \epsilon \quad (15)$$

In region III, a larger fraction of Na^+ has to condense, lowering its activity coefficient slightly compared to the $\epsilon = 0$ case. The numerical results for $\gamma_{\pm}(\text{CaCl}_2)$ and $\gamma_{\pm}(\text{NaCl})$ are

given in Figures 3-7 (broken lines). We notice that in regions II and III $\gamma_{\pm}(\text{CaCl}_2)$ is strongly influenced by the assumption of incomplete condensation. On the other hand, the influence on $\gamma_{\pm}(\text{NaCl})$ is small: there is a slight shift to lower x_{Na} values for the first transition point, i.e., the point where the $\gamma_{\pm}(\text{NaCl})$ curve starts to go down, and this decrease is not quite as sharp as before. However, in the case of $\gamma_{\pm}(\text{NaCl})$ the differences caused by assuming incomplete condensation are virtually within experimental error. The deviation between theory and experimental results at high X and high x_{Na} values of course remains.

As far as $\gamma_{\pm}(\text{CaCl}_2)$ is concerned, we notice that for $X = 16, 9,$ and 4 (Figures 3-5) a value of $\epsilon = 0.1$ gives good agreement with the experimental results. On the other hand, with excess salt letting $\epsilon = 0.1$ yields values of γ_{\pm} which are too low, and higher values of ϵ are required, as shown in Figures 6 and 7. In general, the excess salt condition should yield a better agreement with theoretical treatments,³⁵ and we certainly obtained such an agreement in the single counterion systems with low X values.^{7,8} However the increase of ϵ does seem plausible if we view the microscopic $\text{Na}^+ - \text{Ca}^{2+}$ exchange at the polyion as an equilibrium process similar to the exchange between a macroscopic ion-exchange resin bead and an electrolyte solution. A detailed consideration of such a microscopic exchange equilibrium³⁶ leads to the conclusion that for x_{Na} close to unity the condensed ratio $(1 - \epsilon)$ of Ca^{2+} ions is indeed close to 1 for large X but will become small when X is small, in agreement with our experimental results.

In conclusion, the measurements presented in this paper show the two major effects expected in mixed valency counterion polyelectrolyte systems. First, the increase in the Na^+ activity coefficient as x_{Na^+} decreases confirms the effective removal of the Na^+ ion from the influence of the polyion as Ca^{2+} ions are added. The increase is in quantitative agreement with predictions based on Manning's limiting law. Secondly, the Ca^{2+} activity coefficient decreases strongly as $x_{\text{Ca}^{2+}}$ decreases, but at no point can the Ca^{2+} ion be said to be fully condensed, as is predicted by condensation theory. The degree to which the Ca^{2+} ion is not condensed seems to increase with increasing Cl^- content of the mixtures. One implication of this observation is that in polyelectrolyte mixtures in which only electrostatic long-range interactions are expected to contribute to the excess free energy of the ionic constituents, it will always be possible to remove even trace amounts of divalent ions such as Ca^{2+} or Mg^{2+} by dialysis against, e.g., NaCl , or by ultrafiltration in the presence of excess NaCl . Also, because in this and in previous works we have not found any differences between the activity coefficients of the alkali chlorides, or between the activity coefficients MgCl_2 and CaCl_2 in polyelectrolyte solutions, it is possible to predict activity coefficients in multiionic polyelectrolyte mixtures containing those ions with reasonable confidence, as long as the intercharge distance of the polymer is known. As was stated by Rinaudo and Milas,²⁰ it is important to extend these measurements to other polyelectrolytes, and also to study metal counterions which do not have closed shell electronic configurations. In such cases, specific interactions may be found in addition to the already major effects caused by long-range electrostatic effects studied here.

Acknowledgments. This research was supported by the National Research Council of Canada. One of the authors (K.I.) is grateful to the Killam Trust for support.

Supplementary Material Available: Table I, a listing of mean activity coefficients for NaCl and CaCl_2 (3 pages). Or-

dering information is available on any current masthead page.

References and Notes

- (1) G. S. Manning in "Polyelectrolytes", E. Sélégny, Ed., Reidel Publishing, Dordrecht, Holland, 1974, p 9.
- (2) D. Dolar and D. Kozak in "Abstracts of the IUPAC Symposium on Macromolecules, Leiden", Vol. 1, Inter Scientias, The Hague, 1970, p 363.
- (3) D. Dolar in ref 1, p 97.
- (4) J. Skerjanc, *J. Phys. Chem.*, **79**, 2185 (1975).
- (5) D. Dolar and J. Skerjanc, *J. Chem. Phys.*, **61**, 4106 (1974).
- (6) J. Skerjanc and D. Dolar, *J. Chem. Phys.*, **63**, 515 (1975).
- (7) J. C. T. Kwak, *J. Phys. Chem.*, **77**, 2790 (1973).
- (8) J. C. T. Kwak, M. C. O'Brien, and D. A. MacLean, *J. Phys. Chem.*, **79**, 2381 (1975).
- (9) F. Oosawa, "Polyelectrolytes", Marcel Dekker, New York, N.Y., 1971.
- (10) M. Rinaudo and M. Milas, *Eur. Polym. J.*, **8**, 737 (1972).
- (11) A. Minakata, N. Imai, and F. Oosawa, *Biopolymers*, **11**, 347 (1972).
- (12) M. Mandel and F. Van der Touw in ref 1, p 285.
- (13) G. Muller, F. Van der Touw, S. Zwolle, and M. Mandel, *Biophys. Chem.*, **2**, 242 (1974).
- (14) J. J. Van der Klink, D. Y. H. Prins, S. Zwolle, F. Van der Touw, and J. C. Leyte, *Chem. Phys. Lett.*, **32**, 287 (1975).
- (15) G. S. Manning, *Biopolymers*, **11**, 951 (1972).
- (16) N. DeMarky and G. S. Manning, *Biopolymers*, **14**, 1407 (1975).
- (17) G. S. Manning, *J. Chem. Phys.*, **51**, 924 (1969).
- (18) J. D. Wells, *Proc. R. Soc. London, Ser. B*, **183**, 399 (1973).
- (19) J. D. Wells, *Biopolymers*, **12**, 223 (1973).
- (20) M. Rinaudo and M. Milas, *Chem. Phys. Lett.*, **41**, 456 (1976).
- (21) K. Iwasa and J. C. T. Kwak, *J. Phys. Chem.*, **80**, 215 (1976).
- (22) R. A. Robinson and R. H. Stokes, "Electrolyte Solutions", Butterworths, London, 1959.
- (23) Z. Alexandrowicz, *J. Polym. Sci.*, **56**, 115 (1962).
- (24) R. G. Bates and M. Alfenaar, *Natl. Bur. Stand. U.S., Spec. Publ.*, **No. 314**, 207 (1969).
- (25) J. N. Butler, *Natl. Bur. Stand. U.S., Spec. Publ.*, **No. 314**, 184 (1969).
- (26) R. Huston and J. N. Butler, *Anal. Chem.*, **41**, 200 (1969).
- (27) J. N. Butler and R. Huston, *J. Phys. Chem.*, **71**, 4479 (1967).
- (28) R. D. Lanier, *J. Phys. Chem.*, **69**, 3992 (1965).
- (29) R. A. Robinson and V. E. Bower, *J. Res. Natl. Bur. Stand. U.S., Sect. A*, **70**, 313 (1966).
- (30) See paragraph at end of text regarding supplementary material.
- (31) T. Ueda and Y. Kobatake, *J. Phys. Chem.*, **77**, 2995 (1973).
- (32) Y. M. Joshi and J. C. T. Kwak, to be submitted for publication.
- (33) D. Dolar and K. Juznic, Presented at Int. Conf. Calor. Thermodyn., 1st, Warsaw, Aug 1969 (as quoted in ref 1).
- (34) H. Krakauer, *Biopolymers*, **11**, 781 (1972).
- (35) K. Iwasa, *J. Chem. Phys.*, **64**, 3679 (1976).
- (36) K. Iwasa, unpublished work.

Infrared Studies of Reactions on Oxide Surfaces. 7. Mechanism of the Adsorption of Water and Ammonia on Dehydroxylated Silica

B. A. Morrow,* I. A. Cody, and Lydia S. M. Lee

Department of Chemistry, University of Ottawa, Ottawa, Ontario K1N 6N5, Canada (Received April 30, 1976)

Publication costs assisted by the National Research Council of Canada

The surface of silica is modified in several ways when it has been dehydroxylated by heating under vacuum at temperatures up to 1200 °C. A highly reactive site is generated which is capable of facilitating the dissociative chemisorption of H₂O and NH₃. This site is assumed to be an unsymmetrical siloxane bridge containing an electron deficient silicon atom which can act as a Lewis acid center. Although this site reacts instantaneously with water to yield two SiOH groups which do not hydrogen bond [$\nu(\text{OH}) = 3741 \text{ cm}^{-1}$], the reaction is slow with NH₃ because of the competition between the tendency to coordinate or to dissociate yielding SiOH and SiNH₂ (type I). Symmetrical less reactive siloxane sites are also generated which only react with H₂O to give isolated pairs of hydrogen bonded SiOH groups with infrared bands at 3720 and 3520 cm⁻¹. Finally, the residual isolated hydroxyl groups [$\nu(\text{OH}) = 3748 \text{ cm}^{-1}$] are modified so that at 20 °C they exchange with H₂¹⁸O or they react to a limited extent with NH₃ to give SiNH₂ (type II) and H₂O. Neither process occurs without the prior dehydroxylation. The new hydroxyl species which are generated by the chemisorption of water in both types of siloxane bridge hydrogen bond with excess water and the present results are discussed in terms of previous models for the rehydration of hydrophobic silica.

Thin silica disks (10 mg cm⁻²) are opaque to infrared radiation between about 1350 and 750 cm⁻¹ except for a window of partial transparency between 1000 and 850 cm⁻¹. We have recently shown in parts V and VI^{1,2} (hereafter referred to as V and VI) that two strong bands at 908 and 888 cm⁻¹ and a shoulder near 940 cm⁻¹ appeared if silica was degassed at greater than 400 °C and that the intensity of these bands increased as the degassing temperature increased, reaching a maximum near 1200 °C when about 90% of the isolated surface silanol groups [$\nu(\text{OH}) = 3748 \text{ cm}^{-1}$] had been removed (see Figure 1A).

When a dehydroxylated silica was allowed to react with

H₂O, all three bands disappeared and a new SiOH group was created [$\nu(\text{OH}) = 3741 \text{ cm}^{-1}$]. The bands also disappeared when an excess of NH₃ was added and SiOH and SiNH₂ were formed.² However, when pyridine or trimethylamine was added¹ only the 888- and 940-cm⁻¹ bands disappeared and the spectra indicated that these molecules reversibly coordinated on a Lewis acid site. The total site was assumed to be an asymmetric siloxane bridge containing an electron deficient silicon atom.

Part VI was mainly concerned with questions of reaction stoichiometry, site concentration, and conditions necessary for formation and regeneration of the active site. The present

paper deals with the question of the reaction mechanism and its relevance to the problem of the rehydration of hydrophobic silica.³⁻⁷

Experimental Section

The experimental details have been described previously.¹ The silica used was Cab-O-Sil HS-5 and had a BET (N_2) surface area of $320 \text{ m}^2 \text{ g}^{-1}$. The reaction cell had a volume of about 300 ml so that a 1 Torr dose of reactant corresponds to about $16 \mu\text{mol}$.

Results and Discussion

(a) *Reaction with NH_3* . The infrared spectrum of a silica sample which had been heated at 1200°C under vacuum so as to create the active sites responsible for the bands at 908 and 888 cm^{-1} and a shoulder at 940 cm^{-1} is shown in Figure 1A. All bands disappeared in unison (see VI)² if the silica was titrated with micromole doses of H_2O or BF_3 .⁸ However, with NH_3 the first small dose (about $2 \mu\text{mol}$) caused both of the 908 - and 888-cm^{-1} bands to diminish in unison (Figure 1B) but with the second increment (Figure 1C) the 888-cm^{-1} band diminished substantially, a new relatively sharp band appeared at 932 cm^{-1} and the 908-cm^{-1} band appeared as a shoulder near 913 cm^{-1} . After the spectra were rescanned 5 and 10 min later (Figure 1D,E) and 932-cm^{-1} band had broadened considerably and the transmission near 900 cm^{-1} had decreased. No further changes occurred in the next 3 h or following the addition of another $10 \mu\text{mol}$ dose of NH_3 . If 200 Torr of NH_3 were added (Figure 1F) the weak bands at $913/888 \text{ cm}^{-1}$ immediately disappeared and the intensity at 932 cm^{-1} increased. Accompanying these changes was the progressive growth of bands at 1550 , 3447 , and 3525 cm^{-1} due to $SiNH_2$ and at 3741 cm^{-1} due to $SiOH$ as described in VI (see below for further spectra).

The 932-cm^{-1} band is due to the $Si-N$ stretching mode of $SiNH_2$ ⁹ and the unusual changes in shape and intensity noted above always occurred during a titration sequence with NH_3 . Indeed, this band was so broad at saturation with NH_3 that the transmission at 900 cm^{-1} decreased as $SiNH_2$ was formed whereas it always increased when H_2O or CH_3OH were used. Thus it was difficult to see how the intensity of the 913-cm^{-1} band changed during reaction.

The $\nu(SiN)$ mode of $SiND_2$ is near 882 cm^{-1} and it was possible to observe how the $908\text{-}913\text{-cm}^{-1}$ band behaved during a similar sequence. The spectra on the right in Figure 1 show that after the first dose there was again an even decrease in the intensity of both bands but thereafter the 888-cm^{-1} band decreased more rapidly until after 1 h, most of the sites had been consumed and the 908-cm^{-1} band had shifted to 913 cm^{-1} .

When the Lewis bases pyridine or trimethylamine coordinated with an electron deficient site on dehydroxylated silica¹ only the 888-cm^{-1} band disappeared and the 908-cm^{-1} band shifted to 913 cm^{-1} . With NH_3 it would appear that both chemisorption and coordination occur simultaneously. This is born out upon examination of the NH stretching region.

When >20 Torr of NH_3 was added in one dose a spectrum such as that shown in Figure 1F was immediately observed and at higher frequencies there was a strong band at 3447 cm^{-1} and a weak band at 3525 cm^{-1} which have been assigned² to the symmetric and antisymmetric $\nu(NH)$ modes of $SiNH_2$, respectively. However, if a small dose, <1 Torr or about $5 \mu\text{mol}$, was added an additional weak band was observed at 3417 cm^{-1} (Figure 2A). [A 40 mg cm^{-2} sample was used here in order to obtain spectra of greater intensity.] For

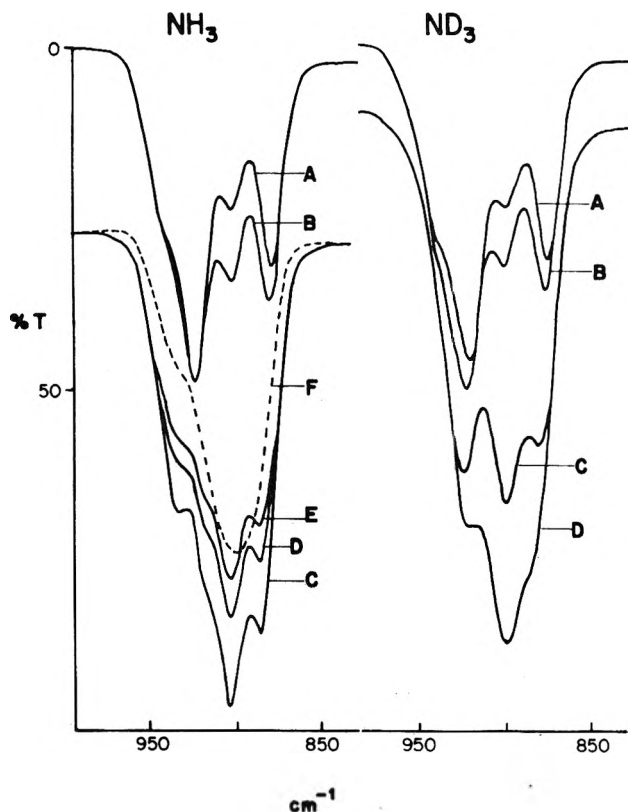


Figure 1. Spectral changes between 1000 and 850 cm^{-1} during the chemisorption of NH_3 and ND_3 on a 10 gm cm^{-2} silica disk which had been degassed at 1200°C under vacuum. NH_3 : (A) Background. (B) After adding $2 \mu\text{mol}$ of NH_3 . (C) After a further $2 \mu\text{mol}$ of NH_3 . (D and E) Repeat scans after (C), scan time 5 min. (F) After adding 200 Torr of NH_3 . ND_3 : (A) Background. (B and C) After adding successive $2 \mu\text{mol}$ doses of ND_3 . (D) Repeat scan after 1 h. The % T scale refers to A and B in each case.

ND_3 the symmetric and antisymmetric $SiND_2$ bands absorb at 2525 and 2628 cm^{-1} and the corresponding new feature is at 2552 cm^{-1} (Figure 2A'). If the cell was left and the spectrum was rescanned 3 h later, the new feature had decreased in intensity and the band due to the symmetric mode had intensified (Figure 2B and 2B'). [At the same time all other bands due to $SiNH_2$ and the 3741-cm^{-1} $SiOH$ band had also increased in intensity.] The appearance of this new feature always coincided with a situation whereby the intensity of the 888-cm^{-1} band was abnormally low, indicative of the formation of a coordinated species.

A broad strong band at 3400 cm^{-1} is normally observed when NH_3 interacts with a silica which has been heated at temperatures low enough to prevent extensive dehydroxylation of the isolated silanols.¹⁰⁻¹² This has been assigned to hydrogen bonded NH_3 and very much weaker bands due to this are usually observed at 3320 and 1625 cm^{-1} along with a broad band near 3000 cm^{-1} due to the perturbed silanols. Blomfield and Little¹⁰ observed a very sharp band at 3420 cm^{-1} after 5 Torr of NH_3 was left in contact with silica which had been degassed at 850°C which they assigned to NH_3 hydrogen bonded to isolated silanols. They found that this band more or less disappeared after condensing the excess ammonia in liquid N_2 . Peri¹¹ also observed a band at 3419 cm^{-1} when excess NH_3 was left in contact with an 800°C degassed silica and, like us, he noted that the intensity of this band decreased with time as the intensity of the $SiNH_2$ bands increased. He attributed this to the ν_3 mode of NH_3 , presumably physically adsorbed on the aerogel. We contend that this band is due to

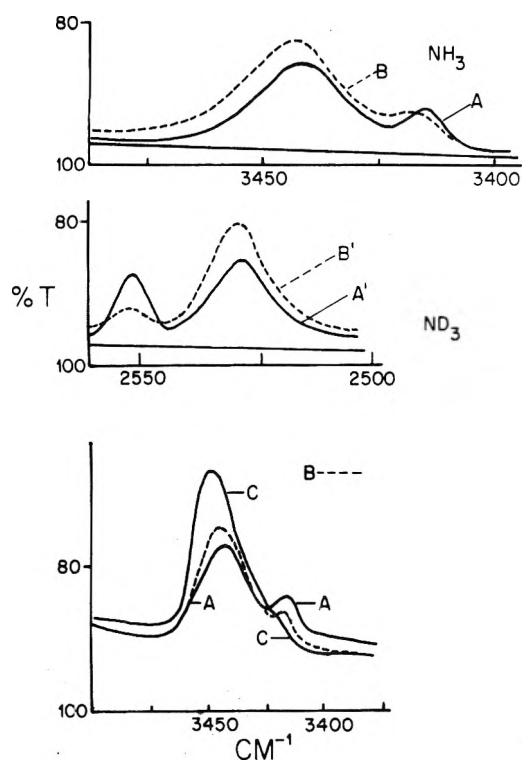
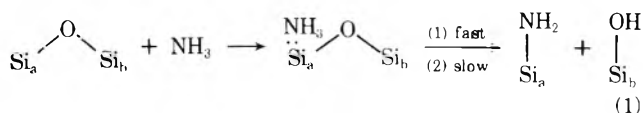


Figure 2. Top and Middle: (A, A') After the adsorption of 5 μmol of NH_3 or ND_3 on a 40 mg cm^{-2} degassed (1100°C) silica. (B, B') Repeat spectrum after 3 h. Bottom: After adsorption of (A) 0.5 Torr, (B) 35 Torr, or (C) 100 Torr of NH_3 on a 40 mg cm^{-2} silica and condensing the excess in liquid N_2 until the P dropped to 10^{-3} Torr. Note that the wavenumber scale is compressed relative to the above by a factor of 2.

NH_3 coordinated on the Lewis acid center described previously.

Further experiments bear this out. Gaseous NH_3 at varying pressures was admitted for 1 min to a cell which contained a 40 mg cm^{-2} silica disk which had been degassed at 1100°C . The excess was condensed into a liquid N_2 trap until the pressure dropped to 10^{-3} Torr (the new band always disappeared rapidly if the excess was pumped away). The initial pressures were 1, 35, and 100 Torr, and the spectra are shown at the bottom of Figure 2. The band at 3417 cm^{-1} was always lower in intensity if the initial pressure was higher whereas the intensity of the symmetric $\nu(\text{SiNH}_2)$ band was higher. If the 3417-cm^{-1} band was due to hydrogen bonded NH_3 its intensity should either increase or remain unaltered as the initial pressure of reactant was increased. On the other hand, if it was due to the antisymmetric NH stretching mode of a coordinated intermediate which was a precursor to the formation of SiNH_2 , then the behavior shown at the bottom of Figure 2 might be rationalized by the following mechanism: We assume the site is an unsymmetrical siloxane bridge² in which one of the silicon atoms (a) is electron deficient (reaction 1). Coordination occurs and there is an initial fast reaction



perhaps involving highly strained sites, and this accounts for the initial instantaneous formation of SiNH_2 and the symmetrical decrease in intensity of the 908- and 888-cm^{-1} bands. After the first addition of NH_3 or ND_3 in the series corresponding to Figure 1 (no $\nu(\text{NH})$ spectra are shown) no band due to coordinated ammonia was observed. With subsequent

doses, this band did appear and the changes with time resembled those shown for the thicker sample (Figure 2), i.e., a continuing slower reaction to yield SiNH_2 . This slower subsequent reaction might arise because a range of site energies exist whereby higher activation energy barriers have to be crossed. That there is a range of Si-N bond energies is perhaps shown by the fact that the 932-cm^{-1} band due to the $\nu(\text{SiN})$ mode is sharp at low product yield (Figure 1C) and broadens enormously at higher coverage extending from about 940 to 910 cm^{-1} .

The rate of chemisorption was always slow even if an excess of NH_3 was apparently present and pressures of the order of 10 Torr were usually necessary to ensure the complete disappearance of the $908/888\text{-cm}^{-1}$ bands. With a 200-mg disk (40 mg cm^{-2}) containing 0.15 sites per 100 \AA^2 (see VI) then 1 Torr of reactant in a cell of 300-ml volume would provide about 10^{19} molecules. With a BET surface area of $320 \text{ m}^2 \text{ g}^{-1}$, the number of sites would also be about 10^{19} . With H_2O or BF_3 a 1 Torr dose of reactant always caused the instantaneous disappearance of the $908/888\text{-cm}^{-1}$ bands. This further indicates that coordination is competing with the tendency toward dissociative chemisorption in the case of NH_3 .

Finally, it is to be noted that if $\nu_a(\text{NH}_3)$ is of too low a wavenumber of $\nu_s(\text{SiNH}_2)$, then the reverse order is to be expected for the deuterated analogues. Considering the NH stretching modes alone and assuming a 1.011 factor anharmonicity correction (see ref 13 for a further discussion of the validity of this treatment), ν_a of ND_3 is predicted to be at 2550 cm^{-1} (observed, 2552 cm^{-1}) and ν_s of SiND_2 is predicted to be at 2518 cm^{-1} (observed, 2525 cm^{-1}).

(b) *Secondary Reactions with NH_3 .* The $\nu_s(\text{NH}_2)$ band was always symmetrical and centered at 3444 cm^{-1} during a titration sequence (Figure 3A) but its peak maximum shifted to 3447 cm^{-1} and a shoulder appeared on the high wavenumber side when >20 Torr of NH_3 was added (Figure 3B). No changes resulted following prolonged evacuation up to 200°C except for the disappearance of the 3417-cm^{-1} band (Figure 3C) but after evacuation for 16 h at 300°C the intensity decreased and the peak maximum shifted to 3450 cm^{-1} (Figure 3D). With further evacuation at higher temperatures these processes continued until after 650°C degassing the weak residual band was symmetrical and centered at 3452 cm^{-1} (Figure 3E). [With 10 mg cm^{-2} samples the intensity at $908/888 \text{ cm}^{-1}$ was also fully restored after degassing at 650°C .] If another small dose of NH_3 was added a weak band centered at 3444 cm^{-1} reappeared and the shoulder of the 3452-cm^{-1} band was still evident (Figure 3F). When 20 Torr of NH_3 was added the spectrum reverted back to that shown in Figure 3B.

The residual intensity at 3452 cm^{-1} after the above degassing sequence to 650°C was always near zero with micromole doses of reactant or when larger pressures had been used (>20 Torr) provided the time of reaction was short (1 min). However, if more than 20 Torr of NH_3 was allowed to react for about 1 h, then the residual intensity at 3452 cm^{-1} was always appreciable after degassing at 650°C . Further, during the degassing up to 650°C the band at 3525 cm^{-1} sharpened and shifted to 3540 cm^{-1} , as noted by Blomfield and Little.¹⁰ A series of spectra are shown at the bottom of Figure 3. [The corresponding shifts of the $\nu(\text{ND})$ bands were not so pronounced and the details could not be so clearly resolved. The 2525-cm^{-1} band shifted to 2529 cm^{-1} and the 2628-cm^{-1} band shifted to 2634 cm^{-1} .] Degassing beyond 650°C caused a slow uniform decrease in the intensity of the $3452/3540\text{-cm}^{-1}$ bands with no further shifts in peak position and they disappeared after degassing at about 1050°C .

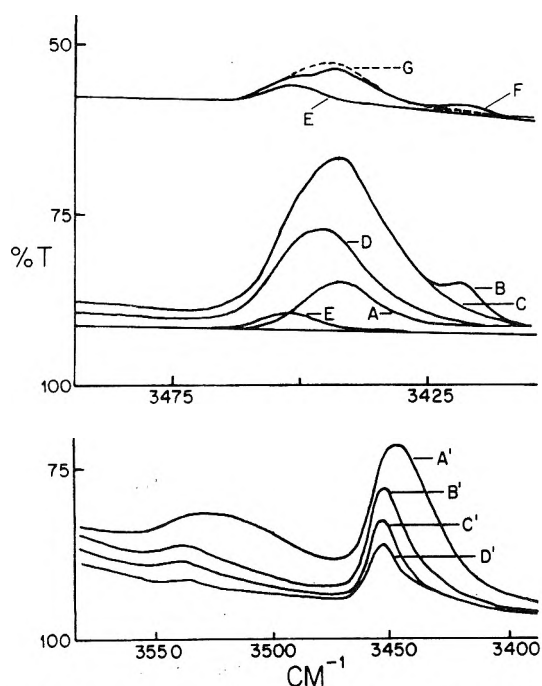


Figure 3. Top: Infrared spectrum near 3450 cm^{-1} following the adsorption and evacuation of NH_3 on a 40 mg cm^{-2} degassed ($1200\text{ }^\circ\text{C}$) silica. (A) After adsorption of $16\text{ }\mu\text{mol}$ and 10-min evacuation. (B) After adding 20 Torr for 1 min and evacuating for 5 min. (C) After 12 h evacuation of (B) at $20\text{ }^\circ\text{C}$ or after 1 h at $200\text{ }^\circ\text{C}$. (D) After evacuation for 16 h at $300\text{ }^\circ\text{C}$. (E) After evacuation for 3 h at $650\text{ }^\circ\text{C}$. (F) After the addition of $2\text{ }\mu\text{mol}$ of NH_3 after (E), no evacuation. (G) After 12 h from (F). The % T scale refers to A–E and E (repeat) to G have been displaced for clarity. Bottom: Spectrum from $3550\text{--}3400\text{ cm}^{-1}$ following (A') adsorption of 25 Torr of NH_3 on a $1200\text{ }^\circ\text{C}$ degassed silica for 2 h and evacuation at $20\text{ }^\circ\text{C}$ for 1 h. Spectral changes after degassing A' at (B') $450\text{ }^\circ\text{C}$ for 2 h; (C') $650\text{ }^\circ\text{C}$ for 1 h; (D') $840\text{ }^\circ\text{C}$ for 1 h.

Blomfield and Little¹⁰ and Peri¹¹ have also reported that the intensity of the SiNH_2 bands increased as a function of initial pressure (for equal reaction time) and as a function of reaction time. We have found that the intensity of the 3748-cm^{-1} band due to residual isolated SiOH groups apparently decreased slightly if high pressures of NH_3 were added, in spite of a slight increase in the intensity of the broad shoulder at 3741 cm^{-1} , and an additional weak feature appeared at 3720 cm^{-1} . These effects are shown in Figure 4 and although the effect was small it was reproducible. These secondary effects were complete in about 1 h as long as more than about 20 Torr of NH_3 was in the reaction cell.

When 1 Torr of HCl was added to a sample which had reacted with sufficient NH_3 so as to just cause the disappearance of the $908/888\text{-cm}^{-1}$ bands then the $3444/3525\text{-cm}^{-1}$ bands instantaneously disappeared, no changes were observed in the $3748/3741\text{-cm}^{-1}$ profile, and a spectrum of NH_4Cl was observed. If the above was repeated after saturation with NH_3 then the spectrum instantaneously changed from that shown in Figure 3A' to 3C'. That is, adding 1 Torr of HCl at $20\text{ }^\circ\text{C}$ produced the same spectral changes as occurred when the sample had been degassed at $650\text{ }^\circ\text{C}$. With time or with higher initial pressures of HCl , the $3452/3540\text{-cm}^{-1}$ bands also disappeared. It has been suggested¹⁰ that part of the intensity at 3520 cm^{-1} might be due to H_2O or to perturbed SiOH groups. This assignment is probably incorrect since none of the spectral features which we have attributed to silanol groups [including the $3720/3520\text{-cm}^{-1}$ bands to be discussed in section d] ever altered when HCl was added.

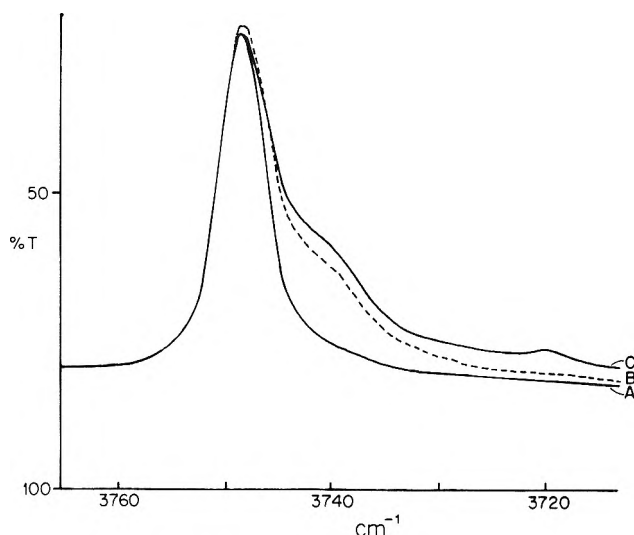
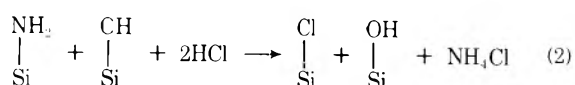


Figure 4. (A) A 10 mg cm^{-2} silica degassed at $1000\text{ }^\circ\text{C}$ for 12 h. (B) After admission of about $10\text{ }\mu\text{mol}$ of NH_3 . (C) After admission of 120 Torr of NH_3 for 30 s and evacuation for 5 min.

(c) *Mechanism of the Secondary Reaction with NH_3 .* The observed shift of the $\nu(\text{NH})$ bands to higher wavenumber is not a surface coverage effect since (a) the reverse shift does not occur on degassing, or when the surface is depopulated after reaction with HCl , and (b) the 3444-cm^{-1} band can be generated even when the 3452-cm^{-1} band is present (Figure 3). Rather it would appear that two types of SiNH_2 species are formed when NH_3 reacts with a partially dehydroxylated silica. We will call these types I and II.

Type I has $\nu(\text{NH})$ bands at 3525 and 3444 cm^{-1} , a sharp $\delta(\text{NH}_2)$ band at 1550 cm^{-1} , and a broad but intense $\nu(\text{SiN})$ band at about 932 cm^{-1} . Type I is formed exclusively by a direct reaction with the active sites as depicted in reaction 1. Type I SiNH_2 is less stable than type II in that it reacts more rapidly with HCl and it can be reversibly removed by degassing at $550\text{--}650\text{ }^\circ\text{C}$. The reaction with HCl is presumed to be as follows:



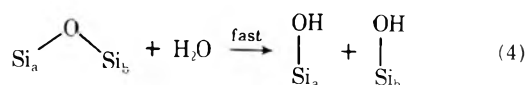
Type II has $\nu(\text{NH})$ bands at 3540 and 3452 cm^{-1} , a sharp $\delta(\text{NH}_2)$ band at 1550 cm^{-1} , and a $\nu(\text{SiN})$ band at 932 cm^{-1} . The band shapes, their relative intensities, and their positions are identical with those which were observed after NH_3 reacted with silica at $650\text{ }^\circ\text{C}$ as described in part IV.⁹ The thermal stability and reactivity with HCl is identical with the latter. The high temperature reaction scheme in part IV⁹ was assumed to involve the normal isolated silanol groups as follows:



and in the present work, in view of the small decrease in intensity of that band, we assume that the same scheme applies. As will be discussed below, the water generated by (3) results in the formation of the weak feature near 3720 cm^{-1} . However, it is to be stressed that this secondary reaction does not occur at $20\text{ }^\circ\text{C}$ unless the silica had been previously dehydroxylated at a temperature above $400\text{ }^\circ\text{C}$.

(d) *Reaction with H_2O .* Since the $908/888\text{-cm}^{-1}$ bands disappeared instantaneously and in unison when a dehy-

droxylated silica was titrated with micromole doses of H₂O, by analogy with (1) we propose the following mechanism:



As discussed in VI,² the unusual breadth of the 3741-cm⁻¹ band generated by reaction with H₂O suggested that two slightly different SiOH groups were generated, each having a $\nu(\text{OH})$ mode near 3741 cm⁻¹. However, a secondary reaction also occurs which is dependent on the initial generation of the above active site.

In part VI we noted that the 3741-cm⁻¹ band developed a tail to low wavenumber toward the end of a titration sequence with H₂O. With an excess of H₂O an additional sharp band developed at 3720 cm⁻¹ accompanied by a very broad feature centered near 3520 cm⁻¹. The spectrum shown in Figure 5B was obtained after 10 Torr of H₂O had been added for 1 h to a new 20 mg cm⁻² sample which had been degassed at 860 °C (Figure 5A), the excess H₂O having been evacuated for 2 h. The shoulder at 3720 cm⁻¹ and the strong band at 3520 cm⁻¹ did not change after prolonged evacuation up to 100 °C. Following evacuation at higher temperatures (Figure 5C, D, and E) both bands decreased in intensity and more or less disappeared if a temperature of 250 °C was used. This type of spectrum and the behavior illustrated upon degassing has been observed by others, particularly by Kiselev's group³⁻⁵ in the USSR, and will be discussed further below. The important point from this work is that the 3520/3720-cm⁻¹ bands were only formed with appreciable intensity after the 908/888-cm⁻¹ bands had disappeared and the new 3741-cm⁻¹ SiOH band had appeared.

With a more highly dehydroxylated sample and with a smaller dose of H₂O all new features in the 3700-cm⁻¹ spectral region can be clearly resolved (Figure 6A and B). A similar sequence using 99% H₂¹⁸O is shown in Figure 6D where the 3741-cm⁻¹ band has now shifted to 3735 cm⁻¹ (see VI) and the 3720-cm⁻¹ band appears as a doublet at 3720 and 3710 cm⁻¹. The broad 3520-cm⁻¹ band (not shown) would not be expected to show any comparable splitting. Upon standing for 16 h in 5 Torr of H₂¹⁸O the 3735-cm⁻¹ band intensified and shifted to 3737 cm⁻¹ and the 3748-cm⁻¹ band decreased in intensity.

If the above reaction was carried out with D₂O using a predeuterated silica, the analogous 3520/3720-cm⁻¹ bands were observed at 2610 and 2740 cm⁻¹ and if a 1:1 mixture of H₂O/D₂O was used no additional bands were observed. Further, if all of the 3748-, 3741-, and 3720-cm⁻¹ bands were present, they exchanged to the same degree as increments of excess D₂O were added and the deuterium containing species were generated.

Finally, the 3720/3520-cm⁻¹ bands could also be generated if excess H₂O was added to a sample which had previously been saturated with NH₃. Therefore, this secondary reaction with H₂O is independent of any changes which might have occurred as a result of the proposed reactions with ammonia. A possible mechanism will be discussed below.

(e) *The Rehydration of Silica.* The rehydration of hydrophobic silica (we will use the term dehydroxylated silica) has been studied by many workers over the past 10 years and a major review of the work up to 1972 has been written by Kiselev and Lygin.⁵ Several more recent studies have also dealt with this problem^{3,4,6} and no clear consensus of the mechanism has yet appeared. All workers have assumed that active aprotic sites are generated in the dehydroxylation reaction although

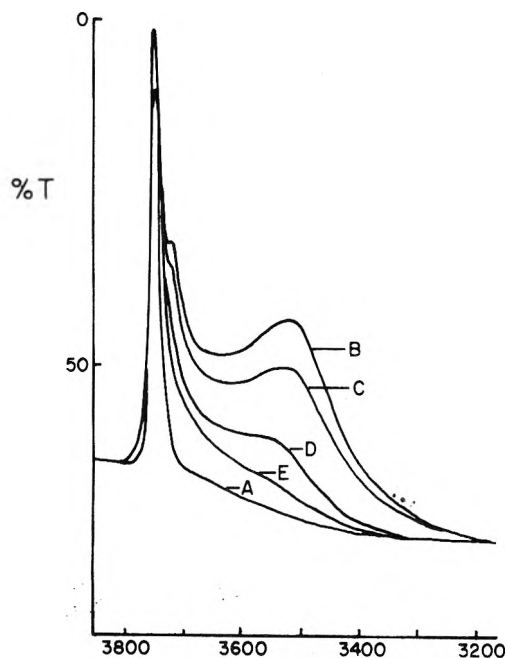


Figure 5. (A) Background spectrum of a 20 mg cm⁻² silica after degassing at 860 °C. (B) After adding 10 Torr of H₂O for 20 min and evacuation for 2 h at 20 °C. (C) Evacuation for 2 h at 150 °C. (D) Evacuation for 12 h at 200 °C. (E) Evacuation for 2 h at 250 °C.

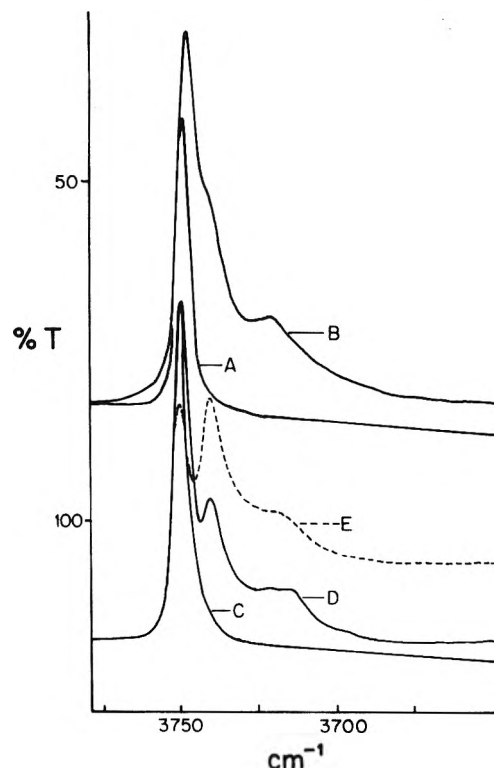


Figure 6. (A) Background spectrum of a 10 mg cm⁻² silica after degassing at 1100 °C. (B) After adsorption of 6 Torr of H₂O for 5 min and evacuation for 5 min at 20 °C. (C) Background spectrum of a 5 mg cm⁻² silica after degassing at 1000 °C. (D) After the adsorption of 0.2 Torr (3 μmol) of 99% H₂¹⁸O. (E) After adding 5 Torr of H₂¹⁸O to D for 16 h and evacuating for 5 min. The % T scale refers to A and B.

no direct spectroscopic proof has been forthcoming. Further, these sites, usually assumed to be strained siloxane bridges, may have varying activity depending on the mode of generation.^{5,14} Thus, with mild heating (<400 °C) adjacent hydrogen

bonded hydroxyls dehydroxylate to liberate water¹⁵⁻¹⁷ and these can be reversibly rehydrated with H₂O vapor at 20 °C. With higher degassing temperatures the remaining isolated hydroxyls are progressively removed and it has been assumed that various types of structural changes must occur, perhaps also accompanied by interparticle sintering giving rise to both extremely stable siloxane bridges which do not readily react with water, and highly strained siloxane bridges which have usual activity.^{5,8,18}

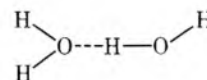
Recent spectroscopic studies have focused attention either on the overtone region^{4,7} from 4000 to 8000 cm⁻¹ or on the $\nu(\text{OH})$ fundamental region^{3,6} from 3000 to 3800 cm⁻¹. In all cases relatively highly hydroxylated samples were used, that is, in comparison with our work there was always a relatively strong residual band due to isolated SiOH groups. Thus, the generation of the 3741-cm⁻¹ band was usually missed. No previous examination below 1000 cm⁻¹ has been reported although this region has been examined in another context.^{19,20} Several workers^{3,5,6} have observed spectra such as those shown in Figure 5 but they have assumed that the generation of the 3720/3520-cm⁻¹ bands was the primary step in the rehydration. This work has shown that the generation of the 3741-cm⁻¹ hydroxyl is the first step as depicted in reaction 1.

The major unresolved question concerning the adsorption of water on dehydroxylated silica has been whether the water hydrogen bonds to the residual SiOH groups, whether it only adsorbs on aprotic centers, or whether both processes occur.^{3-7,21,22} Studies of the adsorption using noninfrared techniques have always indicated that the surface hydroxyl groups are the main adsorption centers.^{5,6,21} Recently Kiselev's group²¹ has shown that, with certain types of infrared spectrometer, the heat generated by the source can heat silica samples up to as high as 80 °C thus making it impossible to compare spectroscopic and nonspectroscopic work if the former is purported to be at 20 °C. He has conclusively shown^{3,4,21} that if the source heating effects are removed then the isolated silanols on dehydroxylated silica fully participate in the adsorption of water. A similar conclusion has been reached by Klier et al.,⁷ who assumed a specific 1:1 interaction in which the isolated silanols were the donors of a hydrogen bond to a single water molecule. [Although we have not been concerned with saturation coverages by H₂O in this work, we have confirmed that we are able to duplicate Kiselev's work either by placing the cell behind the grating, or in the normal sample area. Our spectrometer uses a low current Nernst source and is chopped before the sample so we conclude that beam heating effects are negligible.]

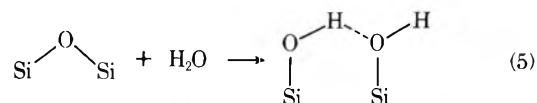
Volkov, Kiselev, and Lygin³ have also found that the bands at 3720 and 3520 cm⁻¹ initially appear at very low surface coverage, growing as adsorption proceeds, and that these bands are the last to be removed during subsequent evacuation, temperatures of about 250 °C being necessary for their removal. They suggested that the first water molecules were adsorbed on the remaining free hydroxyls if the initial degassing temperature was 500 or 700 °C, whereas if 900 or 1100 °C was used, chemisorption on siloxane bridges occurred and the resulting hydroxyls acted as centers for subsequent adsorption of water. They assumed that the 3720/3520-cm⁻¹ bands were due to either "unsymmetrically perturbed" water molecules, or to water dimers. We will now examine this hypothesis in the light of the present results.

The generation of the 3720/3520-cm⁻¹ bands is a secondary process which only occurs after the primary sites which are responsible for the 908- and 888-cm⁻¹ bands have been con-

sumed. The splitting of the 3720-cm⁻¹ band into two equally intense bands at 3720 and 3710 cm⁻¹ when H₂¹⁸O is used suggests that surface SiOH groups (one Si¹⁶OH and the other Si¹⁸OH) are responsible for these features and not molecular water. That is, for an unsymmetrically perturbed water molecule or a dimer (of H₂¹⁸O) only one shifted band at about 3710 cm⁻¹ would have been expected. Furthermore, for a water dimer of the type



envisaged by Volkov et al.³ and first studied in CCl₄ by Magnusson²³ or in nitrogen matrices by Tursi and Nixon²⁴ one would expect to observe additional bands between 3700 and 3650 cm⁻¹ when a 1:1 H₂O/D₂O mixture was adsorbed. Therefore, we conclude that this secondary process also involves a reaction between siloxane sites and water, sites which are slightly less reactive than those responsible for the primary step. We must further assume that the silicon-silicon distance is short enough so that the two SiOH groups can hydrogen bond (the broad band at 3520 cm⁻¹) and that the silicons are symmetric so that there is equal probability of the free SiOH (3720-cm⁻¹ band) containing ¹⁸O or ¹⁶O when 99% H₂¹⁸O is added. The scheme would be:



These hydrogen bonded pairs must be isolated and presumably the concentration is relatively low initially. A fully hydroxylated silica normally only has a broad band near 3550 cm⁻¹ due to hydrogen bonded hydroxyls^{5,14,16,17} (in addition to the 3748-cm⁻¹ band) probably corresponding to chains of such mutually H-bonded species and therefore, the 3720-cm⁻¹ band is not detected because few "terminal" groups exist.

The site depicted in reaction 5 did not react with excess NH₃ because (a) there was no clear evidence for the formation of hydrogen bonded SiOH or of hydrogen bonded SiNH₂, and (b) if excess H₂O was added after saturation with NH₃ the 3720/3520-cm⁻¹ bands continued to grow just as if ammonia had never been added. Therefore, the very weak band at 3720 cm⁻¹ when excess NH₃ was used (see section b) we assume was due to the H₂O liberated in (3) reacting with a few of the symmetric siloxane sites as in (5).

A third process occurs when H₂O vapor is allowed to react with dehydroxylated silica, namely, oxygen-18 exchange of the isolated SiOH groups (Figure 6E). [It is to be stressed that this spectrum represents a genuine O-18 exchange of the 3748-cm⁻¹ band to 3737 cm⁻¹ (see ref 8) not merely an intensification of the 3741-3730-cm⁻¹ profile due to reaction between H₂¹⁸O and the site depicted in (4). The latter reaction yields a different profile centered at 3535 cm⁻¹ and has been discussed in VI.2] Such exchange does not occur at 20 °C if the saturation vapor pressure of H₂¹⁸O is allowed to remain in contact with a nondegassed silica for up to 48 h. Clearly, the dehydroxylation process has altered the reactivity of the residual isolated hydroxyl groups even though the $\nu(\text{OH})$ frequency remains unaltered. It is this altered reactivity that we believe is responsible for the secondary reaction (3) between NH₃ and the isolated SiOH groups, recalling that no reaction occurs without the prior dehydroxylation.

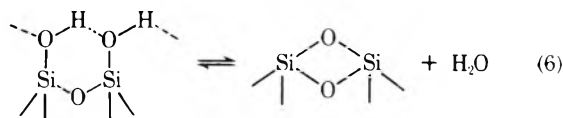
Summary

This work has shown that three consequences follow when the isolated hydroxyl groups are removed from silica by degassing under vacuum at high temperatures. (1) Extremely reactive siloxane bridge sites are generated which facilitate the dissociative chemisorption of H₂O and of NH₃ at 20 °C and which can act as Lewis acid centers for the coordination of the lone pair electrons on nitrogen. (2) Less reactive and presumably symmetric siloxane bridges are formed which rupture with H₂O (but not with NH₃) to yield pairs of SiOH groups which are close enough to hydrogen bond with each other. (3) The residual isolated hydroxyl groups show an unusual reactivity in that they slowly exchange with H₂¹⁸O at 20 °C or they react to a limited extent with NH₃ at 20 °C.

With large quantities of H₂O vapor we observed the same effects which have been reported by Volkov et al.,^{3,4} i.e., the eventual disappearance of all spectral features in the 3750–3700-cm⁻¹ region and the growth of a strong band near 3450 cm⁻¹ due to liquidlike water. Our interpretation of the initial stages of rehydration differs in two ways. First, the apparent intensification observed at 3748 cm⁻¹ (isolated silanols) when the first traces of H₂O were added to a silica which was degassed at 1100 °C (or of its overtone band at 7326 cm⁻¹) was interpreted by Volkov et al.³ and by Davydov et al.⁴ as due to a presumed chemisorption of H₂O on siloxane bridges which simply regenerated normal isolated SiOH groups. We have never observed this during the initial stages of rehydration, but under the apparent low resolution conditions employed in ref 3 and 4, coupled with the relatively intense residual band at 3748 or at 7326 cm⁻¹, it would appear that our 3741-cm⁻¹ shoulder was missed and the composite effect was an apparent intensification at 3748 cm⁻¹.

Secondly, the bands at 3720 and 3520 cm⁻¹ were attributed to molecular water by Volkov et al.³ and by Chuiko et al.⁶ We contend that these can be assigned to the formation of isolated pairs of SiOH groups which are close enough to hydrogen bond. This we assume is the first stage in the true rehydration process which eventually leads to the formation of networks of hydrogen bonded silanols. Undoubtedly with further additions of water, molecular water hydrogen bonds on these and on the isolated hydroxyl groups.^{3,4,7} Our studies have not been concerned with near saturation coverages since it is necessary to be able to examine the overtone region between 8000 and 4000 cm⁻¹ in order to extract useful information,^{4,5,7} a capability we do not possess.

Finally, it has generally been assumed that the reversible rehydration of silicas which have been heated at temperatures below 400 °C is due to simple processes of the type



where the somewhat strained siloxane bridges readily react with water.^{5,15} However, with temperatures above 400 °C the rehydration becomes progressively irreversible and it has been

assumed that structural rearrangement has occurred.^{5,15,25} That the latter is correct has been shown in this work by the appearance of the 908/888-cm⁻¹ bands once heating exceeds about 550 °C (as discussed in VI,² these sites actually start to form at about 400 °C). A secondary structural effect is the altered properties of the isolated SiOH groups.

We have stressed^{1,2} that although the active site depicted in reactions 1 and 4 accounts for the apparent stoichiometry and for the spectroscopic observations, the real site may be considerably more complex. Indeed, our postulated electron deficient silicon atom may be separated from the siloxane bridge. Further, the rather extreme dehydroxylation conditions might have caused a chemical reduction such that the surface layer may have a composition approaching Si₂O₃ which is reported to have infrared bands between 893 and 870 cm⁻¹.^{26,27} Therefore, on the basis of the present results we do not feel that it is fruitful to suggest detailed mechanisms for the above rearrangement.

Acknowledgment. We gratefully acknowledge financial support from the National Research Council of Canada. B.A.M. also acknowledges the help provided by Professor G. A. Somorjai and the staff at the University of California, Berkeley, where this manuscript was written while he was on sabbatical.

References and Notes

- (1) B. A. Morrow and I. A. Cody, *J. Phys. Chem.*, **80**, 1995 (1976).
- (2) B. A. Morrow and I. A. Cody, *J. Phys. Chem.*, **80**, 1998 (1976).
- (3) A. V. Volkov, A. V. Kiselev, and V. I. Lygin, *Russ. J. Phys. Chem.*, **48**, 703 (1974).
- (4) V. Ya. Davydov, A. V. Kiselev, V. A. Lokutsievskii, and V. I. Lygin, *Russ. J. Phys. Chem.*, **48**, 1342 (1974).
- (5) A. V. Kiselev and V. I. Lygin, "Infrared Spectra of Surface Compounds", Wiley, New York, N.Y., 1975.
- (6) A. A. Chuiko, V. A. Sobolev, and V. A. Tertykh, *Ukr. Khim. Zh.*, **38**, 774 (1972) [in Russian].
- (7) K. Klier, J. H. Shen, and A. C. Zettlemoyer, *J. Phys. Chem.*, **77**, 1458 (1973).
- (8) B. A. Morrow and A. Devi, *J. Chem. Soc., Faraday Trans. 1*, **68**, 403 (1972).
- (9) B. A. Morrow, I. A. Cody, and Lydia S. M. Lee, *J. Phys. Chem.*, **79**, 2405 (1975).
- (10) G. A. Blomfield and L. H. Little, *Can. J. Chem.*, **51**, 1771 (1973).
- (11) J. B. Peri, *J. Phys. Chem.*, **70**, 2937 (1966).
- (12) A. A. Tsyganenko, D. V. Pozdnyakov, and V. N. Filimonov, *J. Mol. Structure*, **29**, 299 (1975).
- (13) B. A. Morrow, *J. Chem. Soc., Faraday Trans. 1*, **70**, 1527 (1974).
- (14) M. L. Hair, "Infrared Spectroscopy in Surface Chemistry", Marcel Dekker, New York, N.Y., 1967.
- (15) G. J. Young, *J. Colloid Sci.*, **13**, 67 (1958).
- (16) A. J. Tyler, F. H. Hambleton, and J. A. Hockey, *J. Catal.*, **13**, 35 (1969).
- (17) C. G. Armistead, A. J. Tyler, F. H. Hambleton, S. A. Mitchell, and J. A. Hockey, *J. Phys. Chem.*, **73**, 3947 (1969).
- (18) J. Kunawicz, P. Jones, and J. A. Hockey, *Trans. Faraday Soc.*, **67**, 848 (1971).
- (19) M. Hino and T. Sato, *Bull. Chem. Soc. Jpn.*, **44**, 33 (1971).
- (20) H. A. Benesi and A. C. Jones, *J. Phys. Chem.*, **63**, 179 (1959).
- (21) G. A. Galkin, A. V. Kiselev, and V. I. Lygin, *Russ. J. Phys. Chem.*, **42**, 765 (1968); **43**, 1117, 1292 (1969).
- (22) W. D. Bascom, *J. Phys. Chem.*, **76**, 3188 (1972).
- (23) L. B. Magnusson, *J. Phys. Chem.*, **74**, 4221 (1970).
- (24) A. J. Tursi and E. R. Nixon, *J. Chem. Phys.*, **52**, 1521 (1970).
- (25) T. H. Elmer, I. D. Chapman, and M. E. Nordberg, *J. Phys. Chem.*, **66**, 1517 (1962).
- (26) Y. Nishimura, T. Inagaki, and H. Sasaki, *Fujitsu Sci. Tech. J.*, **2**, 87 (1966).
- (27) A. Toshito and O. Kazumasa, *Chem. Abstr.*, **69**, 6570 (1968).

Dipole Moment Derivatives, Polar Tensors, and Effective Charges of Ammonia and Phosphine

A. B. M. S. Bassi and Roy E. Bruns*

Instituto de Química, Universidade Estadual de Campinas, C.P. 1170, Campinas, S.P., Brasil (Received May 17, 1976)

Publication costs assisted by Universidade Estadual de Campinas

Preferred signs for the dipole moment derivatives of phosphine are selected on the basis of comparison of CNDO calculated values with the experimental alternatives. The atomic polar tensors, effective charges, mean dipole moment derivatives, and anisotropies for the preferred experimental values of this molecule and of ammonia are presented. A recently suggested criterion for the selection of preferred signs based on effective charge values is found to be valid for phosphine but not for ammonia.

Introduction

Preferred sets of signs for the dipole moment derivatives with respect to the normal coordinates, $\partial p/\partial Q_i$, have been determined for almost all of the molecules for which complete experimental intensity data are available. However phosphine is an exception even though its infrared fundamental gas phase intensities have been known for some time.¹ In a localized molecular orbital study of ammonia² CNDO estimates of the derivatives with respect to the symmetry coordinates, $\partial p/\partial S_j$, were compared with the experimental alternative sets of derivatives determined using the intensity data and normal coordinates of ref 1. Preferred signs for $\partial p/\partial Q_i$ are clearly indicated in both the A_1 and E symmetry species. In this report we compare these CNDO values of $\partial p/\partial S_j$ for NH_3 and previously unreported CNDO values for PH_3 with the various experimental alternative sets of derivatives calculated using the normal coordinates corresponding to the refined force fields of Duncan and Mills.³ Their general harmonic force fields, determined using centrifugal distortion and Coriolis constants in addition to the harmonic frequencies of the parent and full deuterated molecules, are very similar to the ones recently obtained by Schlegel et al.⁴ by means of ab initio quantum mechanical calculations. The selection of preferred signs for $\partial p/\partial Q_i$, besides allowing us to perform a comparative study of the dipole moment derivatives of these molecules, permits us to test the hypothesis of Prasad and Singh⁵ that the correct signs correspond to values of the atomic effective charges which show a maximum difference for the central and terminal atoms.

Calculations

The $\partial p/\partial S_j$ values determined from the intensity data of ref 1 and the normal coordinate transformations of ref 3 are presented in Table I. The symmetry coordinates are identical with those of McKean and Schatz¹ (see Table I) except that the bending coordinates are weighted by the equilibrium NH and PH bond lengths so that all of the derivatives have common units of e . Interatomic distances and angles of 1.014 Å and 106° 47' for ammonia and 1.419 Å and 93° 30' for phosphine were used.¹ The molecular orientation relative to a space-fixed Cartesian coordinate system is given in Figure 1. The CNDO⁶ calculations were performed as described previously.⁷ As the theoretical results refer to rotation-free distortions in a space-fixed coordinate system whereas the experimental values imply that the Eckart conditions are sat-

isfied, rotational corrections of +0.014 and -0.048 e for NH_3 and +0.002 and -0.021 e for PH_3 were applied to the experimental values of $\partial p_x/\partial S_3$ and $\partial p_x/\partial S_4$, respectively. These values correspond to S_4 distortions of the internal coordinates such that the angles between the NH and PH bonds and the z axis in Figure 1 remain constant.

The experimental derivatives were transformed to atomic polar tensors, $\mathbf{P}_X^{(\alpha)}$, and effective charges, ξ_α , using the relations⁸

$$\mathbf{P}_X = \mathbf{P}_S \mathbf{U} \mathbf{B} + \mathbf{P}_\rho \beta \quad (1)$$

and

$$\xi_\alpha^2 = \text{TR} [\mathbf{P}_X^{(\alpha)} \mathbf{P}_X^{(\alpha)}] \quad (2)$$

Atomic mean dipole moment derivatives, \bar{p}^α , and anisotropies, β_α^2 , which are related to the effective charge by

$$\xi_\alpha^2 = 3(\bar{p}^\alpha)^2 + \frac{2}{3}\beta_\alpha^2 \quad (3)$$

were calculated using⁹

$$\bar{p}^\alpha = \frac{1}{3} \text{TR} [\mathbf{P}_X^{(\alpha)}] = \frac{1}{3} (p_{xx} + p_{yy} + p_{zz}) \quad (4)$$

and

$$\beta_\alpha^2 = \frac{1}{2} [(p_{xx} - p_{yy})^2 + (p_{yy} - p_{zz})^2 + (p_{zz} - p_{xx})^2 + 3(p_{xy}^2 + p_{yz}^2 + p_{xz}^2 + p_{yx}^2 + p_{zy}^2 + p_{zx}^2)] \quad (5)$$

Results

The CNDO values of $\partial p/\partial S_j$ for NH_3 and PH_3 are compared with the experimental alternatives in Table I. The experimental values for NH_3 are quite similar to those obtained using the normal coordinates of McKean and Schatz.¹ The choice of $\partial p/\partial Q_{3a}$ with a negative sign and $\partial p/\partial Q_1$, $\partial p/\partial Q_2$, and $\partial p/\partial Q_{4a}$ with positive signs, as reported previously² are to be preferred for the values in Table I also.

The comparison of theoretical values with the experimental alternatives for PH_3 is also straight forward. Only the + - - - choice of signs ($\partial p/\partial Q_1$ being positive and the others negative) leads to signs of the experimental $\partial p/\partial S_j$ in agreement with the CNDO signs.

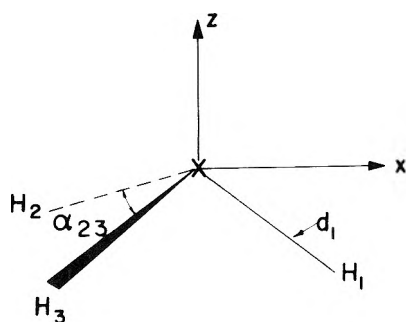
A comparison of the signs of the experimental derivatives for NH_3 and PH_3 is indeed interesting. For both molecules $\partial p_z/\partial S_1$ is positive and $\partial p_z/\partial S_{3a}$ is negative. If intramolecular

TABLE I: Comparison of the Experimental and CNDO Calculated Dipole Moment Derivatives for NH₃ and PH₃ (e)^{a, b}

NH ₃		
A ₁	$\partial p_z / \partial S_1$	$\partial p_z / \partial S_2$
+ + ^c	+0.057	+0.321
+ -	+0.106	-0.302
CNDO	+0.011	+0.303
E		
	$\partial p_x / \partial S_{3a}$	$\partial p_x / \partial S_{4a}$
+ +	+0.018	+0.118
- -	-0.046	-0.022
+ -	+0.028	-0.023
- +	-0.056	+0.119
CNDO	-0.180	+0.109
PH ₃		
A ₁	$\partial p_z / \partial S_1$	$\partial p_z / \partial S_2$
+ +	+0.259	+0.078
+ -	+0.218	-0.115
CNDO (spd)	+0.248	-0.453
E		
	$\partial p_x / \partial S_{3a}$	$\partial p_x / \partial S_{4a}$
+ +	+0.167	+0.094
- -	-0.171	-0.052
+ -	+0.169	-0.056
- +	-0.173	+0.097
CNDO (spd)	-0.402	-0.252

^a Units of electrons, e . $1 \text{ D } \text{\AA}^{-1} = 0.2082e = 3.335 \times 10^{-20} \text{ C}$.

^b The symmetry coordinates are given by: $S_1 = 3^{-1/2}(d_1 + d_2 + d_3)$, $S_2 = 3^{-1/2}r_0(\alpha_{12} + \alpha_{23} + \alpha_{13})$, $S_{3a} = 6^{-1/2}(2d_1 - d_2 - d_3)$, and $S_4 = 6^{-1/2}r_0(2\alpha_{23} - \alpha_{12} - \alpha_{13})$ where d_i and α_{ij} represent the bond and angle coordinates as they are numbered in Figure 1. ^c The different sign possibilities for $\partial p / \partial Q_i$. For example, (+ -) in the A₁ species means that $\partial p_z / \partial Q_1$ is positive and $\partial p_z / \partial Q_2$ is negative. Correspondingly in the E species, those signs indicate that $\partial p_x / \partial Q_3$ and $\partial p_x / \partial Q_4$ are positive and negative, respectively.

**Figure 1.**

charge transfer provided the only significant contributions to the values of these derivatives, their signs imply that electronic charge is transferred in the direction of the moving hydrogens as the NH or PH bond lengths increase. However the localized molecular orbital study of ammonia² indicates that contributions from equilibrium charge movements and distortions of the electronic charge densities described by means of sp polarizations about the central atom are also significant. The net result of all these contributions is considerably larger for PH₃ than for NH₃ as reflected in the larger absolute magnitudes of the experimental phosphine derivatives.

The bending symmetry coordinates for the two molecules show opposite signs for the derivatives, however. In the case of NH₃, the positive signs of $\partial p / \partial S_2$ and $\partial p / \partial S_{4a}$ indicate that electronic charge moves in a direction opposite to that of the hydrogen atoms as S_2 and S_{4a} increase. A bond moment model

description would imply bond moments of the sense $-\text{NH}^+$. The signs of these two derivatives are negative for phosphine implying an opposite flow of charge and a $+\text{PH}^-$ sense for the bond moments. Contrary to the situation for the stretching coordinates, the bending derivatives of NH₃ correspond to larger dipole moment changes than do those of PH₃.

In Table II we present values for the atomic polar tensors calculated using eq 1 and the preferred experimental values of $\partial p / \partial S_j$ in Table I. The atomic polar tensors for P and N are of diagonal form with $\partial p_x / \partial x_\alpha = \partial p_y / \partial y_\alpha$ as dictated by symmetry. The polar tensors for the hydrogen atoms in the xz plane of Figure 1 show off-diagonal elements as large or larger than the diagonal elements. Polar tensors for the other two hydrogen atoms, which are not presented here, have nonzero values for all their elements using this coordinate system. These tensors can be simplified by a rotation of the Cartesian coordinate axes such that one axis is coincident with a bond and the other two are perpendicular to it. However molecular symmetry does not allow the polar tensors of hydrogen a simpler form than the one given in Table II.

The values of the atomic effective charge, mean dipole moment derivative, and anisotropy presented in Table III were calculated by applying eq 2, 4, and 5 to the values in Table II. It is somewhat surprising that the effective charge of nitrogen is smaller than that of phosphorus. For the X₂CY¹⁰ (X = F, Cl; Y = O, S), BX₃¹¹ (X = F, Cl), and CH₃X⁹ (X = F, Cl, Br, I), the effective charge values of the terminal atoms increase as the electronegativity of those atoms increase. These results indicate the opposite trend for a central atom. A relatively small value for the mean dipole moment derivative of the nitrogen atom, which results from a cancellation of positive and negative diagonal elements of $P_X^{(N)}$, leads to a small value of ξ_N in spite of the fact that its anisotropy value is quite large. That the effective charges of central atoms may indeed show different behaviors with respect to atomic properties than the terminal atoms can be seen upon inspection of these values for other molecules. The effective charge of nitrogen in NF₃ is smaller than that of phosphorus in PF₃.^{5,12} Also ξ_C is reported to be smaller than ξ_S for both the XH₄ and XF₄ (X = C, Si) groups.⁵ It should be noted here that Prasad and Singh⁵ state that NH₃ and PH₃ are exceptions to this behavior for central atoms. However they based their observation on ξ_α values corresponding to an apparently incorrect sign choice for $\partial p / \partial Q_i$ of ammonia, which we discuss later. The effective charge values of hydrogen increase with the electronegativity of the central atom in these molecules. This is not a completely general phenomenon, however, as ξ_F in PF₃ is larger than in NF₃.¹²

Recently Prasad and Singh⁵ have suggested that a comparison of the effective charge values for the central and terminal atoms can be used to indicate the correct set of signs for $\partial p / \partial Q_i$. They found that the difference in ξ_α ² values for the central atom and the sum of these values for the terminal atoms is maximum for the preferred sign combinations for several groups of molecules. The preferred sign choice for PH₃ (+ - - -) gives $\xi_P^2 - 3\xi_H^2 = 0.250e^2$ which corresponds to the maximum difference found by Prasad and Singh considering all the possible sign alternatives. For the preferred (+ + + +) choice of NH₃ this difference is $0.036e^2$ whereas several other alternative sign combinations yield larger values. In ref 5 a difference of $0.091e^2$ is reported for the (+ - + +) set of signs. This choice, as indicated by the signs of $\partial p / \partial S_j$ in Table I, necessitates the acceptance of electronic charge flows and distortions in opposite directions for the NH bending motions (i.e., NH bond moments of opposite senses).

TABLE II: Atomic Polar Tensors for NH₃ and PH₃ (e)^a

	$\mathbf{P}_X^{(N)}$			$\mathbf{P}_X^{H_1^1 b}$		
NH ₃ (+ + - +)	+0.110 0 0	0 +0.110 0	0 0 -0.524	-0.101 0 +0.106	0 +0.027 0	-0.187 0 +0.175
	$\mathbf{P}_X^{(P)}$			$\mathbf{P}_X^{(H_1)^b}$		
PH ₃ (+ - - -)	+0.318 0 0	0 +0.318 0	0 0 +0.434	-0.115 0 +0.057	0 -0.097 0	0.072 0 -0.145

^a Units of electrons, *e*. ^b The atomic polar tensors of hydrogen atom number 1 in Figure 1. The atomic polar tensors for the other hydrogen atoms can be generated by rotations as described in ref 9.

TABLE III: Mean Dipole Moment Derivatives, Anisotropies, and Effective Charges of NH₃ and PH₃ (e)^a

XH ₃	\bar{p}^x	β_X^2	ξ_X	$\bar{p}^H b$	$\beta_H^2 c$	$\xi_H b$
NH ₃ (+ + - +)	-0.101	0.402	0.547	0.034	0.127	0.296
PH ₃ (+ - - -)	0.357	0.013	0.625	-0.119	0.014	0.228

^a Units of electrons, *e*, and electrons squared, *e*² (for β_X^2). ^b As these three quantities are invariant to rotations of the Cartesian coordinate axes subscripts for hydrogen are not necessary.

Furthermore the positive value of $\partial p/\partial S_{3a}$ for this set of signs implies that electronic charge moves in a direction opposite to that of the hydrogen atoms. This is contrary to what has been found for *all* the other molecules for which preferred sign combinations have been chosen. Independent of the types of central and terminal atoms, electronic charge has always been found to move in the same direction as the terminal atoms when the bond lengths are increased. A maximum difference of $0.305e^2$ is reported for the (+ - - -) sign choice contrary to the sign choice indicated by the theory. As CNDO calculated values are considered to be more accurate for first row atoms than for those of the second row, ammonia appears to present one exception to the rule proposed by Prasad and Singh.

Acknowledgment. Computer time furnished by the Centro de Computação of the Universidade Estadual de Campinas

and partial financial support from the Financiadora de Estudos e Projetos (FINEP) is gratefully acknowledged.

References and Notes

- (1) D. C. McKean and P. N. Schatz, *J. Chem. Phys.*, **24**, 316 (1956).
- (2) R. E. Bruns, A. B. M. S. Bassi, and P. M. Kuznesof, *J. Am. Chem. Soc.*, submitted for publication.
- (3) J. L. Duncan and I. M. Mills, *Spectrochim. Acta, Part A*, **20**, 523 (1964).
- (4) H. B. Schlegel, S. Wolfe, and F. Bernardi, *J. Chem. Phys.*, **63**, 3632 (1975).
- (5) P. L. Prasad and S. Singh, *J. Chem. Phys.*, in press.
- (6) J. A. Pople and D. L. Beveridge, "Approximate Molecular Orbital Theory", McGraw-Hill, New York, N.Y., 1970.
- (7) G. A. Segal and M. L. Klein, *J. Chem. Phys.*, **47**, 4236 (1967); R. E. Bruns and W. B. Person, *ibid.*, **53**, 1413 (1970).
- (8) W. B. Person and J. H. Newton, *J. Chem. Phys.*, **61**, 1040 (1974).
- (9) J. H. Newton and W. B. Person, *J. Chem. Phys.*, **64**, 3036 (1976).
- (10) A. B. M. S. Bassi and R. E. Bruns, *J. Chem. Phys.*, **62**, 3235 (1975).
- (11) R. E. Bruns and A. B. M. S. Bassi, *J. Chem. Phys.*, **64**, 3053 (1976).
- (12) R. E. Bruns and A. B. M. S. Bassi, unpublished results.

Light Scattering Study of Local Structures in Solutions: Chloroform–Ethanol System

Tadashi Kato and Tsunetake Fujiyama*

Department of Chemistry, Faculty of Science, Tokyo Metropolitan University, Setagaya-ku, Tokyo 158, Japan (Received May 10, 1976)

Publication costs assisted by Tokyo Metropolitan University

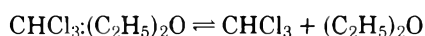
Light scattering spectra were observed for binary solutions of chloroform–ethanol at various concentrations and for various temperatures. The Rayleigh intensities were reduced to concentration fluctuations. The observed temperature and concentration dependencies of concentration fluctuation were explained well if we assumed the existence of an associated complex which was composed of a few ethanol molecules and a chloroform molecule. This result was compared with spectroscopic and thermodynamic data.

Introduction

Local fluctuation of concentration is considered to afford information which is useful to understand the *mixing of liquids* from a molecular viewpoint. Based upon this belief, we have planned a series of studies on analyses of temperature and concentration dependencies of concentration fluctuation through observations of light scattering spectra.¹

First, the relationship between concentration fluctuation and Rayleigh intensities has been theoretically established.² The concentration fluctuations for the chloroform–carbon disulfide system observed by this light scattering method were compared with those determined from the half-band width of the infrared spectrum for the ν_1 fundamental of chloroform-*d*.³

Study of light scattering spectra for the chloroform–diethyl ether system⁴ showed that the observed temperature and concentration dependencies of concentration fluctuation can be explained quite well by considering a (1:1) complex formation between chloroform and diethyl ether molecules and the dissociation equilibrium



The present report concerns itself with the study of the concentration and temperature dependencies of concentration fluctuation for binary solutions of chloroform–ethanol through the observation of light scattering spectra. Our interests lie in the possibility of determining local structures in solutions where the local structures are unknown.

Experimental Section

The samples used in the present study were commercially available reagents. Ethanol was purified by distillation after elimination of water by zeolite A-3. Chloroform was purified by column chromatography on alumina in order to eliminate water and ethanol. The binary solution of ethanol and chloroform was made dust-free by the use of a millipore filter FG of 0.2- μm pore size. Mole fractions of sample solutions were determined from the weight and density of each component. Density data were found in the International Critical Tables.⁵

Light scattering spectra were obtained by using a spectrometer designed and constructed in our laboratory. The spectrometer is composed of a He–Ne gas laser source (NEC, GLG108) and a pressure scanning Fabry–Perot interferometer. Details of the spectrometer have been reported elsewhere along with the reliability of the spectrometer.

The temperature of the samples was controlled by a high

temperature cell which was made by the authors. A temperature constancy of $\pm 1^\circ\text{C}$ was obtained with the apparatus.

The sampling procedure for the observation of light scattering spectra at a given concentration was repeated several times, until at least three spectra whose Rayleigh intensities were almost the same were obtained. Of these samples, the sample which showed the least Rayleigh intensity was chosen as the best sample. Then, light scattering spectra were observed for this best sample at temperatures of 20, 35, and 45 $^\circ\text{C}$. The observation was repeated five times and this averaged value was chosen as an observed intensity data.

Results and Discussion

Light Scattering Spectra and Concentration Fluctuation. Figure 1 shows the light scattering spectra for the ethanol–chloroform system. It is seen from the figure that the Rayleigh intensity increases in magnitude on passing from pure liquids to binary solutions. After separating the Rayleigh part from the observed spectra, a Rayleigh intensity was expressed relative to a Rayleigh intensity of pure chloroform. Then, the concentration fluctuation, $\langle(\Delta x)^2\rangle$, was calculated from the relation²

$$N\langle(\Delta x)^2\rangle = \frac{RT^2}{M(\partial n/\partial x)_{P,T}} \left[\frac{S}{S_0} \left(\frac{n_0}{n}\right)^2 \left(\frac{\rho}{\rho_0}\right) \frac{(\partial n_0/\partial T)_{P,x}}{C_{P_g}^\circ} - \frac{(\partial n/\partial T)_{P,x}}{C_{P_g}} \right] \quad (1)$$

where R is the gas constant, M the mean molecular weight, T the absolute temperature, n the refractive index, ρ the density, C_{P_g} the specific heat per gram, N the total number of molecules of the field within which the concentration fluctuation is considered, and (S/S_0) is an intensity ratio of Rayleigh lines. The suffix zero specifies the quantities related with pure chloroform.

In Figure 2, the concentration fluctuations thus obtained are plotted against the mole fraction, x , of ethanol for different temperatures. The dashed line of Figure 2 corresponds to the concentration fluctuation expected for an ideal binary solution. It is seen from the figure that the observed concentration fluctuation is generally larger than that of an ideal solution. The concentration fluctuation takes a maximum value at $x = 0.5$ for an ideal solution, while the observed concentration fluctuation takes a maximum value at the mole fraction of about 0.3 for an ethanol–chloroform system. In the region where x is smaller than 0.6, the concentration fluctuation assumes much larger values than that of an ideal solution. As the temperature increases, the magnitude of the concentration

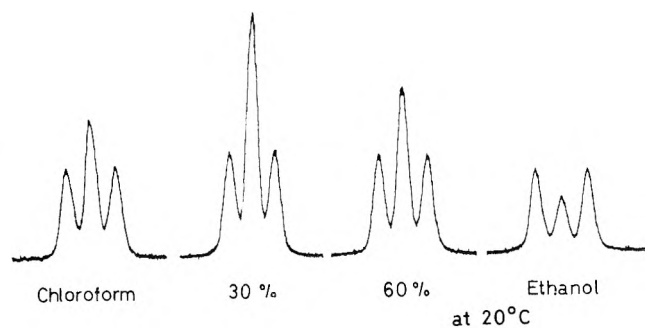


Figure 1. Observed light scattering spectra for the ethanol-chloroform system at 20 °C. The concentration is expressed in terms of mole percent of ethanol.

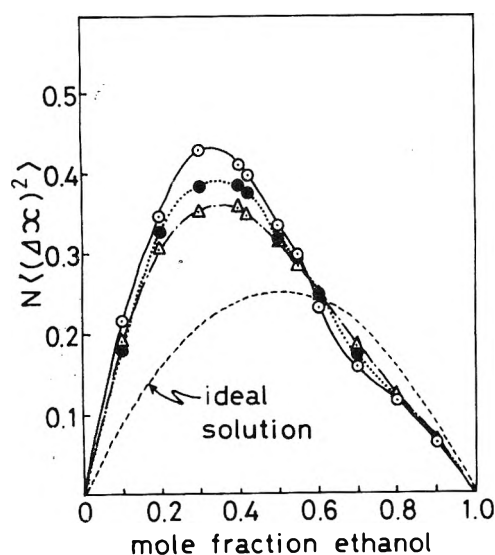


Figure 2. Observed concentration fluctuation for the ethanol-chloroform system at temperatures of: (—○—) 20 °C; (· · · ● · · ·) 35 °C; (---△---) 45 °C.

fluctuation decreases in this concentration range. On the other hand, in the region where x is larger than 0.6, the concentration fluctuation assumes smaller values than those of an ideal solution and increases in magnitude as the temperature increases.

These specific concentration and temperature dependencies of the concentration fluctuation may arise from intermolecular interactions between ethanol and chloroform molecules. Taking into account the probable intermolecular interactions such as hydrogen bonding formation, we tried to estimate possible local structures expected for an ethanol-chloroform system through theoretical consideration of the observed concentration and temperature dependencies of the concentration fluctuation.

Theoretical Consideration of $\langle(\Delta x)^2\rangle$. Instead of considering intermolecular interactions directly, we introduce a concept of an associated complex.

Consider a binary solution whose components are molecules A and B. The concentration fluctuation within the region which contains a constant number, N , of molecules can be estimated from the number fluctuation of molecule A, $\langle(n_A - \bar{n}_A)^2\rangle$

$$\begin{aligned} \langle(x_A - \bar{x}_A)^2\rangle &= \left\langle \left[\frac{n_A}{N} - \left(\frac{\bar{n}_A}{N} \right) \right]^2 \right\rangle \\ &= \frac{1}{N^2} \langle(n_A - \bar{n}_A)^2\rangle \quad (2) \end{aligned}$$

where \bar{x}_A is a macroscopic mean mole fraction of molecule A. The number fluctuation corresponding to the right-hand side of eq 2 is reduced to the relation

$$\langle(n_A - \bar{n}_A)^2\rangle = \langle n_A(n_A - 1) \rangle + \bar{n}_A - (\bar{n}_A)^2 \quad (3)$$

The necessary terms of eq 3 are obtained from the relations

$$\bar{n}_A = \sum_{n_A=0}^N n_A f(n_A) \quad (4)$$

and

$$\langle n_A(n_A - 1) \rangle = \sum_{n_A=0}^N n_A(n_A - 1) f(n_A) \quad (5)$$

where $f(n_A)$ is a probability of finding n_A number of molecule A in the region being considered. Under the assumption that a binary solution is ideal, $f(n_A)$ is expressed as

$$f(n_A) = \frac{N!}{n_A!(N - n_A)!} P_A^{n_A} (1 - P_A)^{N - n_A} \quad (6)$$

because there is no intermolecular interaction in the system and because sizes of component molecules are the same. P_A of eq 6 is the probability of a molecule being A. In the present treatment, P_A is equal to the mole fraction, \bar{x}_A , of molecule A. Combining eq 4, 5, and 6, we can calculate the number fluctuation of molecule A

$$\langle(n_A - \bar{n}_A)^2\rangle = NP_A(1 - P_A) = N\bar{x}_A(1 - \bar{x}_A) \quad (7)$$

Setting $\ln f(n_A) = \phi(n_A)$ and expanding $\phi(n_A)$ around the n_A value at which $\phi(n_A)$ assumes a maximum value, that is, around n_A^* , then the relation

$$\phi(n_A) = \phi(n_A^*) - \frac{1}{2} \left[\frac{N}{n_A^*(N - n_A^*)} \right] (n_A - n_A^*)^2 \quad (8)$$

is obtained, where terms higher than cubic with respect to $(n_A - n_A^*)$ are neglected. As n_A should be equal to a mean value of n_A within the region, \bar{n}_A , and $P_A = \bar{x}_A = \bar{n}_A/N$, we obtain

$$\phi(n_A) = \phi(\bar{n}_A) - \frac{1}{2} \left[\frac{N}{NP_A(1 - P_A)} \right] (n_A - \bar{n}_A)^2 \quad (9)$$

Inserting eq 7

$$\phi(n_A) = \phi(\bar{n}_A) - \frac{1}{2} \left[\frac{(n_A - \bar{n}_A)^2}{\langle(n_A - \bar{n}_A)^2\rangle} \right] \quad (10)$$

Thus, the expression for $f(n_A)$ is obtained as

$$f(n_A) = f(\bar{n}_A) \exp \left[- \frac{1}{2} \frac{(n_A - \bar{n}_A)^2}{\langle(n_A - \bar{n}_A)^2\rangle} \right] \quad (11)$$

which shows a Gaussian distribution of $f(n_A)$. At the same time, the number fluctuation of a molecule A is expressed in the form

$$\langle(n_A - \bar{n}_A)^2\rangle = - \frac{1}{[d^2\phi(n_A)/dn_A^2]_{n_A = \bar{n}_A}} \quad (12)$$

Equations 11 and 12 tell us the number fluctuation in solutions can be calculated from eq 12 as long as N is large enough to make $f(n_A)$ a Gaussian distribution.

In the above discussion for an ideal solution, the probability of a number of molecules A being n_A for a given configuration was considered to be $P_A^{n_A}(1 - P_A)^{N - n_A}$ because the molecules behave independently. At the same time all the possible configurations were assumed to occur with an equal probability. In the actual solutions, however, the form of $f(n_A)$ would be rather complicated, because the species of molecules sur-

rounding the particular molecule in consideration may be affected by a molecular species of the central molecule. In order to simplify the theoretical treatment, we place restrictions on the range within which the effect of an existence of a particular molecular extends. As an example, consider the case where molecules A have a strong tendency to associate with each other. We assume, in this case, that a few molecules of A behave as a single associated molecule and that the associated molecule is independent of the other molecules. Let the number of molecules which form an associated molecule be l . Then the number of associated molecules is n_A/l , where n_A is the number of molecules A out of N molecules. As we are observing the deviation from a mean molecular number in the sense of a probability, it is not necessary to consider dynamical changes inside of the associated molecule. It is enough to consider the averaged structure of the molecules. In other words, if we determine the l value from the observed concentration fluctuation, the l value obtained is not necessarily an integer. Based upon this model, theoretical formulas were obtained for two different situations: (I) association between molecules of the same species (case I), and (II) association between molecules both of the same and different species (case II).

Concentration Fluctuation for Case I (A_l , B_m Type). Consider a case where associated molecules have the form of A_l and B_m , and they behave as independent molecules. Let the numbers of molecules which behave independently be x and y for species A_l and B_m , respectively. Then there exist relations

$$\begin{aligned} n_A &= lx \\ N - n_A &= my \end{aligned} \quad (13)$$

where n_A is the number of molecules of A. In this case it is enough to count the number of configurations of A_l molecules, instead of those of A molecules. Therefore $f(n_A)$ is expressed as

$$f(n_A) = \frac{(x+y)!}{x!y!} P_x^x (1-P_x)^y \quad (14)$$

where P_x is the probability of a molecule being an associated molecule A_l , i.e., $P_x = \bar{x}/(\bar{x} + \bar{y})$. Substituting eq 14 into eq 12, we obtain

$$\langle (n_A - \bar{n}_A)^2 \rangle = \bar{n}_A(N - \bar{n}_A)[lN - (l-m)\bar{n}_A]/N^2 \quad (15)$$

In the derivation of eq 15, Stirling's formula is used since N is large. Thus, we finally obtain the expression for concentration fluctuation

$$\begin{aligned} N\langle (\Delta x_A)^2 \rangle &= N\langle (x_A - \bar{x}_A)^2 \rangle \\ &= \bar{x}_A(1 - \bar{x}_A)[l - (l-m)\bar{x}_A] \end{aligned} \quad (16)$$

Concentration Fluctuation for Case II. Two subcases will be considered.

(a) Where \bar{x}_A is small, we may consider a simplified model system which is composed from associated molecules of $A_l B_m$ and B_m types. Let the amount of $A_l B_m$ and B_m be x and y , respectively. Then the relations which correspond to eq 13 are

$$\begin{aligned} n_A &= lx \\ N - n_A &= m(x-y) \end{aligned} \quad (17)$$

Therefore $f(n_A)$ becomes

$$f(n_A) = \frac{(x+y)!}{x!y!} P_x^x (1-P_x)^y \quad (18)$$

Following the same procedure as in the preceding paragraph, the fluctuation of n_A is

$$\langle (n_A - \bar{n}_A)^2 \rangle = \bar{n}_A(N - \bar{n}_A)[lN - (l+m)\bar{n}_A]/N^2 \quad (19)$$

The corresponding concentration fluctuation is calculated to be

$$\langle (\Delta x_A)^2 \rangle = \bar{x}_A(1 - \bar{x}_A)[l - (l+m)\bar{x}_A] \quad (20)$$

(b) Where \bar{x}_A is large. In this case, we consider a model system which is composed from associated molecules of A_l and $A_l B_m$ types, the amount of A_l and $A_l B_m$ being x and y , respectively. Then the relations corresponding to eq 13 or 17 are

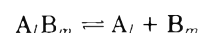
$$\begin{aligned} n_A &= l(x+y) \\ N - n_A &= my \end{aligned} \quad (21)$$

Thus, the concentration fluctuation becomes

$$N\langle (\Delta x_A)^2 \rangle = \bar{x}_A(1 - \bar{x}_A)[(l+m)\bar{x}_A - l] \quad (22)$$

Comparison with Experimental Results. Figures 3 and 4 show the calculated concentration fluctuations for the systems (A_l , B_l) and (A_l , B), respectively. It can be seen from the figures that concentration fluctuation increases as the association number, l , increases. The dashed lines of the figures indicate the calculated concentration fluctuation expected for an ideal binary solution. We also see from Figure 4 that the fluctuation maximum deviates from $\bar{x}_A = 0.5$ more largely as l increases. The theoretical curve corresponding to $l = 2$ or $l = 3$ of Figure 4 seems to explain the experimental results of Figure 2 in the sense that the concentration fluctuation takes on much larger values than those of ideal binary solutions in a low concentration range of ethanol. The theoretical curves of Figure 4, however, cannot explain the experimental results of Figure 2 in a high concentration range of ethanol. Figures 5, 6, and 7 show the theoretical curves calculated from eq 20 or 22. It is seen from these figures that the concentration fluctuation can assume smaller values than those of an ideal binary solution. It is also seen that the concentration fluctuation can take on a zero value at certain mole fractions. Therefore the fluctuation curves have two distinct maxima. Comparing the results of Figures 5, 6, and 7 with the observed concentration fluctuation of Figure 2, we can understand that the theoretical curves corresponding to $l = 2, 3$, and 4 of Figure 5 can explain the general features of the experimental results of Figure 2 in the sense that concentration fluctuation is larger at a low ethanol concentration and smaller at a high ethanol concentration than that of an ideal binary solution. The existence of two maxima near $\bar{x}_A = 0.3$ and $\bar{x}_A = 0.8$ is also predicted by the theories. However, the observed fluctuation does not assume zero value at any mole fraction, which indicates the defect in the present theory.

Modification of Theory. We start by considering the reason for the calculated concentration fluctuation assuming a zero value. In the present model, there is a concentration at which the macroscopic mole fraction coincides with the number ratio of the component species of an associated molecule, and so, only an association of type $A_l B_m$ can exist. This arises from the fact that complete association is assumed in the preceding theory. Thus we modify the theory by considering a dissociation equilibrium of the form



From the conclusion of the preceding paragraph, we may confine our model in the dissociation equilibrium of the form

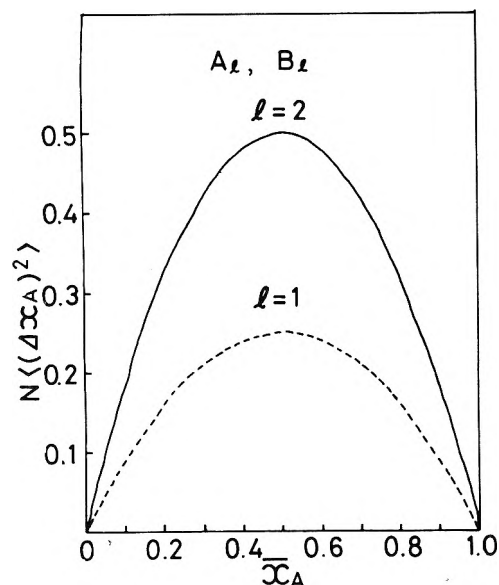


Figure 3. Theoretical values of concentration fluctuation calculated from eq 16 for $l = m$.

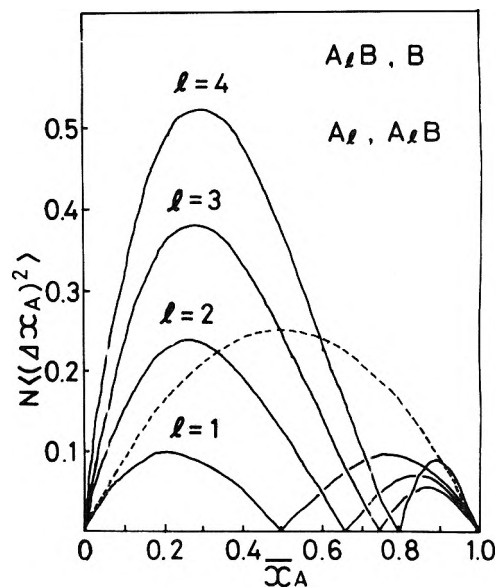


Figure 5. Theoretical values of concentration fluctuation calculated from eq 20 and 22 for $m = 1$ and $l = 1, 2, 3, 4$.

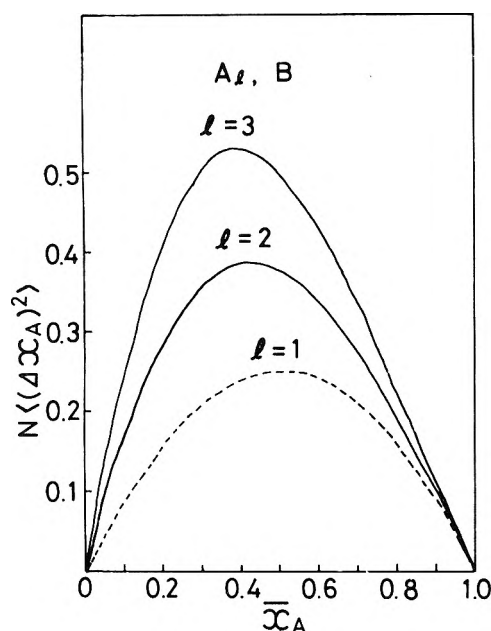
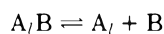


Figure 4. Theoretical values of concentration fluctuation calculated from eq 16 for $m = 1$ and $l = 1, 2, 3$.



that is, the system under consideration is composed of associated molecules, $A_l B$ and A_l , and a free molecule, B . Then the amounts of the components, $\bar{n}_{A_l B}$, \bar{n}_{A_l} , and \bar{n}_B , are related to each other

$$\frac{\bar{n}_{A_l B}}{N'} = K \left(\frac{\bar{n}_{A_l}}{N'} \right) \left(\frac{\bar{n}_B}{N'} \right) \quad (23)$$

where

$$N' = n_{A_l B} + n_{A_l} + n_B$$

and K is an equilibrium constant in an usual sense. Let the amounts of molecules which behave independently of each other be expressed as $x = n_{A_l}$, $y = n_{A_l B}$, and $z = n_B$. Then, the relations corresponding to eq 13, 17, and 21 are

$$n_A = l(x + y)$$

$$N - n_A = y + z \quad (24)$$

Thus, x , y , and z cannot be determined uniquely in this case and, therefore, f is a function of two mutually independent variables. If we chose n_A and $n_{A_l B}$ as the two variables, f is expressed as,

$$f(n_A, n_{A_l B}) = \frac{(x + y + z)!}{x!y!z!} P_x^x P_y^y (1 - P_x - P_y)^z \quad (25)$$

The calculation of concentration fluctuation for a two variable case is almost similar with that for a single variable case. If we distinguish these two variables by 1 and 2, we obtain the expressions

$$\langle (n_1 - \bar{n}_1)^2 \rangle = \frac{\beta_{22}}{\beta_{11}\beta_{22} - \beta_{12}^2} \quad (26)$$

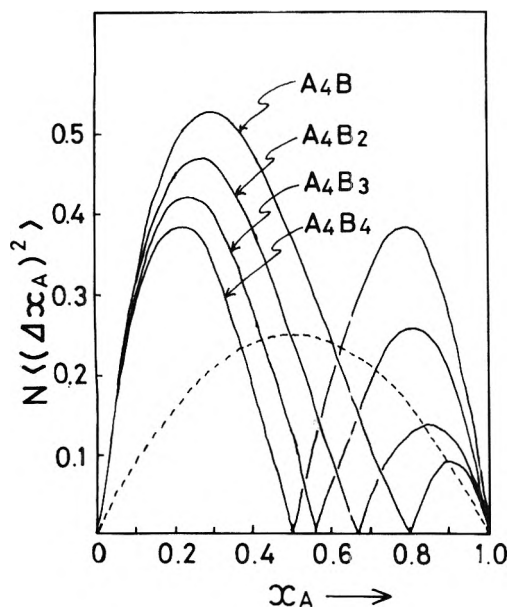


Figure 7. Theoretical values of concentration fluctuation calculated from eq 20 and 22 for $l = 4$ and $m = 1-4$.

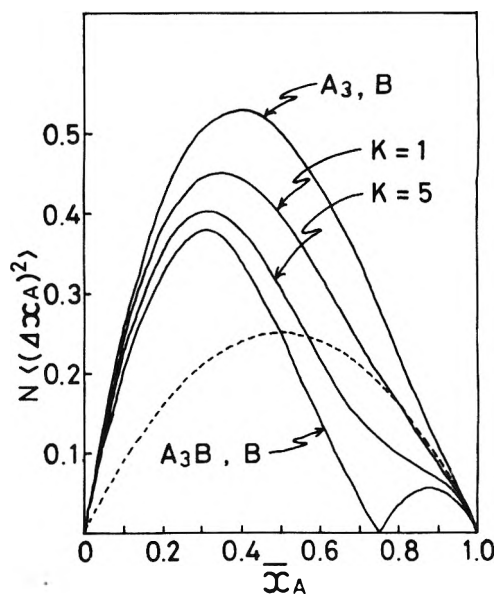


Figure 9. Theoretical values of concentration fluctuation calculated from eq 31 for $l = 3$ and $K = 1$ and 5 .

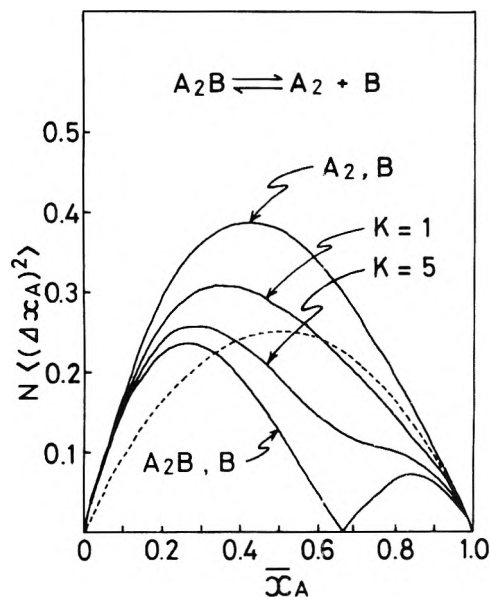


Figure 8. Theoretical values of concentration fluctuation calculated from eq 31 for $l = 2$ and $K = 1$ and 5 .

and

$$\beta_{ij} = - \left[\frac{\partial^2 \phi(n_1, n_2)}{\partial n_i \partial n_j} \right]_{n_i = n_i, n_j = \bar{n}_j} \quad (27)$$

Thus, we obtain the relations

$$\langle (n_A - \bar{n}_A)^2 \rangle = \bar{n}_A (N - \bar{n}_A) \times [lN - (l-1)\bar{n}_A - 2l\bar{n}_{A/B}] / N^2 \quad (28)$$

and

$$N \langle (\Delta \bar{x}_A)^2 \rangle = \bar{x}_A (1 - \bar{x}_A) [l - (l-1)\bar{x}_A - 2l\bar{n}_{A/B}/N] \quad (29)$$

As, $\bar{n}_{A/B}$ is calculated from eq 23 to be

$$2l\bar{n}_{A/B}/N = l - (l-1)\bar{x}_A - [l - (l-1)\bar{x}_A]^2 - 4lR\bar{x}_A(1 - \bar{x}_A)]^{1/2} \quad (30)$$

where

$$R = K/(K+1)$$

We finally obtain the expression for concentration fluctuation

$$N \langle (\Delta x_A)^2 \rangle = \bar{x}_A (1 - \bar{x}_A) \{ [l - (l-1)\bar{x}_A]^2 - 4lR\bar{x}_A(1 - \bar{x}_A) \}^{1/2} \quad (31)$$

The theoretical curves calculated from eq 31 are shown in Figure 8 ($l = 2$) and Figure 9 ($l = 3$). The resulting theoretical curves explain the general features of the experimental results of Figure 2 very well.

Temperature Dependence of Concentration Fluctuation. Figure 2 shows the characteristic temperature dependence of the concentration fluctuation for the ethanol–chloroform system. The main three characteristics are: (1) the fluctuation decreases with increasing temperature in the low ethanol mole fraction range, (2) the fluctuation increases with increasing temperature in the high ethanol mole fraction range, and (3) the two maxima observed at 20 °C gradually change into a single maximum with increasing temperature. The effect of temperature seems to make the concentration fluctuation approach the theoretical curve of an ideal binary solution. The theoretical curves of Figure 5 show that the decrease in l corresponds to the items (1) and (2). The decrease in K , on the other hand, correspond to the item (3). The decrease in l corresponds to the decrease of mutual association of ethanol, while the decrease in K to the decrease of association between ethanol and chloroform. The best fit between the calculated and observed concentration fluctuation was obtained by setting $l = 3$ and $K = 4$ for 20 °C and $l = 2.5$ and $K = 2$ for 45 °C. The final results for theoretical calculation are shown in Figure 10.

Concentration Fluctuation and Local Structure. In the preceding paragraph, a theoretical consideration of the concentration fluctuation has been given. The final l and K values obtained from the theory afford very interesting information about local structures in a chloroform–ethanol system. In a chloroform–ethanol system at 20 °C, three ethanol molecules and one chloroform molecule behave as a single molecule. This argument should be understood, of course, in a probability

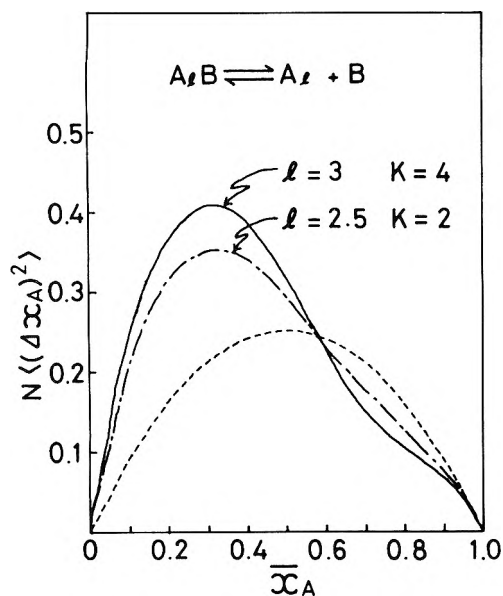


Figure 10. Final results of theoretical calculation corresponding to experimental values at 20 and 45 °C.

sense. Perhaps, ethanol molecules form a local structure in a ethanol–chloroform system, the unit of which is composed of a few ethanol molecules. The growth of a local structure which is composed of larger numbers of ethanol might be prevented by the existence of chloroform molecules which form hydrogen bonding with an ethanol molecule.

As the temperature increases, the local structure breaks. The l value change from 3 to 2.5 with increasing temperature from 20 to 45 °C may indicate a slight decrease in the tendency of self-association between ethanol molecules. The K value change from 4 to 2 in the same temperature range indicates a considerable decrease of the association between ethanol and chloroform molecules.

In order to see the reliability of the present result, it is important to discuss the above results in comparison with experimental information, such as thermodynamic quantities. Thermodynamic quantities, for example, heats of solution, are to be related with situation changes on passing from pure liquids to solution, while concentration fluctuations directly reflect information about a solution. Figure 11 shows the heat of solutions observed for chloroform–ethanol⁶ and carbon tetrachloride–ethanol⁷ systems. In a carbon tetrachloride–ethanol system, the heat of solution takes on positive values for the whole concentration range. This has been explained as a breakdown of hydrogen bonding between ethanol molecules by the presence of carbon tetrachloride molecules. In a chloroform–ethanol system, on the other hand, the heat of solution can take on negative values, because new types of hydrogen bonding are formed between chloroform and ethanol molecules. Thus, the concentration dependency of the heat of solution for a chloroform–ethanol system may be explained by two main factors. One is an endothermic factor due to the breakdown of hydrogen bonding between ethanol molecules and the other is an exothermic factor due to the formation of hydrogen bonds between ethanol and chloroform molecules. The concentration dependence of the endothermic process may be explained approximately by the heat of solution data for a carbon tetrachloride–ethanol system which are shown in Figure 11.

The concentration dependence of the exothermic process,

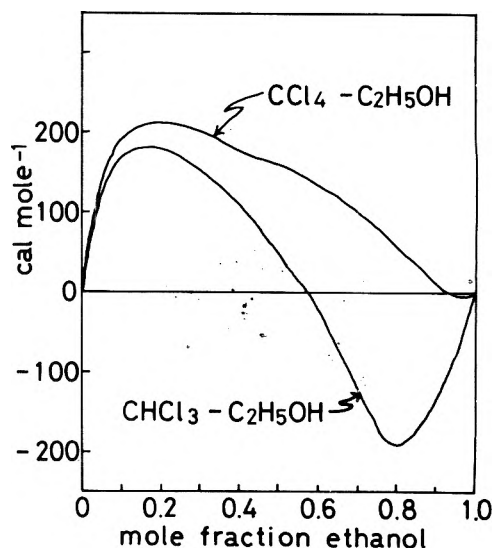


Figure 11. Heat of solution for the ethanol–chloroform system (from ref 6) and for the ethanol–carbon tetrachloride system (from ref 7) at 45 °C.

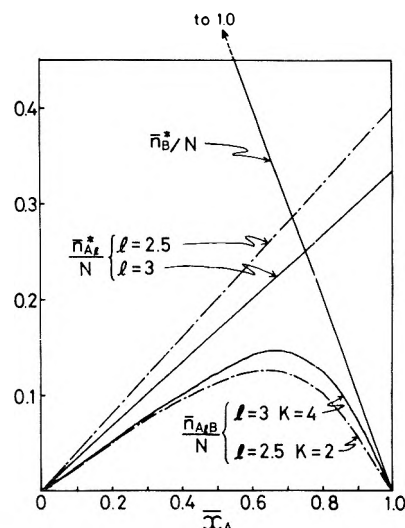


Figure 12. $\bar{n}_{A,B}/N$ values calculated from eq 23 for ($l = 3, K = 4$) and for ($l = 2.5, K = 2$). $n_{A_i}^*$ and n_B^* correspond to complete dissociation.

on the other hand, may be explained by the concentration dependence of $\bar{n}_{A,B}/N$. As the $\bar{n}_{A,B}/N$ value obtained from eq 30 is an averaged value of an associated molecule, $A_l B$, the heat of hydrogen bond formation between chloroform and ethanol is almost proportional to the $\bar{n}_{A,B}/N$ value, which is shown in Figure 12. If these ideas are reasonable, the concentration dependence curve of the heat of solution for a chloroform–ethanol system can be compared to the synthesized curve by adding two curves: the concentration dependence curve of heat of solution for a carbon tetrachloride–ethanol system and the concentration dependence curve of $\bar{n}_{A,B}/N$ which is multiplied by a hydrogen bonding energy between ethanol and chloroform. In other words, the heat of dissociation of hydrogen bonding between ethanol molecules exceeds the heat of hydrogen bond formation between ethanol and chloroform molecules where the concentration of ethanol is small, which results in a positive heat of solution in the ethanol–chloroform system. Where the ethanol concentration is large, on the other hand, the heat of hydrogen bond for-

mation between ethanol and chloroform molecules exceeds the heat of dissociation of hydrogen bonding between ethanol molecules, which results in a negative heat of solution in the ethanol-chloroform system.

It has been known from infrared spectral analyses that a few alcohol molecules form associated complexes, although their structures and populations have not been completely established yet. Fletcher⁸ studied the absorption spectra of the *n*-decane solution of ethanol-*d*₁ in the region of 1.9–2.2 μm. He concluded that there exist monomers, acyclic tetramers, and cyclic tetramers with the relative population of 1:3.4:10.9, respectively at 25 °C. He also studied the absorption spectra of methanol at 40, 80, and 120 °C.⁹ He found the coexistence of monomers, dimers, and tetramers in the gas phase. In the chloroform-ethanol system also, the associated complex structures may be rather complicated. In the present work, however, a single value, *l*, is assumed for the number of ethanol

molecules which form an associated complex. This theoretical treatment is certainly oversimplified, but the present results of $l = 3 \sim 2.5$ are not unreasonable if we consider that *l* is an averaged value of association numbers which correspond to various types of polymer ethanols.

References and Notes

- (1) K. Iwasaki, M. Tanaka, and T. Fujiyama, *Bunko Kenkyu*, **25**, 134 (1976).
- (2) K. Iwasaki, M. Tanaka, and T. Fujiyama, *Bull. Chem. Soc. Jpn.*, **49**, 2719 (1976).
- (3) T. Fujiyama, M. Kakimoto, and T. Suzuki, *Bull. Chem. Soc. Jpn.*, **49**, 606 (1976).
- (4) K. Iwasaki, Y. Katayanagi, and T. Fujiyama, *Bull. Chem. Soc. Jpn.*, in press.
- (5) "International Critical Tables", McGraw-Hill, New York, N.Y., 1926.
- (6) G. Scatchard and C. L. Raymond, *J. Am. Chem. Soc.*, **60**, 1278 (1938).
- (7) J. A. Barker, I. Brown, and F. Smith, *Discuss. Faraday Soc.*, **15**, 142 (1953).
- (8) A. N. Fletcher, *J. Phys. Chem.*, **76**, 2562 (1972).
- (9) A. N. Fletcher, *J. Phys. Chem.*, **75**, 1808 (1971).

Dielectric Studies of Amino Acid Conformation

Joseph A. Walder

Department of Chemistry, Northwestern University, Evanston, Illinois 60201 (Received February 19, 1976)

Publication costs assisted by the National Institute of General Medical Sciences

The dielectric properties of a number of structurally rigid aqueous amino acids have been reexamined in terms of the Kirkwood theory for the dielectric polarization of polar liquids. Those in which the charged groups are not enclosed in a common hydration sphere have an effective dipole moment, as defined by Kirkwood, substantially less than the true molecular moment calculated on the basis of charge separation. Thus molecular moments and mean intercharge distances for aqueous amino acids cannot be calculated directly from the dielectric properties. Nonetheless, the pattern of the dielectric behavior in a structurally homologous series of amino acids may still provide conformational information. It is shown on this basis, contrary to previous interpretation, that long chain α,ω -amino acids (greater than C₆) have allowed internal rotational motion in aqueous solution. The lower members in this series appear to exist in the extended configuration.

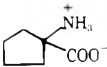
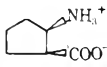
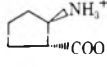
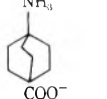
Among the methods that have been used to gain insight into the structure of small molecules in solution, dielectric measurements have been particularly suitable for the aqueous amino acids. Such investigations provided the principal evidence that in water the neutral form of these species existed as a dipolar or zwitterion.^{1,2} With this result, Wyman was able to apply dielectric studies to the conformational analysis of a variety of dipolar ions.^{2,3} Based on an empirical treatment of the data he interpreted the dielectric behavior of the α,ω -amino acids to indicate that these species existed in water as the freely rotating chains.² Later Kirkwood gave theoretical support to the empirical approach of Wyman and made direct calculations of the root-mean-square intercharge distances for these species.⁴ The calculated values were in very good agreement with those calculated on the assumption of free rotation about carbon-carbon bonds with either the methods of Kuhn⁵ or Eyring.⁶

Recently Edward et al. have extended these studies of the

α,ω -amino acids to higher members in the series.^{7,8} In contrast to previous findings their observations led them to conclude that these species adopt the fully extended conformation in water. It can be shown, however, that the pattern in the dielectric behavior of this series is not consistent with the extended configuration and in fact indicates the presence of allowed rotational motion although not to the extent of free rotation as was previously thought. In addition their studies of certain structurally well-defined amino acids require that there be given an altered interpretation of the measured dipole moments of dipolar ions from that of Kirkwood.⁸

Extending the approach of Onsager, Kirkwood⁹ developed the theory for the dielectric behavior of polar liquids to a stage that remains the most applicable form to this day. From this it becomes apparent that the dipole moment of a molecule, when in a polar solvent, cannot be obtained from dielectric measurements alone. Rather the dielectric properties are related to the moment $\bar{\mu}$, equal to $(\bar{\mu} \cdot \bar{\mu})^{1/2}$ where $\bar{\mu}$ is the dipole

TABLE I: Dipole Moments for Rigid Amino Acids

Amino acid		$\bar{\mu}^a$	$ \bar{\mu} = eR^b$
$H_3^+NCH_2COO^-$	(I)	16.2	14.9
	(II)	14.6	14.9
	(III)	13.3	14.4
	(IV)	15.9	21.4
	(V)	27.9	32.2

^a Calculated from the data of Edward et al.⁸ ^b Intercharge distances calculated using the bond lengths and angles given in Table II with the aid of CPK models.

moment of the molecule and $\bar{\mu}$ the sum of the dipole moment of the molecule and the moment which it induces in its neighbors by hindering their rotation relative to itself.

For aqueous dipolar ions the relationship between $\bar{\mu}$ and the dielectric constant, ϵ , assumes a particularly simple form:⁴

$$\bar{\mu} = 3.30\delta^{1/2} \quad \delta = \frac{\epsilon - \epsilon_0}{c} \quad (1)$$

where c is the molar concentration of the dipolar ion, ϵ_0 the dielectric constant of the pure solvent, and δ the so-called dielectric increment. Although $\bar{\mu}$ is formally a function of composition, saturated aqueous solutions of all aliphatic amino acids correspond to a mole fraction of less than 0.05. Accordingly, for these species δ is generally constant throughout their entire range of solubility.

For structural information $|\bar{\mu}|$ is the moment of interest but unfortunately it cannot in practice be obtained from the value of $\bar{\mu}$. Kirkwood showed, however, that for glycine $\bar{\mu}$ differed by less than 5% from $|\bar{\mu}|$, calculated on the basis of charge separation.¹⁰ Hence, he concluded that for the aliphatic amino acids, $|\bar{\mu}|$ is to a close approximation equal to $\bar{\mu}$ itself.⁴ With this assumption and eq 1 we have

$$e\bar{R} = |\bar{\mu}| = \bar{\mu} = 3.30\delta^{1/2} \quad (2)$$

where e is the elementary charge and \bar{R} the root-mean-square dipole separation. Using eq 2 we may then calculate \bar{R} in a straightforward fashion from dielectric measurements.

Recently several other amino acids have been studied in which the intercharge distance is structurally fixed (Table I).⁸ In agreement with Kirkwood's assumption $\bar{\mu}$ is approximately equal to $|\bar{\mu}|$ for compounds I (glycine), II, and III. However for IV and V, $\bar{\mu}$ is considerably less than $|\bar{\mu}|$. The differences between $\bar{\mu}$ and $|\bar{\mu}|$ for IV and V, 5.5 and 4.3 D, respectively, are too large to be explained by any factors that might effect $|\bar{\mu}|$ such as dipole-dipole interactions or dipole induction in bonds neighboring charged groups. The values of $|\bar{\mu}|$ calculated on the basis of charge separation according to the first relation in eq 2 are to a close approximation correct. Consequently the differences between $\bar{\mu}$ and $|\bar{\mu}|$ for IV and V must reflect the effects of interactions with neighboring water molecules upon the effective moment $\bar{\mu}$. Thus there must be some aspect of the hydration of IV and V that is not shared by glycine, II, and III. One possibility suggests itself. Solvating water molecules will surround the charged ends of these dipolar ions as shown

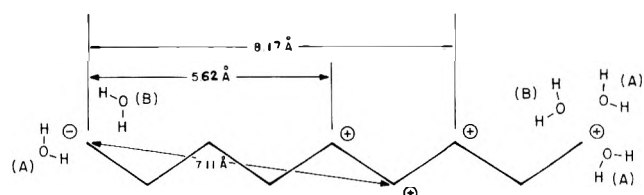


Figure 1. The planar projection of 8-amino-octanoic acid in the extended configuration. Water molecules are depicted hydrating the charged ends of the dipolar ion. Those water molecules labeled B provide backside hydration. End-to-end distances are shown for the C₄, C₅, and C₆ α,ω -amino acids to demonstrate the stepwise increase in extended chain length.

in Figure 1. Those water molecules labeled A are oriented in such a way that their moments add to the moment of the molecule. Those labeled B, providing backside hydration, are so oriented that their moments detract from that of the molecule. For glycine, II, and III the intercharge distance is too small to permit backside hydration; both the amino and carboxyl groups are encased in a common hydration sphere. Hence $\bar{\mu}$ will more nearly equal $|\bar{\mu}|$ for these compounds than for IV and V in which backside hydration can take place.

From the definition of $\bar{\mu}$ we may write

$$\bar{\mu} = (|\bar{\mu}|^2 + \bar{\mu} \cdot \bar{\mu}_{ind})^{1/2} \quad (3)$$

where $\bar{\mu}_{ind}$ is the moment induced in neighboring molecules. Knowing $\bar{\mu}$ and $|\bar{\mu}|$ we can calculate the component of $\bar{\mu}_{ind}$ along the direction of $\bar{\mu}$. For IV and V this is approximately 9.6 and 8.0 D, respectively, equivalent to the moment of four-five water molecules. This is not too large to be accounted for by backside hydration if one considers that both charged groups are subject to this hydration and that the effect extends beyond the first hydration sphere. The argument of course assumes that hydrating water molecules on the backside of the charged groups are more rigidly oriented than those hydrating the outer faces. This is not unreasonable since the hydrocarbon portion of the dipolar ion should result in an ordering of the surrounding water. In any case, it is clear that for the amino acids in which the charged groups are sufficiently far apart to be separately hydrated, $\bar{\mu}$ is substantially less than $|\bar{\mu}|$.

Thus the approximate equivalence of $\bar{\mu}$ and $|\bar{\mu}|$ found for glycine cannot be expected for all aliphatic amino acids. Generally the intercharge distance is sufficient to permit separate hydration of both charged groups in which case $\bar{\mu}$ will be considerably less than $|\bar{\mu}|$. As such a direct calculation of \bar{R} from eq 2, as performed by Kirkwood, will usually be in serious error. In the series of α,ω -amino acids, glycine is the only member in which the charged groups are enclosed in a common hydration sphere. Its value of $\bar{\mu}$ then is expected to be disproportionately large. That this is so is reflected in the fact that $\bar{\mu}_{\beta\text{-ala}} - \bar{\mu}_{\text{gly}}$ is far smaller than for any other adjacent homologues in the series (Table II).

Although eq 2 cannot be considered valid, the relationship between $|\bar{\mu}|$ and $\bar{\mu}$ should remain relatively constant for those members in a homologous series of dipolar ions which present similar structural features. Accordingly the pattern in the dielectric behavior of such a series may provide conformational information even though the precise intercharge distances cannot be calculated. Based on an approximately linear relationship between δ and R_{max}^2 , the square of the extended chain length, Edward and co-workers have proposed that the aqueous dipolar ions of the α,ω -amino acids adopt the fully extended configuration.⁸ However, as shown in Figure 2, this

TABLE II: Increments in R_{\max} and $\tilde{\mu}$ between the α, ω -Amino Acids.^a

$C_n - C_{n+1}$	$\Delta R_{\max}, \text{\AA}^b$	$\Delta \tilde{\mu}, \text{D}^c$
$C_2 - C_3$	1.54	1.2
$C_3 - C_4$	0.98	3.2
$C_4 - C_5$	1.49	4.7
$C_5 - C_6$	1.06	3.2
$C_6 - C_7$	1.42	3.4
$C_7 - C_8$	1.10	2.6
$C_8 - C_9$	1.36	3.2
$C_9 - C_{10}$	1.14	3.1

^a R_{\max} and $\tilde{\mu}$ for glycine are 3.10 \AA and 16.2 D, respectively. ^b The negative charge was taken to lie between the oxygen atoms along the line of the $C_1 - C_2$ bond. The positive charge of the ammonium group was assumed to lie 0.25 \AA beyond the nitrogen atom on the $C_\omega - N$ bond. All C-C and C-C-N bond angles were assumed to be 109.5°. The $C_1 - C_2$ bond length was taken to be 1.52 \AA , all other C-C bond lengths 1.54 \AA , and the $C_\omega - N$ bond length 1.4 \AA . ^c Calculated from data in ref 8.

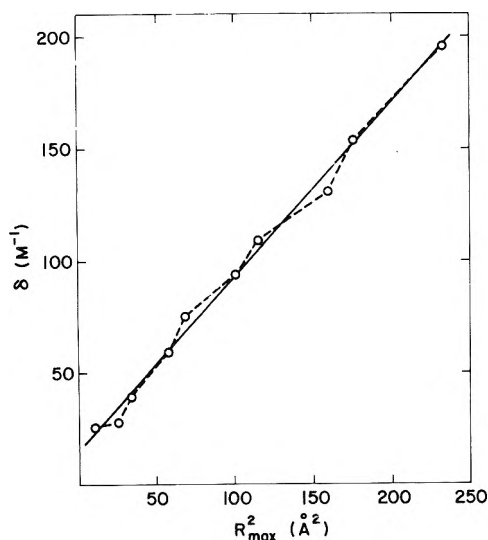


Figure 2. Plot of δ vs. R_{\max}^2 , the square of the extended chain length (data from Edward et al.).⁸ The dotted line indicates the regular stepwise variation in δ .

interpretation neglects a striking stepwise variation in δ as a function of R_{\max}^2 . This pattern results from the fact that R_{\max} increases in a stepwise fashion with the number of carbon atoms in the chain, n , whereas $\tilde{\mu}$ does not.

The basis for the alternating pattern in R_{\max} can be seen in the planar projections of the extended structures (Figure 1). For the values of R_{\max} given by Edward et al.^{7,8} the increment in R_{\max} when proceeding from an even to odd carbon chain number is always 1.82 \AA while that from an odd to even carbon chain number is 0.69 \AA . A consideration of the geometry involved, however, indicates that the variation cannot be fixed but rather should dampen with increasing chain length.

Repeating these measurements (Table II) we have found: (1) that the amplitude of the variation is less than given by Edward and co-workers, and (2) that the variation does in fact dampen with increasing chain length. If the aqueous α, ω -amino acids existed in the extended configuration a similar variation would be expected for the increments in $\tilde{\mu}$ (Table II).¹¹ This appears to hold through C_5 . Recall that the disproportionately small increment in $\tilde{\mu}$ between glycine and β -alanine is due to the abnormally large value of $\tilde{\mu}$ for glycine which is not representative of the series. The increment in $\tilde{\mu}$ between the C_4 and C_5 amino acids is approximately 1.5 times that between the C_3 and C_4 amino acids in accord with the increments in R_{\max} . After C_5 the increments in $\tilde{\mu}$ are essentially invariant¹² and do not at all reflect the pattern in R_{\max} .¹³ Therefore, from at least 7-aminoheptanoic acid through 10-aminodecanoic acid some degree of rotational motion must be allowed.

The forces responsible for limiting the internal rotation of the α, ω -amino acids must in large measure be due to hydration, particularly of the charged end groups. For the lower members in the series (through $C_5 - C_6$), these forces appear to be sufficient to freeze the molecules in the extended configuration. With increasing chain length, the effects of the end group hydration decrease, and the internal degrees of freedom increase, resulting in the development of rotational motion. Since an exact relationship between $|\tilde{\mu}|$ and $\tilde{\mu}$ cannot be obtained the precise extent to which internal rotation is allowed cannot be determined from these data alone.

Acknowledgment. This investigation was supported in part by Grant No. GM-09280 from the National Institute of General Medical Sciences, U.S. Public Health Service, to Professor I. M. Klotz. The author is grateful to Professor Klotz for helpful discussions.

References and Notes

- (1) J. Wyman, Jr., and T. L. McMeekin, *J. Am. Chem. Soc.*, **55**, 908 (1933).
- (2) J. Wyman, Jr., *Chem. Rev.*, **19**, 213 (1936).
- (3) J. Wyman, Jr., *J. Phys. Chem.*, **43**, 143 (1939).
- (4) J. G. Kirkwood in "Proteins, Amino Acids and Peptides", E. J. Cohn and J. T. Edsall, Ed., Reinhold, New York, N.Y., 1943, pp 294-296.
- (5) W. Kuhn, *Z. Phys. Chem.*, **175A**, 1 (1935).
- (6) H. Eyring, *Phys. Rev.*, **2**, 39, 746 (1932).
- (7) J. T. Edward, P. G. Farrell, and J. L. Job, *J. Phys. Chem.*, **77**, 2191 (1973).
- (8) J. T. Edward, P. G. Farrell, and J. L. Job, *J. Am. Chem. Soc.*, **96**, 902 (1974).
- (9) J. G. Kirkwood, *J. Chem. Phys.*, **7**, 911 (1939).
- (10) For glycine the interchange distance is structurally fixed. Other contributions to the moment are relatively small.
- (11) The so-called even-odd effect found for the nematic to isotropic transition temperatures of certain liquid crystals is an example where such a pattern does result when aliphatic chains are in the extended configuration. See S. Marčelja, *J. Chem. Phys.*, **60**, 3599 (1974).
- (12) The dielectric increment of 11-aminoundecanoic acid was also determined (see ref 8), but had to be done at 40 °C because of solubility problems. The increment in $\tilde{\mu}$ between the C_{10} and C_{11} amino acids was unexpectedly large, probably reflecting aggregation of the C_{11} species. For this reason, the $C_{10} - C_{11}$ increment was not included in Table II.
- (13) The pattern of increments in R_{\max} after C_5 is sensitive to the exact bond lengths and angles chosen. With variation of these parameters, however, we have found R_{\max} to always increase in a stepwise fashion and all increments in R_{\max} after C_5 to be greater than the $C_3 - C_4$ increment. Neither of these relations are found in $\tilde{\mu}$.

Study of Relaxational Mechanisms in Dimethyl Sulfoxide in Water by Optical Digital-Correlation Spectroscopy

P. W. Drake[†] and R. Meister*

Department of Electrical Engineering, The Catholic University of America, Washington, D.C. 20064 (Received May 22, 1976)

Publication costs assisted by The Catholic University of America

The binary mixture 0.3 mole fraction Me₂SO in H₂O has been studied employing optical digital-correlation spectroscopy over the temperature range from -18 to -115 °C. The measurement of the concentration fluctuation times and the isothermal structural relaxation times in this system shows that the correlator technique can be effective in separating multiple relaxation processes. The isothermal structural relaxation function was found to be represented by a single time which is quite rare in viscous liquids. The measured concentration times yield mutual diffusion coefficients over the reported temperature range.

Introduction

In the spectrum of light scattered by a viscoelastic liquid, the shape and intensity of the polarized Rayleigh line (central component of the spectrum) are governed by the combined effect of thermal diffusion and longitudinal stress relaxation on the fluctuations in density responsible for the scattering.^{1,2} In the case of a binary mixture the concentration fluctuations also contribute to the central spectrum. Fishman and Mountain,³ assuming a single structural relaxation process, have developed a theoretical relationship for the spectral distribution of the scattered light for such a binary mixture. The theoretical normalized correlation function of the scattered field is given by

$$G_n(t)_1 = a_1 \exp(-Dq^2t) + a_2 \exp(-\chi q^2t) + a_3 \exp(-\Gamma_M t) + a_4 \exp(-\Gamma_\beta t) \cos \omega_\beta t \quad (1)$$

where D is the mutual diffusion coefficient, χ the thermal diffusivity, $(1/\Gamma_M) = \tau_{st}$ the structural relaxation time, q is the magnitude of the scattering wave vector, \mathbf{q} , given by $|\mathbf{q}| = q = 2nq_0 \sin(\phi/2)$ where \mathbf{q}_0 is the wave vector of the incident light, n the refractive index, ϕ is the scattering angle, the coefficients are normalized as $a_1 + a_2 + a_3 + a_4 = 1$, ω_β the Brillouin shift, and Γ_β the line width.

Dimethyl sulfoxide (Me₂SO)-water mixture was selected for this binary mixture study. The particular mixture chosen was 0.3 mole fraction because nuclear magnetic relaxation⁴ and recent ultrasonic⁵ studies on this mixture have shown that single relaxation processes adequately represent the measurement. Published results to date using digital correlation spectroscopy (DCS) to study structural relaxation in other viscoelastic liquids have needed to employ distributions of relaxation times to characterize the relaxation process.⁶⁻⁸ The Me₂SO/H₂O mixture in the range of 0.2-0.4 mole fraction has a large temperature dependence of viscosity, and is glass forming, making it suitable for studying by the digital correlation technique. The DCS method has proven useful for probing structural relaxation phenomena in the range from 10^{-6} to 10^2 s.

Experimental Section

The dimethyl sulfoxide (Me₂SO) sample was Fisher certified grade, and mixed with double-distilled deionized water.

[†] Present address: Peter W. Drake, Manhattan Hall 209, Manhattan College, Bronx, N.Y. 10471.

The 30% mole fraction Me₂SO in water mixture tested was mixed by weight to better than 0.05%. The samples were filtered in a closed multipass system employing in series the optical cross dewar and millipore filter (142 mm diameter, 0.65- μ m pore size) to remove dust. No further purification was done.

For this temperature dependent study a vessel containing the sample was built in the form of an optical cross fused into a dewar and has been described by Pinnow et al.⁹ Temperature control was effected by regulating the flow of cold N₂ gas through coils immersed in the dewar. Temperatures were monitored by a thermocouple in the bath. The temperature of the bath was stable to better than ± 0.1 °C over the course of each measurement throughout the observation range from -115 to 0 °C. There was a constant temperature offset of between 1 and 1.5 °C between the bath and the sample over this range. The temperatures at which these data are reported are estimated uncertain to ± 0.3 °C, although the stability was considerably better than this.

In obtaining the correlator results a 1.4-W Ar⁺ laser (Coherent Radiation) operating at 5145 Å (limited to operating at 200 mW to avoid local heating of the sample due to absorption of the laser light) was focussed with a short focal length lens (hard focussed) to produce a well-defined scattering region in the liquid for the light scattering study. The light scattered through 90° was then passed thru a pin hole aperture (spatially filtered) to define a phase coherent correlation volume, and detected by a photomultiplier assembly (Malvern type RR50). The photopulses output are then fed into a digital correlator (Malvern Type K7023) with 24 channels operated in a single clipped mode yielding the correlation function of the incoming photoelectron counts which is related to the normalized autocorrelation function of the scattered light, $G_n(t)$, by

$$C_k(t) = a + b |G_n(t)|^2 \quad (2)$$

where a and b are coefficients determined by the experimental conditions. Reference 7 presents an excellent review of the parameters effecting a and b . For the present study it should be observed that b is a function of the clipping level, spatial coherence of the detected light, and the effects of finite sampling time (the actual finite sampling time called "bin size" of the correlator is θ). It is this latter contribution which permits the effective "filtering out" of various contributions to the scattered spectrum. Jakeman et al.^{10,11} have shown that

for Lorentzian light this correction factor to the intensity of the autocorrelation function is $(\sin(\Gamma\theta)/\Gamma\theta)^2$, where $\Gamma = 1/\tau$ and θ is the sampling bin size. All of the correlator data was obtained by superimposing shapes of $C_k(t)$ obtained with at least five different sampling times, to ensure that the exact shape of the correlation function was obtained. The different sampling times were chosen to ensure overlap of correlograms. The correlograms so obtained were matched in these overlapping regions by first considering the one obtained from the longest sampling time (bin size) from which the dc scattering background and slope were determined. Having these constants, correlograms for shorter bin sizes were, in turn, adjusted to fit the preceding function by sliding vertically and matching lines in the overlapping region. In this way the detailed normalized correlation function was determined. The apparatus and data collection system employed here has been described in detail by Lai et al.⁷

Results

The 0.3 mole fraction Me₂SO in H₂O binary mixture has been studied over the temperature range from -18 to -115 °C employing digital correlation spectroscopy. This temperature range corresponds to a viscosity range of from 20 cP to approximately 10^7 P. Throughout this range the thermal diffusivity, $\chi = \lambda/\rho_0 C_p$ (where ρ_0 is density of liquid, λ is the thermal conductivity, C_p is the specific heat at constant pressure), is much greater than the mutual diffusion coefficient, D , governing the dissipation of concentration fluctuations. Typically χ is of the order 10^{-3} to 10^{-4} cm²/s for viscous liquids while the largest value of observed D is 9×10^{-6} cm²/s. Over the temperatures reported the contribution to the observed spectrum from thermal diffusivity (entropy fluctuations) is negligible. Considering use of DCS in the high viscosity region ($>10^4$ P) the Mountain and Brillouin lines are generally separable because the decay time Γ_B^{-1} of the correlation functions associated with the Brillouin component is short compared with the average structural relaxation time which determines the relaxation rate of the Mountain component. Under this condition the term with the a_4 coefficient in eq 1 can be neglected and eq 1 becomes

$$G_n(t) = a_1 \exp(-Dq^2t) + a_3 \exp(-\Gamma_M t) \quad (3)$$

The first term represents the correlation function associated with concentration fluctuations; the second term represents the density correlation function. The contribution due to the concentration fluctuations should be exponential and have a q^2 dependence while the contribution due to structural relaxation is independent of q .

The characteristic decay time for the density correlation function is τ_{st} and for the concentration function is $\tau_c = 1/Dq^2$, thus the spectrum can be separated dependent on the relative magnitudes of τ_c and τ_{st} . When $\tau_c \gg \tau_{st}$, appropriate selection of the sampling time θ in the range, $10 < \tau_c/\theta < 100$, will yield a measured correlation function of the form

$$C_k'(t) = a + b \exp(-2Dq^2t) \quad (4)$$

The measurements show that $\tau_c \approx 10^3 \tau_{st}$ and eq 4 describes the contribution due to concentration fluctuations. A typical measurement of the concentration correlation function is given in Figure 1. To verify the identity of this component of the scattered spectrum a qualitative check on the q dependence was made. With the optical cross dewar employed the scattering angle could be varied from 80 to 100° using the side port while a scattering angle of approximately $8 \pm 3^\circ$ could be measured using the entrance port. The ratio of the observed

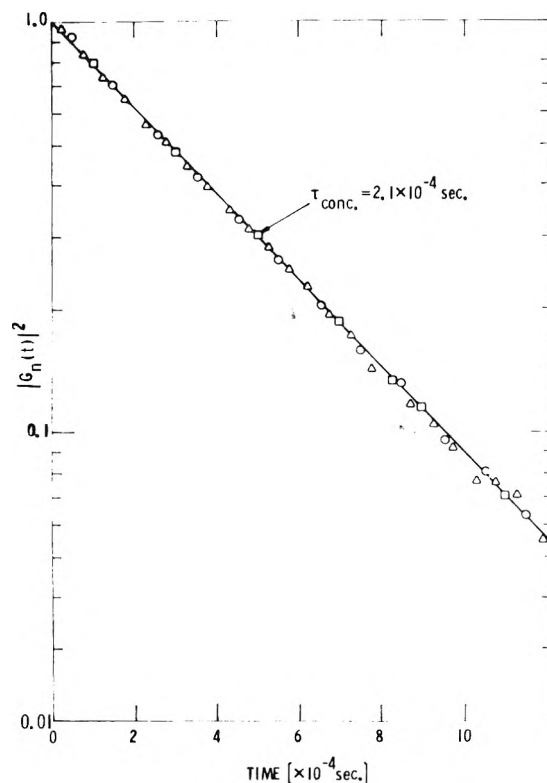


Figure 1. Concentration fluctuation correlation function vs. time for various bin sizes at -75 °C. 0.3 mole fraction of Me₂SO in H₂O.

relaxation times was $\tau(80^\circ)/\tau(100^\circ) = 1.3$ and the ratio of the scattering vectors is: $q^2(98^\circ)/q^2(82^\circ) = 1.3$. The ratio of the observed relaxation time for a scattering angle of $8 \pm 3^\circ$ was found to be $\tau(8^\circ)/\tau(90^\circ) \approx 60$ and the calculated ratio based on the q^2 dependence is $\tau(8^\circ)/\tau(90^\circ) = 51$. On the basis of these measurements it is concluded that the measured correlation times are q^2 dependent and follow the relation $\tau_c = 1/Dq^2$. The measured τ_c are presented in Figure 2 vs. reciprocal temperature.

The deviation of the Me₂SO-H₂O mixture from an ideal mixture can be considered from the measurements of both mutual diffusion coefficients, D , obtained here and self-diffusion coefficients available from NMR measurements.⁴ A relationship between these parameters and the rate of change of chemical potential $\partial\mu/\partial c$ (osmotic pressure) is given by $D = \alpha^*(\partial\mu/\partial c)$, where α^* is the mass transport coefficient containing the self-diffusion constants and the concentrations of the two species.^{12,13} A calculation of the osmotic pressure utilizing the self-diffusion constants from NMR⁴ and an extrapolation of Figure 2 to determine the mutual diffusion coefficient yields 270 ± 100 [J/cm³]. Theoretical determination of the osmotic pressure assuming an ideal mixture can be calculated.¹⁴ The value for the ideal mixture is found to be 490 J/cm³. Departure from ideality was to be expected in light of the significant heat of mixing for the 0.3 Me₂SO in H₂O mixture.¹⁵ For a point of reference it is noted that Berge¹⁴ found experimentally, on the bases of an analysis of the Rayleigh intensity, that $(\partial\mu/\partial c)_{\text{expt}} = 260 \pm 40$ J/cm³ for the binary system carbon disulfide-acetone while the calculation for the ideal case yielded $(\partial\mu/\partial c)_{\text{theor}} = 757$ J/cm³ for their system.

The contribution from the density fluctuations was evident at the lower range of temperatures studied, -85 to -115 °C. By varying the sampling bin time θ it is observed that at a time scale substantially shorter than that of the concentration

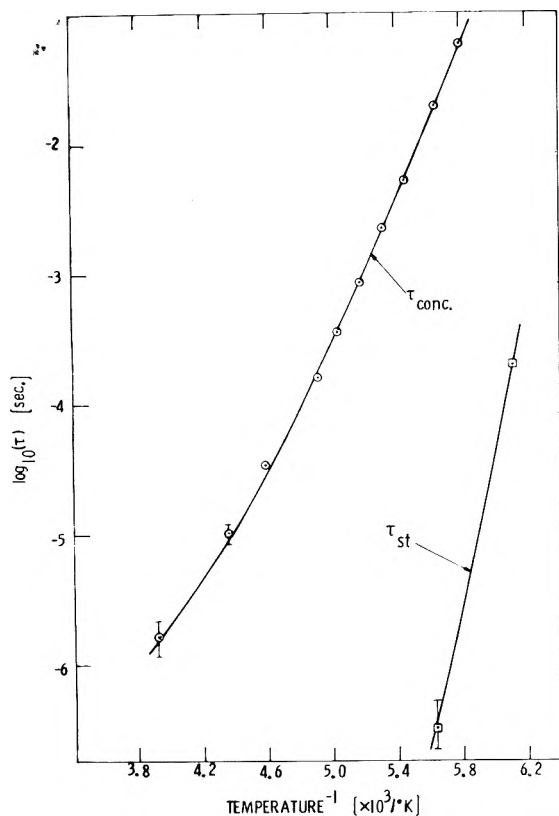


Figure 2. Structural and concentrational relaxation times (τ 's) as function of inverse temperature.

fluctuations the correlation function due to density fluctuations could be independently observed. Choosing $\theta \leq \tau_c/1000$, the observed correlation function was of the form

$$C_k''(t) = a + b \exp(-2t/\tau_{st}) \quad (5)$$

A typical plot of $|G_n(t)|^2$, the exponential part of C_k'' , at -110°C is shown in Figure 3 and is well described by a simple exponential. This relaxation process was checked for possible q dependence and was found, within experimental uncertainty, to be independent of q . To eliminate the possibility that the observed results might be associated with both molecular reorientational motions as well as with density fluctuations, polarized (I_{VV}) and depolarized (I_{VH}) scattering intensity measurements were made. I_{VV} (i.e., polarized scattering) is the intensity of the scattered light with the incident light and the scattered light perpendicular to the scattering plane and is associated with both density and reorientational fluctuations. I_{VH} (depolarized scattering) is the intensity of the scattered light with the incident light perpendicular to the scattering plane and the scattered light parallel to the scattering plane and is associated only with molecular reorientation. These measurements provided a ratio I_{VV}/I_{VH} greater than 200 which indicates that scattering associated with molecular reorientation is not an important mechanism in this study. The results support identification with the density fluctuations. The measured structural relaxation times, τ_{st} , are plotted in Figure 2 along with τ_c .

A recent ultrasonic absorption study⁵ has provided data on structural relaxation times and also available are NMR relaxation times. It has been suggested that the NMR times represent the end over end tumbling of the Me_2SO molecules, which for 0.3 mole fraction Me_2SO in H_2O are approximately equal to the orientational times of the H_2O molecules in the

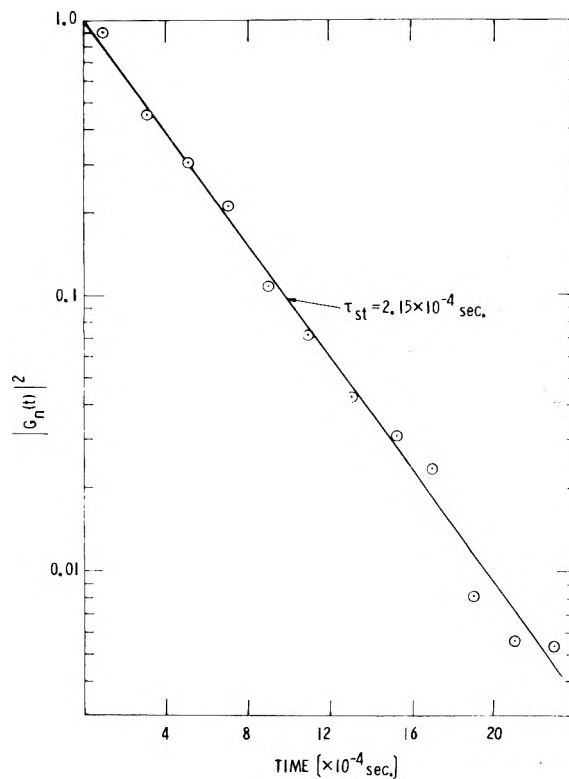


Figure 3. Structural correlation function vs. time at -110°C .

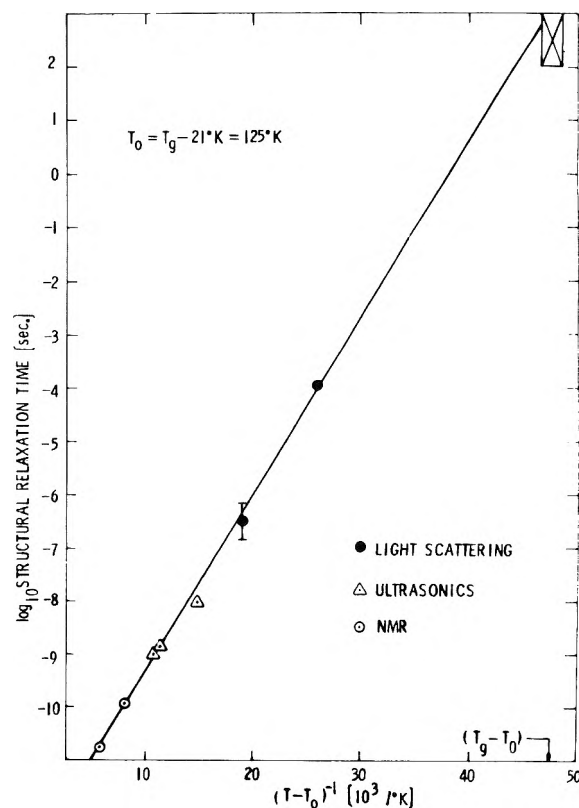


Figure 4. Composite structural relaxation times vs. $(T - T_0)^{-1}$. \boxtimes , approximate relaxation time at the glass temperature.

system derived from the intrarelation process. These various times and the light scattering times obtained from this study are plotted in Figure 4 as a function of $(T - T_0)^{-1}$. The

measured glass transition temperature T_g , obtained by calorimetric techniques,¹⁶ and the associated approximate relaxation time, $\tau_{st}^E \approx 10^2 - 10^3$ s, are represented in Figure 4. The transport properties of viscous liquids are frequently non-Arrhenius and can usually be described by a temperature dependence of the form, $\tau = A \exp[B/(T - T_0)]$, where A and B are experimentally determined parameters and T_0 is an operationally defined "ideal glass" temperature related to the glass transition temperature T_g . This smooth fit of the three sets of data in Figure 4 yielded $T_0 = T_g - 21$ K = 125 K. This fit suggests that for the 0.3 mole fraction Me₂SO in H₂O system the ultrasonic, NMR, and light scattering techniques are all observing the structural relaxation process. Fitting limited viscosity data for this system, Schichman¹⁷ obtained a $T_0 = 120$ K, which is in close agreement with the T_0 found by the DCS method.

The simultaneous measurement of the concentration fluctuation times, τ_c , and the isothermal structural relaxation time, τ_{st} , in Me₂SO in H₂O shows that the correlator technique can be effectively employed to measure and separate multiple relaxation processes. The Me₂SO in H₂O results also show that the isothermal structural relaxation function is single, which is quite rare in viscous liquids and similar to pure water.

Acknowledgment. This research was supported by the Office of Naval Research Contract No. 00014-75-C-0585.

References and Notes

- (1) R. D. Mountain, *J. Res. Natl. Bur. Stand., Sect. A*, **70**, 207 (1966).
- (2) C. J. Montrose, V. A. Solovgey, and T. A. Litovitz, *J. Acoust. Soc. Am.*, **43**, 117 (1968).
- (3) L. Fishman and R. D. Mountain, *J. Phys. Chem.*, **74**, 2175 (1970).
- (4) K. J. Packer and D. J. Tomlinson, *Trans. Faraday Soc.*, **67**, 1302 (1971).
- (5) W. Madegosky, NOL (private communication).
- (6) C. Demoulin, C. J. Montrose, and N. Ostrowski, *Phys. Rev. A*, **9**, 1740 (1974).
- (7) C. C. Lai, P. B. Macedo, and C. J. Montrose, *J. Am. Ceram. Soc.*, **58**, 120 (1975).
- (8) J. F. Dill, P. W. Drake, and T. A. Litovitz, *Am. Soc. Lubr. Eng., Trans.*, **18**, 202 (1975).
- (9) D. A. Pinnow, S. J. Candau, J. T. LaMacchia, and T. A. Litovitz, *J. Acoust. Soc. Am.*, **43**, 131 (1968).
- (10) E. Jakeman, C. J. Oliver, and E. R. Pike, *J. Phys. A*, **3**, 145 (1970).
- (11) E. Jakeman, E. R. Pike, and S. Swain, *J. Phys. A*, **4**, 517 (1971).
- (12) P. Debye, *Phys. Rev. Lett.*, **14**, 783 (1965).
- (13) B. Chu, F. J. Schoenes, and W. P. Kao, *J. Am. Chem. Soc.*, **90**, 3042 (1968).
- (14) M. DuBois and P. Berge, *Phys. Rev. Lett.*, **26**, 121 (1971).
- (15) F. Rallo, F. Rodante, and P. Silvestroni, *Thermochim. Acta*, **1**, 311 (1970).
- (16) D. H. Rasnoussen and A. P. MacKenzie, *Nature (London)*, **220**, 1315 (1968).
- (17) S. A. Schichman and R. L. Amey, *J. Phys. Chem.*, **75**, 98 (1971).

The Significant Determination of the Permanent Dipole Moment of a Solute in Solution¹

R. Finsy* and R. Van Loon*

Faculteit van de Wetenschappen, Vrije Universiteit Brussel, Brussels, Belgium (Received June 7, 1976)

An extrapolation method based on the Onsager-Kirkwood-Fröhlich theories is reported for determining the dipole moment of a polar molecule in solution in a nonpolar solvent. To illustrate the method the dipole moment of 1,1,1-trichloroethane was determined in solution in six different solvents yielding $1.70_5 \pm 0.02$ D, almost independent of the nature of the solvent. When calculated with the Debye equation the apparent dipole moment values vary by about 0.12 D as a function of the solvent. Experimental assessment of the Kirkwood-Fröhlich correlation factor showed a weak tendency to parallel orientation of neighboring dipolar axis in pure liquid 1,1,1-trichloroethane.

1. Introduction

Determination of the permanent dipole moment of a polar molecule in the liquid state has very often led to a diversity of values for one and the same molecule,² especially when determined in different solvents.

In this paper it will be illustrated by the determinations of the dipole moment of 1,1,1-trichloroethane (TCE) in different solvents that the variation of the apparent dipole moment values as function of the solvent, sometimes called the "solvent effect",³ can be explained by the incorrect treatment of the internal field in the Debye theory; the latter being only correct at infinite dilution of a polar solute in a nonpolar solvent if both solvent and solute molecules have the same polarizability.⁴

To show this, extrapolation methods, based on respectively the Onsager-Kirkwood-Fröhlich (OKF) theories and the Debye theory, are reported and compared for determining the dipole moment of a polar molecule in solution in a nonpolar solvent. In addition the methods using the OKF theories allow an experimental assessment of the Kirkwood-Fröhlich correlation factor in the pure polar liquid and in binary mixtures of a polar and a nonpolar component.

As an example the frequently studied polar TCE was investigated. The TCE molecule and three of the solvent molecules (2,2-dimethylpropane, tetrachloromethane, and cyclohexane) being nearly spherical and having comparable molar volumes were especially chosen to approach the theoretical models as far as possible. The dipole moment was also determined in three currently used solvents consisting of

TABLE I: Dielectric Constants of Some Pure Liquids

Liquid	ϵ (at t , °C)	$-(\partial\epsilon/\partial t) \times 10^4$	$\frac{1}{2}(\partial^2\epsilon/\partial t^2) \times 10^5$	Probable error $\times 10^3$	Temp range
2,2-Dimethylpropane (neopentane)	1.831 (0)	+15.6		2	-16 + 9.6
Cyclohexane	2.015 (25)	14.8		2	+5.4 + 50
Tetrachloromethane (carbon tetrachloride)	2.228 (25)	20.0		2	-20 + 50
Benzene	2.278 (25)	20		2	+25 + 50
1,4-Dimethylbenzene (<i>p</i> -xylene)	2.260 (25)	31		4	25-50
1,3,5-Trimethylbenzene (mesitylene)	2.273 (25)	18		4	25-50
1,1,1-Trichloroethane (TCE)	7.953 (0)	383	16.5	6	-20 + 15
	7.945 (0)	372	10.8	4	0 + 50

"nonspherical" molecules (benzene, 1,4-dimethylbenzene, and 1,3,5-trimethylbenzene).

2. Experimental Section

2.1. Apparatus and Products. The capacitance of a three electrode stainless steel cell, in vacuo (C_0) and filled with the liquid to be studied (C), is measured with a transformer ratio-arm bridge Wayne-Kerr B-221 A at a frequency of 1592 Hz.

In vacuo the capacitance was given by $C_0 = (6.4225 + 0.0001t)$ pF (t is the temperature in °C), with a reproducibility of 0.0005 pF. About 10 cm³ of liquid is introduced in the cell by vacuum distillation. The dielectric constant ϵ of the studied liquid is given by $\epsilon = C/C_0$.

The cyclohexane, tetrachloromethane (carbon tetrachloride), benzene, 1,4-dimethylbenzene (*p*-xylene), and 1,3,5-trimethylbenzene (mesitylene) were Merck products pro analysi dried on molecular sieves, purity about 99.9% controlled by gas-liquid chromatography. The 2,2-dimethylpropane (neopentane) was a Phillips Petroleum Co. product of 99.83% purity. The 1,1,1-trichloroethane (methylchloroform) was a raw Fluka or Merck product; after several washings with H₂SO₄, Na₂CO₃, and water, and drying on anhydrous CaCl₂ it was distilled; its final purity (about 99.9%) was controlled by gas-liquid chromatography. Determinations of volume changes for nine solvent-solute mixtures were made by density measurements at different temperatures following Kratky et al.⁵ with an Anton Paar DMA 10 densimeter, whose precision was improved by measuring the period of oscillation of the cell with an external seven-digit frequency counter. The final precision of about 5×10^{-5} g/ml was governed by the ultimate temperature control of the measuring cell which was within ± 0.03 °C. The measured densities of the pure components were, within the experimental uncertainty, in agreement with the values reported by Timmermans.⁶ The volume change on mixing v_e of all investigated systems was less than 0.4 cm³/mol, and for the TCE/tetrachloromethane mixtures v_e was in agreement with the literature data.⁷⁻⁹

2.2. Dielectric Constants of the Pure Liquids. The dielectric constants of the pure liquids were measured at temperature intervals of about 4 °C in the ranges given in Table I. These measurements were fitted to a power series in the temperature using a least-squares criterion and a F-test¹⁰ to retain only the significant terms in the power series. The coefficients of these series are also given in Table I, together with the probable error (for 95% confidence limits) on the dielectric constants. The data on cyclohexane, tetrachloromethane, benzene, 1,4-dimethylbenzene, and 1,3,5-trimethylbenzene are in excellent agreement with the selected values of the National Bureau of Standards.¹¹ For 2,2-dimethylpropane no values for the dielectric constant were found in the literature. The

determined dielectric constant of TCE agrees within 1% with the literature values¹²⁻¹⁶ and within 0.5% with the more recent values.^{15,16}

2.3. Dielectric Constants of Some Solutions. Measurements of the dielectric constant of several solutions with the volume fraction of TCE ranging from about 0.1 to 0.9 in tetrachloromethane, 2,2-dimethylpropane, and cyclohexane and of dilute solutions with volume fraction of TCE ranging from about 0.05 to 0.20 in benzene, 1,4-dimethylbenzene, and 1,3,5-trimethylbenzene were performed and analyzed in the same way as for the pure liquids. Results are listed in Tables II-V.

The probable error on the reported volume fractions of the solutions is about 2×10^{-4} , except for the TCE/2,2-dimethylpropane solutions where the probable error was about 5×10^{-4} .

3. Determination of the Permanent Dipole Moment and the Kirkwood-Fröhlich Orientation Correlation Factor in Solution

For a binary mixture of a nonpolar substance with dielectric constant ϵ_1 and a polar substance with permanent dipole moment μ and high frequency permittivity ϵ_∞ , the Onsager-Kirkwood-Fröhlich formulation gives¹⁵

$$\frac{4\pi\rho\mu^2}{3kT} = \left(\frac{3}{\epsilon_\infty + 2}\right)^2 \frac{2\epsilon + \epsilon_\infty}{2\epsilon + \epsilon_1} \times \left[\frac{2\epsilon + \epsilon_\infty}{3\epsilon} \frac{\epsilon - \epsilon_1}{\varphi} - (\epsilon_\infty - \epsilon_1) \right] \quad (1)$$

where ρ is the number density in the pure polar liquid; φ is the volume fraction in the polar component; ϵ is the dielectric constant of the mixture, and $g(\varphi)$ is the Kirkwood orientation correlation factor, obeying $\lim_{\varphi \rightarrow 0} g(\varphi) = 1$.

The Debye treatment gives, with the same notations

$$\frac{4\pi\rho\mu^2}{3kT} = \frac{9}{(\epsilon_1 + 2)(\epsilon_\infty + 2)} \left[\frac{\epsilon_\infty + 2}{\epsilon + 2} \frac{\epsilon - \epsilon_1}{\varphi} - (\epsilon_\infty - \epsilon_1) \right] \quad (2)$$

In the derivation of eq 1 and 2 it is assumed that the molar volume v_m of the mixture is given as $v_m = (1 - x)v_1 + xv_2$, where v_1 and v_2 are respectively the molar volumes of the pure nonpolar solvent and the pure polar solute, x is the mole fraction of the polar component (this is equivalent to stating that the solutions present no volume changing on mixing). This assumption is verified within 0.4% for the least favorable case of the investigated mixtures (cf. section 2.1).

The determination of the dipole moment in solution is carried out by extrapolating the right-hand side of eq 1 and 2 to infinite dilution. The extrapolation is performed in the two following ways.

3.1. With the experimental values of ϵ , ϵ_1 , and φ , and an estimate for ϵ_∞ , one calculates the right-hand side of eq 1 and 2,

TABLE II: Dielectric Constants of Some Solutions of 1,1,1-Trichloroethane in Tetrachloromethane in the Temperature Range 25 to 50 °C

Vol fraction in TCE	ϵ at 25 °C	$-(\partial\epsilon/\partial t)$ $\times 10^4$	$\frac{1}{2}(\partial^2\epsilon/\partial t^2)$ $\times 10^6$	Probable error $\times 10^3$
0.0607	2.439	30		2
0.0792	2.505	49		2
0.1878	2.914	66	19	2
0.3006	3.377	117	55	3
0.3946	3.785	146	109	4
0.5033	4.297	144	62	4
0.5940	4.749	207	69	6
0.6828	5.211	226	62	4
0.7787	5.747	254	56	6
0.9184	6.569	300	55	4

TABLE III: Dielectric Constants of Some 1,1,1-Trichloroethane/Cyclohexane Mixtures in the Temperature Range 5 to 45 °C

Vol fraction in TCE	ϵ at 25 °C	$-(\partial\epsilon/\partial t)$ $\times 10^4$	$\frac{1}{2}(\partial^2\epsilon/\partial t^2)$ $\times 10^6$	Probable error $\times 10^3$
0.0669	2.247	28.2	2	2
0.1121	2.412	38.8	5.6	2
0.2212	2.838	66.3	15	2
0.2769	3.072	82.5	19	3
0.3902	3.580	117	29	4
0.4959	4.098	154	43	5
0.5989	4.632	191	48	6
0.7088	5.253	238	66	6
0.8002	5.797	275	77	6
0.9133	6.505	329	94	6

TABLE IV: Dielectric Constants of Some 1,1,1-Trichloroethane/2,2-Dimethylpropane Mixtures in the Temperature Range -20 to +10 °C

Vol fraction in TCE	ϵ at 25 °C	$-(\partial\epsilon/\partial t)$ $\times 10^4$	$\frac{1}{2}(\partial^2\epsilon/\partial t^2)$ $\times 10^6$	Probable error $\times 10^3$
0.0957	2.220	39.1	6	2
0.1589	2.496	55.7	15	2
0.2577	2.964	83.7	27	2
0.3626	3.507	111	31	3
0.4362	4.001	142	50	3
0.5702	4.801	192	72	3
0.6689	5.389	225	101	3
0.7634	6.073	268	112	2
0.8841	6.966	322	151	4

which we will represent respectively by $Y_{\text{Ons}}(\varphi)$ and $Y_{\text{Deb}}(\varphi)$, as a function of the volume fraction. Then $Y_{\text{Ons}}(\varphi)$ and $Y_{\text{Deb}}(\varphi)$ are fitted with a power series in φ using a least-squares criterion and the values $Y_{\text{Ons}}(0)$ and $Y_{\text{Deb}}(0)$ at infinite dilution are obtained together with their probable error estimated from the variance-covariance matrix of the coefficients of the power series.

The value of the dipole moment is given by

$$\mu_{\text{Ons}} = \left[\frac{3kT}{4\pi\rho} Y_{\text{Ons}}(0) \right]^{1/2} \quad (3)$$

and

$$\mu_{\text{Deb}} = \left[\frac{3kT}{4\pi\rho} Y_{\text{Deb}}(0) \right]^{1/2} \quad (4)$$

respectively.

The probable error $\delta\mu$ on μ is estimated by

TABLE V: Dielectric Constants of Dilute Solutions of 1,1,1-Trichloroethane in Benzene, 1,4-Dimethylbenzene, and 1,3,5-Trimethylbenzene in the Temperature Range 25 to 30 °C

Vol fraction in TCE	ϵ at 25 °C	$-(\partial\epsilon/\partial t)$ $\times 10^4$	$\frac{1}{2}(\partial^2\epsilon/\partial t^2)$ $\times 10^6$	Probable error $\times 10^3$
TCE in Benzene				
0.0505	2.443	30	3.1	2
0.0964	2.601	38	3.8	2
0.1301	2.717	45	7.7	2
0.2110	3.010	60	53	3
TCE in 1,4-Dimethylbenzene				
0.0638	2.473	31		2
0.0894	2.561	35	6.9	2
0.1612	2.811	53	143	5
0.2020	2.962	59	130	4
TCE in 1,3,5-Trimethylbenzene				
0.0672	2.497	23	2.7	2
0.1090	2.636	38	7.4	2
0.1542	2.793	45	7.6	2
0.1936	2.936	56	128	2

$$\frac{\delta\mu}{\mu} \approx \frac{1}{\epsilon_{\infty} + 2} \delta\epsilon_1 + \frac{1}{2Y(0)} \left(\frac{3}{\epsilon_{\infty} + 2} \right)^2 \delta\epsilon_{\infty} + \frac{1}{2Y(0)} \delta Y(0) \quad (5)$$

In the derivation of eq 5 the probable errors on temperature and density are neglected and it is assumed that $\epsilon_1 \approx \epsilon_{\infty}$; $\delta Y(0)$ is the probable error on $Y(0)$.

The values of the Kirkwood-Fröhlich correlation factor g as a function of the concentration are readily obtained by

$$g(\varphi) = \frac{Y_{\text{Ons}}(\varphi)}{Y_{\text{Ons}}(0)} \quad (0 \leq \varphi \leq 1) \quad (6)$$

3.2. The second extrapolation method involves the analytical limits for $\varphi \rightarrow 0$ of eq 1 and 2, which are, respectively, using $\lim_{\varphi \rightarrow 0} g = 1$:

$$\frac{4\pi\rho\mu^2}{3kT} = \left(\frac{3}{\epsilon_{\infty} + 2} \right)^2 \frac{2\epsilon_1 + \epsilon_{\infty}}{3\epsilon_1} \times \left[\frac{2\epsilon_1 + \epsilon_{\infty}}{3\epsilon_1} \left(\frac{\partial\epsilon}{\partial\varphi} \right)_{\varphi=0} - (\epsilon_{\infty} - \epsilon_1) \right] \quad (7)$$

and

$$\frac{4\pi\rho\mu^2}{3kT} = \frac{9}{(\epsilon_1 + 2)(\epsilon_{\infty} + 2)} \times \left[\frac{\epsilon_{\infty} + 2}{\epsilon_1 + 2} \left(\frac{\partial\epsilon}{\partial\varphi} \right)_{\varphi=0} - (\epsilon_{\infty} - \epsilon_1) \right] \quad (8)$$

One first extrapolates $(\epsilon - \epsilon_1)/\varphi$ for $\varphi \rightarrow 0$ yielding $(\partial\epsilon/\partial\varphi)_{\varphi=0}$. This is done by means of a least-squares criterion fitting $(\epsilon - \epsilon_1)/\varphi$ with a power series in φ . Next the right-hand sides of eq 7 and 8, which we will denote respectively by $Z_{\text{Ons}}(\varphi)$ and $Z_{\text{Deb}}(\varphi)$, are calculated at infinite dilution from the data for ϵ_1 , ϵ_{∞} , and $(\partial\epsilon/\partial\varphi)_{\varphi=0}$.

Finally the value of μ is given by

$$\mu_{\text{Ons}} = \left[\frac{3kT}{4\pi\rho} Z_{\text{Ons}}(0) \right]^{1/2} \quad (9)$$

and

$$\mu_{\text{Deb}} = \left[\frac{3kT}{4\pi\rho} Z_{\text{Deb}}(0) \right]^{1/2} \quad (10)$$

The probable error is now given by using the same assumptions as for eq 5

$$\delta\mu = \frac{\mu}{2Z(0)} \left(\frac{3}{\epsilon_\infty + 2} \right)^2 \left\{ \frac{\epsilon_\infty}{\epsilon_\infty + 2} \left(\frac{\partial\epsilon}{\partial\varphi} \right)_{\varphi=0} \delta\epsilon_1 + \delta\epsilon_\infty + \delta \left[\left(\frac{\partial\epsilon}{\partial\varphi} \right)_{\varphi=0} \right] \right\} \quad (11)$$

Both methods 3.1 and 3.2 will be used in the following sections to determine the dipole moment of TCE in different solvents.

4. Estimates of the High Frequency Permittivity of TCE

In order to calculate the value of the permanent dipole moment of TCE we need to know its high frequency permittivity ϵ_∞ , which is in both the Onsager–Kirkwood–Fröhlich (OKF) and Debye theories a characteristic of the induced part of the polarization (total deformation polarization) of the polar component.

4.1. From measurements in the gas phase¹⁷ one obtains for the total molar polarizability $P = (4\pi N_a \alpha / 3)$ (N_a is the Avogadro number) of TCE: $P = (27.0 \pm 1) \text{ cm}^3$, which yields for the liquid state

$$\epsilon_\infty = (2.15 - 0.002t) \pm 0.06 \quad (12)$$

4.2. Absorption and dispersion measurements between 5 and 40 GHz¹⁸ if represented by the simple Debye frequency relations give

$$\epsilon_\infty = (2.47 - 0.004t) \pm 0.04 \quad (13)$$

This value must be too high as it neglects the higher frequency Poley absorption.^{19–23}

4.3. Alternatively one can account for the Poley absorption by putting $\epsilon_\infty = n_{\text{IR}}^2$, where n_{IR}^2 is the square of the refractive index at the high frequency termination of the Poley absorption.²⁴

Measurements performed at the National Physical Laboratory, U.K., with the dispersive Fourier transform spectroscopy technique,²⁵ yield at 25 °C and a frequency of 3 THz (wave number 100 cm^{-1}):

$$\epsilon_\infty = n^2(3 \text{ THz}) = 2.126 \pm 0.01 \quad (14)$$

in agreement with estimate (12).

4.4. Often^{26,27} ϵ_∞ is put equal to n_{D}^2 or to $1.05 n_{\text{D}}^2$ (n_{D} is the refractive index at the sodium D line). This gives at 20 °C

$$\epsilon_\infty = n_{\text{D}}^2 = 2.067_6 \quad (15)$$

and

$$\epsilon_\infty = 1.05 n_{\text{D}}^2 = 2.170_9 \quad (16)$$

4.5. An approximate estimate, based on assumed additivity of polarizabilities, is

$$\alpha(\text{TCE}) = \frac{3}{4}\alpha(\text{CCl}_4) + \frac{1}{4}\alpha(\text{CH}_3)_4 \quad (17)$$

This yields

$$\epsilon_\infty = (2.182 - 0.0018t) \pm 0.003 \quad (18)$$

in good agreement with estimates (12) and (14).

It has to be pointed out that the values of the permanent moment of TCE are however not very sensitive to the choice of ϵ_∞ . From eq 5 or 11 and with the data for TCE one finds in a first approximation $\partial\mu/\partial\epsilon_\infty \simeq -0.25 \text{ D}$ so that taking n_{D}^2 or $1.05 n_{\text{D}}^2$ or estimates (12), (14), or (18) for ϵ_∞ will lead to a spread of only 0.03 D for the dipole moment values. However estimates of ϵ_∞ by extrapolations of complex permittivity data,

estimate (13), can give underestimations of about 0.1 D for the dipole moment of TCE.

5. Discussion

5.1. *Dipole Moment of TCE.* The values of the permanent moment of TCE in solution in the six different solvents are calculated at different temperatures with estimate (18) for ϵ_∞ and eq 3, 4 and 9, 10; (methods 3.1 and 3.2, respectively). The apparent variation of μ as a function of temperature does not exceed 0.02₆ D. The mean values over the considered temperature intervals are listed in Table VI. The results show that both extrapolation methods yield the same value ($1.70_5 \pm 0.02 \text{ D}$) for the permanent moment of TCE. This value appears to be solvent independent within the experimental uncertainty, when determined using the OKF theories, while when calculated with the Debye equation a familiar solvent effect was observed: the value of the dipole moment ranges from 1.67 to 1.80 D with decreasing dielectric constant (or polarizability) of the solvent, the differences between the values of μ^2 calculated with eq 7 and 8 being proportional to $(\epsilon_\infty - \epsilon_1)$. This is clearly shown when rewriting eq 7, (OKF at infinite dilution) as

$$\begin{aligned} \frac{4\pi\rho\mu^2}{3kT} = & \frac{9}{(\epsilon_1 + 2)(\epsilon_\infty + 2)} \left[\frac{\epsilon_\infty + 2}{\epsilon_1 + 2} \left(\frac{\partial\epsilon}{\partial\varphi} \right)_{\varphi=0} - (\epsilon_\infty - \epsilon_1) \right] \\ & - 12(\epsilon_\infty - \epsilon_1) \left(\frac{\partial\epsilon}{\partial\varphi} \right)_{\varphi=0} \frac{(\epsilon_1 - 1)}{\epsilon_1(\epsilon_\infty + 2)(\epsilon_1 + 2)^2} \\ & + 2(\epsilon_\infty - \epsilon_1)^2 \frac{(\epsilon_1 - 1)}{\epsilon_1^2(\epsilon_1 + 2)^2(\epsilon_\infty + 2)^2} \\ & \times \left[3\epsilon_1(\epsilon_1 + 2) + 2(\epsilon_1 - 1) \left(\frac{\partial\epsilon}{\partial\varphi} \right)_{\varphi=0} \right] \quad (19) \end{aligned}$$

The first term on the right-hand side of eq 19 is the right-hand side of eq 8 (Debye at infinite dilution), while the other terms are, for the studied liquids, small corrections; the term in $(\epsilon_\infty - \epsilon_1)^2$ is several orders of magnitude smaller than the one in $(\epsilon_\infty - \epsilon_1)$.

5.2. *Orientation Correlations.* One sees from Figure 1 that the Kirkwood–Fröhlich orientation correlation factor g , calculated with eq 6, increases with the concentration of TCE in tetrachloromethane, 2,2-dimethylpropane, and cyclohexane from unity to about 1.14 in pure TCE. This corresponds to a weak tendency toward a parallel alignment of the dipolar axis of neighboring TCE molecules. The fact that g is not equal to one at the higher concentrations and in pure TCE also shows that inaccurate estimates of its dipole moment will be obtained when calculated with the Onsager equation (eq 1 with $g = 1$), especially for the pure polar liquid in which case the dipole moment will be overestimated by about 0.1 D.

5.3. *Comparison with Some Results from the Literature.* Values of the dipole moment of TCE, obtained from measurements in solution in different solvents, are reported in the recent literature and range from 1.65 to 1.87 D.^{1,13,16,28–33} As some controversial statements^{16,30} are formulated about “reasonable” differences in the reported values we will examine very briefly the reported methods, which are mainly three: the Halverstadt–Kumler (HK) method,³⁴ the Debye equation for (one) dilute solution as reported by Crossley and Walker,³⁰ and the Onsager equation for the pure polar liquid.

The HK method is based on the Debye equation³⁵ and therefore assumes the local field to be equal to the Lorentz field. So one can expect that the apparent dipole moment of TCE will vary by about 0.1 D as a function of the solvents

TABLE VI: Dipole Moment of 1,1,1-Trichloroethane in Solution^a

Solvent	Section 3.1 method ^b		Section 3.2 method ^c		Probable error	Temp range, °C
	μ_{Ons}	μ_{Deb}	μ_{Ons}	μ_{Deb}		
2,2-Dimethylpropane	1.71 ₄	1.79 ₇	1.74 ₂	1.79 ₁	0.04	-20 + 10
Cyclohexane	1.68 ₆	1.72 ₃	1.69 ₇	1.71 ₄	0.02	0 + 50
Tetrachloromethane	1.70 ₅	1.70 ₁	1.70 ₄	1.69 ₁	0.02	+25 + 50
Benzene	1.70 ₇	1.68 ₇	1.69 ₈	1.67 ₈	0.02	25-50
1,4-Dimethylbenzene	1.70 ₆	1.68 ₅	1.68 ₇	1.66 ₈	0.02	25-30
1,3,5-Trimethylbenzene	1.72 ₂	1.69 ₉	1.69 ₅	1.67 ₅	0.02	25-50

^a Mean values over the reported temperature ranges. ^b Determined with the extrapolation method described in section 3.1. ^c Determined with the extrapolation method described in section 3.2.

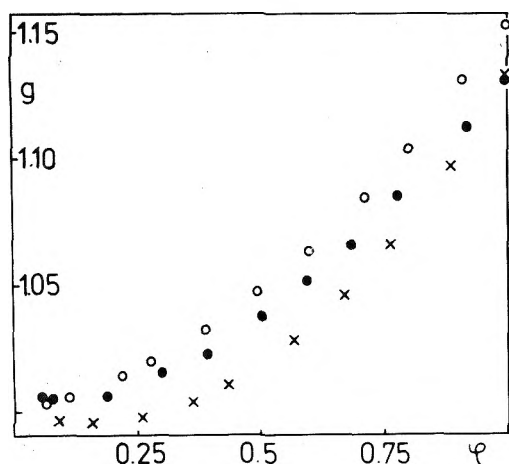


Figure 1. Orientation correlation factor g of 1,1,1-trichloroethane in solution in (X) 2,2-dimethylpropane at -20°C , (O) cyclohexane at 25°C , and (●) tetrachloromethane at 25°C .

used, in a way similar with our results when calculated with the Debye equation. In particular the values of the dipole moment are expected to decrease with increasing solvent polarizability (or dielectric constant). This is clearly so for the reported values determined with the HK method: 1.66 D in benzene and 1.75 D in *n*-hexane;³³ 1.70 D in benzene;²⁸ 1.73 D in tetrachloromethane.²⁹ These results are within the experimental uncertainty in agreement with our "Debye" results.

The same remarks hold for the method of Crossley and Walker,³⁰ which follows straightforwardly from the Debye equation. On the basis of measurements on one dilute solution with volume fraction of about 0.05, values ranging from 1.65 to 1.87 D in several solvents are reported³⁰⁻³² using this method. Besides the fact that the Debye equation is likely to induce an apparent variation of about 0.1 D as a function of the solvent, the experimental uncertainty involved in this method is of the same order of magnitude; e.g., in 1,4-dimethylbenzene the following values are given: 1.65 D at 25°C ³¹ and 1.76 D at 25°C .³²

The third method (Onsager equation) will overestimate, as shown in section 5.2, the value of the dipole moment of TCE up to about 0.1 D in the pure polar liquid, due to the neglect of orientation correlations. This explains the rather elevated value determined by Clemett and Davies¹³ in the pure polar liquid (1.78 ± 0.02 D), and the apparent variation of the dipole moment of TCE in solution in benzene as a function of the concentration in TCE, observed by Turner et al.¹⁶ (μ ranges from 1.73 to 1.86 D). It should be noted that the value reported

by these authors at their lowest concentration in TCE (mole fraction 0.25) is in agreement with ours, as in this region g is almost equal to one.

In the gas phase the following values are reported: 1.77 ± 0.02 D,³⁶ 1.79 ± 0.02 D,¹⁷ and more recently $1.75_5 \pm 0.01_5$ D.³⁷ The values we obtained in solution are somewhat smaller, although the difference with the recent and accurate data, determined by Stark effect in the microwave region,³⁷ is not very significant. Hereby it should be observed that the validity of the OKF theories is limited by the assumption that the molecules can be treated as point dipoles embedded in spheres with isotropic and uniform polarizability. The real solvent and solute molecules, however, present also higher order moments, whose influence may be negligible for intermolecular distances large compared to the molecular dimensions (i.e., in dilute gases) but can become considerable in the liquid phase. This could eventually explain the small difference (as far as it is significant) between the value of the dipole moment of TCE obtained here ($1.70_5 \pm 0.02$ D) and the gas phase value of Holm et al.³⁷ ($1.75_5 \pm 0.01_5$ D).

6. Conclusion

The value of the dipole moment of TCE in solution, determined with the proposed extrapolation methods and calculated with the OKF equation, is independent, within experimental uncertainty, of the solvents used and amounts to $1.70_5 \pm 0.02$ D. Calculated with the Debye equation this value increases from 1.67 to 1.80 D with decreasing polarizability (or dielectric constant) of the solvent. The effect is due to the incorrect treatment of the local field in the Debye theory.

The value of $1.70_5 \pm 0.02$ D is in agreement with the recent literature data if we take into account the following: (a) using the Onsager equation for the pure polar liquid the value of the dipole moment of TCE is overestimated by about 0.1 D due to the neglect of orientation correlations between neighboring TCE molecules; (b) estimates of ϵ_∞ , based on extrapolations to infinite frequency of complex permittivity data with help of the dynamic Debye equations, are not acceptable and lead to underestimated values of the dipole moment of TCE by about 0.1 D.

More generally it seems recommendable to bear in mind the following statements when determining the dipole moment of a polar molecule in solution in a nonpolar solvent: (a) the nonpolar solvent molecules should be as far as possible similar in structure, specific volume, and polarizability to the polar molecule investigated. In particular the difference between the polarizabilities of solvent and solute should be as small as possible. (b) The theoretical equations relating the dielectric constant of the solution to the dipole moment of the polar

molecules should preferably be based on the OKF theories, not on the Debye theory.

Acknowledgment. The authors are grateful to Professor A. Bellemans for providing experimental facilities in the Dielectrics Laboratory of the "Université Libre de Bruxelles".

References and Notes

- (1) This work was supported in part by the Belgian "Fonds National de la Recherche Scientifique".
- (2) See, e.g., A. L. McClellan, "Tables of Experimental Dipole Moments", Vol. 1, W. H. Freeman and Co., San Francisco, Calif., 1963; Vol. 2, Raha Enterprises, El Cerrito, Calif., 1974.
- (3) C. P. Smyth, "Dielectric Behaviour and Structure", McGraw-Hill, New York, N.Y., 1955, p 40.
- (4) (a) L. Onsager, *J. Am. Chem. Soc.*, **58**, 1486 (1936); (b) J. H. Van Vleck, *Mol. Phys.*, **24**, 341 (1972).
- (5) O. Kratky, H. Leopold, and H. Stabinger, *Z. Angew. Phys.*, **27**, 273 (1969).
- (6) J. Timmermans, "Physico-Chemical Constants of Pure Organic Compounds", Vol. 1, Elsevier, Amsterdam, 1950; Vol. 2, Elsevier, Amsterdam, 1965.
- (7) V. Mathot and A. Desmyer, *J. Chem. Phys.*, **21**, 782 (1953).
- (8) I. Prigogine and V. Mathot, *J. Chem. Phys.*, **20**, 49 (1952).
- (9) J. Jeener and M. Lambert, *Discuss. Faraday Soc.*, **22**, 85 (1956).
- (10) See, e.g., P. R. Bevington, "Data Reduction and Error Analysis for the Physical Sciences", McGraw-Hill, New York, N.Y., 1969, p 195.
- (11) A. A. Maryott and E. R. Smith, *Natl. Bur. Stand. Circ.*, **No. 514**, (1951).
- (12) R. S. Holland, G. N. Roberts, and C. P. Smyth, *J. Am. Chem. Soc.*, **78**, 20 (1956).
- (13) C. Clemett and M. Davies, *Trans. Faraday Soc.*, **58**, 1705 (1962).
- (14) S. Mallekarjun and N. E. Hill, *Trans. Faraday Soc.*, **61**, 1389 (1965).
- (15) R. Van Loon, S. Fuks, and A. Bellemans, *Bull. Soc. Chim. Belg.*, **76**, 202 (1967).
- (16) E. M. Turner, D. W. Anderson, L. A. Reich, and W. E. Vaughan, *J. Phys. Chem.*, **74**, 1275 (1970).
- (17) A. A. Maryott, M. E. Hobbs, and P. M. Gross, *J. Am. Chem. Soc.*, **63**, 659 (1941).
- (18) R. Van Loon and R. Finsy, *J. Phys. D (Appl. Phys.)*, **8**, 1232 (1975).
- (19) Y. Leroy, E. Constant, C. Abbar, and P. Desplanques, *Adv. Mol. Relaxation Processes*, **1**, 273 (1967).
- (20) M. Davies, G. W. F. Pardoe, J. E. Chamberlain, and H. A. Gebbie, *Trans. Faraday Soc.*, **64**, 847 (1968).
- (21) N. E. Hill, W. E. Vaughan, A. H. Price, and M. Davies, "Dielectric Properties and Molecular Behaviour", Van Nostrand, London, 1969, p 305.
- (22) R. Van Loon and R. Finsy, *Rev. Sci. Instrum.*, **45**, 523 (1974).
- (23) R. Finsy and R. Van Loon, *J. Chem. Phys.*, **63**, 4831 (1975).
- (24) See, e.g., M. Evans, *Spectrochim. Acta, Part A*, **31**, 609 (1975).
- (25) J. Chamberlain, C. E. Gibbs, and H. A. Gebbie, *Infrared Phys.*, **9**, 185 (1969).
- (26) Reference 21, p 241.
- (27) C. J. F. Böttcher, "Theory of Electric Polarization", 2d ed, Vol. 1, Elsevier, Amsterdam, 1973, pp 173 and 180.
- (28) R. J. W. Le Fèvre and G. L. D. Ritchie, *J. Chem. Soc.*, 4933 (1963).
- (29) R. J. W. Le Fèvre, J. V. Radford, G. L. D. Ritchie, and P. J. Stiles, *J. Chem. Soc. B*, 148 (1968).
- (30) J. Crossley and S. Walker, *J. Chem. Phys.*, **45**, 4733 (1966).
- (31) J. Crossley and S. Walker, *J. Chem. Phys.*, **48**, 4742 (1968).
- (32) J. Crossley and C. P. Smyth, *J. Am. Chem. Soc.*, **91**, 2482 (1969).
- (33) G. Klages and R. Langpape, *Z. Naturforsch. A*, **15**, 964 (1960).
- (34) I. F. Halverstadt and W. D. Kumler, *J. Am. Chem. Soc.*, **64**, 2988 (1942).
- (35) See, e.g., W. J. Taylor, *J. Phys. Chem.*, **79**, 1817 (1975); also J. W. Smith, "Electric Dipole Moments", Butterworths, London, 1955, p 54.
- (36) R. H. Wiswall and C. P. Smyth, *J. Chem. Phys.*, **9**, 356 (1941).
- (37) R. Holm, M. Mitzlaff, and H. Hartmann, *Z. Naturforsch. A*, **23**, 307 (1968).

A Study of the Solvent Effect on the Lowest Triplet State of Hydroxybenzaldehydes

K. A. Martin, G. Moller, and A. M. Nishimura*

Department of Chemistry, Wichita State University, Wichita, Kansas 67208 (Received April 7, 1976)

Publication costs assisted by the National Institute of Health and the Petroleum Research Fund

The phosphorescence microwave double resonance methods were used to observe the effects of inter- and intramolecular hydrogen bonding and chlorinated solvents on the lowest triplet state of *o*-, *m*-, and *p*-hydroxybenzaldehydes. Correlation of the vibronic activity observed in the optical phosphorescence spectra, the total rate constants for the dynamic processes is phosphorescence decays, and the zero field splittings due to spin-spin and spin-orbit interactions are noted as a function of both intra- and intermolecular hydrogen bonding and external heavy atom effect. The nature of the triplet state of the hydroxybenzaldehydes is definitely that of π, π^* in benzoic acid, a strongly hydrogen bonding host. In *p*-xylene and phenol hosts, the triplet state of *o*-hydroxybenzaldehyde is n, π^* . In the chlorinated host, *p*-dichlorobenzene, the nature of the phosphorescent triplet state of the hydroxybenzaldehyde is π, π^* with admixtures of the $^3n, \pi^*$ state.

Introduction

The study of hydrogen bonding has been renewed within the last few decades because of its vital importance in biological systems.¹ Since all bonds involve electrons, perturbations caused by hydrogen bonding would be expected to be detectable if a method of observing electronic changes sensitive to such perturbations existed. Recently in the study of the excited triplet electronic state of aromatic carbonyl molecules, extremely sensitive methods of phosphorescence microwave double resonance (PMDR) have been used to monitor electronic structures which are very responsive to intra- and in-

termolecular perturbations.²⁻⁵ Several workers have attempted to correlate the nature of the phosphorescent triplet state of some aromatic carbonyl molecules to:²⁻⁴ (1) the vibronic activity of the phosphorescence spectra, (2) the kinetic parameters for the radiative relaxation process due to phosphorescence, and (3) the magnitude of the triplet state zero field splitting (zfs) parameters resulting from electron spin-spin and spin-orbit interactions.

These past studies have shown that excited triplet state energies are strongly influenced by external solvent matrices. However, no attempts were made to specify the host type.

Since hydrogen bonding is known to perturb the electronic structure of molecules, the magnitude of the three aforementioned features should be sensitive to such perturbations. In this paper, we report some results of a study designed to detect the effects on the nature and the properties of the triplet state in the presence of intermolecular and/or intramolecular hydrogen bonding.

Experimental Section

The guest molecules investigated in the study were *p*-hydroxybenzaldehyde (*p*-HBA), *m*-hydroxybenzaldehyde (*m*-HBA), and *o*-hydroxybenzaldehyde (*o*-HBA). These guests were purified by multiple vacuum distillation or sublimation. The hosts included *p*-dichlorobenzene (DCB), *p*-xylene, phenol, and benzoic acid. DCB was obtained from Fisher Scientific Co. and was extensively zone refined under an inert atmosphere for an equivalent of over 200 passes. *p*-Xylene was purchased from J. T. Baker Chemical Co. and purified by shaking with concentrated sulfuric acid, washed, dried, and chromatographed. Finally, the solvent was subjected to multiple vacuum distillation. The phenol host, purchased from Mallinckrodt Chemical Works, was recrystallized from methanol and sublimed under vacuum. The solution for each guest-host combination investigated was sealed under vacuum in a thin-walled pyrex ampoule which was fitted into a slow wave helical structure attached to a semirigid 50- Ω stainless steel coaxial cable suspended in a liquid helium cryostat equipped with a quartz optical tip. Single crystals containing appropriate guest molecules were grown in a standard Bridgman furnace at room temperature for DCB and benzoic acid or in a cold room for *p*-xylene host. Single crystals were cut from the resulting ingots, mounted inside the slow wave helix, and immersed in liquid helium.

For experiments requiring a continuous excitation source, a 100-W xenon-mercury high-pressure arc lamp was used. Adequate filtering was accomplished by means of a solution containing NiSO₄ and CoSO₄ and a Corning 7-54 filter. The lamp was placed in a 45° configuration to a 0.75 m Czerny-Turner spectrometer with $\leq 100\text{-cm}^{-1}$ slits. A cooled EMI 6256B photomultiplier tube was used for detection of the phosphorescence. To obtain temperatures below 4.2 K, the vapor above the liquid helium was pumped and temperatures as low as 1.4 K were routinely obtained as determined by vapor pressure measurements of the liquid helium.

For phosphorescence decay measurements, a vibronic band of the phosphorescence (usually the 0,0 band) was isolated with the spectrometer and the excitation source was extinguished in about 2 ms by an electronically controlled mechanical shutter, or alternatively, the decay was measured following a xenon flash lamp excitation of 10- μs duration.

The zero field transitions of the triplet sublevels were detected by microwave induced delayed phosphorescence (MIDP) technique.^{6,7} The technique requires an appreciable difference in the populations of the two sublevels when the transition is adiabatically swept with the microwave power subsequent to the extinguishing of the excitation light. The phosphorescence decay is monitored via the spectrometer-photomultiplier combination. When the swept microwave energy is momentarily in resonance with the zero field transition, the populations of the two levels connected by the microwave power is perturbed, resulting in a sudden change in the phosphorescence intensity. In some cases the microwave power and/or sweep rate were adjusted such that an inversion of the populations in the coupled levels was achieved resulting in larger echoes.⁸

The microwave field was generated in the slow wave helix by a Hewlett-Packard sweep generator amplified by a 1-W TWT amplifier and terminated with the semirigid 50- Ω coaxial assembly. An Alfred microwave sweeper with appropriate plug-in was used in several cases (*vide infra*) where simultaneous pumping of two zero field transitions was necessary. The microwave sweep was calibrated using a Hewlett-Packard Model 540B transfer oscillator in conjunction with a Phillips 6630 frequency counter.

In several cases two of the transitions could be observed in the manner just described, but the detection of the third transition required either the continuous pumping of a different transition with another microwave generator or the monitoring of a weak phosphorescence band of an asymmetric vibration, or a combination of the two methods.

Results and Discussion

The fundamental vibrations as assigned from the phosphorescence spectra for the hydroxybenzaldehydes in DCB host are listed in Table I. These assignments are consistent with ir and vibronic data for benzaldehydes⁹⁻¹² and substituted phenols.^{13,14} Shown in Figure 1 are the phosphorescence spectra at 1.4 K of the three hydroxybenzaldehydes in DCB and *o*-HBA in *p*-xylene host. For *p*-HBA in DCB, nearly all fundamental vibrations have measurable intensity, but especially prominent is the 697- cm^{-1} ring mode which has been observed in prior studies to be sensitive to the position and type of substituent on the benzaldehyde.¹² This mode is considerably less intense for *p*-HBA in the other two hosts.

The phosphorescence spectrum of *m*-HBA in DCB host exhibits two particularly intense bands, one associated with the out-of-plane aldehydic C-H bend (1002 cm^{-1}) and the other at 102 cm^{-1} which could be due either to the torsion modes of the hydroxyl group or the phosphorescence origin of the same molecule in an inequivalent site. For *o*-HBA in DCB, most of the ring modes are apparent, but the bulk of the vibronic intensity arises from the vibrations associated with the aldehyde substituent. The out-of-plane C-H bend (1004 cm^{-1}) is still dominant, but the carbonyl stretching mode (1686 cm^{-1}) accounts for a considerable portion of the intensity.

The *p*-HBA in the *p*-xylene host spectrum is quite similar to that found in DCB host. The significant differences are the absence of the intense 697- cm^{-1} band that dominates the spectrum in DCB and the increased intensity and slight frequency shift of the out-of-plane aldehydic C-H band. The phosphorescence spectrum of *m*-HBA in *p*-xylene host consists of two subspectra, one originating at 24 856 cm^{-1} and the other red shifted by 189 cm^{-1} (*cf.* Figure 1). Dual origins are also observed for *p*-HBA and *m*-HBA in phenol, the predominant characteristics of which are shown in Table II. The phosphorescence spectrum associated with the origin having the slower phosphorescence decay rate constants exhibits more intensity in the out-of-plane aldehydic C-H bend and ring modes while the subspectrum originating with the faster rate constant has strong intensity in only the in-plane carbonyl stretching frequency. This effect could be due to guest molecules in inequivalent sites, phosphorescence originating from the same molecule but from two closely spaced triplet states, or the existence of a multi-minimum potential energy surface (*vide infra*).

A large difference exists in the phosphorescence spectra for *o*-HBA in DCB and in *p*-xylene (*cf.* Figure 1). In the *p*-xylene host, *o*-HBA phosphorescence shows the disappearance of the ring mode and the predominance of the carbonyl stretching

TABLE I: Assignments of the Fundamental Vibrations (cm^{-1}) of Hydroxybenzaldehydes in DCB at 1.4 K^a

Mode ^b	Wilson ^c notation	<i>o</i> -HBA	<i>m</i> -HBA	<i>p</i> -HBA
In-Plane Modes (a')				
C=O stretch		1686	1702	1702
$\nu(\text{CC})$	8a	1609	1616	1620
$\nu(\text{CC})$	8b	1603	1607	1598
$\nu(\text{CC})$	19a	--	1531	1514
Aldehyde C-H bend		1457	1463	1464
$\nu(\text{CC})$	19b	1485	1463?	1441
$\nu(\text{CC})$ or $\beta(\text{CH})$	14 or 3	--	1371	1364
$\nu(\text{C-OH})$	7a	1253	1272	1241
$\nu(\text{C-CHO})$	13	1209	1117?	1214 or 1226
$\beta(\text{O-H})$		1159	1182	1166
$\beta(\text{CH})$	9a or 9b	1154	1153	1166
$\beta(\text{CH})$	9b or 15	--	1109	1097
$\beta(\text{CH})$	18a or 18b	1030	1101	19
$\alpha(\text{CCC})^d$	1	802	916	841
$\alpha(\text{CCC})^d$	12	711	759	718
$\alpha(\text{CCC})^d$	6b	628	647	653
$\alpha(\text{CCC})^d$	6a	525	528	447
C-CHO bend ^e	9b	--	426	424
C-OH bend ^e	15	236	156	181
Out-of-Plane Modes (a'')				
Aldehyde C-H bend		1004	1002	1016
$\gamma(\text{CH})$	17a	848?	891	951
$\gamma(\text{CH})$	5	943	946	918
$\gamma(\text{CH})$	11 or 17b	933	873	858
$\gamma(\text{CH})$	10a	856	787	810
$\phi(\text{CC})$	4	717	678	697
$\phi(\text{CC})$	16b	440	461	510
$\phi(\text{CC})$	16a	532	557	403
C-OH bend ^e	10b	234	271	342
O-H bend		307	300	
C-CHO bend ^e	11	194		204
C-CHO torsion		145	125	154
C-OH torsion			102?	

^a Question marks indicate tentative assignments. -- indicates modes not observed. ^b ν , stretching modes; β , C-H in-plane deformation; α , in-plane ring deformation; γ , C-H out-of-plane deformation; ϕ , out-of-plane skeleton deformation. ^c Descriptions are most accurate for *p*-HBA. Notation from ref 25. ^d Radial skeletal modes sensitive to nature and position of substituents. ^e These mode are strongly coupled and the descriptions are only approximate.

mode. This effect has been observed by others and correlates well with an n, π^* lowest triplet state.^{2,15} The phosphorescence spectrum of *o*-HBA in phenol is dominated by the C=O stretching mode extending to its third harmonic.

The energies of the carbonyl stretching mode in each of the systems under study are listed in Table III. The lower frequencies of this mode in *o*-HBA relative to the *m*-HBA and *p*-HBA is attributed to intramolecular hydrogen bonding expected in this isomer. No drastic shift in the C=O stretching frequency is observed in the hydroxyl substituted benzaldehydes in phenol host as compared to the *p*-xylene host, indicating that the intermolecular hydrogen bond in phenol may not be a significant effect when compared to other interactions.

Shown in Table IV is a summary of the zfs observed by optical detection of the zero field transitions by MIDP. The axis system used in this paper is shown in Figure 2. The

TABLE II: Observed Average Rate Constants and Relative Vibronic Activity of Hydroxybenzaldehydes Exhibiting Phosphorescence Subspectra at 1.4 K

Guest/ host	Phos- phores- cence origins, cm^{-1}	Average phos- phores- cence rate constants ^a k_{av}	Relative peak intensities ^b	
			C-H out-of- plane bend	C=O Stretch- ing
<i>m</i> -HBA/ <i>p</i> -xylene	24 856	---	---	0.85
<i>m</i> -HBA/ phenol	24 667	13.2	0.85	0.45
<i>p</i> -HBA/ phenol	24 775	1733	---	0.90
	24 268	91	0.46	0.67
	24 969	100	---	0.32
	25 121	52	0.33	0.13

^a $k_{av} = (k_z + k_y + k_x)/3$. ^b Band intensities reported as fraction of the intensity of the corresponding origin. --- indicates band not observed.

TABLE III: Observed Carboxyl Stretching Modes (in cm^{-1}) for Hydroxybenzaldehydes in Several Hosts at 1.4 K

Guest	Host	DCB	<i>p</i> -Xylene	Phenol ^a	Benzoic acid
<i>o</i> -HBA		1686	1693	1600-1700	1688
<i>m</i> -HBA		1702	1716	1719	1695
<i>p</i> -HBA		1702	1720	1713	1716

^a Reported energies for the subspectrum corresponding to the faster decaying origins.

TABLE IV: Observed Zero Field Transition Frequencies in MHz ($\pm 5\%$) for Hydroxybenzaldehydes in Several Hosts at 1.4 K^a

Guest	Host	Benzoic acid	Phenol ^b	<i>p</i> -Xy- lene	<i>p</i> -Di- chloro- benzene
<i>o</i> -Hydroxybenzal- dehyde		5100			6680
		2925			4527
<i>m</i> -Hydroxybenz- aldehyde		3220	8320	8100	5571
		3135	6150	6200	4204
			2150	1400	
<i>p</i> -Hydroxybenza- ldehyde		7070	6500	4816	7065
		3665	3000	4207	3720
		3450	3500		3350

^a Blanks indicate transitions which could not be observed by methods used. ^b zfs reported are those for the longer lived of the dual subspectra.

principal axes of this system diagonalizes the zero field tensor according to $H = DS_z^2 + E(S_x^2 - S_y^2)$. The ordering of the zero field levels $\tau_z > \tau_y > \tau_x$ was extrapolated from past work with high-field Zeeman studies on benzaldehydes,⁴ substituted benzaldehydes,^{4,16} and aromatic ketones.¹⁶ The relative energy ordering of the zero field states was determined uniquely by analysis of the MIDP data.

The energy of the 0,0 band along with the kinetic rate parameters for the phosphorescence process for all the systems

TABLE V: Total Phosphorescence Decay Rate Constants in sec^{-1} ($\pm 5\%$) for Hydroxybenzaldehydes in Several Hosts at 1.4 K

Guest	Host	Benzoic acid	Phenol ^a	<i>p</i> -Xylene	<i>p</i> -Dichlorobenzene
<i>o</i> -Hydroxybenzaldehyde	0,0 (cm^{-1})	24 765	24 426	24 576	24 637
	k_z	16	8.4×10^3	2.8×10^3	87
	k_y	3.0	140	83	3.0
	k_x	0.67	350	820	14
<i>m</i> -Hydroxybenzaldehyde	0,0 (cm^{-1})	23 294	24 268 (24 775)	24 667	24 125
	k_z	5.5	78 (4.5×10^3)	35	27
	k_y	0.73	5.0 (200)	1.7	2.0
	k_x	1.4	7.7 (500)	2.8	1.1
<i>p</i> -Hydroxybenzaldehyde	0,0 (cm^{-1})	24 630	25 121 (24 969)	25 176	25 187
	k_z	6.2	47 (270)	50	44
	k_y	0.33	0.77 (6.2)	3.0	1.5
	k_x	1.1	3.4 (33)	2.3	2.1

^a Values in parentheses refer to decay constants and energy of phosphorescence origins of an observed subspectrum. Cf. text.

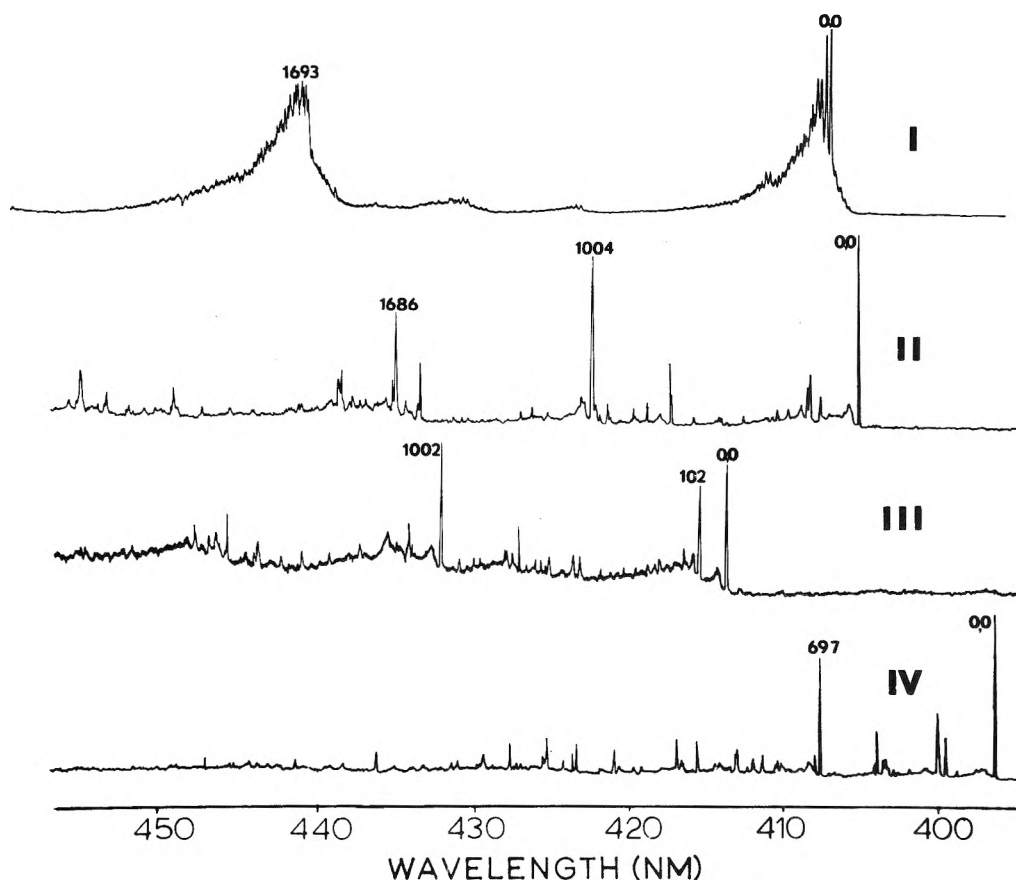


Figure 1. Single crystal phosphorescence spectra at 1.4 K of (I) *o*-hydroxybenzaldehyde in *p*-xylene, (II) *o*-hydroxybenzaldehyde in *p*-dichlorobenzene, (III) *m*-hydroxybenzaldehyde in *p*-dichlorobenzene, and (IV) *p*-hydroxybenzaldehyde in *p*-dichlorobenzene.

studied are given in Table V. The kinetic parameters for the phosphorescence decay process were measured by a combination of methods described by Tinti and El-Sayed at low (~ 1.4 K) and high (≥ 4.2 K) temperatures.¹⁷ The rate parameters were obtained by considering the total decay at very low temperatures, assuming the spin-lattice relaxation processes can be neglected. The decomposition of the phosphorescence intensity decay upon shuttering the excitation light yields three first-order exponential rate parameters since the emission intensity decays according to

$$I(t) = \sum_i k_i r N_i(0) e^{-k_i t}$$

where $k_i r$ is the radiative rate constant, $N_i(0)$ is the steady state population, and k_i is the total rate constant. The subscript index refers to the individual sublevels in the triplet state. The rate constants obtained in this manner were found to be self-consistent with the time-dependent MIDP measurements. The decay of the phosphorescence intensity following excitation with a xenon flash directly yields the rate constant of the fastest emitting sublevel. At high temperatures the phosphorescence decays as an average of all three components of the triplet state. This is due to thermalization of the populations in the sublevels caused by increased spin-lattice relaxation rates. In all cases studied, at 4.2 K the

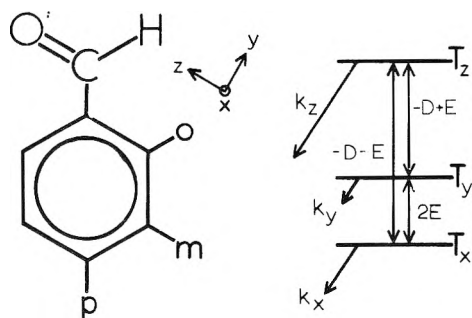


Figure 2. Structure of *o*-, *m*-, and *p*-hydroxybenzaldehyde with the directions of the principal axes of the zero field tensor and the energy level ordering scheme of the phosphorescent triplet spin sublevels with the corresponding decay rate constants measured in this study.

spin–lattice relaxation process was found to be slow as compared to other relaxation processes and the required higher temperatures were obtained by allowing the helium to fall below the sample, where the sample temperature was estimated at ~ 10 K.

The phosphorescence spectra of *m*-HBA in phenol shows two distinct subspectra. The salient feature is the distinct difference in rate constants of these two spectra (cf. Table V). The faster decaying phosphorescence origin at $24\,775\text{ cm}^{-1}$ has an average lifetime of 0.58 ms and a longer-lived origin lying 507 cm^{-1} lower in energy has a lifetime of 33 ms. The ratio of the origin intensities of the former to the latter is 1.46:1 at 1.4 K and 0.95:1 at 4.2 K. The phosphorescence emission spectrum taken at 77 K, although broad, definitely shows a marked predominance of the subspectrum associated with the slower decaying origin. MIDP techniques while monitoring the 0,0 origin at $24\,775\text{ cm}^{-1}$ failed to yield echoes in the phosphorescence decay signals. Dual origins are also observed for *p*-HBA in phenol in which the faster decaying of the two origins lies 154-cm^{-1} red shifted with an average lifetime of 10 ms whereas the original band at $25\,121\text{ cm}^{-1}$ has a lifetime of 60 ms (cf. Table V). At 1.4 K, the ratio of the intensities of the higher to the lower energy origin bands are 0.96:1. At 77 K, the thermal broadening of the phosphorescence bands makes assignment of the emission to the two subspectra difficult.

The dual origins in the above systems may be caused by several factors. They may arise from guest molecules occupying energetically inequivalent host sites, from different guest–host pair combinations, or from multimimum potential surfaces in energetically closely spaced states as postulated by Hochstrasser and others.^{18,19} Although past studies on benzaldehydes have shown that the mixing of the lowest $^3\pi,\pi^*$ with a nearby $^3n,\pi^*$ state becomes significant when the energy separating the two states is roughly less than 500 cm^{-1} ,⁴ as seen in Tables IV and V, the zfs and kinetic data reflect a $^3\pi,\pi^*$ state for *p*-HBA in phenol and do not reflect such mixing even though there is relatively small energy separating the two origins (ca. 150 cm^{-1}). In addition, the intensity ratio of the bands in the two subspectra is dependent upon the rate at which the phenol host crystal is grown (ca. $\pm 10\%$). Also, in the case of *p*-HBA in phenol, the faster decaying origin exhibits significantly larger zfs.²⁰ These results appear to support the cause of the dual origin as arising from different guest–host pair combinations. However, the arguments presented above do not exclude other interpretations and further experiments are currently being conducted to distinguish between these and other possibilities.

In comparing the kinetic data of Table V of *o*-, *m*-, and

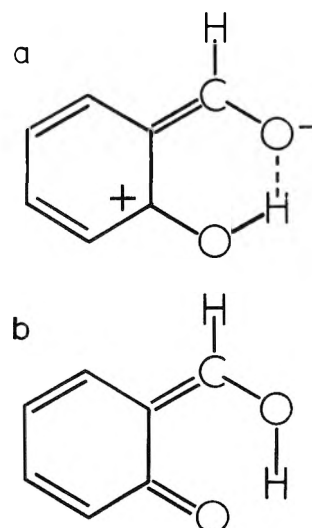


Figure 3. Possible valence bond structures for internally hydrogen bonded *o*-hydroxybenzaldehyde. Structure a adapted from ref 21, b from ref 22.

p-HBA in *p*-xylene and DCB hosts, a cursory interpretation is that the external heavy atom effect does not noticeably shorten the phosphorescence lifetime of the $^3\pi,\pi^*$ emitting triplet sublevels. The reason may be that the gain in radiative strength via external spin–orbit coupling is offset by the relatively larger interaction of the $^3n,\pi^*$ state with the chlorinated host molecules, thereby lowering the degree of admixture with the phosphorescent $^3\pi,\pi^*$ state. The net result is the overall decrease in the decay rate constants.

The hydroxybenzaldehydes in benzoic acid reflect the expected results of strong hydrogen bonding. The zfs and the total phosphorescence rate constants shown in Tables IV and V are characteristic of pure $^3\pi,\pi^*$ state. In general, these $^3\pi,\pi^*$ states show a red shift of the triplet 0,0 band and a considerable increase in the phosphorescence lifetimes.

Examination of Table V shows an effect unique to the systems containing *o*-HBA in phenol and in *p*-xylene hosts. The trend observed in the energies of the $T_1 \rightarrow S_0$ transition in strongly hydrogen bonded molecules would normally be expected to blue and red shift for $^3n,\pi^*$ and $^3\pi,\pi^*$ states, respectively. Although the ca. 640-cm^{-1} red shift of the phosphorescence 0,0 band of *o*-HBA relative to *p*-HBA in either phenol and *p*-xylene hosts is consistent with a $^3\pi,\pi^*$ triplet state, the large magnitude of the phosphorescence decay rate constants can only be explained in terms of the emission originating from an $^3n,\pi^*$ state. In addition the overall features of the vibronic fine structure in the phosphorescence spectra complements this interpretation (cf. Figure 1). One possible explanation for the anomaly is the existence of valence bond structures as shown in Figure 3 postulated for *o*-HBA.^{21,22} In fact Lamola and Sharp have suggested a radiationless deactivation route involving such a tautomer in *o*-hydroxy aromatic carbonyl molecules.²² The shifts observed in the carbonyl stretching frequency as previously discussed for *o*-HBA relative to *m*- and *p*-HBA would support such structures as contributing to the total electronic structure.

Significantly, *o*-HBA in DCB host does not show features characteristic of n,π^* phosphorescent states, although the phosphorescence properties of the *same* guest molecule in phenol and *p*-xylene crystals exhibited are those for pure $^3n,\pi^*$ state as discussed above. The phosphorescence rate constants, the vibronic activity in the phosphorescence spectrum, and

TABLE VI: Observed Zero Field Splitting Energies^a in cm⁻¹ and Phosphorescence Rate Constants in sec⁻¹ for Substituted Benzaldehydes in Several Hosts at 1.4 K

Guest	Host	<i>p</i> -Xylene	<i>p</i> -Dichlorobenzene
<i>p</i> -Hydroxybenzaldehyde	0,0 (cm ⁻¹)	25 176	25 183
	<i>k_z</i>	50	44
	<i>k_y</i>	3.0	1.5
	<i>k_x</i>	2.3	2.1
	<i>-D</i>	0.150	0.180
<i>p</i> -Methoxybenzaldehyde ^b	0,0 (cm ⁻¹)	25 000	24 750
	<i>k_z</i>	46	34
	<i>k_y</i>	0.96	1.2
	<i>k_x</i>	2.4	1.4
	<i>-D</i>	0.201	0.158
<i>p</i> -Methylbenzaldehyde ^b	0,0 (cm ⁻¹)	25 260	25 060
	<i>k_z</i>	120	70
	<i>k_y</i>	2.7	0.96
	<i>k_x</i>	11	3.0
	<i>-D</i>	0.412	0.208
<i>p</i> -Chlorobenzaldehyde ^b	0,0 (cm ⁻¹)	24 880	24 930
	<i>k_z</i>	140	93
	<i>k_y</i>	6.4	4.9
	<i>k_x</i>	10.0	7.9
	<i>-D</i>	-0.4033	-0.260
	<i>E</i>	0.0567	0.0587

^a Energy ordering of the zero field states is assumed to be $\tau_z > \tau_y > \tau_x$. For entries in which all three transitions were not observed (cf. Table IV) the assignments were extrapolated (cf. text).
^b Values from ref 2.

the zfs of *o*-HBA in DCB all tend to correlate with a lowest $^3\pi, \pi^*$ phosphorescent state. Two possible explanations follow. The first is that intermolecular forces experienced by the guest molecules in DCB host could compete with the perturbation of the intramolecular type. Specifically, the hydrogen bonding of the carbonyl group with the hydroxyl proton is no longer as facile because of the competitive hydrogen bonding between the chlorine and hydroxyl moieties. Another possible explanation of the $^3n, \pi^*$ admixture of the lowest $^3\pi, \pi^*$ state is that

the chlorine heavy atom host enhances the radiative depopulation via vibronic coupling to the spin and spin-orbit interaction, such as those reported by El-Sayed in halonaphthalenes.²³ As previously discussed, the increased vibronic activity of *o*-HBA induced by the DCB host as compared to the other two hosts gives support to such an interpretation.

The mechanism for relaxation from the triplet state of the hydroxybenzaldehydes is by direct spin-orbit coupling which mixes states of different orbital types, viz.



Thus, if the lowest triplet state is $^3n, \pi^*$, then direct spin-orbit interaction would couple the triplet state with a $^1\pi, \pi^*$ state and vice versa. Since we observe that τ_x is more radiative than τ_y in most systems which we studied, as seen in Table IV, τ_x must gain its radiative property via asymmetric vibrations which couple $^3\pi, \pi^*$ with states of n, π^* and/or σ, π^* types. Implicit in this discussion is the assumption that the C_{2v} point group is a good description of the symmetry in the excited state. The fact that our data, in most cases, indicate $k_z \gg k_x > k_y$ (cf. Table V) seems to make valid the assumption that the symmetry of the excited triplet state of these carbonyl molecules can best be described by a more symmetric C_{2v} group. Additionally, in the study of substituted benzenes, nitrogen containing naphthalene heterocycles,²⁴ and aromatic carbonyls,^{2,5} the symmetry criteria of the entire molecule were not found to be an accurate description of the experimentally determined spectroscopic properties such as those reported here.

The effect of substituents on the lowest triplet state of benzaldehyde is summarized in Table VI. The observed trend is that the interaction of the lowest $^3\pi, \pi^*$ state with a higher $^3n, \pi^*$ state is less when the substituent is considered electron donating. In addition a comparison of the phosphorescence decay rate constants and zero field splitting parameters of a given para-substituted guest molecule in the two hosts, *p*-xylene and DCB, indicates possible hydrogen bond formation with the DCB host, since hydrogen bonding tends to raise the $^3n, \pi^*$ energy thereby lowering the coupling between the $^3n, \pi^*$ and $^3\pi, \pi^*$ state. The effects of the substituents' position on the triplet state is shown in Table VII. The magnitudes of the rate constants and the zfs reflect π, π^* states with some degree of n, π^* character, with the exception of *m*-chlorobenzaldehyde in DCB which is distinctly $^3n, \pi^*$.

In view of the strong dependent nature of the lowest triplet π, π^* state on the proximity of the nearby n, π^* triplet state,

TABLE VII: Observed Zero Field Transitions in MHz and Phosphorescence Rate Constants in sec⁻¹ for Various Isomers of Substituted Benzaldehyde in *p*-Dichlorobenzene^a

	0,0 (cm ⁻¹)	<i>k_z</i>	<i>k_y</i>	<i>k_x</i>	Microwave transitions
<i>o</i> -Chlorobenzaldehyde	24 925	94	5.8	58	9 565
					6 025
					3 575
<i>m</i> -Chlorobenzaldehyde	24 795	250	92	180	12 375
					8 600
					3 750
<i>o</i> -Tolualdehyde	24 740	160	2.3	22	9 940
					5 090
					4 910
<i>m</i> -Tolualdehyde	24 646	60	1.5	3.1	6 580
					3 928
					2 663

^a Energy ordering of the zero field states is assumed to be $\tau_z > \tau_y > \tau_x$.

any generalization on the effects of hydrogen bonding in aromatic carbonyl molecules must consider external as well as substituent effects. The exact mechanisms for the electronic relaxation process via the phosphorescent triplet state can be explained only in terms of specific cases. Qualitatively, however, strongly interacting hosts such as those capable of hydrogen bonding will decrease the mixing of the $^3n, \pi^*$ with the lowest $^3\pi, \pi^*$ state in the hydroxybenzaldehydes.

Acknowledgment. Acknowledgment is made to the donors of the Petroleum Research Fund, administered by the American Chemical Society, for partial support of this work. We also thank the Wichita State University Research Committee and the National Institutes of Health for supporting this research. The liquid helium used in this work was kindly donated by the Kansas Refined Helium Company.

References and Notes

- (1) For example, G. C. Pimentel and A. L. McClellan, "The Hydrogen Bond", W. H. Freeman, San Francisco, Calif., 1960; and L. Pauling, "The Nature of the Chemical Bond", Cornell University Press, Ithaca, N.Y., 1960.
- (2) A. M. Nishimura and D. S. Tinti, *Chem. Phys. Lett.*, **13**, 278 (1972).
- (3) T. H. Cheng and N. Hirota, *Chem. Phys. Lett.*, **13**, 194 (1972); **14**, 415 (1972).
- (4) T. H. Cheng and N. Hirota, *Mol. Phys.* **27**, 281 (1974); H. Hayashi and S. Nagakura, *ibid.*, **27**, 969 (1974).
- (5) See, for example, M. A. El-Sayed, *J. Chem. Phys.*, **54**, 680 (1971); *Acc. Chem. Res.*, **4**, 23 (1971); "Excited States", Vol. I, E. C. Lim, Ed., Academic Press, New York, N.Y., 1974, and references therein.
- (6) J. Schmidt, W. S. Veeman, and J. H. van der Waals, *Chem. Phys. Lett.*, **4**, 341 (1969).
- (7) D. A. Antheunis, J. Schmidt, and J. H. van der Waals, *Chem. Phys. Lett.*, **6**, 255 (1970).
- (8) C. B. Harris and R. J. Hoover, *J. Chem. Phys.*, **56**, 2199 (1972).
- (9) V. B. Singh and I. S. Singh, *Ind. J. Pure Appl. Phys.*, **6**, 682 (1968).
- (10) O. N. Singh, M. P. Skivastava, and I. S. Singh, *Curr. Sci.*, **36**, 630 (1967).
- (11) G. E. Campagnaro and J. L. Wood, *J. Mol. Struct.*, **6**, 117 (1970).
- (12) K. A. Martin, Masters Thesis, University of California, Davis, Calif., 1973.
- (13) J. H. S. Green, D. J. Harrison, and W. Kynaston, *Spectrochim. Acta, Part A*, **27**, 2199 (1971).
- (14) D. L. Cummings and J. L. Wood, *J. Mol. Struct.*, **20**, 1 (1974).
- (15) S. P. McGlynn, T. Azumi, and M. Kinoshita, "Molecular Spectroscopy of the Triplet State", Prentice-Hall, Englewood Cliffs, N.J., 1969.
- (16) A. M. Nishimura and J. S. Vincent, *Chem. Phys. Lett.*, **13**, 89 (1972).
- (17) D. S. Tinti and M. A. El-Sayed, *J. Chem. Phys.*, **54**, 2529 (1971).
- (18) R. M. Hochstrasser and C. A. Marzocco, "Molecular Luminescence", E. C. Lim, Ed., W. A. Benjamin, New York, N.Y., 1969.
- (19) A. J. Duben, L. Goodman, and M. Koyanagi, "Excited States", Vol. I, E. C. Lim, Ed., Academic Press, New York, N.Y., 1974.
- (20) Zero field transitions at 12 400 and 5250 MHz were observed for *p*-HBA in phenol while monitoring the 24 969-cm⁻¹ origin.
- (21) G. Porter and P. Suppan, *Trans. Faraday Soc.*, **61**, 1164 (1965).
- (22) A. A. Lamola and L. J. Sharp, *J. Phys. Chem.*, **70**, 2634 (1966).
- (23) M. A. El-Sayed, *Acc. Chem. Res.*, **1**, 7 (1968), and references therein.
- (24) A. M. Nishimura, D. S. Tinti, and J. S. Vincent, *Chem. Phys. Lett.*, **12**, 360 (1971).
- (25) E. B. Wilson, Jr., *Phys. Rev.*, **45**, 706 (1934).

Effects of Intermolecular Interaction on Protein Diffusion in Solution

Wilfrid B. Veldkamp*

Center for Materials Science and Engineering, The Department of Electrical Engineering, Massachusetts Institute of Technology, Cambridge, Massachusetts 02139

and Joseph R. Votano

The Department of Biology, Massachusetts Institute of Technology, Cambridge, Massachusetts 02139 (Received April 5, 1976)

Publication costs assisted by MIT Health Science

The effects of macromolecular interactions on the mutual diffusion coefficient of normal oxygenated hemoglobin in salt solutions were studied. The dependence of the mutual diffusion coefficient on the protein concentration up to 20 g % or 3.1 $\mu\text{mol}/\text{cm}^3$ was obtained by photon correlation spectroscopy. In addition, independent measurements were made of the isothermal osmotic compressibility and shear viscosity at the same temperature and over the same concentration range. These measurements were used to test the validity of the so-called generalized Stokes-Einstein relationship proposed in the literature. The diffusion data for protein concentrations of up to 7 g % follow this relationship if the expression for the friction coefficient uses the solvent viscosity. At higher concentrations, the data deviated substantially from the relationship. However, at concentrations higher than 14 g %, the data agreed again when the friction coefficient contained the solution viscosity as measured by viscometry. In this study, at a pH of 7.2, a temperature of 21 °C, and an ionic strength of 0.125, hemoglobin molecules behaved as noninteracting particles in solution for concentrations below 7 g %, but with further increases in concentration weak intermolecular interaction are evident. The dominant interactions are the excluded volume effect and a much smaller electrostatic contribution.

I. Introduction

In a monodisperse macromolecular solution where laser light is scattered predominantly by the macromolecules, the relevant quantity measured by photon correlation spectroscopy¹ is the pair-pair correlation function

$$G^2(K, t) = \left\langle \sum_{m, n} \sum_{p, q} e^{-i\mathbf{K} \cdot (\mathbf{R}_m(t) - \mathbf{R}_n(t))} e^{i\mathbf{K} \cdot (\mathbf{R}_p(0) - \mathbf{R}_q(0))} \right\rangle \quad (1)$$

where N is the total number of macromolecules in the scat-

tering volume, and \mathbf{K} is the scattering vector. $\mathbf{R}_p(0)$ and $\mathbf{R}_m(t)$ denote the position coordinates of macromolecules p and m at time zero and t , respectively, and the large brackets denote an average over the N -particle distribution function $P^N(\mathbf{R}, t)$ of the macromolecules in solution. In a very dilute solution, where macromolecules can be regarded as noninteracting, $P^N(\mathbf{R}, t)$ should factorize into a product of N one-particle distribution functions $P^1(\mathbf{R}_j, t)$, each satisfying a simple diffusion equation. Under this condition, eq 1 can be evaluated easily to become

$$G(K, t) = 1 + |F(K, t)|^2 \quad (2)$$

where the dynamic structure factor $F(K, t)$ equals

$$F(K, t) = \left\langle \sum_i^N \sum_m^N e^{-i\mathbf{K}\cdot\mathbf{R}_i(t)} e^{i\mathbf{K}\cdot\mathbf{R}_m(0)} \right\rangle \quad (3)$$

and reduces to

$$\begin{aligned} F(K, t) &\rightarrow F_s(\mathbf{K}, t) = \langle e^{-i\mathbf{K}\cdot\mathbf{R}(t)} e^{i\mathbf{K}\cdot\mathbf{R}(0)} \rangle \\ &= e^{-DK^2t} \end{aligned} \quad (4)$$

As shown recently by Altenberger and Deutch,² even if one considers the long-range hydrodynamic interaction among macromolecules given by the Oseen tensor in the equation governing the N -particle distribution function $P^N(\mathbf{R}, t)$, the solution of this equation, when used with eq 3, gives a result equivalent to eq 4. In addition to these long-range hydrodynamic interactions in a concentrated solution, equally important short-range interactions arise from the excluded volume effect of the finite size macromolecules. Therefore, the validity of the simple result expressed in eq 4 is rather questionable. Nevertheless, our consistent experimental observation is that the K and t dependence follows the simple functional dependence expressed in eq 4 to the highest concentration measured. Thus, it is possible to define *experimentally* a "mutual diffusion coefficient" D_m corresponding to a single Fourier component of the concentration fluctuation defined by the scattering vector, \mathbf{K} , in a concentrated protein solution by fitting the measured correlation function to eq 2. Our purpose in this paper is to investigate the dependence of D_m on temperature, concentration, viscosity, and other thermodynamic parameters that characterize the solution.

For spherical noninteracting particles in the limit of very low concentrations, D_m reduces to D_0 , which is given by the Stokes-Einstein relationship

$$D_0 = k_B T / f_0 \quad (5)$$

where f_0 is the friction coefficient of the Brownian particle. For a macroscopic spherical particle, the friction coefficient is given by the Stokes formula

$$f_0 = 6\pi\eta_0 a \quad (6)$$

where η_0 is the solvent viscosity at temperature T and a is the radius of a Brownian particle.

At finite concentrations, the interparticle interaction in terms of a potential of average force, $U(r_{ij})$, must be taken into account. Phillies³ recently considered this case and derived the following generalization of eq 5:

$$D_{mA} = \left(\frac{\delta\Pi}{\delta C_A} \right)_{p,T} \frac{(1-\phi)}{f_A} \quad (7)$$

In this equation, Π is the osmotic pressure of an imperfect gas of Brownian particles

$$\Pi = k_B T C_A - \frac{2\pi C_A^2}{3} \int_0^\infty dr r^3 \left(\frac{\delta\Pi}{\delta r} \right) g_{AA}(r) \quad (8)$$

in terms of the pair correlation function $g_{AA}(r)$ of the Brownian particles. C_A and f_A are the concentration and friction coefficient, respectively, of species A or the Brownian particle in a concentrated solution. f_A may or may not be given by expression 6. It is an ill-defined quantity in this theory. The correction factor $(1-\phi)$ arises from the fact that eq 5 is derived in the solvent-fixed frame, whereas light scattering measurements are performed in the volume-fixed frame. $\phi = C_A v_A$ where v_A is the partial specific volume of the Brownian particle. The correction disappears at infinite dilution. In relating the light scattering measurement to the theory, we assume $D_{mA} = D_m$.

In this study, quasi-elastic light scattering measurements determined the D_m values of the protein over a broad concentration range at constant ionic strength and pH. Isothermal viscosity and osmotic pressure measurements were also made on identically prepared protein solutions. Osmotic compressibility values were obtained from the pressure data by numerical differentiation. These values and the concentration dependence of the viscosity data were used to compare the calculated and observed concentration dependent diffusion coefficient, D_m . Various forms of the frictional coefficient, f_A , have been used to make this comparison.

The protein used in this study is normal oxygenated hemoglobin A, HbA-O₂, with a molecular weight of 64 500 and molecular dimensions of $50 \times 55 \times 65$ Å. Due to the physiological importance of this macromolecule, its preparation and its physical and chemical properties have been studied extensively.⁴

II. Materials and Methods

A. HbA Preparation. All procedures for preparing hemoglobin, HbA, were done at 4 °C. To remove the plasma and buffy coat, freshly drawn blood samples in heparin were washed and centrifuged with 0.9% NaCl four times at 1200g. The erythrocyte cells were freeze-lyzed by a method similar to Wilson's.⁵ The hemoglobin lysate, diluted 4-to-1 with distilled water, was centrifuged for 1 h at 20 000g. The hemoglobin supernatant was concentrated to 25 g/dl by ultrafiltration using an Amicon with an XM-50 membrane. The HbA solution was then dialyzed extensively in a closed flask for 24 h against a 50 mM bis-tris buffer, pH 7.2, and 100 mM NaCl. A buffer-to-hemoglobin volume of 100 to 1 was used in dialysis with one buffer change after 12 h. Following dialysis, a series of solutions of varying hemoglobin concentrations were made up and stored in droplet form at 77 K. Before performing the light scattering measurements, the HbA solution was centrifuged at 20 000g for 1 h. The HbA concentration was measured in the light scattering cell at the completion of each experiment and was based on a molar extinction coefficient of $\epsilon 11\,500 \text{ M}^{-1} \text{ cm}^{-1}$ per heme at 5400 Å. Also, the amount of methemoglobin was ascertained at this time by the Hegesh method.⁶ In all light scattering experiments, the final amount of methemoglobin never exceeded 4%.

B. Viscosity Measurements. Hemoglobin viscosity was measured over a broad concentration range at various temperatures, using a Cannon-Manning semimicro viscometer, Model 75-A440. Before performing viscosity measurements, the viscometer was calibrated by using a certified viscosity standard, N1.0, from the Cannon Instrument Co., State College, Pa. The kinematic viscosities at given concentration and temperature were converted to centipoise by multiplying the kinematic viscosity by the measured density of the hemoglobin solution.

C. Osmotic Pressure Measurements. Osmotic pressure in

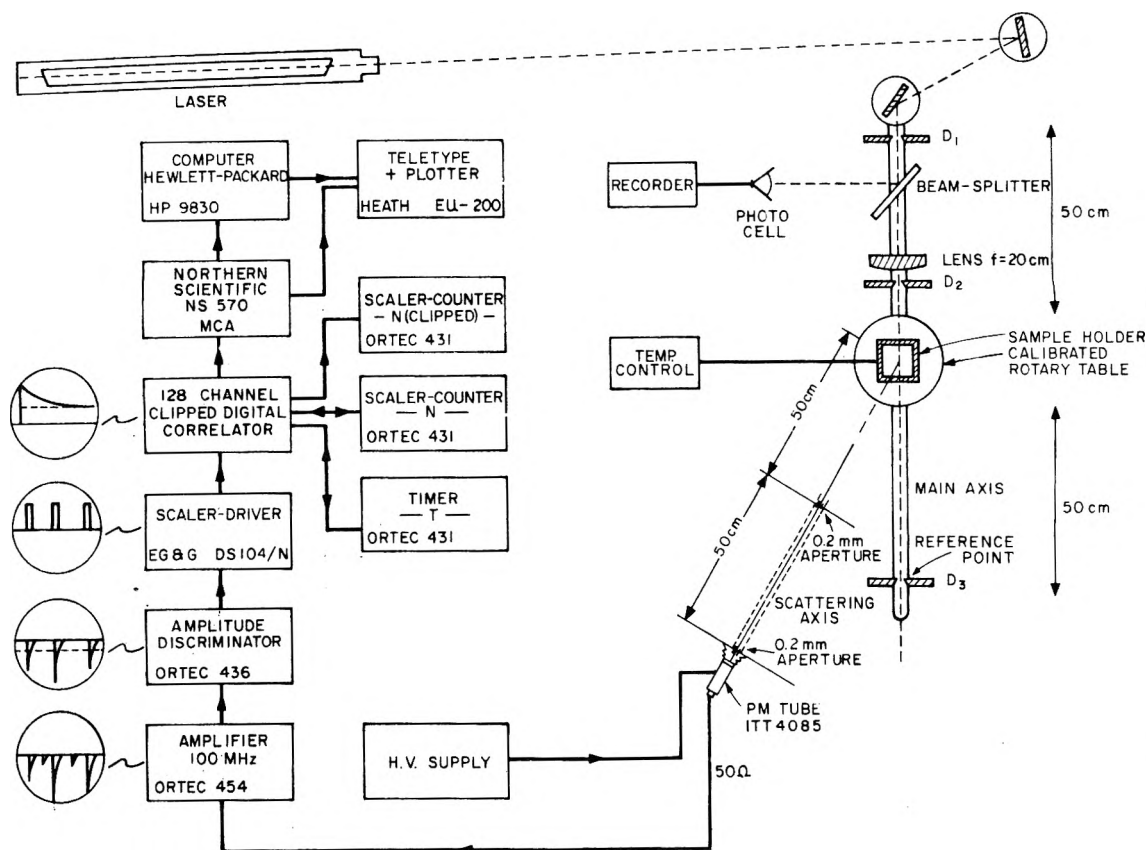


Figure 1. Schematic layout of the photon correlation spectrometer.

HbA solutions in the concentration range of 0.5 to 20 g % was measured on a modified Hewlett and Packard Mechrolab high-speed osmometer, Model 501. This type of osmometer functions similarly to a Hepp osmometer when a reduced pressure is applied to the solvent side of the semipermeable membrane to prevent any net flow of solvent through the membrane into the compartment containing the macromolecular component plus solvent. By reducing the atmospheric pressure on the elevator reservoir, the colloidal osmotic pressure values of concentrated HbA solutions could be measured rapidly. The semipermeable membrane was EP5 (Schleicher & Schuell), which has an exclusion limit at a molecular weight of 5000. Before the membrane was installed in the osmometer, it was soaked for 48 h at 4 °C in deionized distilled water and then soaked again for another 24 h in the appropriate buffered salt solution. Measurements of the osmotic pressure, Π , for a given hemoglobin solution were repeated until the observed values of Π were within ± 0.02 cmHg. Usually, after the first three determinations, the dynamic equilibrium values for Π on successive samples at the same concentration were reproducible. To ensure that the membrane permeability was not altered and that the composition of the buffered solvent remained constant in the lower osmotic pressure chamber, the solvent reference value needed to obtain Π was ascertained before a number of determinations of Π were made for a given hemoglobin concentration.

D. *Quasi-Elastic Light Scattering Measurements.* The apparatus for these experiments is shown in Figure 1. A 50-mW He-Ne laser provided the light (6328 Å), which is to some extent absorbed by the oxyhemoglobin. Light sources of shorter wavelengths, such as from an argon laser, should not be used because the fluorescent activity of the hemoglobin molecule is too strong. The absence of heating effects in the

hemoglobin was determined by looking for local solute and solvent turbulence or flows by beating the scattered light with specular reflections of the cell window. This sensitive technique can detect flow velocities from micrometers per second to meters per second. No such average flow pattern was observed in the focused beam at any scattering angle. The scattered light was collimated by two pinholes to within one coherent solid angle. The detected photon pulses were amplified and standardized into pulses of 30-ns width and 5-V amplitude.

A 128-channel clipped digital correlator was used. This correlator is basically equivalent to the full correlator in the sense that both give the correlation function $G(K,t)$ of the particle number fluctuations in the scattering medium. Methods of photon correlation spectroscopy have been discussed in more detail in a recent article.¹ The measured temporal correlation function $G(K,t)$ of a homodyne experiment can be expressed in the form

$$G(K,t) = \langle n \rangle^2 \{ 1 + F(A)F(B) |F(K,t)|^2 \} \quad (9)$$

where $\langle n \rangle$ is the average number of photon counts detected, and $F(A)$ is a factor between 0 and 1, depending on the scattering geometry. $F(A)$ is approximately one for detection areas up to one coherence area and is approximately $(1/M)$ when the detector area is M times larger than the coherence area.

$F(B)$ equals $(1+k)/(1+\langle n \rangle)$ where k is the clipping level of the autocorrelator. The correlation time is related to $(2DK^2)^{-1}$. The data in the form of photon counts in a particular channel of the multichannel analyzer are analyzed using the cumulant expansion technique.⁷ All light scattering measurements were made at a scattering angle of 90°. Index of refraction measurements of concentrated HbA solutions

yielded a linear concentration dependence of the form $n = 1.3357 + 0.0128\chi$ at 21 °C and $n = 1.3332 + 0.0135\chi$ at 35 °C with χ in 10^7 mol/cm³. This refractive index was used in the evaluation of magnitude of the scattering vector, $\mathbf{K} = (4\pi n/\lambda) \sin \theta/2$.

The scattering cell was a 0.3 cm³ black anodized aluminum holder with glass windows on three sides. The cell was mounted on a thermoelectric temperature control unit. Inlet and outlet ports of the cell were designed such that the flow pattern would sweep the entire cell volume, particularly the cell windows.

Cell and sample cleaning is extremely important in obtaining meaningful and consistent results. Before each measurement, the cell was flushed with 500 cell volumes of triple-distilled deionized water through two Millipore filters, one 250 Å of Type VSWP, followed by either a 0.22- or 0.45- μ m filter of Type GSWP. Then, the system was flushed with the buffer solvent. To prevent exposing the cleaned cell to the unfiltered environment, the hemoglobin was injected via a junction between the two filters.

III. Experimental Results

The mutual diffusion coefficients of oxygenated hemoglobin were measured over a concentration range between 0.15 and 3.10 μ mol/cm³ (or 1 to 20 g %) at two temperatures, 21 and 34.5 °C. Each data point, D_m , in Figure 2 represents an average of 12 measurements of D_m on two different samples. Error-bar length represents the variance in the distribution of the D_m values at a given concentration. As HbA concentration increases, a larger Millipore filter pore size (0.45 μ m) is required, so that the amount of foreign particles such as dust and minute amounts of fragmented vesicles from the lysis process increases slightly. These particles accounted mainly for the moderate increase in the variance of the D_m values at higher hemoglobin concentrations. In Figure 2, the observed D_m values are independent of concentration within experimental error, up to approximately 1.6 μ mol/cm³. Following this linear behavior, a steep decline in the observed D_m values occurred at a volume packing fraction of approximately 15%.

The possibility of appreciable dimer formation to account for the decrease in the D_m values with higher HbA concentrations has been ruled out for the following reasons. The diffusion coefficient of a dimer considered as an equivalent prolate ellipsoid yields an approximate diffusion coefficient of $0.74D_0$. Calculation of the Z averaged diffusion coefficient revealed that at concentrations of 2.8 and 3.1 μ mol/cm³, the number of dimers would have to be 28 and 62% of the total molecules, respectively, to account for the observed D_m values. Such extensive dimerization did not appear in the cumulant analysis of the correlation function. The data points in Figure 2 were obtained from the first cumulant k_1 via $D = -k_1/2K^2$. These data were also checked for higher cumulants. In a typical run the magnitude of the variance as defined by the second cumulant k_2 , $(k_2/k_1^2)^{1/2} \times 100\%$ was between 10 and 22%. Further evidence of the lack of dimer or higher aggregates comes from ultracentrifugation studies.⁸ The possibility of laser-induced aggregation during the experiment was ruled out by the absence of any increase in intensity of the monitored scattered light. However, it must be remembered that, as concentration increases, the assumption of independent particles, or, alternatively, of a Gaussian random process becomes invalid. Then, the non-Gaussian correction term in eq 2 is of the order ζ^3/V , where ζ is the correlation range of the interacting macromolecules, and V is the linear dimension of the scattering volume subtended by the detector.⁹ As seen in

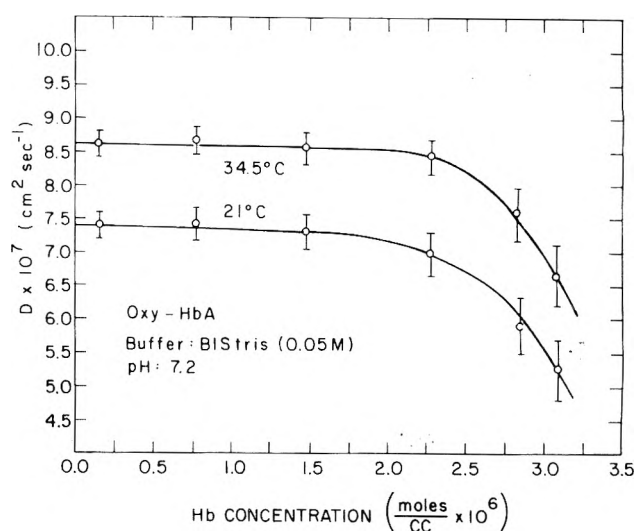


Figure 2. Mutual diffusion coefficient of normal oxygenated HbA as a function of HbA concentration. Each data point represents an average of 12 measurements of D_m on two different samples.

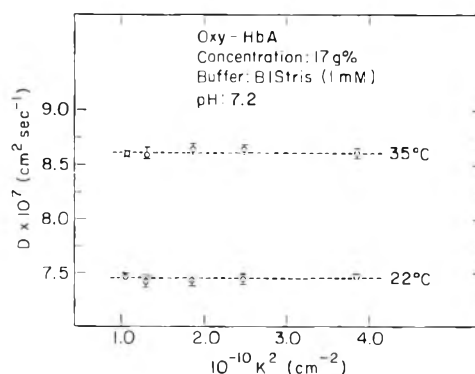


Figure 3. Dependence of the oxygenated HbA mutual diffusion coefficient on K^2 .

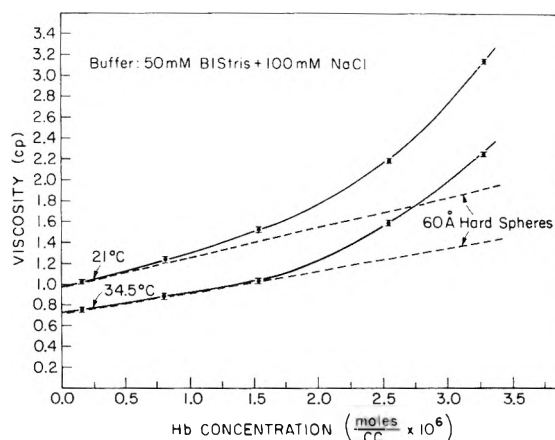


Figure 4. Viscosity of oxygenated HbA as a function of concentration at 21 and 34.5 °C, as well as hard-sphere predictions by Peterson and Fixman.¹⁰

Figure 3, the lack of any K^2 dependence of D_m means that for a macromolecule of radius r , $(Kr)^2 \ll 1$; thus, the contribution of ζ^3/V can be considered negligible.

The measured values of viscosity at 21 °C are shown in Figure 4. Measurements at 34.5 °C were made also to determine if any pronounced differences in viscosity dependence

TABLE I: Taylor Series Expansion Coefficients in HbA Concentration for Viscosity, Normalized Diffusion Data, and Osmotic Pressure, Fitted to their Respective Total Number of Measurements

TAYLOR SERIES EXPANSION COEFFICIENTS					
$Y = C_0 + C_1 X + C_2 X^2 + C_3 X^3 + C_4 X^4 + \dots \left(X = \frac{\text{moles}}{\text{cc}} \times 10^7 \right)$					
COEFFICIENT	VISCOCITY (cp) $Y = \eta$		RELATIVE DIFFUSION $Y = D/D_0$		OSMOTIC PRESSURE (ATM $\times 10^2$) $Y = \Pi$
	21° C	34.5° C	21° C	34.5° C	21° C
C_0	9.5011×10^{-1}	7.3190×10^{-1}	1.0000	1.0000	-5.8184×10^{-2}
C_1	3.8888×10^{-2}	1.3608×10^{-2}	-2.0458×10^{-2}	-3.9587×10^{-3}	2.3838×10^{-1}
C_2	-9.4257×10^{-4}	1.5516×10^{-6}	4.8225×10^{-4}	1.2970×10^{-3}	3.0169×10^{-3}
C_3	5.5308×10^{-5}	3.1724×10^{-4}	-8.1768×10^{-5}	-2.0722×10^{-4}	-2.0747×10^{-3}
C_4	0	0	5.6156×10^{-6}	1.4048×10^{-5}	2.1038×10^{-4}
C_5	0	0	-1.6703×10^{-7}	-4.1859×10^{-7}	-5.0056×10^{-6}
C_6	0	0	1.5181×10^{-9}	4.3092×10^{-9}	0

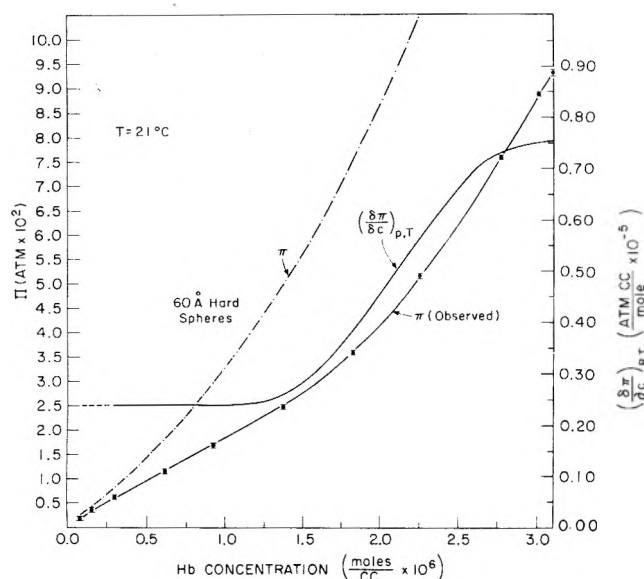


Figure 5. Osmotic pressure measurements of oxygenated HbA as a function of concentration, osmotic compressibility vs. concentration as obtained by numerical differentiation, and hard-sphere predictions by Rice and Gray.¹¹

occurs at higher temperatures. These experiments provided some measure of the concentration dependence of the frictional coefficient and allowed f_A in eq 7 to be expressed in terms of an experimentally determined parameter, the viscosity. At both temperatures, the viscosity was linear at low concentrations and followed the calculated hard-sphere predictions to a first-order approximation given by Peterson.¹⁰ The rapid rise in viscosity at higher concentrations cannot be described by this hydrodynamic theory. Table I lists the coefficients of the power series expansion in concentration for the solid curves found to fit the observed data points in Figure 2.

The osmotic pressure and compressibility values of hemoglobin solutions with ionic strength and pH identical with

those used to determine the D_m values of HbA are shown in Figure 5. Also shown is the osmotic pressure for a gas composed of 60-Å diameter hard spheres as calculated by the formulation of Rice and Gray.¹¹ No corrections of the observed Π values were made for the Donnan pressure effect, since the calculated contribution was extremely small because the magnitude of the ionic strength was high and because the hemoglobin was approximately at its isoelectric point.⁴

The shape of the osmotic pressure curve is in reasonable agreement with that measured by Adair¹² for the bovine and sheep hemoglobin at a similar ionic strength and pH. Both of these results show linear behavior in Π at concentrations less than $1.4 \mu\text{mol}/\text{cm}^3$ and nonlinear behavior in the range from 2.6 to $3.1 \mu\text{mol}/\text{cm}^3$. In our measurements, a small discontinuity in Π existed below $0.20 \mu\text{mol}/\text{cm}^3$. Such a discontinuity in the initial slope of Π vs. concentration for protein measurements is not uncommon.¹³ To calculate the osmotic compressibility, a fourth-order power series expansion in concentration was used to fit the pressure data. This fit gave a variance of less than 1% between the observed and calculated Π values. In computing the fit of the pressure curve, the small discontinuity in Π at the two lowest concentrations was removed by determining the slope by least squares in the concentration range from 0.30 to $0.93 \mu\text{mol}/\text{cm}^3$ and by then using the computed Π values to fit the complete pressure curve. This procedure was essential, since the magnitude of $(\delta\Pi/\delta C)_{P,T}$ is sensitive to any fluctuation in the osmotic pressure data. Tabulated in Table I are Taylor series coefficients for the fitted osmotic pressure curve at 21° C.

IV. Discussion of Results

Several aspects of the observed concentration and temperature dependence of D_m deserve note (see Figure 2). The initial linearity of D_m and its decrease after $1.6 \mu\text{mol}/\text{cm}^3$ (or 10 g %) were in fair agreement with self (tracer) diffusion coefficient measurements reported by Riveros-Moreno and Wittenberg¹⁴ and measurement of mutual and tracer diffusion coefficients by Keller, Canales, and Yum.¹⁵ At 3 g % or less, the D_m values determined by use of the diaphragm method¹⁵

were in good agreement with those of Figure 2, except at moderate concentrations (3–7 g %) where a small concentration dependency was observed. The largest difference, 13%, in the value of D_m occurred at $3.1 \mu\text{mol}/\text{cm}^3$. These disagreements may be due to differences in the D_m measuring techniques. The light scattering technique is a direct nonperturbative method, whereas the diaphragm technique to measure D_m makes use of a macroscopic concentration gradient across a cell membrane. The diaphragm technique determines an integral diffusion coefficient from which a calculated D_m value is obtained (eq 3 of ref 15).

At low Hb concentration, the relationship between D_m values at two different temperatures is

$$D_m(T_1) = D_m(T_2) \frac{\eta(T_2) T_1}{\eta(T_1) T_2} \quad (10)$$

where $\eta(T)$ is the viscosity of the solvent at a given temperature. At 34.5°C , the D_m values should be $10.5 \times 10^{-7} \text{ cm}^2/\text{s}$ instead of the observed value of $8.6 \times 10^{-7} \text{ cm}^2/\text{s}$. As shown by the measured macroscopic viscosities at 34.5°C (see Figure 4), viscosity did not change abnormally; as expected, these observed η 's were smaller than those at 21°C . However, from other light scattering measurements on dilute Hb solutions at various temperatures (to be published), there is a definite decrease in the D_m temperature dependence above 27°C . Below 27°C , the temperature behavior at low HbA concentrations is predicted by the Stokes–Einstein relationship, eq 5, for noninteracting particles.

This ideal behavior is also apparent in the linear dependence of Π on the concentration, up to approximately 7 g %, as shown in Figure 5. From the virial expansion of the osmotic pressure Π in concentration

$$\Pi = RT(C + BC^2 + \dots) \quad (11)$$

it can be seen that, within experimental accuracy, the second virial coefficient B is zero in this low concentration range. Here, R and T are the gas constant and absolute temperature, respectively, and C is given in mol/cm^3 . Also, from a plot of Π/C , using the above expression, a value of $4.76 \text{ cm}^3/\text{g}$ is obtained for B in the higher concentration range, after conversion from cm^3/mol . This value agrees reasonably well with the value of $5.10 \text{ cm}^3/\text{gm}$ from Adair's data.¹² Calculations of the electrostatic interactions and interactions due to protein surface charge fluctuations,¹⁶ although approximate, indicate that the contributions of these interactions and of the Donnan effect to the value of B are negligible. Therefore, the main contribution to B is from the excluded volume effect.¹⁷ This contribution is $3.96 \text{ cm}^3/\text{g}$, using a hydration value¹⁸ of 0.24 g of $\text{H}_2\text{O}/\text{g}$ of Hb and a partial specific volume of $0.75 \text{ cm}^3/\text{g}$. Consequently, the contribution of electrostatic interactions to B is approximately $0.8 \text{ cm}^3/\text{g}$; clearly, normal hemoglobin interactions under these conditions are mainly repulsive in nature.

To ascertain the range in which the generalized Stokes–Einstein relation, eq 7, can describe the observed D_m values of hemoglobin, a concentration-dependent form of the frictional coefficient, f , as defined by eq 6 is needed. The evaluation of f over a large concentration range is either too difficult to interpret if obtained directly experimentally, as in ultracentrifugation studies, or theoretical formulation of f is limited to dilute solutions and simple interaction potentials. However, it is worthwhile to examine the trend of f/f_0 with protein concentration, as given by the hydrodynamic treatment of Pyun and Fixman,¹⁹ by diffusion data of Keller et al.,¹⁵ and by calculations using our experimental values of D_m and $(\delta\Pi/\delta C)_{p,T}$.

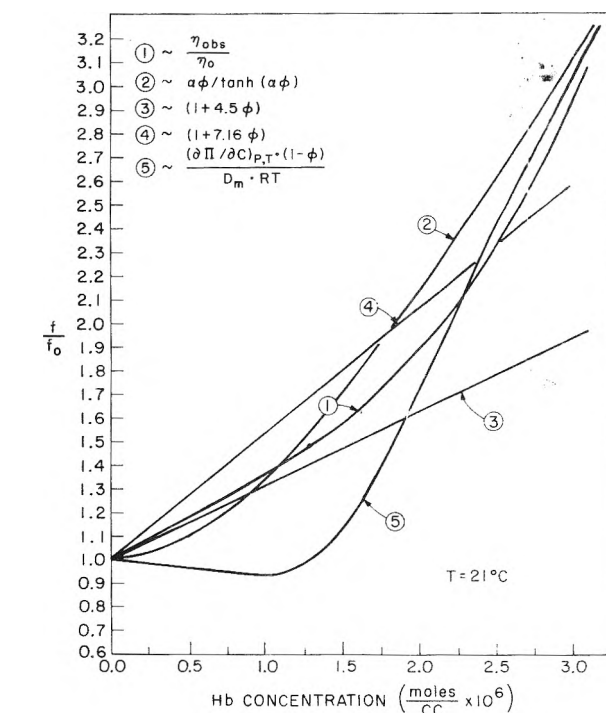


Figure 6. Normal frictional coefficient of oxygenated HbA for five models of f used in conjunction with Stokes law, $f = 6\pi a\eta$: (1) use of the solution viscosity η_{sol} , (2) data of Keller et al.,¹⁵ (3) hydrodynamic hard-sphere calculations by Peterson and Fixman,¹⁰ (4) hydrodynamic soft-sphere calculations by Peterson and Fixman,¹⁰ (5) from osmotic compressibility and quasi-elastic light-scattering data.

$(\delta C)_{p,T}$. By use of eq 5 and 7, the expression for the observed (f/f_0) becomes

$$f/f_0 = \frac{D_0(\delta\Pi/\delta C)_{p,T}(1-\phi)}{D_m RT} \quad (12)$$

where ϕ is the Hb partial specific volume.

The numbered formulations of f/f_0 in Figure 5 show the results of this comparison. Formulations 1 and 5 are self-explanatory. Formulation 2 was found to fit the hemoglobin data of Keller et al. when $\alpha = 21.5$. Lastly, formulations 3 and 4 are the hydrodynamic expressions in which the perturbation of the solvent velocity alone is considered, and velocity perturbations by solute molecules on one another, together with those of the solvent, are taken into account. There is little agreement of hydrodynamic curves 3 and 4 with the observed curve 5; this finding may be taken to mean that long-range hydrodynamic effects are negligible even at dilute protein concentrations. At these low concentrations curve 5 is in bad agreement with curve 1 if the observed solvent viscosity is used; however, in the high concentration range an unexpected agreement between these curves occurs with the use of the solution's viscosity.

Another way to see the pronounced effect of the use of solution and solvent viscosities is by the normalization of D_m given by

$$D_m/D_0 = \frac{(\delta\Pi/\delta C)_{p,T}(1-\phi)}{RT\eta_r} \quad (13)$$

where η_r is the relative viscosity—the ratio of the solution viscosity to the solvent viscosity. The three macroscopic parameters, D_m , $(\delta\Pi/\delta C)_{p,T}$, and η_r , in this expression, measured by independent means, can be used in a comparison between the observed D_m/D_0 ratio and that calculated from eq 5 and 7. Figure 6 presents this comparison with and without the

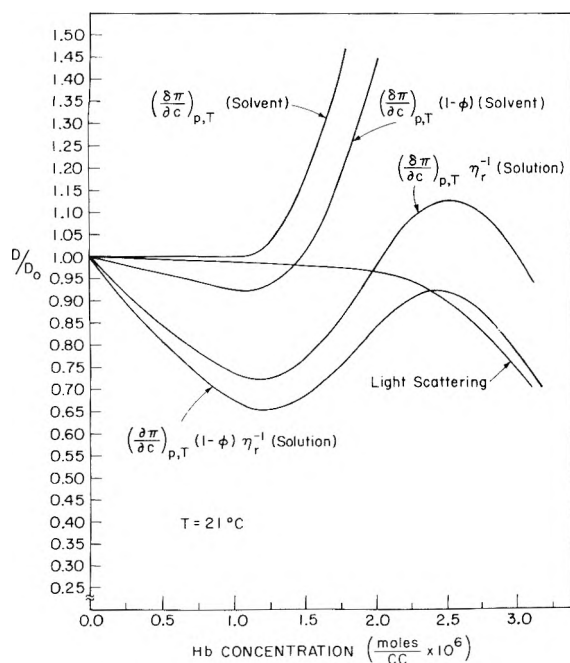


Figure 7. Normalized oxygenated HbA diffusion coefficient as a function of concentration (obtained by photon correlation spectroscopy), and predictions of the generalized Stokes–Einstein eq 7 with solution viscosity and solvent viscosity and with and without the solvent backflow correction factor $(1 - \phi)$. Note, clearly eq 7 predicts the diffusion coefficient at low concentrations when the solvent viscosity is used and when solvent backflow is ignored; at high concentrations, the solution viscosity and solvent backflow corrections provide agreement with the measured data.

correction factor for solvent and solution viscosities. The factor $(1 - \phi)$, reflecting the backflow of the solvent due to the motion of macromolecules in a constant-volume system, is not negligible, even at low Hb concentration, partly because the specific volume used in calculating ϕ included the hydration layer. A value of $0.99 \text{ cm}^3/\text{g}$ for the specific hydrodynamic volume was used for ϕ , and a spherical hydration shell was assumed. Although ϕ has a finite value, it can only be estimated; therefore, the other case, where $\phi = 0$, is also presented.

At low to moderate concentrations (up to $1.2 \mu\text{mol}/\text{cm}^3$), where B equals zero, the observed and calculated D_m/D_0 ratio are in good agreement when solvent viscosity is used. For $B > 0$, eq 7 predicts an increase in the D_m/D_0 ratio, since the motion of solute molecules in concentration gradients should increase under a repulsive ensemble average force, but in fact, the observed ratio is constant, within experimental accuracy, up to $2.2 \mu\text{mol}/\text{cm}^3$. This discrepancy in the observed behavior of D_m/D_0 can be explained qualitatively: a changed microscopic viscosity and a resultant changed frictional coefficient oppose a rapid relaxation of concentration gradients. This assumption is reinforced since the observed η values of hemoglobin at 21°C follow the viscosity values calculated from the well-known Huggins equation¹⁷

$$\eta = \eta_0[1 + [\eta]C + k[\eta]^2C^2] \quad (14)$$

to within 4%, up to $2.8 \mu\text{mol}/\text{cm}^3$, using $[\eta] = 0.036 \text{ dl/g}$ for the intrinsic viscosity of Hb and $k = 2$. For solid uncharged spheres, the value of the Huggins constant, k , should be approximately 2, both from theoretical models²⁰ and from measurements.²¹ The onset of hydrodynamic interactions responsible for a change in the microscopic viscosity can account for the nonlinear behavior of the observed viscosity with

concentration. In fact, for $k = 2$, a nonnegligible change in the microviscosity should occur around a hemoglobin concentration of $1.5 \mu\text{mol}/\text{cm}^3$ —where B becomes positive (see Figure 4). Therefore, it seems plausible that an increased value of f could counterbalance the effect of the ensemble average force, $\langle F \rangle$, assuming, of course, the magnitude of the frictional coefficient is the same or nearly so everywhere in solution.

Agreement between the observed D_m/D_0 values and the values obtained from eq 7, using the solution viscosity (see Figure 6), at high concentrations, must be taken with reservation, since there is no way to determine whether the observed D_m actually depicts the expected transition from solvent viscosity to the viscosity affected by protein intermolecular interactions, i.e., protein– H_2O to protein–protein interactions. Therefore, in this concentration range, the applicability of the generalized Stokes–Einstein relationship, when used in conjunction with the Stokes formulation, is questionable.

This study has addressed repulsive interactions—the least complicated of intermolecular interactions. It has been shown that the observed behavior of D_m for Hb can be predicted from independent thermodynamic measurements, in conjunction with the Stokes formulation for f , when the concentration is less than $1.1 \mu\text{mol}/\text{cm}^3$. In general the mutual diffusion coefficients of globular proteins are expected to follow the Stokes–Einstein relationship, $k_B T/6\pi a \eta$, at low concentrations and at sufficient ionic strength and pH. In this study, however, the relationship held to a much higher concentration, $1.5 \mu\text{mol}/\text{cm}^3$. As has been shown for bovine serum albumin,²² this is not a general feature of proteins. Apparently, in our study, the nearly twofold increase in viscosity may be balanced by an increase in $(\delta\Pi/\delta C)$ (via the excluded volume effect). Although the exact accompanying change in the microviscosity with concentration is indeterminable, one would expect some change in D_m outside the experimental accuracy. The generalized Stokes–Einstein relationship, eq 7, offers the best available interpretation of the lack of any change in D_m in the range from low to moderate protein concentrations.

Another hydrodynamic model, proposed by Broersma,²³ based on a nonuniform solvent viscosity whose magnitude depends upon the distance, r , away from a particle of radius, a , yields a normalized diffusion coefficient dependence of the form $D_0/D_m = 1 + l(\eta/\eta_0 - 1)$, where l is a parameter dependent on molecular shape and hydration sphere. With $l = 0.13$, a reasonable fit to the observed D_0/D_m data could be obtained.

Only further investigation and, hopefully, better qualitative hydrodynamic models will result in a more accurate physical representation of the diffusional process for macromolecules.

Acknowledgments. The authors wish to thank Professors A. Rich and S. Chen for valuable discussions and the use of their laboratory equipment. This work was supported in part by Contract No. AEC-AT (11-1)3352. J.R.V. acknowledges financial support from the NIH Postdoctoral Fellowship, No. GM53334-03.

References and Notes

- (1) S. Chen, W. Veldkamp, and C. Lai, *Rev. Sci. Instrum.*, **46**, 1356 (1975).
- (2) A. Altenberger and J. Deutsch, *J. Chem. Phys.*, **59**, 894 (1973).
- (3) G. Phillies, *J. Chem. Phys.*, **60**, 976 (1974).
- (4) E. Antonini and M. Brunori, "Frontiers of Biology", A. Neuberger and E. Tatume, Ed., North Holland Publishing Co., Amsterdam, Chapter 5.
- (5) W. Wilson, M. Luzzana, J. Penniston, and S. Johnson, *Proc. Natl. Acad. Sci. U.S.A.*, **71**, 1260 (1974).

- (6) E. Hegesh and N. Gruener, *Clin. Chem. Acta*, **36**, 679 (1970).
 (7) D. Koppel, *J. Chem. Phys.*, **57**, 4814 (1972).
 (8) R. Briehl and S. Ewert, *J. Mol. Biol.*, **80**, 445 (1973).
 (9) P. Tartaglia and S. Chen, *J. Chem. Phys.*, **58**, 4389 (1973).
 (10) J. Peterson and M. Fixman, *J. Chem. Phys.*, **39**, 2516 (1963).
 (11) S. Rice and P. Gray, "Statistical Mechanics of Simple Liquids", Interscience, New York, N.Y., 1965.
 (12) G. Adair, *Proc. R. Soc. London, Ser. A*, **120**, 573 (1928).
 (13) G. Scatchard, *J. Am. Chem. Soc.*, **68**, 2315 (1946).
 (14) V. Riveros-Moreno and J. Wittenberg, *J. Biol. Chem.*, **247**, 895 (1972).
 (15) K. Keller, E. Canales, and S. Yum, *J. Chem. Phys.*, **75**, 379 (1971).
 (16) J. Kirkwood and J. Shumaker, *Proc. Natl. Acad. Sci. U.S.A.*, **38**, 863 (1952).
 (17) C. Tanford, "Physical Chemistry of Macromolecules", Wiley, New York, N.Y., 1961.
 (18) B. Schoenborn, R. Featherstone, P. Vogelhut, and C. Suskind, *Nature (London)*, **202**, (1964).
 (19) C. Pyun and M. Fixman, *J. Chem. Phys.*, **41**, 937 (1964).
 (20) R. Simha, *J. Appl. Phys.*, **23**, 1020 (1952).
 (21) P. Cheng and H. Schachman, *J. Polym. Sci.*, **16**, 9 (1955).
 (22) G. Phillies, Sc.D. Thesis, M.I.T., 1973, unpublished.
 (23) S. Broersma, *J. Chem. Phys.*, **28**, 1158 (1958).

Kinetics of Dissociation of Ferric Chloride Complexes. Stability Constants of Inner- and Outer-Sphere Complexes

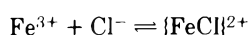
H. A. Schwarz* and R. W. Dodson

Department of Chemistry Brookhaven National Laboratory, Upton, New York 11973 (Received June 10, 1976)

Publication costs assisted by Brookhaven National Laboratory

The inner-sphere complex FeCl^{2+} is selectively produced by the reaction of thallium(II) chloride with Fe(II) in pulse radiolysis experiments. The approach to equilibrium of this system indicates that at 25 °C and 1 M ionic strength the equilibrium mixture contains an appreciable component of the outer-sphere complex, $\text{Fe}^{3+}, \text{Cl}^-$. The equilibration mechanism is $\text{Fe}^{3+} + \text{Cl}^- \rightleftharpoons \text{FeCl}^{2+}$ ($K_{in} = k_1/k_{-1}$), $\text{FeCl}^{2+} + \text{Cl}^- \rightleftharpoons \{\text{FeCl}_2\}^+$ (K_2), $\text{Fe}^{3+} + \text{Cl}^- \rightleftharpoons \text{Fe}^{3+}, \text{Cl}^-$ (K_{out}), $\text{Fe}^{3+}, \text{Cl}^- + \text{Cl}^- \rightleftharpoons \{\text{FeCl}_2\}^+$ ($K_4 = k_4/k_{-4}$). It is found that $K_{in} = 3.0 \text{ M}^{-1}$, $K_{out} = 2.2 \text{ M}^{-1}$, $K_2 = 1.3 \text{ M}^{-1}$, $k_{-1} = 7.3 \text{ s}^{-1}$, and $k_{-4} = 5.3 \text{ s}^{-1}$. An interpretation of published data indicates that the extinction coefficient of FeCl^{2+} varies only slightly with ionic strength and that K_{out} is also nearly independent of ionic strength between 1 and 4 M while K_{in} increases by a factor of 5 in this range.

The equilibrium constant of the reaction



where $\{\text{FeCl}\}^{2+}$ includes both inner- and outer-sphere complexes, increases markedly with ionic strength. It has been assumed that any outer-sphere complex effects in this reaction are negligible.^{1,2} Information on the relative contributions of inner- and outer-sphere complexes can be obtained from the effects of Fe^{3+} and Cl^- concentrations on the rate of approach to equilibrium. The kinetic results at 6 M² and 9 M³ ionic strength do not require any outer-sphere complex. Kinetic data at 0.6 M ionic strength⁴ were interpreted as requiring approximately equal proportions of the two complexes at equilibrium.

The oxidation of iron(II) by thallium(II) chloride complexes selectively produces inner-sphere FeCl^{2+} .⁵ The kinetics and the ratio of initial and final absorbances found for the approach to equilibrium at 1 M ionic strength are reported here. They demonstrate the importance of outer-sphere complexes at 1 M ionic strength.

Experimental Section

The materials and the preparation of solutions were as described before.^{5,6} The concentrations in the reaction mixture containing thallium were $2.5 \times 10^{-4} \text{ M}$ Tl(III), $1.00 \times 10^{-3} \text{ M}$ Tl(I), and $1.00 \times 10^{-3} \text{ M}$ Fe(II). The Fe(II) concentrations in reaction mixtures without thallium were either 5.1×10^{-3} or $10.2 \times 10^{-3} \text{ M}$. All solutions contained 1.00 M acid.

The anions present were ClO_4^- and Cl^- . The solutions were deaerated with argon.

The pulse radiolysis equipment and thermostat were described earlier.^{5,6} A deuterium arc was used as the light source, and absorbances were measured at 340 nm (near the FeCl^{2+} peak) except as otherwise noted. The optical path length was 6.1 cm. The reaction mixtures were at 25.0 °C when pulsed. The dose delivered in each pulse produced $1.8 \times 10^{-6} \text{ M}$ Fe(III) in solutions containing thallium. A higher dose, producing $15 \times 10^{-6} \text{ M}$ Fe(III), was used for solutions not containing thallium.

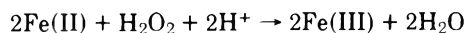
Results

The pulse radiolysis of solutions containing thallium and chloride produces Tl(II) by Cl_2^- oxidation of Tl(I) and hydrogen atom reduction of Tl(III). The Tl(II) rapidly equilibrates with chloride to form complexes.⁶ All forms of Tl(II) oxidize Fe(II) to Fe(III) but its higher chloride complexes produce exclusively inner-sphere FeCl^{2+} .⁵ All reactions of Tl(II) are complete in 10^{-3} s , leaving a solution with FeCl^{2+} present at a concentration exceeding the equilibrium concentration. In the subsequent approach to equilibrium, the absorbance of the solution is observed to decay by first-order kinetics, that is:

$$A = (A_0 - A_\infty)e^{-kt} + A_\infty \quad (1)$$

The blank against which the absorbance is measured is the solution just before the radiation pulse. The half-life of this

decay is less than 0.1 s. There is also a slow production of Fe(III) by

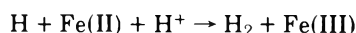


This reaction contributes less than 20% of the total Fe(III) and its half-life is 12 s under our experimental conditions.⁷ Consequently its effect is negligible.

The absorbance of the solution was followed for at least 3 half-lives. The parameters A_0 , A_∞ , and k were evaluated by a least-squares fit of the data to eq I. The standard deviations of the observed absorbances from the calculated values were less than ± 0.0001 absorbance unit, or generally about $\pm 0.5\%$ of the initial absorbance. Four pulses were given to each sample. The initial and final absorbances decreased by about 3% with each pulse. This effect is largely due to the back reaction of Tl(II) with FeCl_2^{2+} . The rate constant, k , should be independent of this reaction, and R , the ratio of A_∞ to A_0 , is expected to be much less sensitive to number of pulses than A_0 and A_∞ . Indeed, there was no discernible effect of number of pulses on either k or R . Values of k and R are given in Table I.

We have found that inner-sphere FeCl_2^{2+} in excess of the equilibrium amount can also be produced in the absence of thallium by the reaction of Cl_2^- with Fe(II). Jayson et al.,⁸ in a pulse radiolysis study of deaerated solutions containing Fe(II) and Cl^- , did not observe any slow decay attributable to FeCl_2^{2+} . Their Fe(II) concentration was a factor of 10 smaller than ours, and it is likely that hydrogen atoms reduced the FeCl_2^{2+} product instead of reacting with Fe(II).

Table I includes some rate constants measured in the absence of thallium. The amount and rate of Fe(II) oxidation by the hydrogen peroxide produced during the radiation pulse were measured separately by following the absorbance change of the solution between 1 and 5 s after the pulse. The contribution of the hydrogen peroxide reaction to the absorbance change during the FeCl_2^{2+} relaxation is not negligible in this case, primarily because of the higher Fe(II) concentration. The data were corrected for the hydrogen peroxide effect before fitting to eq I. Rate constants calculated without this correction were 3 to 10% higher than those tabulated. Values of R (i.e., A_∞/A_0) for the ferrous solutions without thallium were higher than those in the presence of thallium by a factor of about 3. This effect is expected, as the pathway forming FeCl_2^{2+} in the system is only one of several modes of production of Fe(III). The values of R were also scattered, probably because of reaction of hydrogen atoms with FeCl_2^{2+} or with traces of oxygen in competition with the slow reaction



Discussion

The rate constants for the approach of FeCl_2^{2+} to equilibrium, given in Table I, do not increase linearly with chloride concentration, as would be expected if a single inner-sphere complex were involved. The curvature of such a plot is negative, whereas participation of a second inner-sphere complex, $\text{FeCl}_2^+\text{Cl}^-$, would produce positive curvature. Furthermore, the ratio of the initial slope to intercept is 2.2 M^{-1} . If the outer-sphere complex were negligible in comparison to the inner-sphere complex, then the slope would be expected to be 5.2 M^{-1} , the stability constant for monochloro Fe(III) species.²

We will discuss the results in terms of the following reactions:

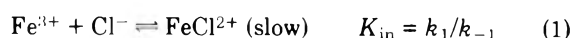
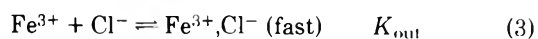
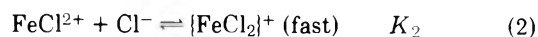


TABLE I: Rate Constants and Final to Initial Absorbance Ratios for Ferric Chloride Approach to Equilibrium in 1 M Acid Solutions at 25 °C

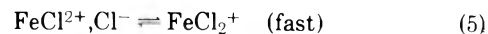
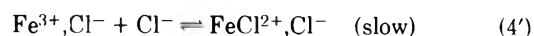
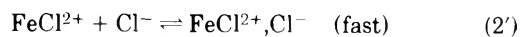
$[\text{Cl}^-]$, M	k , s^{-1}	f^a	R_{exptl}	R_{calcd}
0.0051	7.4	0.50	0.040	0.030
0.0082	7.5	0.58	0.049	0.042
0.0100 ^b	7.3			
0.0100 ^c	7.4			
0.0172	7.7	0.70	0.074	0.069
0.0441	8.1	0.85	0.132	0.133
0.050 ^b	8.1			
0.050 ^c	8.2			
0.089 ^d	8.7	0.93	0.218	0.216
0.089	8.7	0.93	0.213	0.216
0.089 ^e	8.6	0.93	0.210	0.216
0.090	8.9	0.93	0.213	0.216
0.100 ^b	9.1			
0.100 ^c	9.2			
0.300	12.0	0.99	0.443	0.438
0.600	15.4	1.00	0.590	0.585
0.900	17.4	1.00	0.666	0.668

^a The fraction of Fe(III) produced as inner-sphere chloride complexes. ^b No thallium present, $5 \times 10^{-3} \text{ M Fe(II)}$. ^c No thallium present, $1 \times 10^{-2} \text{ M Fe(II)}$. ^d 320 nm. ^e 370 nm.



$$K_4 = \frac{k_4}{k_{-4}} = \frac{K_2 K_{\text{in}}}{K_{\text{out}}}$$

Only three of the four equilibria are independent, as is noted by expressing K_4 in terms of the others. FeCl_2^{2+} is the inner-sphere complex and $\text{Fe}^{3+},\text{Cl}^-$ is the outer-sphere complex. The symbol $\{\text{FeCl}_2\}^+$ represents the sum of the inner-inner complex, FeCl_2^+ , and the inner-outer complex, $\text{FeCl}_2^+\text{Cl}^-$, assumed to be in rapid equilibrium. Mechanistically, reactions 2 and 4 probably involve only $\text{FeCl}_2^{2+},\text{Cl}^-$ and could be written



from which $K_2 = K_2'(1 + K_5)$ and $k_{-4} = k_{-4}'/(1 + K_5)$. Reaction 2' is an ion pair formation and will be diffusion limited. Reaction 4' is similar to reaction 1 with just the addition of a chloride in the outer sphere. Consequently it is reasonable to expect it to be slow. Reaction 5 is assumed to be fast by analogy with the corresponding reaction of $\text{FeOH}^{2+},\text{Cl}^-$.⁹ By "fast" is meant equilibrium is established in less than 0.01 s.

Hydrolyzed species are present in small proportions. Consequently the equilibrium constants and particularly the rate constants (which are strongly acid dependent^{1,2}) are composite constants. Such effects do not influence the interpretation of the data inasmuch as all experiments were performed at constant acid concentration.

The ratio of final to initial absorbances, R , is determined by the first three equilibria. If it is assumed that the inner-sphere complexes are solely responsible for light absorption in this region, then

$$R = \frac{K_{in}[Cl^-](1 + K_2[Cl^-])}{\{1 + (K_{in} + K_{out})[Cl^-] + K_{in}K_2[Cl^-]^2\}f} \quad (II)$$

where f is the fraction of the total iron species formed as inner-sphere complexes. For solutions containing thallium, f can be calculated from⁵

$$f = \frac{0.37 \times 10^4[Cl^-] + 2.4 \times 10^7[Cl^-]^2 + 2.3 \times 10^9[Cl^-]^3 + 1.7 \times 10^{10}[Cl^-]^4}{0.67 + 5.6 \times 10^4[Cl^-] + 5 \times 10^7[Cl^-]^2 + 2.3 \times 10^9[Cl^-]^3 + 1.7 \times 10^{10}[Cl^-]^4}$$

which is the ratio of the rate at which Tl(II) reacts with Fe(II) to produce $FeCl_2^{2+}$ to the total rate of production of Fe(III). The value of f is near one for most of the chloride concentrations used here (as may be seen from Table I). Note that eq II does not contain extinction coefficients. This is the result of assuming only inner-sphere complexes absorb light. In other words, R should be wavelength independent. This is tested at three wavelengths, shown in Table I. There is perhaps a slight increase in R at shorter wavelengths, as might be expected if Fe^{3+}, Cl^- is absorbing light with the peak of its spectrum further out toward the UV.

Equation II can be rearranged to

$$y = K_{in} + K_{in}K_2[Cl^-](1 - Rf) \quad (III)$$

where $y = Rf\{1 + (K_{in} + K_{out})[Cl^-]\}/[Cl^-]$. The sum $K_{in} + K_{out}$ is $5.2 M^{-1}$ at $25^\circ C$ and $1 M$ ionic strength.² A plot of y vs. $[Cl^-](1 - Rf)$ is shown in Figure 1, from which $K_{in} = 3.0 M^{-1}$, $K_2 = 1.3 M^{-1}$, and $K_{out} = 2.2 M^{-1}$ (by difference). Values of R computed from eq (II) with these stability constants are given in Table I for comparison with the observed results. Note that two points at the lowest chloride concentration are not included in Figure 1. The nature of the function y is such as to grossly overemphasize the experimental errors at these concentrations. Also, reaction of chlorine atoms with Fe(II) and back reaction of Tl(II) with $FeCl_2^{2+}$ would cause the method of computing f to yield values which are too large. Such effects become negligible at higher chloride concentrations.

The effects of several assumptions merit consideration: (i) The above mechanism does not include a complex with two outer-sphere chlorides, $Fe^{3+}, 2Cl^-$. If such a complex is included and assumed to have negligible absorbance, then

$$y = K_{in} + K_{in}K_2[Cl^-]\{1 - Rf(1 + r)\}$$

where r is the ratio of $Fe^{3+}, 2Cl^-$ to $\{FeCl_2\}^+$. The data preclude a value of r greater than 0.2. The intercept, K_{in} , is not significantly affected by any r , but if r is chosen as 0.1, for instance, K_2 would be calculated to be $1.5 M^{-1}$.

(ii) The inclusion of a finite extinction coefficient for Fe^{3+}, Cl^- leads to a lower estimate of K_{in} . For instance, a choice of 200 for $\epsilon(Fe^{3+}, Cl^-)$ would result in an estimate of $2.8 M^{-1}$ for K_{in} .

(iii) If f is assumed to be 1 at $[Cl^-] > 0.04$, K_{in} would be estimated as $3.3 M^{-1}$.

It should be noted that K_2 is defined for the formation of $\{FeCl_2\}^+$ from $FeCl_2^{2+}$. The more usual definition of the second stability constant would be

$$K_2' = \frac{[\{FeCl_2\}^+]}{[FeCl_2^{2+}] + [Fe^{3+}, Cl^-][Cl^-]}$$

or $K_2' = K_2K_{in}/(K_{in} + K_{out})$, which is $0.8 M^{-1}$ (but still does not include any outer-outer, or $Fe^{3+}, 2Cl^-$, complex). The estimate of K_2 from the slope of the line in Figure 1 will be influenced by any medium effect due to the replacement of

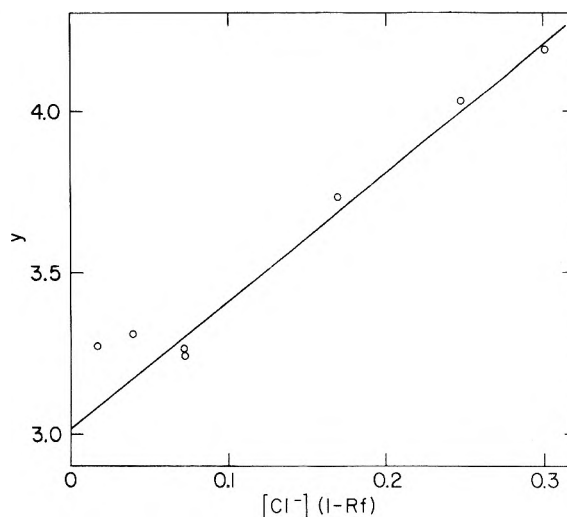


Figure 1. Test of eq 3 which expresses the chloride dependence of the ratio of final to initial absorbances. Ionic strength is $1 M$, temperature $25^\circ C$.

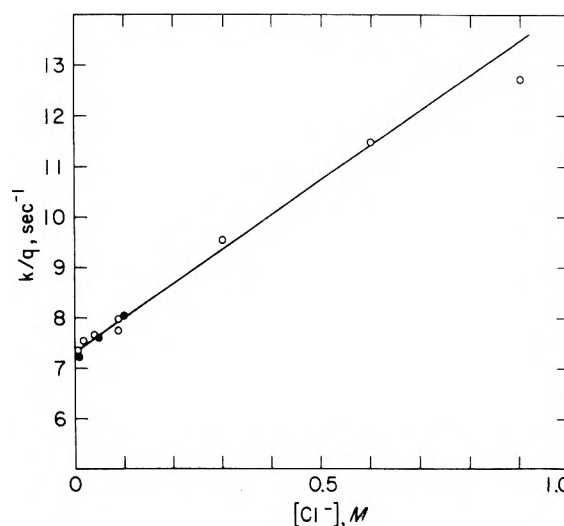


Figure 2. Test of eq 5 which expresses the chloride dependence of the rate constant k . Ionic strength is $1 M$, temperature $25^\circ C$: (O) thallium present, (●) thallium absent.

ClO_4^- by Cl^- . Such an effect is of much less consequence in estimating the intercept, K_{in} . The value of $0.8 M^{-1}$ for K_2' agrees well with the conclusion of Rowley and Sutin that K_2' is about $1 M^{-1}$.²

Reactions 1 to 3 do not suffice to explain the chloride variation of k . Reaction 4 offers an additional pathway for introducing or removing chloride from the inner coordination sphere. Reactions 1 to 4 lead to the following expression for the rate constant for approach to equilibrium:

$$k = (k_{-1} + k_{-4}K_2[Cl^-]) \left\{ \frac{1}{1 + K_2[Cl^-]} + \frac{K_{in}([Cl^-] + [Fe(III)])}{1 + K_{out}([Cl^-] + [Fe(III)])} \right\} \quad (IV)$$

In deriving this equation it was assumed that pseudo-first-order kinetics apply, which will be the case if either $[Fe(III)] \gg [Cl^-]$ or $[Cl^-] \gg [Fe(III)]$. The latter is true in our experiments, so

$$k/q = k_{-1} + k_{-4}K_2[Cl^-] \quad (V)$$

TABLE II: Ionic Strength Variation of Inner- and Outer-Sphere Stability Constants of Monochloro Fe(III) Complexes Derived from Average Extinction Coefficients

I, M	$\bar{\epsilon}^a$	ϵ_{in}^b	$K_{in} + K_{out}^c$ M^{-1}	K_{in} M^{-1}	K_{out} M^{-1}
1.00	1380	2500 ^c	5.2	2.9	2.3
3.00	1710	2620	9.8	6.4	3.4
4.00	2090	2670	17.3	13.5	3.8
5.00	2520	2730	36.3	33.5	2.8
6.00	2710	2790	110	107	3 ^d

^a Reference 2, 340 nm. ^b Linear interpolation between 1 and 6 M, 340 nm. ^c Reference 5. ^d Assumed.

where

$$q = \frac{1}{1 + K_2[Cl^-]} + \frac{K_{in}[Cl^-]}{1 + K_{out}[Cl^-]}$$

A plot of k/q vs. $[Cl^-]$ is shown in Figure 2, from which $k_{-1} = 7.3 \text{ s}^{-1}$ and $k_{-4} = 5.3 \text{ s}^{-1}$. The deviations from the line are somewhat larger than the experimental error, possibly because of medium effects. Unpublished results of Po and Sutin,¹⁰ in which k was measured in a stopped-flow apparatus at chloride concentrations up to 0.5 M, are in agreement with our data to better than 2%. Values from the literature for k_{-1} at 25 °C and 1 M ionic strength, 1 M acid, are 7.24^{11} and 6.8 s^{-1} .⁹

Campion et al.¹² report a value of $12 \text{ M}^{-1} \text{ s}^{-1}$ at 3 M ionic strength for the Fe(II) catalysis of $FeCl_2^{2+}$ decomposition.¹³ This pathway should be negligible at our concentrations, and indeed no effect of Fe(II) on the rate constant is observed between 10^{-3} and 10^{-2} M (Table I).

Rowley and Sutin² measured $K_{in} + K_{out}$ in equilibrated systems and determined k by a stopped-flow method at 6 M ionic strength under conditions such that $[Fe(III)] \gg [Cl^-]$ and sufficiently low $[Cl^-]$ that $[FeCl_2^+]$ was negligible. Under these conditions, eq IV reduces to

$$k = k_{-1} \left\{ 1 + \frac{K_{in}([Fe(III)] + [Cl^-])}{1 + K_{out}([Fe(III)] + [Cl^-])} \right\}$$

They found k to be nearly linear in $[Fe(III)] + [Cl^-]$. The ratio of initial slope to intercept was 107 M^{-1} , which on the basis of the above equation would be K_{in} . The sum $K_{in} + K_{out}$ was 110. In other words, K_{out} is negligible compared to K_{in} at 6 M ionic strength.

Rowley and Sutin gave extinction coefficients of the monochloro Fe(III) species between 1 and 6 M ionic strength derived from spectrophotometric measurements. These are average extinction coefficients and are related to the extinction coefficient of the inner-sphere complex by

$$\bar{\epsilon} = \epsilon_{in} \frac{K_{in}}{K_{in} + K_{out}} \quad (VI)$$

(assuming the outer-sphere complex contribution to $\bar{\epsilon}$ is negligible). Their values are given in column 2 of Table II along with their values of $K_{in} + K_{out}$ in column 4. If it is assumed that K_{out} is 3 M^{-1} at 6 M ionic strength, which is consistent with the above discussion, then from eq VI ϵ_{in} is 2790 at 6 M ionic strength. The value of ϵ_{in} at 1 M ionic strength is 2500.⁵ It is clear, then, that the much larger variation of $\bar{\epsilon}$ with ionic strength, seen in Table II, can be explained as due to varying proportions of inner- and outer-sphere complexes. In other words, eq VI can be used to calculate separate values for K_{in} and K_{out} . In order to do this we will assume that ϵ for $FeCl_2^{2+}$ can be found at the various concentrations by linear interpolation between the 1 and 6 M values. The values so computed are given in Table II. The value of 2.9 for K_{in} at 1 M ionic strength obtained by this method is in good agreement with the value of 3.0 reported above. Values of K_{out} at 4 M and below are quite insensitive to the linear interpolation assumption. It would appear that K_{out} is relatively insensitive to ionic strength in this region whereas K_{in} varies by a factor of 5.

Wendt and Strehlow⁴ reported that $K_{out} = 2 \pm 1$ on the basis of pressure jump measurements of the rate of $FeCl_2^{2+}$ relaxation in 0.027 M H^+ . It was necessary for them to assume that k_{-4} was negligible in comparison to k_{-1} . We do not find this to be the case in 1 M acid, but it may be so at their acid concentration where the overall rate of relaxation is much faster. It is not clear whether the agreement of our value of K_{out} with theirs is significant or fortuitous in view of the very different populations of hydrolyzed species in the two experiments.

Acknowledgment. We express our appreciation to Drs. J. K. Rowley and N. Sutin for helpful discussions. This research was carried out at Brookhaven National Laboratory under contract with the U.S. Energy Research and Development Administration.

References and Notes

- (1) H. Coll, R. V. Nauman, and P. W. West, *J. Am. Chem. Soc.*, **81**, 1284 (1959).
- (2) J. K. Rowley and N. Sutin, *J. Phys. Chem.*, **74**, 2043 (1970).
- (3) T. C. King and J. K. Rowley, *J. Phys. Chem.*, **75**, 1113 (1971).
- (4) H. Wendt and H. Strehlow, *Z. Elektrochem.*, **66**, 228 (1962).
- (5) H. A. Schwarz and R. W. Dodson, *J. Phys. Chem.*, submitted for publication.
- (6) R. W. Dodson and H. A. Schwarz, *J. Phys. Chem.*, **78**, 892 (1974).
- (7) H. N. Po and N. Sutin, *Inorg. Chem.*, **7**, 621 (1968).
- (8) G. G. Jayson, B. J. Parsons, and A. J. Swallow, *J. Chem. Soc., Faraday Trans. 1*, **69**, 1597 (1973).
- (9) R. E. Connick and C. P. Coppel, *J. Am. Chem. Soc.*, **81**, 6389 (1959).
- (10) Unpublished work by H. N. Po and N. Sutin; private communication from N. Sutin.
- (11) H. N. Po and N. Sutin, as reported in ref 2.
- (12) R. J. Campion, T. J. Conocchioli, and N. Sutin, *J. Am. Chem. Soc.*, **86**, 4591 (1964).
- (13) T. J. Conocchioli, G. Nancollas, and N. Sutin, *J. Am. Chem. Soc.*, **86**, 1453 (1964).

A Simple Theory of Surface Tension at Low Vapor Pressure

H. Ted Davis* and L. E. Scriven

Departments of Chemical Engineering and Materials Science, University of Minnesota,
Minneapolis, Minnesota 55455 (Received June 9, 1976)

Publication costs assisted by the National Science Foundation

A simple lattice model is used to derive an expression relating the surface tension to the internal pressure of the bulk condensed phase in equilibrium with its vapor. The expression, although derived with the aid of a molecular model, depends only on the thermodynamic properties of the bulk condensed phase. Comparison of theory with experiment is quite good for several liquids. Predicted values are low in most cases. The average absolute error is 17% of the experimental value.

The stress tensor of a system of classical particles interacting via a pairwise additive intermolecular potential may be expressed in the form

$$\mathbf{T}(\mathbf{r}_1) = \mathbf{T}^K(\mathbf{r}_1) + \mathbf{T}^V(\mathbf{r}_1) \quad (1)$$

where the kinetic part of the stress tensor is

$$\mathbf{T}^K(\mathbf{r}_1) = -n(\mathbf{r}_1)kT \mathbf{I} \quad (2)$$

and the interaction part (to be precise, the part contributing to the interfacial tension) is¹

$$\mathbf{T}^V = \frac{1}{2} \int \frac{d\mathbf{u}(r_{21})}{dr_{21}} \frac{\mathbf{r}_{12}\mathbf{r}_{12}}{r_{12}} \times n(\mathbf{r}_1)n(\mathbf{r}_1 + \mathbf{r}_{21})g(r_{12},\mathbf{r}_{21})d^3r_{21} \quad (3)$$

where \mathbf{I} is the unit tensor, $u(r_{21})$ the pair potential, n the density, and g the pair correlation function.

In what follows, we consider a dilute vapor phase of bulk density n_v in equilibrium with a dense condensed phase of bulk density $n_c \gg n_v$. We restrict our attention to a planar system, i.e., one in which the density varies only in the x direction. We use the Fowler-Kirkwood-Buff approximation² to the density profile, namely

$$n(x) = n_c \quad x < 0 \\ = n_v \approx 0 \quad x > 0 \quad (4)$$

We also assume that for the purpose of evaluating thermodynamic functions the structure of the condensed phase can be approximated by that of a simple cubic lattice, i.e.

$$g(\mathbf{r}_{21}) = \sum_j^N a^3 \delta(\mathbf{r}_{21} - \mathbf{R}_j) \quad (5)$$

where a^3 is the volume of the simple cubic unit cell (and, therefore, $n_c = a^{-3}$) and \mathbf{R}_j is the position of the j th lattice site relative to the position of particle 1.

With eq 4 and 5, the expression for \mathbf{T}^V can be reduced to the form

$$\mathbf{T}^V(z_1) = \frac{1}{2a^3} \sum_{j, X_j < -x_1}^N u'(R_j) \frac{\mathbf{R}_j \mathbf{R}_j}{R_j} \quad (6)$$

where X_j is the x component of \mathbf{R}_j . For a simple cubic lattice, approximating eq 6 by keeping terms through the fifth nearest neighbor contributions, we find the principal stress difference is

$$T_{zz}^V(x_1) - T_{xx}^V(x_1) = \frac{1}{2a^2} [u'(a) + \sqrt{2}u'(\sqrt{2}a) + 2u'(2a) + \frac{6}{\sqrt{5}}u'(\sqrt{5}a)] \quad x_1 = 0 \\ = \frac{1}{2a^2} [2u'(2a) + \frac{6}{\sqrt{5}}u'(\sqrt{5}a)] \\ = 0 \quad x_1 = -2a, -3a, \dots \quad x_1 = -a \quad (7)$$

The interfacial tension γ is defined as the integral across the interface of this difference between the transverse and the normal stress components, i.e.

$$\gamma = \int_{-\infty}^{\infty} (T_{zz}^V - T_{xx}^V) dx \quad (8)$$

Assuming continuity of the stress tensor, we can evaluate γ from the results of eq 7 by linear interpolation of the values of $T_{zz}^V - T_{xx}^V$ across successive lattice planes. Thus

$$\gamma = \sum_{\text{lattice planes}} a (\text{average value of } T_{zz}^V - T_{xx}^V \text{ between successive planes})$$

or

$$\gamma = \frac{1}{4a} [u'(a) + \sqrt{2}u'(\sqrt{2}a) + 6u'(2a) + \frac{18}{\sqrt{5}}u'(\sqrt{5}a)] \quad (9)$$

Let us next consider the thermodynamic energy function U of the lattice model considered here. Keeping contributions through fifth nearest neighbors, we find

$$U = U^K(T) + 6N[u(a) + 2u(\sqrt{2}a) + \frac{4}{3}u(\sqrt{3}a) + u(2a) + 4u(\sqrt{5}a)] \quad (10)$$

where $U^K(T)$ is the ideal gas limit of U . Noting that $V = Na^3$, we can put the volume derivative of U in the form

$$\left(\frac{\partial U}{\partial V}\right)_{T,N} = \frac{1}{3a^2N} \left(\frac{\partial U}{\partial a}\right) = \frac{2}{a^2} \times [u'(a) + 2\sqrt{2}u'(\sqrt{2}a) + 4\sqrt{3}u'(\sqrt{3}a) + 2u'(2a) + \frac{20}{\sqrt{5}}u'(\sqrt{5}a)] \quad (11)$$

TABLE I: Surface Tensions of Several Liquids

Substance	T, K	γ , dyn/cm	
		Eq 12 ^a	Expt ^b
Benzene	293	24.4	28.9
Benzene	333	22.4	23.7
Benzene	353	21.1	21.2
n-Heptane	293	19.8	20.1
n-Heptane	313	18.6	18.2
n-Heptane	333	15.5	14.3
Diethyl ether	273	18.8	18.9
Diethyl ether	298	17.5	16.7
Argon	84	8.4	13.3
Argon	90	7.7	11.8
Nitrogen	78	6.7	8.8
Nitrogen	90	5.7	6.0
Oxygen	71	9.7	18.0
Oxygen	89	9.0	13.4
Methane	90.7	9.1	18.7
Methane	120	9.0	11.0
Carbon tetrachloride	288	23.5	27.7
Carbon tetrachloride	343	19.8	20.9

^a Bulk phase thermodynamic data taken from J. S. Rowlinson, "Liquids and Liquid Mixtures", Butterworths, London, 1959. ^b J. J. Jasper, *J. Phys. Chem. Ref. Data*, 1, 841 (1972).

The quantity $(\partial U/\partial V)$ is referred to as the "internal pressure".

We shall now make the final assumption of our model. This is that the quantity in the square bracket of eq 9 can be approximated by the quantity in the square bracket of eq 11. For nonpolar fluids this should be a fairly good approximation. For example, if u goes as r^{-6} , then the ratio of the square bracketed term in eq 9 to that in eq 11 is 0.89. With this assumption the final form of the interfacial tension is

$$\gamma = \frac{1}{8n_c^{1/3}} \left(\frac{\partial U}{\partial V} \right)_{T,N} \quad (12)$$

Thus, we have succeeded in determining the interfacial tension solely in terms of the thermodynamic properties of the bulk condensed phase. The molecular details have been eliminated. An implication of eq 12 is that the excess Helmholtz free energy to create interface of area dA is equal to the change in the bulk phase internal energy upon changing the volume by amount $n_c^{1/3} dA/8$ at constant temperature and number of particles N .

In Table I, surface tensions predicted by eq 12 are compared with experimental values for a variety of liquids. The overall agreement is quite good, especially considering the oversimplifications of the model leading to eq 12.

It is interesting that a century and a half ago, Young³ suggested that the interfacial tension can be estimated as one-third of the product of the range of the attractive potential and the cohesive force, or in Rayleigh's⁴ terminology, the intrinsic pressure of attraction of fluid across an imaginary plane interface. If the range of the potential is assumed to be equal to $n_c^{-1/3}$ and if the intrinsic pressure is equated to $(\partial U/\partial V)_T$, then Young's estimate of the surface tension is the same as eq 12 except that the factor of $1/8$ in eq 12 would be $1/3$. Rayleigh points out that Young's argument should have led to a factor of $3/20$ instead of $1/3$, a correction bringing Young's estimate even closer to eq 12.

Acknowledgment. The authors wish to thank NSF for financial support of the research reported here.

References and Notes

- (1) J. H. Irving and J. G. Kirkwood, *J. Chem. Phys.*, **18**, 817 (1950).
- (2) J. G. Kirkwood and F. P. Buff, *J. Chem. Phys.*, **17**, 338 (1949).
- (3) T. Young, "Supplement to the Encyclopaedia Britannica", 1816. See T. Young's "Miscellaneous Works", Vol. I, G. Peacock, Ed., John Murray, Albemarle Street, London, 1855, p 461.
- (4) Lord Rayleigh, *Phil. Mag.* **XXX**, 285, 456 (1890). See also Lord Rayleigh, "Scientific Papers", Vol. III, Dover Publication, New York, N.Y., 1964, p 404.

Pulse Radiolysis Study of Geminate Recombination in Charge Transfer Systems

Koichiro Hayashi, Dagmar Lindenau, Wolfram Schnabel, and Masahiro Irie*

The Hahn-Meitner-Institut für Kernforschung, Berlin GmbH, 1 Berlin 39, West Germany and the Institute of Scientific and Industrial Research, Osaka University, Suita, Osaka 565, Japan (Received May 3, 1976)

Publication costs assisted by the Hahn-Meitner-Institut für Kernforschung

Geminate recombination of ion pairs formed from the excited charge transfer complex of α -methylstyrene-pyromellitic dianhydride was studied by the pulse radiolysis technique. Radiation-induced ionic dissociation of the complex is found to occur from both excited singlet and triplet states. The recombination rate of the ions thus formed depends on the electronic state from which they are formed. Ion pairs formed from the singlet complex recombine faster than those from the triplet state. The difference in the decay behavior is discussed from the view point of spin conservation in ion pairs immediately after their generation.

Introduction

The reactions of primary products initially formed non-homogeneously in radiation as well as photochemistry have been studied extensively both from the theoretical and the experimental point of view.¹⁻⁸ There are two methods for obtaining information about the very early events, such as geminate recombination of isolated pairs (radical pairs, positive hole-electron pairs, and cation-anion pairs). One is the scavenger method using a presumed relationship between scavenger concentration and time.¹ Another, more powerful method is the direct observation of processes, which has become possible by the development of pulse techniques. By the latter method the study of the early events has advanced remarkably.

Recently, Eisenthal et al. have succeeded in observing directly the geminate recombination of iodine atoms formed in solvent cages by picosecond flash photolysis using a mode locked laser.⁵ The geminate recombination of positive charge-electron pairs has been much more extensively studied with the pulse radiolysis technique,^{1,2,4,7} since the lifetime of ion pairs is longer than that of radical pairs and it is more easy to detect them. The recombination of isolated cation-anion pairs in polar solvent, however, has been scarcely elucidated, since the formation of isolated cation-anion pairs of organic compounds is limited to special systems such as excited charge transfer complexes.^{6,9,10}

In previous work,⁹ we have directly observed the geminate recombination of associated cation-anion pairs, generated from α -methylstyrene-tetracyanobenzene complexes in methylene chloride solution by laser flash photolysis. We found that the recombination rate depends on the electronic state of the precursor. Ottolenghi et al. also measured directly the geminate recombination of photochemically produced ion pairs of pyrene radical cations and *N,N*-dimethylaniline radical anions.⁶ As reported earlier¹⁰ the dissociation of excited charge transfer complexes into ion pairs in polar solvents cannot only be induced by uv light but also by high-energy radiation such as γ rays. The purpose of this paper is to elucidate in detail the process of geminate recombination of cation-anion pairs generated by irradiating a solution of the CT complex of α -methylstyrene and pyromellitic dianhydride with 50-ns pulses of 15-MeV electrons. The results thus ob-

tained should be used to compare the behavior of radiation and photochemically produced ion pairs.

Experimental Section

The solvents 1,2-dichloroethane (DCE) and tetrahydrofuran (THF) used were of spectrometric grade and dried over CaH_2 . α -Methylstyrene was purified as described before.¹⁰ Pyromellitic dianhydride (PMDA) was sublimated before use. The samples were deaerated by bubbling with purified argon for 30 min.

The pulse radiolysis facility of the Hahn-Meitner-Institute was used. The samples were irradiated with 50-ns pulses of 15-MeV electrons from a L-band linear accelerator (Vickers Co. Ltd.). The signals were displayed on a Tektronix 7623 storage oscilloscope. To avoid photoionization, the analyzing light had to pass through cutoff filters, which absorbed light below 455 nm.

Results and Discussion

(I) "Fast" Ionic Dissociation and Association. Figure 1 shows a typical transient absorption after an electron pulse recorded at 664 nm, obtained in a 1:1 (v/v) mixture of DCE and THF containing 2.7 M α -methylstyrene and 7.5×10^{-1} M PMDA. The trace is composed of two curves indicating the existence of two intermediates. One intermediate is formed immediately during the pulse and disappears within a few microseconds while the other intermediate grows in slowly and decays within several hundred microseconds.

In order to identify the two intermediates, transient absorption spectra were recorded immediately and 20 μs after the pulse. The spectra are shown in Figure 2A and 2B. They are both attributed to the absorption of the PMDA radical anion,¹² though the absorption maxima differ slightly. This result indicates that the same radical anion is formed from two different precursors with different lifetimes in this system.

As is shown in Figure 3 the rapidly growing absorption increases with increasing concentration of added α -methylstyrene, which is known to form a charge transfer complex with PMDA.¹¹ Thus, this increase of the absorption is due to the increase of the concentration of the α -methylstyrene-PMDA complex. In the absence of α -methylstyrene the rapidly growing absorption was not observed. Thus, it appears that the fast growing absorption is due to a species formed by the ionic dissociation of the CT complex. It is assumed that the dissociation occurs from CT complexes being in excited singlet states. The formation of ions from the excited singlet

* Address correspondence to this author at The Institute of Scientific and Industrial Research, Osaka 565, Japan.

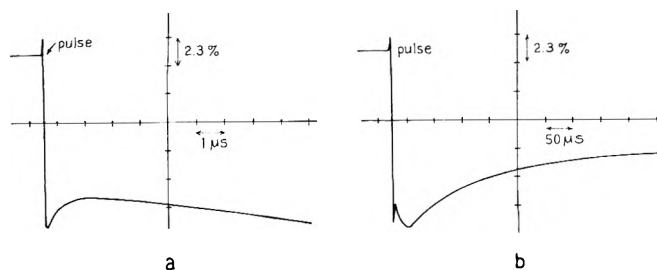


Figure 1. Oscillograms obtained at 664 nm in the pulse radiolysis of a solution containing 2.7 M α -methylstyrene and 7.5×10^{-3} M PMDA in a solvent mixture of THF and DCE (volume ratio of 1:1) at room temperature.

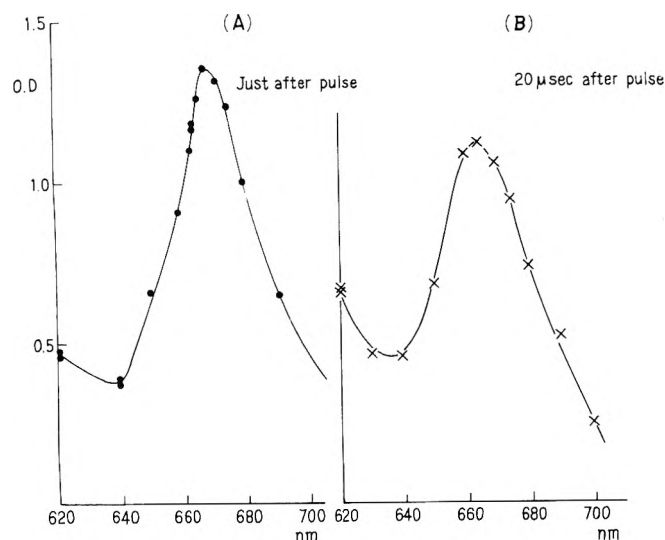


Figure 2. Transient absorption spectra obtained in the pulse radiolysis of a solution containing 0.97 M α -methylstyrene and 9.4×10^{-3} M PMDA in a solvent mixture of THF and DCE (volume ratio of 1:1) at room temperature: (A) immediately after and (B) 20 μ s after the pulse.

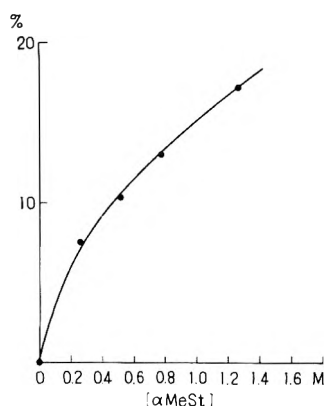


Figure 3. Dependence of the yield of the PMDA radical anion formed during the pulse on the concentration of α -methylstyrene added to the solution containing 1.0×10^{-2} M of PMDA in a solvent mixture of THF and DCE (volume ratio of 1:1).

state coincides with the previous observation at 77 K.¹⁰ It has been reported recently⁹ that upon uv irradiation (λ 347 nm) of the complex PMDA- α -methylstyrene dissociation into ions occurred only from the triplet state. Dissociation from the lowest excited singlet state was not observed. The intersystem crossing rate is faster than the dissociation rate in the lowest excited singlet state. However, the fact that PMDA anion radicals are generated very fast upon irradiation with high-

energy radiation makes it very probable that the dissociation occurs in this case from excited states of the singlet system. It is assumed that higher excited singlet states (i.e., states above the first excited state) of the complexes are involved. In principle PMDA and α -methylstyrene could react with charged species generated during the radiolysis of the solvent components, thus giving rise to the transient absorption observed. However, DCE and THF were chosen as solvent constituents because of their strong capability of reacting with electrons (DCE) and positively charged species (THF), thus forming relatively stable unreactive ions. It is, therefore, highly improbable that the observed ionic species are formed by a direct electron capture or a positive charge transfer in this mixed solvent.

The fast growing radical anions of PMDA decay about one hundred times faster than the slowly formed ions. The rapid decay is attributable to geminate recombination. The position of the absorption maximum of the ions at 670 nm is slightly shifted to higher wavelengths relative to the absorption maximum of free ions at 664 nm observed in pure THF. The red shift is considered to be due to the interaction of the radical anion with the positive partner.¹⁰ The interaction between the partners of the ion pairs is assumed to cause a rapid recombination resulting in fast geminate recombination. The recombination rate observed in this case is, however, slow compared with the rate measured during the flash photolysis experiments, where the absorption of the ions decayed within a few tenths of a nanosecond. This suggests that the interaction in ion pairs produced by high-energy radiation is weaker than in ion pairs produced by uv light. This assumption corresponds to the finding that by irradiating the PMDA-ethylbenzene complex in a glassy matrix at 77 K the shift of the ions formed by γ irradiation is smaller than that of ions produced by uv light irradiation.¹⁰ This indicates that ion pairs formed by high-energy radiation interact less strongly than ion pairs produced photochemically.

(II) "Slow" Ionic Dissociation and Association. The transient absorption shown in Figure 1 depicts not only the fast but also the slow ionic dissociation process. It is assumed that in the slow process PMDA radical anions are formed from a rather stable precursor, presumably a complex in the excited triplet state. In order to substantiate this assumption, the effect of triplet quenchers was examined. It was found that in the presence of oxygen or air the slowly growing component was not formed, as shown in Figure 4A and 4B, though the formation of the fast component was not influenced. The slow component, however, was always detectable after oxygen was removed by bubbling with argon, as demonstrated by the oscilloscope trace in Figure 4D. Fluorenone, which frequently acts as triplet quencher, also prevented the formation of the slowly growing component (Figure 4C). These results are taken as evidence that in the slow process of ion formation a triplet precursor is involved.

Figure 5 shows the time dependence of the transient absorption observed at the maximum of the PMDA radical anion spectrum as a function of the α -methylstyrene concentration. In the absence of α -methylstyrene the absorption at 664 nm also increases slowly. It is assumed that the PMDA anion radicals thus detected arise from the dissociation of triplet excited THF-PMDA complexes. If α -methylstyrene is present in the solution a portion of the absorption is formed within the pulse. This portion increases with increasing α -methylstyrene concentration. Simultaneously the portion of the slowly growing absorption decreases. In the presence of α -methylstyrene both types of PMDA complexes exist. The fraction

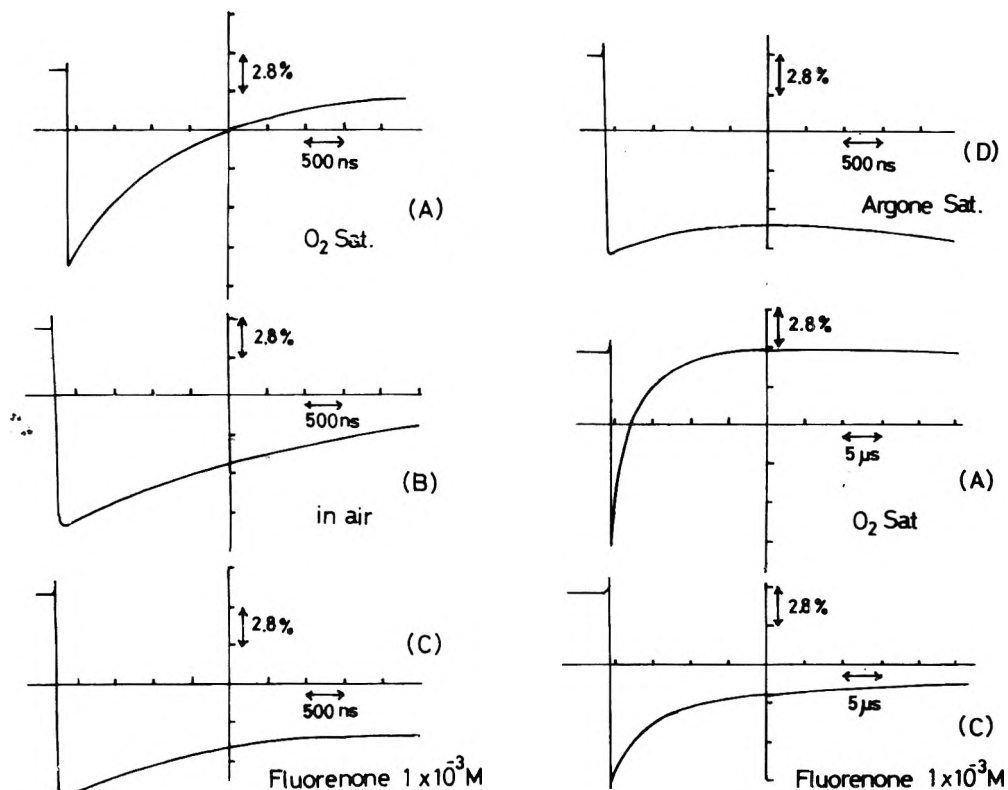


Figure 4. Oscillograms recorded at 664 nm in the pulse radiolysis of solutions containing 9.7×10^{-1} M α -methylstyrene and 9.4×10^{-3} M PMDA in a solvent mixture of THF and DCE (volume ratio of 1:1) in the presence of (A) oxygen, (B) air, (C) 1×10^{-3} M fluorenone, and (D) argon (saturated).

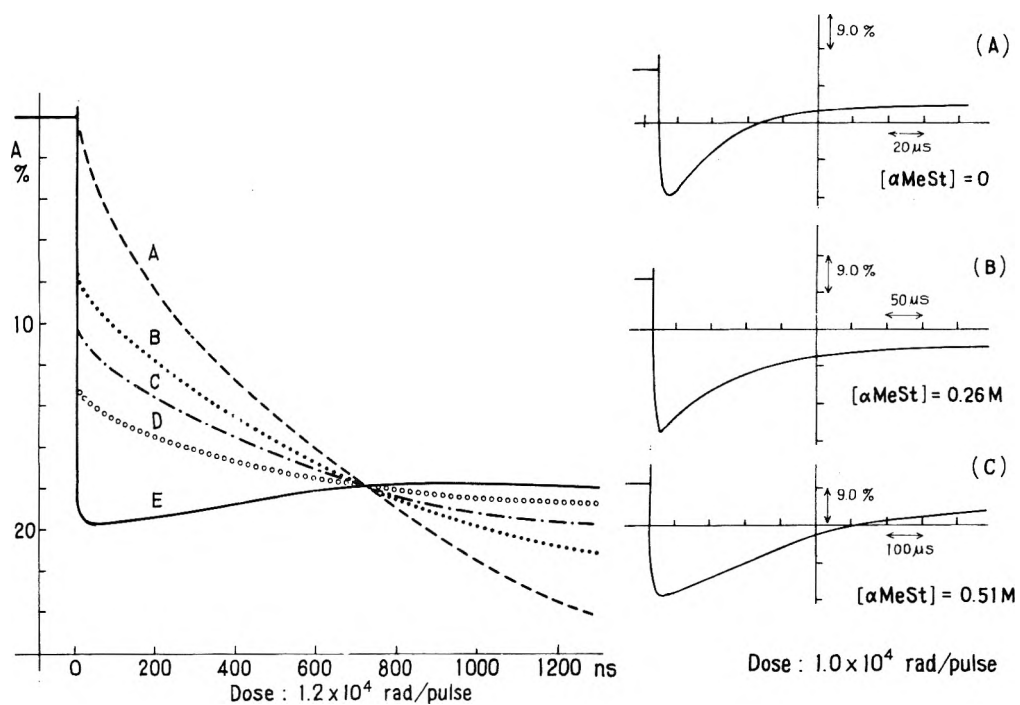


Figure 5. Oscillograms recorded at 364 nm in the pulse radiolysis of solutions containing various amounts of α -methylstyrene and 1.0×10^{-2} M PMDA in a solvent mixture of THF and DCE (volume ratio of 1:1) at room temperature. Concentrations of α -methylstyrene: (A) 0 M, (B) 0.26 M, (C) 0.51 M, (D) 0.77 M, (E) 1.29 M.

of α -methylstyrene-PMDA complexes increases with increasing α -methylstyrene concentration. If the concentration of the latter becomes greater than about 1.3 M, the fraction of PMDA-THF complexes can be considered as negligible. Then the observed changes of the absorption at 664 nm are

exclusively due to the dissociation of α -methylstyrene-PMDA complexes. The same conclusion is arrived at by considering the rates of decay of the ions formed from triplet precursors at various α -methylstyrene concentrations. As shown in Table I the half-life increases from 40 to 430 μ s by increasing the

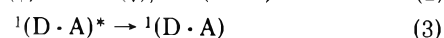
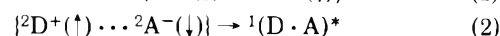
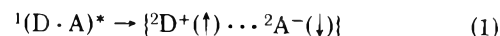
TABLE I: Half-Life and Maximum Absorption at 664 nm for Solutions Containing Varying Amounts of α -Methylstyrene^a

Concn of α MeSt, M	A % max	$\tau_{1/2}$, μ s
0	29.3	40
0.26	36.4	220
0.51	26.9	270
0.77	25.5	370
1.29	13.9	430

^a [PMDA] = 1×10^{-2} M, THF:DCE = 1:1 (v/v), dose 1.0×10^4 rad; pulse length 50 ns.

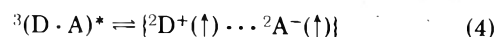
α -methylstyrene concentration from 0 to 1.29 M. This result is attributed to a difference of the recombination rates of the two kinds of ion pairs. Obviously, ion pairs formed by dissociation of THF-PMDA complexes recombine faster than ion pairs stemming from the dissociation of α -methylstyrene-PMDA complexes. The question arose whether the observed decay of the absorption at λ 664 nm is due to combination of homogeneously distributed free ions or to the recombination of rather strongly interacting ion pairs, i.e., to geminate recombination of ions. Evidence for geminate recombination infers from the fact that the observed decay follows first-order kinetics. Further on it was expected that the decay time should vary with the absorbed dose per pulse if random combination and geminate recombination of ions would be competing reactions. However, an indication for a substantial portion of random combination could not be obtained. By varying the absorbed dose per pulse from 4×10^3 to 9.3×10^3 rad the time $\tau_{2/3}$ (time for a decrease of the absorption to $2/3$ of its initial value) remained constant within the error limit ($\tau_{2/3} = 240 \pm 20$ μ s). (Experimental conditions during these experiments: [PMDA] = 7.5×10^{-3} M; [α MeSt] = 2.7 M; [THF]:[DCE] = 1:1 (v/v).)

(III) *Association Mechanism.* The decay behavior of the ions depends on the electronic state of the precursor as stated above. A similar behavior was found during the investigation of the uv light induced dissociation of α -methylstyrene-tetracyanobenzene complexes.⁹ In that case it was found that the decay rate of ions formed from singlet states was much faster than that of ions formed from complexes in the triplet state. As was suggested already in the previous paper⁹ the remarkable difference of the decay rates becomes understandable by taking into account the role of spin conservation during the recombination of ion pairs. When the spin-lattice relaxation time T_1 is greater than the recombination time T_R an ion pair formed from a singlet state recombines to form $^1(D \cdot A)^*$ without changing the initial spin state:

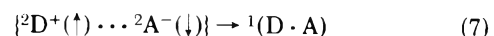
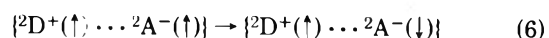
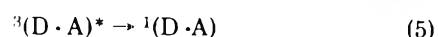


A $^1(D \cdot A)^*$ complex formed by recombination of an ion pair quickly deactivates to the ground state complex and its lifetime is therefore very short.

In the case of ion pairs generated from triplet excited α -methylstyrene-pyromellitic dianhydride complexes evidence for a strong interaction between the ions is obtained from the fact that the absorption at 664 nm decays according to a first-order law. This indicates that free ions are not formed. Further respective evidence infers from the fact that decay times several orders of magnitude lower were found than spin correlation times calculated by Brocklehurst^{3b} for isolated ions. If free ions would exist in the solution the spin correlation would be retained for a period much shorter than the observed decay time and the latter should be also shorter. Thus the observed effects may be explained by the following mechanism: the ion pair formed from the triplet state has a total spin quantum number of one during the time T_1 :



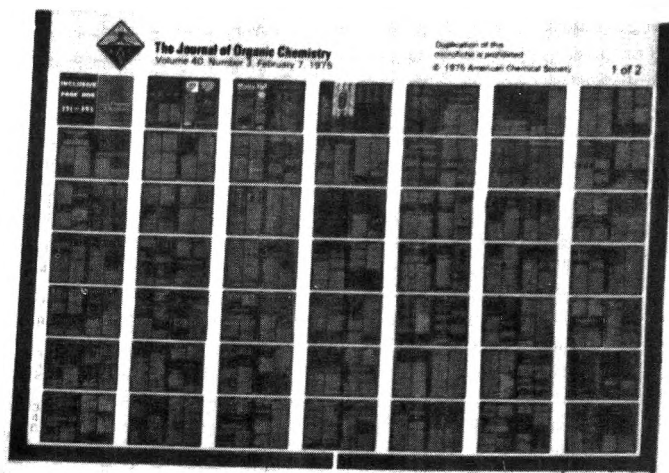
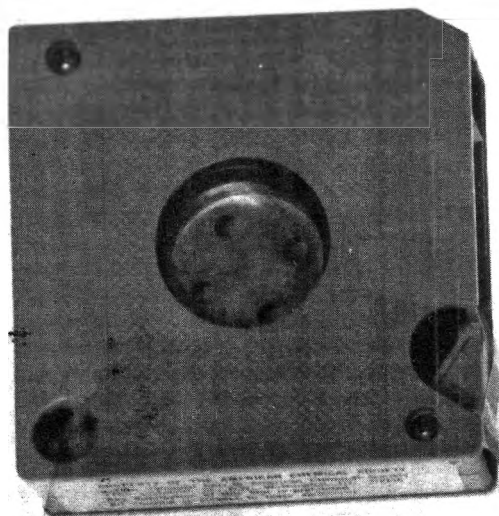
Equilibrium 4 will endure until either $^3(D \cdot A)^*$ complexes are deactivated to ground state complexes (process 5) or inversion of the spins of the radical ions occurs (process 6):



The rather slow rates of reactions 5 and 6 are considered to cause the observed slow decay rate of those ion pairs formed from CT complexes in the triplet state.

References and Notes

- (1) A. Mozumder and J. L. Magee, *Int. J. Radiat. Phys. Chem.*, **7**, 83 (1975).
- (2) K. Y. Lam and J. W. Hunt, *Int. J. Radiat. Phys. Chem.*, **7**, 317 (1975).
- (3) (a) B. Brocklehurst, *Chem. Phys.*, **2**, 6 (1973); (b) *Chem. Phys. Lett.*, **28**, 357, 361 (1974).
- (4) M. P. DeHaas, J. M. Warman, P. P. Infelta, and A. Hummel, *Chem. Phys. Lett.*, **31**, 382 (1975).
- (5) K. B. Eisenthal, *Acc. Chem. Res.*, **8**, 118 (1975).
- (6) D. M. Goodall, N. Orbach, and M. Ottolenghi, *Chem. Phys. Lett.*, **26**, 365 (1974).
- (7) F. Dainton, M. B. Ledyer, R. May, and G. A. Salmon, *J. Phys. Chem.*, **77**, 45 (1973).
- (8) E. Zador, J. M. Warman, L. H. Luthiens, and A. Hummel, *J. Chem. Soc., Faraday Trans. 1*, **70**, 227 (1974).
- (9) M. Irie, H. Masuhara, K. Hayashi, and N. Mataga, *J. Phys. Chem.*, **78**, 341 (1974).
- (10) M. Irie, S. Irie, Y. Yamamoto, and K. Hayashi, *J. Phys. Chem.*, **79**, 699 (1975).
- (11) M. Irie, S. Tomimoto, and K. Hayashi, *J. Polym. Sci., Part A*, **10**, 3235 (1972).
- (12) Y. P. Pilette and K. Weiss, *J. Phys. Chem.*, **75**, 3805 (1971).



MICROFORMS

American Chemical Society publications in microform

MICROFILM OR MICROFICHE?

With the ACS microform program you can receive either, or both

Microfilm

All periodical publications back to volume one

Copying privileges included with current subscriptions

All non-print supplementary materials provided free on microfiche

Archival quality silver halide film supplied as you request; positive or negative; 16 or 35mm; cartridge, reel, or cassette.

For microfilm information:

Special Issues Sales

American Chemical Society
1155 16th Street, N.W.
Washington, D.C. 20036
(202) 872-4363

Microfiche

Current issues of primary journals, beginning with January 1975

Individual issues or full volumes available

Supplementary materials also available on microfiche

Fiche supplied are archival quality silver halide, negative, 105 x 148mm (4" x 6"); 24x, with eye legible headers, start and end targets, and page numbers

For microfiche information:

Business Operations

Books and Journals Division
American Chemical Society
1155 16th Street, N.W.
Washington, D.C. 20036
(202) 872-4444

